AFOSR-TR- 91 1 2035
February 1991
(Distrib. Nov. 1991)

FINAL TECHNICAL REPORT
to

US AIR FORCE OFFICE OF SCIENTIFIC RESEARCH

Bolling Air Force Base
Washington DC 20332-6448

AFOSR Grant No. 89-0223

TRANSPORT PHENOMENA AND INTERFACIAL KINETICS IN MULTIPHASE COMBUSTION SYSTEMS

Principal Investigator: **Daniel E. Rosner**

Period Covered: 1 January 1989 to 31 December 1990

Yale University
High Temperature Chemical Reaction Engineering Laboratory
Department of Chemical Engineering
PO Box 2159 YS, New Haven CT 06520 USA

The views and conclusions contained in this document are those of the authors and his research colleagues and should not be interpreted as necesarily the official policy or the endorsements, either expressed or implied, of the Air Force Office of Scientific Research or the U.S. Government

FINAL TECHNICAL REPORT (February 1991)

AFOSR Grant No. 89-0223

TRANSPORT PHENOMENA AND INTERFACIAL KINETICS IN MULTIPHASE COMBUSTION SYSTEMS

Principal Investigator: **Daniel E. Rosner**

Yale University
High Temperature Chemical Reaction Engineering Laboratory
Department of Chemical Engineering
PO Box 2159 YS, New Haven CT 06520 USA

Table of Contents

REPORT DOCUMENTATION PAGE

Form Approved
OMB No. 0704-0188

1. AGENCY USE ONLY (Leave blank)	2. REPORT DATE	3. REPORT TYPE AND DATES COVERED
	February 1991	Final Report: 1/1/89 to 12/31/90

4. TITLE AND SUBTITLE

TRANSPORT PHENOMENA AND INTERFACIAL KINETICS IN MULTIPHASE COMBUSTION SYSTEMS (U)

5. FUNDING NUMBERS

PE - 61102F
PR - 2308
SA - BS
G - AFOSR 89-0223

6. AUTHOR(S)

Daniel E. Rosner

7. PERFORMING ORGANIZATION NAME(S) AND ADDRESS(ES)

HIGH TEMPERATURE CHEMICAL REACTION ENGINEERING LABORATORY
YALE UNIVERSITY
BOX 2159, YALE STATION
NEW HAVEN, CONNECTICUT 06520 U.S.A.

8. PERFORMING ORGANIZATION REPORT NUMBER

9. SPONSORING/MONITORING AGENCY NAME(S) AND ADDRESS(ES)

AFOSR/NA
Building 410
Bolling AFB DC 20332-6448

10. SPONSORING/MONITORING AGENCY REPORT NUMBER

11. SUPPLEMENTARY NOTES

12a. DISTRIBUTION/AVAILABILITY STATEMENT

Approved for public release; distribution is unlimited

12b. DISTRIBUTION CODE

13. ABSTRACT (Maximum 200 words)

This *final report* summarizes Yale High Temperature Chemical Reaction Engineering Laboratory research activities (under Grant AFOSR 89-0223) for the two-year period ending 31 Dec.1990. Our techniques and results are outlined in the following specific sections/areas:

2.1. TRANSPORT PROPERTIES OF AGGREGATED SUBMICRON PARTICLES: EXPERIMENTS AND THEORY
2.2. MULTIPHASE TRANSPORT THEORY
2.2.1 TRANSPORT BEHAVIOR OF NONSPHERICAL AGGREGATED PARTICLES
2.2.2 INERTIAL EFFECTS ON THE TRANSPORT OF SUBMICRON PARTICLES ACROSS NON-ISOTHERMAL BOUNDARY LAYERS
2.2.3 THERMOPHORETIC EFFECTS ON THE COAGULATION DYNAMICS OF COMBUSTION-GENERATED PARTICLES
2.2.4 'MOMENT' METHODS FOR TRANSPORT PROBLEMS INVOLVING PARTICLE POPULATIONS
2.2.5 KINETICS AND MORPHOLOGY OF CVD-MATERIALS
2.2.6 VAPOR PHASE 'IGNITION' IN CVD-BOUNDARY LAYERS

20 presentations and 11 archive journal publications have resulted from this research program. Copies of all publications are included in the Appendices (Section 6) of this report.

14. SUBJECT TERMS

soot transport, multiphase flow, boundary layer theory, thermophoresis, aggregates, non-spherical particles, boron

15. NUMBER OF PAGES

151

16. PRICE CODE

17. SECURITY CLASSIFICATION OF REPORT	18. SECURITY CLASSIFICATION OF THIS PAGE	19. SECURITY CLASSIFICATION OF ABSTRACT	20. LIMITATION OF ABSTRACT
Unclassified	Unclassified	Unclassified	UL

TRANSPORT PHENOMENA AND INTERFACIAL KINETICS IN MULTIPHASE COMBUSTION SYSTEMS

1. INTRODUCTION

The performance of ramjets burning slurry fuels (leading to condensed oxide aerosols and liquid film deposits), gas turbine engines in dusty atmospheres, or when using fuels from non-traditional sources (*e.g.*, shale-, or coal-derived), depends upon the formation and transport of small particles across non-isothermal combustion gas boundary layers (BLs). Even airbreathing engines burning "clean" hydrocarbon fuels can experience *soot* formation/deposition problems (*e.g.*, combustor liner burnout, accelerated turbine blade erosion and "hot" corrosion). Moreover, particle formation and transport are important in many chemical reactors used to synthesize or process aerospace materials (turbine blade coatings, optical waveguides, ...). Accordingly, our research is directed toward providing chemical propulsion systems engineers and materials-oriented engineers with new techniques and quantitative information on important particle- and vapor-mass transport mechanisms and rates.

The purpose of this report is to summarize our research methods and accomplishments under AFOSR Grant 89-0223 (Technical Monitor: J.M.Tishkoff) during the 2-year period: 1 January 1989-31 December 1990. Readers interested in greater detail than contained in Section 2 are advised to consult the published papers cited in Sections 2 and 5. Copies of any of these published papers (Sections 5.1,5.2) or preprints (Section 5.3) can be obtained by writing to the PI: Prof. Daniel E. Rosner, at the Department of Chemical Engineering, Yale University, Box 2159 Yale Station, New Haven CT 06520-2159 USA. Comments on, or examples of, applications of our research (Section 3.4) will be especially welcome.

An interactive experimental/theoretical approach has been used to gain understanding of performance-limiting chemical-, and mass/energy transfer-phenomena at or near interfaces. This included the further development and exploitation of seeded laboratory flat flame burners (Section 2.1), flow-reactors (Sections 2.2.5 and 2.3), and new optical diagnostic techniques (Section 2.3). Resulting experimental rate data, together with the predictions of asymptotic theories (Section 2), were used as the basis for proposing and verifying simple viewpoints and rational engineering correlations for future design/optimization studies.

2. RESEARCH ACCOMPLISHMENTS AND PUBLICATIONS

Most of the results we have obtained under Grant AFOSR 89-0223 can be divided into the subsections below:

2.1. TRANSPORT PROPERTIES OF AGGREGATED SUBMICRON PARTICLES: EXPERIMENTS AND THEORY

The ability to reliably predict the *thermophoretic* properties of isolated and aggregated flame-generated particles (carbonaceous soot, Al_2O_3, ...) is important to many technologies, including chemical propulsion and refractory materials fabrication. In 1989 we reported preliminary measurements of the *thermophoretic diffusivity* ($\alpha_T D$) of flame-generated submicron TiO_2(s) "soot" particles using a $TiCl_4$(g)-seeded low strain-rate counterflow laminar diffusion flame technique (Gomez and Rosner, 1990, 1991). Inferred ($\alpha_T D$)-values based on *observed* particle-free-zone thicknesses, LDV measurements of $v_z(z)$ (*via* $v_r(z)$) and measured (thermocouple) temperature gradients were well within 7% of values expected using Waldmann's kinetic theory approach *for an isolated dense spherical particle*. Similar conclusions were reached in earlier, rather different experiments on flame-generated submicron "soots", both organic (*eg.*, Eisner and Rosner, 1985) and inorganic (Rosner and Kim, 1984) even though the soot "particles" in these systems are heavily aggregated. Our most recent theoretical studies provide an interesting

explanation and confirmation for this remarkable and quite useful *insensitivity of (orientation-averaged) $\alpha_T D$ to aggregate particle size and morphology*; *viz.* addition of a primary particle to an aggregate containing N such spherical particles increases the thermal force and drag by nearly the same amount, and this is true in both Knudsen number limits. Our results in the near-continuum limit ($Kn_p<<1$) are shown in Fig 2.1-1 (Rosner *et. al.*, 1991) and even smaller departures from unity are found in the free-molecule limit ($Kn_p>>1$). In marked contrast, it should be emphasized that the Brownian diffusion-, inertial-, and *optical*-properties of such aggregates are quite *sensitive* to size (N) and morphology. There are many interesting consequences of these differences both for predicting particle *deposition* rates and for *sampling* combustion-generated aerosols (Rosner *et.al.*, 1991).

2.2. MULTIPHASE TRANSPORT THEORY

2.2.1 TRANSPORT BEHAVIOR OF NONSPHERICAL AGGREGATED PARTICLES

Because of the need to accurately predict the Soret 'diffusion' of large, highly *nonspherical* molecules (*e.g.*, polycyclic aromatic soot precursors and large metal-organic vapors used to deposit thin films with useful optical properties) and the thermophoretic transport of *nonspherical* submicron particles (*e.g.*, long soot aggregates) we have continued our research on predicting the *shape*- and orientation-dependence of their thermal diffusion velocities (Garcia-Ybarra & Rosner, 1989), and *photophoretic* velocities (Rosner, *et.al.*, 1989, Mackowski, 1990), including the implications of these effects for agglomeration rates (Park and Rosner, 1989a) and combustion deposits formed from agglomerated particles. Our recent theoretical studies of the transport properties of asymmetric two-sphere aggregates (see Fig.2.2-1 and Mackowski, 1990) reveal a strong tendency for them to *align* themselves with respect to the local value of **grad** T_g, despite the inevitable randomizing effects of Brownian rotation in a bath gas of local temperature T_g. Moreover, unsymmetrical binary aggregates (*eg*. aggregates comprised of two diferent size spheres, or spheres of different thermophysical or optical properties) are expected to exhibit "anomalous" Brownian motion, which will probably render "dynamic light scattering" (DLS) techniques unreliable for such particles. Because particle size and shape also affect Brownian diffusivities, we initiated the development of useful engineering methods for predicting total mass deposition rates from 'coagulation-aged' *distributions* of suspended particles — including 'fractal' agglomerates and linear chains of uniform sized "primary" spherical particles (see, *e.g.*, Rosner, 1989; and Rosner and Tassopoulos, 1989, and Rosner, 1990)).

2.2.2 INERTIAL EFFECTS ON THE TRANSPORT OF SUBMICRON PARTICLES ACROSS NON-ISOTHERMAL BOUNDARY LAYERS

Another important example of the competition between *submicron particle inertia* and particle *thermophoresis* (Park and Rosner, 1989b) has been clarified for the case of particle-laden laminar boundary layers on surfaces with streamwise curvature, as in the case of combustion turbine blades) (Konstandopoulos and Rosner, 1991). Even for particles small enough to be characterized by small (subcritical) Stokes numbers ($Stk<<1$), large inertial effects on convective-phoretic mass transfer rates are found when $Stk(Re)^{1/2}=O(1)$.

In principle, thermophoresis "alone" can also be used to "clean" a dusty gas well below the "inertial threshold", especially if heat addition to the gas is a simultaneous goal. For this reason we calculated (Park and Rosner, 1990) the (dimensionless, stretched) thickness of the "dust-free" layer adjacent to a hot wall toward which a heavily loaded submicron dusty gas is directed. This is the same phenomenon we exploit in our counterflow flame measurements of $(\alpha_T D)_p$ (Section 2.1) except these calculations were for hot *solid* walls and included high (non-negligible) particle mass loadings.

2.2.3 THERMOPHORETIC EFFECTS ON THE COAGULATION DYNAMICS OF COMBUSTION-GENERATED PARTICLES

Our recent studies of submicron particle migration in host-gas temperature gradients and radiation fields (see, *eg.*, Rosner, *et. al.*, 1991, Castillo *et. al.*, 1990), Mackowski, D.W., 1990) suggest that even spherical particles thermally out of equilibrium with their local host gas can *coagulate* with particle-particle encounter rate constants quite different from the usual "isothermal" Brownian values. This leads to *unusual population dynamics*, including the possibility that initially broad coagulating "overheated" particle populations can become *narrower* than ordinary "self-preserving" populations. This is illustrated in Fig. 2.2-3 (Rosner *et al.*, 1991), which shows the predicted dependence of the (log-normal) *spread* parameter, σ_g, and geometric *mean size*, d_g, on dimensionless elapsed time for radiatively heated carbonaceous particles in the near-continuum limit. We have also investigated the frequently occurring converse case: *ie.* the strong tendency of radiatively *cooled* large particles to grow still larger by rapidly "scavenging" smaller ones. Because of the formal analogy between our thermophoretically-augmented Brownian coagulation rate constant and earlier expressions derived for the coagulation of electrostatically *charged* particles, we anticipate that similar effects would be observed in "unipolar" soot aerosol systems.

2.2.3 ROLE OF SOOT PARTICLE PHOTOPHORESIS IN COMBUSTORS WITH HIGH RADIATIVE HEAT FLUXES

Small suspended particles can drift (exhibit 'phoresis') as a result of nonuniform photon-induced particle heating in a 'host' gas. Our earlier analysis (Mackowski,1989) of the *photophoretic velocity* of aerosol particles (which includes both the 'free-molecular' and the more important 'slip-flow' regimes) showed that *photophoresis* can be a significant transport mechanism for micron-sized *absorbing* particles in high radiative transfer combustion environments (see, *e.g.*, Fig 2.6-1 of Castillo, Mackowski and Rosner,1990). To demonstrate this we have predicted dimensionless transport coefficients (proportional to the ordinary Stanton number for mass transport) as a function of radiative/convective energy flux ratio and carbonaceous particle size for laminar boundary layer flow past a cooled solid surface. Large effects on the deposition rate of intermediate size absorbing particles (*eg.*, between 1 and 10 micrometers) were found if the radiative flux is comparable to or exceeds the ordinary (Fourier) energy flux. For details the reader should consult Castillo, Mackowski and Rosner, 1990.

2.2.4 'MOMENT' METHODS FOR TRANSPORT PROBLEMS INVOLVING PARTICLE POPULATIONS

Many flow problems involving coagulating and migrating particle populations can be solved conveniently by deriving/integrating a closed set of differential equations for selected "moments" of the particle size distribution (PSD-)function. This is particularly true when the PSD *shape* is relatively simple (*e.g.*, single mode log-normal) and does not markedly change as a result of the participating phenomena. One such class of problems occurs in the *theory of aerosol sampling---i.e.* correcting PSD instrument data for the systematic size-dependent effects of wall losses and/or coagulation in the *upstream* sampling tube. We have recently shown that the necessary correction factors can be calculated by direct upstream integration of a closed set of 3 moment equations (Rosner and Tassopoulos, 1991). As a representative example, Fig. 2.2-4 shows the correction factor for total particle number density as a function of the scaled length of the sampling system and the spread parameter of the aerosol measured at the instrument (for turbulent gas flow in the absence of appreciable coagulation). These methods can be readily generalized to include diabatic sampling tubes, as encountered in extracting soot samples from jet engine combustors.

2.2.5 KINETICS AND MORPHOLOGY OF CVD-MATERIALS

A small impinging jet (stagnation flow) reactor has been designed and built for studying the CVD-rates of refractory films on inductively heated substrates (see, also, Section 2.2.6 below). To help understand the topography of CVD film surfaces in the limit when thermally driven mass

transfer *dominates* concentration diffusion we recently completed a linear stability theory (Castillo, *et.al.*,1991; jointly supported by NASA-Lewis RC)).

2.2.6 VAPOR PHASE 'IGNITION' IN CVD BOUNDARY LAYERS

Optimizing the growth rate and properties of CVD films growing on heated surfaces will often require reactor design/flow conditions such that the onset of external diffusion limitations approximately coincides with the onset of homogeneous reactions within the vapor BL (Rosner *et.al.*, 1990, 1991). For this purpose, a simple asymptotic CVD theory is being developed which exploits the high activation energy of the *homogeneous* reactions.

2.3 GASIFICATION KINETICS OF SOLID BORON AND PYROLITIC GRAPHITE

Because of the energetic potential of boron as a solid fuel (or fuel additive) and the likely role of *surface* reactions involving the gaseous oxidant $B_2O_3(g)$ in the processes of fine boron-particle ignition, combustion and extinction, we previously completed and have now submitted for publication flow reactor measurements of the intrinsic kinetics of the gasification of B(s) at surface temperatures between about 1300K and 2100K (Zvuloni *et. al.*, 1989, Zvuloni, 1990). While the chemical propulsion implications of these measurements are emphasized in our AIAA publication (Zvuloni *et. al.*, 1991), the experimental techniques and the mechanistic implications of our results are emphasized in full-length manuscripts now being prepared for *J. Phys. Chem.* (Zvuloni, Rosner and Gomez, 1991) and for a forthcoming symposium on the combustion of boron-based solid fuels (Gomez *et. al.*, 1991). As mentioned in our previous Final Report we also completed a preliminary set of measurements of the remarkably efficient gasification of *pyrolytic graphite* by OBOBO(g) (Zvuloni *et. al.*, 1990c). These measurements, which have not yet been supplemented or written up for publication, will have interesting implications for boron-containing systems in which are present suspended organic soot particles and/or pyrolytic graphite containment walls.

3. ADMINISTRATIVE INFORMATION: PERSONNEL, PRESENTATIONS, APPLICATIONS, "COUPLING" ACTIVITIES

The following sections summarize some pertinent 'non-technical' facets of the abovementioned Yale HTCRE Lab/AFOSR research program:

3.1 Personnel

The present results (Sections 2 and 5) are due to the contributions of the personnel listed in Table 3.1-1. It will be noted that, in addition to the results themselves, this program has simultaneously contributed to the research training of a number of students and recent PhDs, who will now be in an excellent position to make future contributions to critical technologies oriented toward high-performance air-breathing chemical propulsion, and/or high-tech materials processing.

Table 3.1-1 Summary of *Research Participants* on AFOSR Grant :89-0223
TRANSPORT PHENOMENA AND INTERFACIAL KINETICS IN MULTIPHASE COMBUSTION SYSTEMS

Name	Status[a]	Date(s)	Principal Research Activity[b]
Castillo,J.	PDRA-VS	'89,'90	theory of vapor condens. in BLs
Collins,J.	GRA	'89,'90	CVD of ceramic coatings
Garcia-Ybarra,P.	PDRA-VS	'89,'90	kinetic theory of thermophoresis
Gomez, A.	PDRA-I	'89,'90	meas. of particle transp. props.
Konstandopoulos,A.G†	GRA	'89,'90	thermophoresis/inertia coupling
Labowsky,M.	VS	'89,'90	method of images calculations
Mackowski,D.W.	PDRA	'89,'90	aggregates, photophoresis
Rosner, D.E.	PI	'89,'90	program direction-Xport theory/exp
Tassopoulos,M.†	GRA	89,'90	aggregate particle deposition

a PDRA=Post-doctoral Research Asst GRA= Graduate Research Assistant
I = Instructor PI = Principal Investigator VS = Visiting Scholar
b See Section 5 for specific references cited in text (Section 2)
† PhD work expected to be complete by mid '91

3.2 Cooperation with USA-Industry

The research summarized here was supported by AFOSR under Grant 89-0223 (completed 31 December 1990). During this two year period the Yale HTCRE Laboratory has also been the beneficiary of smaller grants from U.S. corporations, including GE, Textron-Lycoming, DuPont, SCM-Chemicals, Babcox and Wilcox, Shell and Union Carbide, as well as the feedback and advice of scientists/engineers from each of these corporations and Combustion Engineering (now ABB). We appreciate this level of collaboration, and expect that it will accelerate inevitable applications of our results in areas relevant to their technological objectives (see, also, Section 3.4, below).

3.3 Presentations and Research Training

Apart from the publications itemized in Section 5 and our verbal presentations (of progress) at regular AFOSR Contractors Meetings (including the Boron Workshop), our results have also been presented at annual conferences of the following professional organizations:

AAAR	Combustion Inst.
AIChE	Fine Particle Society
ASME	Electrochemical Soc.
MRS	IHTC-9(Intersociety)

In addition, during the period: 1/1/89 -12/31/90, seminars have been presented at the following Universities:

Princeton UNED-Madrid Technion (Haifa)

In all, a total of 20 talks were given by Yale-HTCRE people based in part on the results of this 2-year research program.

This program involved the PhD dissertation research of two graduate students (A.G.Konstandopoulos and M. Tassopoulos; cf. Table 3.1-1) expected to complete their degree requirements in 1991, and one (J. Collins) expected to complete his work (jointly sponsored by NASA-Lewis RC) in 1992.

3.4 Known Applications of Yale-HTCRE Lab Research Results

It has been particularly gratifying to see direct applications of some of this AFOSR-supported particle and vapor mass transfer research and high temperature interfacial kinetcs research in more applications-oriented investigations reported in recent years. Indeed, the writer would appreciate it if further examples known to the reader can be brought to our attention.

The PI's transport *textbook/treatise* (Rosner,1986,1988,1990) entered its *third* reprinting in 1990, indicating sustained worldwide interdisciplinary interest. As noted in the preface, much of the presentation of combustion-related topics is the result of the author's OSR sponsored research on these (or closely related) subjects.

Our earlier AFOSR- and NASA- sponsored studies of O- and N-atom recombination on thermal protection system surfaces and *incomplete energy accommodation* (for a review, see, eg., Halpern and Rosner(1982)) have apparently been playing a significant role in recent EEC (Hermes vehicle), Russian (Buran), and Japanese R&D on glide re-entry vehicles (Dr. C.D Scott of NASA-Johnson Space Center,Houston TX 77058 is familiar with these recent applications as well as relevant follow-on studies at NASA). Likewise, our earlier studies of the chemical attack of SiC by O- and/or N-atoms are evidently being used to help interpret recent arcjet materials response measurements at NASA-Johnson Space Center (D.M.Curry). Our results on the chemical attack of boron by OBOBO(g)(see Zvuloni *et. al.* (1991) have been recently incorporated in mathematical models of boron particle ignition/combustion/extinction (Aerodyne Corp., Princeton Univ., UCSD).

Our new results on the thermophoretic properties of aggregated soot particles (Section 2.2.1) strengthens considerably the basis of "thermophoretic sampling", already widely used in the combustion research community (based on our earlier studies (Eisner and Rosner(1985), and Dobbins and Megaridis(1987)) as a supplement to 'optical' methods (including dynamic light scattering), whose interpretation is complicated by aggregation effects.

Further explicit examples are provided in work at MIT, and Sandia CRF, both groups having incorporated our rational correlation of *inertial particle impaction* (*e.g.* a cylinder in cross-flow) in terms of an *effective Stokes numbe.* (Israel and Rosner, 1983, Rosner, 1986). This concept has also proven useful to correlate inertial impaction in external *supersonic* flows and internal flow fixed bed filters.

We were also pleased to recently learn (letter dated 1 August 1989) about applications of our earlier AFOSR and DOE-supported research (on the correlation of inertial impaction by cylinders in crossflow) by the National Engineering Laboratory (NEL) of Glasgow, Scotland (Contact: Dr. Andrew Jenkins). NEL is apparently developing mass-transfer prediction methods applicable to waste-heat recovery systems, as well as pulverized coal-fired boilers.

In the area of alkali sulfate vapor deposition in combustion turbine systems additional applications of our predictive methods (for "chemically frozen" and LTCE multicomponent laminar boundary layers) are being made by British Coal Corporation-Power Generation Branch, Cheltenham, England (Dr. J. Duxbury, I.Fantom contacts) in connection with their topping cycles which will run gas turbines on the products of fluidized bed coal combustors/gasifiers.

Our recent work on Soret-transport effects in CVD systems (see, eg., Rosner(1980) and our follow-on studies on the prediction of transport-shifted CVD "phase diagrams") promise to be of use to AF contractors producing fibers for high performance composite materials.

Clearly, other fruitful *opportunities* for applications of our recent mass transfer/interfacial kinetics research now exist in many R&D programs currently supported by the US Air Force.

4.CONCLUSIONS

In the OSR-sponsored Yale HTCRE Lab research during 1989 and 1990, briefly described above, we have shown that new methods for rapidly measuring vapor- and particle-mass transfer rates , combined with our recent advances in mass transport theory, provide useful means to identify and incorporate important, but previously neglected, mass transport phenomena in many propulsion engineering and materials engineering design/optimization calculations.

Despite formidable complexities to be overcome in the design and operation of power plants utilizing a broad spectrum energetic fuels the abovementioned techniques and results (Section 2) are indicative of the potentially useful simplifications and generalizations which have emerged from our present fundamental AFOSR-funded research studies of combustion-generated particle transport mechanisms and interfacial reactions. It is hoped that this report and its supporting (cited) papers will facilitate the refinement and/or incorporation of some of the present ideas into design and test procedures of greater generality and reliability. This work has also helped identify new directions where research results would have a significant impact on future engineering practice.

5. REFERENCES

5.1 CITED BACKGROUND PUBLICATIONS (*Predecessor* OSR Grants)

Eisner, A.D. and Rosner, D.E., "Experimental Studies of Soot Particle Thermophoresis in Non-Isothermal Combustion Gases Using Thermocouple Response Techniques", *Combustion and Flame* **61**, 153-166 (1985); see, also: *J PhysicoChemical Hydrodynamics*, **7**, 91-100 (1986)

Halpern, B. and Rosner, D.E.,"Incomplete Energy Accommodation in Surface-Catalyzed Reactions", in **Heterogeneous Atmospheric Chemistry**, *Geophysical Monograph Series* **26**,167-172 (1982)

Israel, R. and Rosner, D.E., "Use of a Generalized Stokes Number to Determine the Aerodynamic Capture Efficiency of Non-Stokesian Particles from a Compressible Gas Flow", *Aerosol Sci.Tech.***2**,45-51 (1983)

Mackowski, D.W.,"Photophoresis of Aerosol Particles in the Free-molecular and 'Slip-Flow' Regimes", *Int. J. Heat Mass Transfer* (Pergamon) **32**,(5),843-854 (1989)

Rosner, D.E., **Transport Processes in Chemically Reacting Flow Systems**, Butterworth-Heinemann (Stoneham MA) 1986; Third Printing 1990)

Rosner, D.E.,"Thermal (Soret) Diffusion Effects on Interfacial Mass Transport Rates", *Physiocochemical Hydrodynamics* **1**,159-185 (1980)

Rosner, D.E. and Kim, S.S., "Optical Experiments on Thermophoretically Augmented Submicron Particle Deposition From 'Dusty' High Temperature Gas Flows", *The Chemical Engrg. J.* (Elsevier) **29**, [3],147-157 (1984)

5.2 PUBLICATIONS WHICH APPEARED (Based on this AFOSR Program)

Castillo, J. and Rosner,D.E.,"Theory of Surface Deposition from a Unary Dilute Vapor-Containing Stream Allowing for Condensation Within the Laminar Boundary Layer", *Chem.Eng. Sci.* **44** 925-937,(1989); see, also: *ibid.* **44** (4) 939-956(1989).

Castillo, J.L., Mackowski, D.W., and Rosner, D.E., "Photophoretic Contribution to the Transport of Absorbing Particles Across Combustion Gas Boundary Layers", *Progress in Energy and Combustion Science* **16**, 253-260, (1990)

Garcia-Ybarra, P., and Rosner, D.E., "Thermophoretic Properties of Small Nonspherical Particles and Large Nonspherical Molecules," *AIChE J.*, **35** [1], 139-147 (1989)

Mackowski, D.W., "Phoretic Behavior of Asymmetric Particles in Thermal Non-equilibrium with the Gas: Two-Sphere Aggregates", *J. Colloid and Interface Science* **140**, (1), 138-1576 (1990)

Park, H.M., and Rosner, D.E., "Effect of Coagulation in the Boundary Layer on the Size Distribution of Thermophoretically Deposited Particles", *Chem. Engrg. Sci.* **44** (10) 2225-2231, (1989a)

Park, H.M., and Rosner, D.E., "Combined Inertial and Thermophoretic Effects on Particle Deposition Rates in Highly Loaded Dusty Gas Systems", *loc.cit.* **44** (10), 2233-2244 (1989b)

Rosner, D.E., Mackowski, D.W.,and Garcia-Ybarra, P.,"Size- and Structure-Insensitivity of the Thermophoretic Transport of Aggregated 'Soot' Particles in Gases", *Comb. Sci. Tech.* **80**,(1-3), 87-101,(1991)

Rosner, D.E. and Tassopoulos, M., "Deposition Rates from Streams Containing 'Polydispersed' Particle Populations of Arbitrary Spread", *AIChE J.* **35** (9), 1497-1508 (1989); see, also:"Total Mass Deposition Rates from 'Polydispersed' Aerosols"; *AIChE J.* **35** (1), 164-167 (1989)

Zvuloni, R., **Flow Reactor Studies of the High Temperature Gasification Kinetics of Solid Boron and Carbon and Their Chemical Propulsion Implications**, PhD Dissertation, Dept. Chemical Engineering, Yale University, New Haven CT, May 1990

Zvuloni, R., Gomez, A., and Rosner, D.E., "Direct Measurements of the High Temperature Kinetics of Solid Boron Gasification by its Higher Oxide $B_2O_3(g)$: Chemical Propulsion Implications", *A.I.A.A. -J. Propulsion and Power* **7** (1) 9-13, (1991)

5.3 CITED PAPERS SUBMITTED FOR PUBLICATION OR IN PREPARATION

Castillo, J.L., Garcia-Ybarra, P., and Rosner, D.E., "Morphological Instability of a Thermophoretically Growing Deposit", *J. Crystal Growth* (in press, 1991)

Gomez, A., and Rosner, D.E., "Thermophoretic Effects on Particles in Counterflow Laminar Diffusion Flames " (in preparation, 1991)

Gomez, A., Rosner, D.E. and Zvuloni, R., "Recent Studies of the Kinetics of Solid Boron Gasification by $B_2O_3(g)$ and Their Chemical Propulsion Implications", invited paper for *Proc. 2d Int. Sympos. on Special Topics in Chemical Propulsion*: **Combustion of Boron-Based Solid Propellants and Solid Fuels**, (in press 1991)

Konstandopoulos, A.G. and Rosner, D.E.,"Inertial Effects on Thermophoretic Transport of Small Particles to Walls With Streamwise Curvature---I. Experiment, II. Theory", Prepared for Submission to *Int. J. Heat Mass Transfer* (Pergamon)

Mackowski, D.W., Tassopoulos, M. and Rosner, D.E., "Effect of Radiative Heat Transfer on the Coagulation Rates of Combustion-Generated Particulates", Central States Mtg. - The Combustion Inst., 21-24 April 1991, Nashville, TN.; (to be submitted to *Int. J. Heat Mass Transfer* (Pergamon) (1991))

Park, H.M., and Rosner, D.E., "Thermophoretically Induced Phase Separation in Highly-Loaded 'Dusty' Gas Mixtures", (to be submitted 1991)

Rosner, D.E., Konstandopoulos, A.G., Tassopoulos, M. and Mackowski, D.W, "Deposition Dynamics of Combustion-Generated Particles: Summary of Recent Studies of Particle Transport Mechanisms, Capture Rates, and Resulting Deposit Microstructure/Properties", *Proc. Engineering Foundation Conference*: **Inorganic Transformations and Ash Deposition During Combustion**, (in press 1991)

Rosner, D.E., Mackowski, D.W, Tassopoulos, M., Castillo, J.L. and Garcia-Ybarra, P., "Effects of Heat Transfer on the Dynamics and Transport of Small Particles in Gases", AIChE Annual Mtg. - (S.W.Churchill Birthday Symposium), November 1990, Chicago Il; *I/EC-Research* (in press 1991)

Rosner, D.E., Castillo, J.L., and Tassopoulos, M. "Role of High Activation Energy Homogeneous Reactions in Limiting CVD-Rates and Deposit Quality for Heated Surfaces", Paper 55d, AIChE Annual Mtg., Chicago, IL, November 15, 1990; Prepared for Submission to *J. Electrochem Soc.*, 1991

Rosner, D.E. and Tassopoulos, M.,"Direct Solutions to the Canonical 'Inverse' Problem of Aerosol Sampling Theory: Coagulation and Size-dependent Wall Loss Corrections for Log-Normally Distributed Aerosols in Upstream Sampling Tubes", *J. Aerosol Sci.* (in press 1991)

Zvuloni, R., Rosner, D.E., and Gomez, A., "OBOBO(g) as a Gasifier of Graphite: Measurements and Implications", (in preparation, 1991a)
Zvuloni, R., Rosner, D.E. and Gomez, A., "Role of Water Vapor on the Gasification Kinetics of Solid Boron by its Higher Oxide $B_2O_3(g)$", *AIAA. J. Propuls. Power* (in press 1991)
Zvuloni, R., Rosner, D.E., and Gomez, A., "High Temperature Kinetics of Solid Boron Gasification By its Higher Oxide $B_2O_3(g)$: Flow Reactor Techniques, Rate Measurements and Their Chemical Implications", *J. Phys. Chem.* (to be submitted, 1991)

ABBREVIATIONS

BL	boundary layer
CVD	chemical vapor deposition
DLS	dynamic light scattering
HTCRE	High Temperature Chemical Reaction Engineering (Lab)
Kn_p	Knudsen number (based on particle dimension)
LBL	laminar boundary layer
LDV	laser-Doppler velocimetry
LTCE	local thermochemical equilibrium
MIPES	microwave-induced plasma emission spectroscopy
O( )	order of magnitude ( )
Pr	Prandtl number (of host gas mixture)
TBL	turbulent boundary layer
Re	Reynolds number
Sc	Schmidt number based on particle Brownian diffusivity
Stk	Stokes number based on particle stopping time
R&D	research and development
PI	principal investigator
PSD	particle size distribution
QE	quasi-equilibrium
VCE	vapor/condensate equilibrium

YALE UNIVERSITY

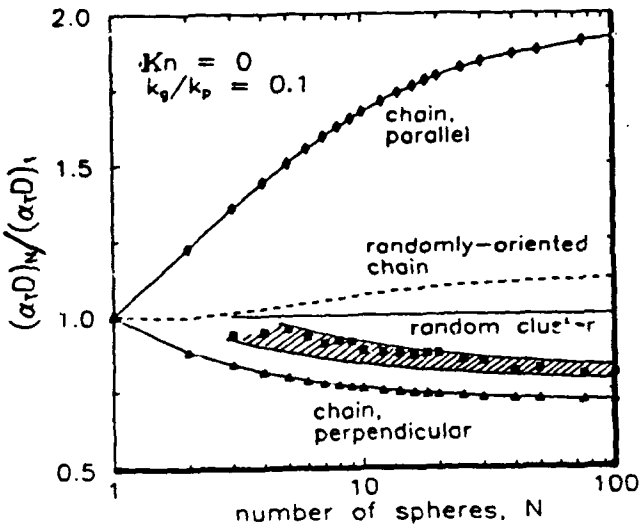

Fig 2.1-1 Predicted normalized thermophoretic diffusivity of aggregates containing N-primary spheres; near-continuum limit, conductivity ratio=0.1 (after Rosner *et.al.* 1991)

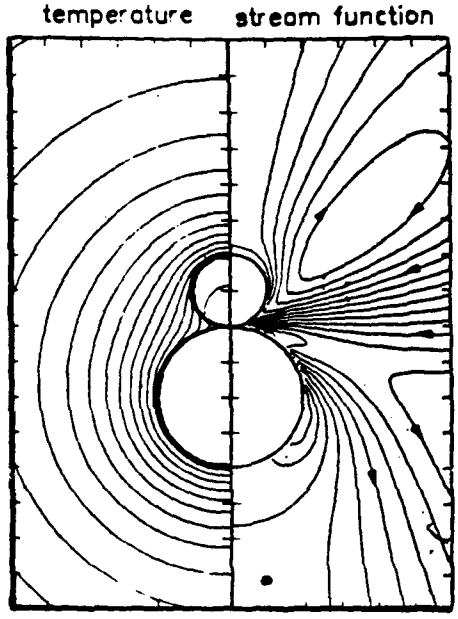

Fig.2.2-1 Predicted isotherms and streamlines in the vicinity of an asymmetric two-sphere aggregate with identical radiative properties but a size ratio of 2 (k_g/k_p=0.1, Kn_p<<1) (after Mackowski,1990)

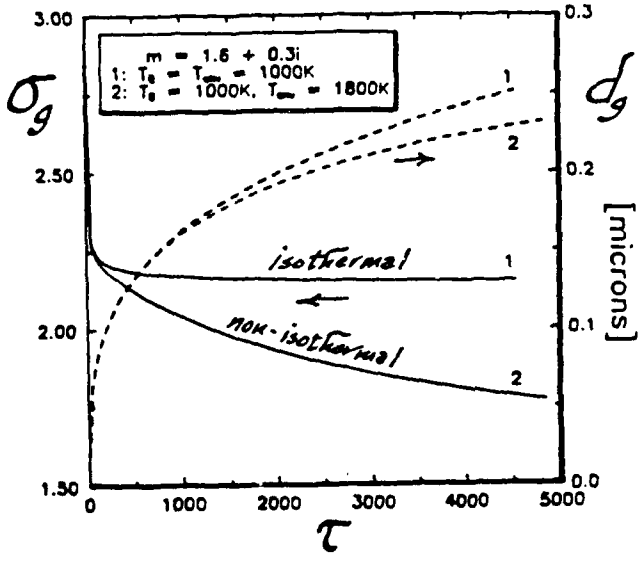

Fig 2.2-3 Predicted evolution of soot PSD parameters for coagulating populations of carbonaceous spherical particles; effects of particle "overheating" in the high pressure limit (after Mackowski *et al.*,1991, Rosner *et.al.* 1990)

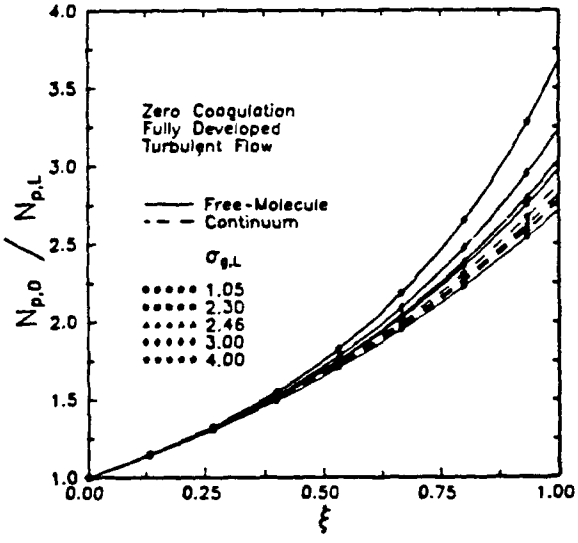

Fig.2.2-4 Effect of size-dependent particle losses to the walls of an upstream sampling tube; correction factors to be applied to measured total particle number densities using a tube of rescaled L/d. (For turbulent gas flow in both particle Knudsen number limits) (after Rosner and Tassopoulos,1991)

REPORT DOCUMENTATION PAGE

Form Approved
OMB No. 0704-0188

1. AGENCY USE ONLY (Leave blank)	2. REPORT DATE	3. REPORT TYPE AND DATES COVERED
	1991	Journal Publication

4. TITLE AND SUBTITLE
"Size- and Structure-Insensitivity of the Thermophoretic Transport of Aggregated "Soot" Particles in Gases"(U)

5. FUNDING NUMBERS
PE - 61102F
PR - 2308
SA - BS
G - AFOSR 89-0223

6. AUTHOR(S)
D. E. ROSNER, D. W. MACKOWSKI and P. GARCIA-YBARRA

7. PERFORMING ORGANIZATION NAME(S) AND ADDRESS(ES)
HIGH TEMPERATURE CHEMICAL REACTION ENGINEERING LABORATORY
YALE UNIVERSITY
BOX 2159, YALE STATION
NEW HAVEN, CONNECTICUT 06520 U.S.A.

8. PERFORMING ORGANIZATION REPORT NUMBER

9. SPONSORING/MONITORING AGENCY NAME(S) AND ADDRESS(ES)
AFOSR/NA
Building 410
Bolling AFB DC 20332-6448

10. SPONSORING/MONITORING AGENCY REPORT NUMBER

11. SUPPLEMENTARY NOTES

12a. DISTRIBUTION/AVAILABILITY STATEMENT
Approved for public release; distribution is unlimited

12b. DISTRIBUTION CODE

13. ABSTRACT (Maximum 200 words)

Abstract—There is now convincing theoretical and experimental evidence, assembled and discussed here, for the remarkable insensitivity of the orientation-averaged *thermophoretic* properties of aggregated particles to aggregate size and structure (morphology), as well as the nature of gas/surface scattering. Indeed, theoretical consideration of straight chains, and uniformly "packed" quasi-spherical agglomerates, as well as recent experimental data on soot aggregate transport in/from laminar flames at atmospheric pressure, indicates that the orientation-averaged thermophoretic diffusivity, $\langle \alpha_T D \rangle_N$, of an aggregate containing N primary particles is usually within about 8% of the $(\alpha_T D)_1$-value for a single "primary" sphere in the free-molecule regime and within about 21% in the continuum limit. Among other things, this implies that, especially in the free-molecule regime, thermophoretically-dominated transport rates can be adequately predicted *without* a detailed knowledge of the size and morphology (-distribution) of the aggregated particles or the nature of gas/particle surface scattering, which is definitely *not* the case for particle transport by Brownian diffusion or inertial drift (see, *e.g.*, Rosner, 1991). This result also implies that thermophoretic particle sampling from "low pressure" flames (Dobbins and Megaridis, 1987) does not itself introduce a significant bias in the relative populations of various sampled aggregate sizes and morphologies.

14. SUBJECT TERMS	15. NUMBER OF PAGES
soot, aggregated particles, thermophoresis,diffusion	15
	16. PRICE CODE

17. SECURITY CLASSIFICATION OF REPORT	18. SECURITY CLASSIFICATION OF THIS PAGE	19. SECURITY CLASSIFICATION OF ABSTRACT	20. LIMITATION OF ABSTRACT
Unclassified	Unclassified	Unclassified	UL

#181

Combust. Sci. and Tech., 1991, Vol 80 (1-3) 87-101 (1991)

Size- and Structure-Insensitivity of the Thermophoretic Transport of Aggregated "Soot" Particles in Gases

D. E. ROSNER, D. W. MACKOWSKI and P. GARCIA-YBARRA *Yale University, Department of Chemical Engineering, High Temperature Chemical Reaction Engineering Laboratory, New Haven, CT 06520-2159, U.S.A.*

(Received November 26, 1990; in final form May 14, 1991)

Abstract—There is now convincing theoretical and experimental evidence, assembled and discussed here, for the remarkable insensitivity of the orientation-averaged *thermophoretic* properties of aggregated particles to aggregate size and structure (morphology), as well as the nature of gas/surface scattering. Indeed, theoretical consideration of straight chains, and uniformly "packed" quasi-spherical agglomerates, as well as recent experimental data on soot aggregate transport in/from laminar flames at atmospheric pressure, indicates that the orientation-averaged thermophoretic diffusivity, $\langle \alpha_T D \rangle_N$, of an aggregate containing N primary particles is usually within about 8% of the $(\alpha_T D)_1$-value for a single "primary" sphere in the free-molecule regime and within about 21% in the continuum limit. Among other things, this implies that, especially in the free-molecule regime, thermophoretically-dominated transport rates can be adequately predicted *without* a detailed knowledge of the size and morphology (-distribution) of the aggregated particles or the nature of gas/particle surface scattering, which is definitely *not* the case for particle transport by Brownian diffusion or inertial drift (see, *e.g.*, Rosner, 1991). This result also implies that thermophoretic particle sampling from "low pressure" flames (Dobbins and Megaridis, 1987) does not itself introduce a significant bias in the relative populations of various sampled aggregate sizes and morphologies. As a corollary, local gas temperature and soot volume fraction estimates based on mass transfer rates- or thermocouple response-methods (Eisner and Rosner, 1985, 1986) will be negligibly influenced by the inevitably uncertain sizes and morphologies of the prevailing soot agglomerates. Since the optical properties (*e.g.*, effective cross-sections for light-scattering and extinction) of soot aggregates are now known to be size- and structure-*sensitive* (Mackowski, 1987, 1988, Dobbins, Santoro, and Semerjian, 1990. Dobbins and Megaridis, 1991)) we anticipate that the drag *vs.* thermal force "compensation" effects that produce $\langle \alpha_T D \rangle$-values *insensitive* to aggregate *size* (N), *and structure, and the nature of gas molecule/surface scattering* will find important R & D applications for many systems in which agglomeration occurs. It is also concluded that thermophoretic means would *not* be useful to rapidly separate various asymmetric particle morphologies unless orientation-averaging is suppressed, perhaps using external fields (**E**, **B**).

Key words: Soot, aggregated particles, mass transport, thermophoresis, agglomerates; Brownian diffusion.

1 INTRODUCTION

In many technologies, including those involving organic- and inorganic "soot" production in combustors, fine suspended particles are formed by chemical reactions and/or the physical nucleation of vapors, yet coalescence rates are unable to compete with the inevitable coagulation rates, leading to highly "aggregated" particles (see, *e.g.*, Ulrich *et al.*, 1977, 1982, Megaridis and Dobbins, 1990). These aggregates are comprised of much smaller "primary" particles, frequently themselves highly spherical and remarkably "monodispersed" (narrow-spread in primary particle diameters). The simultaneous presence of many aggregate sizes and morphologies evidently complicates the task of predicting the evolution and transport of such "particles", including their deposition or capture. It also complicates the research task of measuring their numbers and characteristics, especially *in situ* using optical techniques (see, *e.g.*, Dobbins, Santoro, and Semerjian, 1990). The purpose of this paper is to point out that whereas the Brownian diffusion-, inertial-and/or optical properties of such aggregates are indeed quite sensitive to aggregate size and morphology, the *thermophoretic properties* of such particles (*i.e.*, their migration behavior in reponse to an

imposed temperature gradient in the gas phase) are remarkably *insensitive* to aggregate size and morphology, with rather important research and technological implications briefly discussed below.

The situation will be seen to be particularly striking in the free-molecule limit where, for example, it is known that an aggregate containing 100 primary particles would necessarily have an orientation-averaged Brownian diffusion coefficient $\langle D_N \rangle$ less than 4.6% ($=(100)^{-2/3}$) that of the primary sphere, and $\langle D_N \rangle$ could itself easily differ by nearly an order of magnitude depending upon the aggregate morphology (*e.g.*, linear?, quasi-spherical, fractal-like?, . . .) (see, *e.g.*, Rosner, 1990, Rosner *et al.*, 1991). In contrast, we show below that the orientation-averaged thermophoretic diffusivity $\langle \alpha_T D \rangle_N$ defined by the drift velocity expression:

$$\mathbf{V}_T = \langle \alpha_T D \rangle_N (-\mathbf{grad}\ T_g)/T_g, \tag{1}$$

is within about 8% of the value for an isolated "primary" sphere in the same gaseous environment for all aggregate sizes (designated *via* the integer index N for the number of primary particles in the linear aggregate). The underlying reason for this will be seen to reside in the similar way in which both the net *thermal force* and the aggregate *drag* depend upon aggregate size and morphology. This approximate "cancellation" of size- and morphology-effects also occurs in the near-continuum (high-pressure-) limit, but to a somewhat smaller extent. In the discussion below we consider both Knudsen number limits ($Kn \ll 1$ and $Kn \gg 1$), bearing in mind that future research will be necessary to better characterize the transport behavior of such aggregates in the more difficult "transition" regime (intermediate Knudsen numbers).

2 EVIDENCE FOR THE SIZE- AND STRUCTURE-INSENSITIVITY OF $\langle \alpha_T D \rangle_N$

While admittedly incomplete, there is already convincing evidence, both theoretical and experimental, for the insensitivity of $\langle \alpha_T D \rangle_N$ to both aggregate size, N, and morphology, especially in the free-molecule limit and (to a somewhat smaller extent) in the near-continuum limit. The evidence is briefly reviewed in each of the subsections below. For additional details the reader is directed to the specific references cited (Section 5).

2.1 *Chain-like (Elongated) Particles in the Free-Molecule Limit*

In free molecule flow the insensitivity of particle thermophoretic transport to particle structure can be considered separately under two different viewpoints: *size* and *shape* effects. First, because thermal as well as resistance forces are both proportional to the particle cross-section, this factor cancels and the induced thermophoretic velocity does not depend on particle *size* (*i.e.*, mean cross-section). Second, although non-spherical particles exhibit differential cross-sections depending on each particular orientation, these shape effects almost cancel out when averaged over all possible orientations attained by the non-spherical particles due to Brownian rotation. As a consequence, the orientation-averaged thermophoretic velocity is only weakly dependent on particle morphology due to these shape effects. Detailed calculations have been carried out recently for sphero-cylindrical particles by García-Ybarra and Rosner (1989). Their results concerning the particle aspect-ratio dependence are summarized and discussed briefly in the following.

Focusing attention only in the resistance and thermal forces acting on a sphero-cylindrical particle (*i.e.*, a cylinder of length L and radius R with hemispherical caps on both ends) moving with velocity $\mathbf{V}$ relative to a carrier gas subjected to a temperature gradient **grad** T_g, the total force on the particle can be written:

$$\mathbf{F} = -N_g \pi R^2 \sqrt{2\pi m k_B T_g} \cdot (\mathscr{R} \cdot \mathbf{V} + \tfrac{3}{4} v \mathscr{T} \cdot \mathbf{grad} \ln T_g), \tag{2}$$

where N_g, m and v are the local molecular number density, the molecular mass and the kinematic viscosity of the carrier gas, respectively, k_B is the Boltzmann constant and T_g the common absolute temperature. The dimensionless thermal force matrix $\mathscr{T}$ and the resistance matrix $\mathscr{R}$, when referred to the principal symmetry axis of the sphero-cylinder, are found to be

$$\mathscr{T}_{11} = \mathscr{T}_{22} = \tfrac{8}{3} + \frac{2L}{R}\left(1 - \frac{a}{4}\right), \tag{3}$$

$$\mathscr{T}_{33} = \tfrac{8}{3} + \frac{L}{R} a, \tag{4}$$

$$\mathscr{R}_{11} = \mathscr{R}_{22} = \mathscr{T}_{11} + a\frac{\pi}{3}\left(1 + \frac{3L}{4R}\right), \tag{5}$$

$$\mathscr{R}_{33} = \mathscr{T}_{33} + a\frac{\pi}{3}, \tag{6}$$

$$\mathscr{R}_{ij} = \mathscr{T}_{ij} = 0, \quad (i \neq j). \tag{7}$$

Here a is the *diffuse reflection fraction* of the impinging molecules. The subscript 3 refers to the coordinate axis along the sphero-cylinder and the subscripts 1, 2 to the other orthogonal axes on the normal plane. The quasi-steady thermophoretic velocity of the particle is obtained by equating the components of $\mathbf{F}$ to zero in Eq. (2). Thus,

$$\mathbf{V}_T = -\tfrac{3}{4} v (\mathscr{R}^{-1} \cdot \mathscr{T}) \cdot \mathbf{grad} \ln T_g, \tag{8}$$

which shows that $\mathbf{V}_T$ does not depend on particle cross-section (particle size) and that, in general, $\mathbf{V}_T$ and **grad** T_g will have different directions. By averaging over all particle orientations (assuming equiprobability in the absence of a net torque) we obtain

$$\langle \mathbf{V}_T \rangle = -(\tfrac{3}{4} v)\, \tfrac{1}{3} \cdot \mathrm{Trace}(\mathscr{R}^{-1} \cdot \mathscr{T})\, \mathbf{grad} \ln T_g \tag{9}$$

Note that the proportionality factor can be identified with the orientation-averaged product $\langle \alpha_T D \rangle$ of the binary thermal diffusion factor α_T and the Brownian diffusion coefficient D, by analogy with the equivalent result of kinetic theory of gases for a quasi-Lorentzian gas of spheres (Mason, 1957; Waldmann and Schmitt, 1966) where

$$[\alpha_T D]_{sph} = \frac{3v}{4(1 + a\pi/8)}, \tag{10}$$

Then, from Eq. (9) we can write

$$\frac{\langle \alpha_T D \rangle}{[\alpha_T D]_{sph}} = \frac{1 + a\pi/8}{3} \cdot \left(\frac{2\mathscr{T}_{11}}{\mathscr{R}_{11}} + \frac{\mathscr{T}_{33}}{\mathscr{R}_{33}}\right). \tag{11}$$

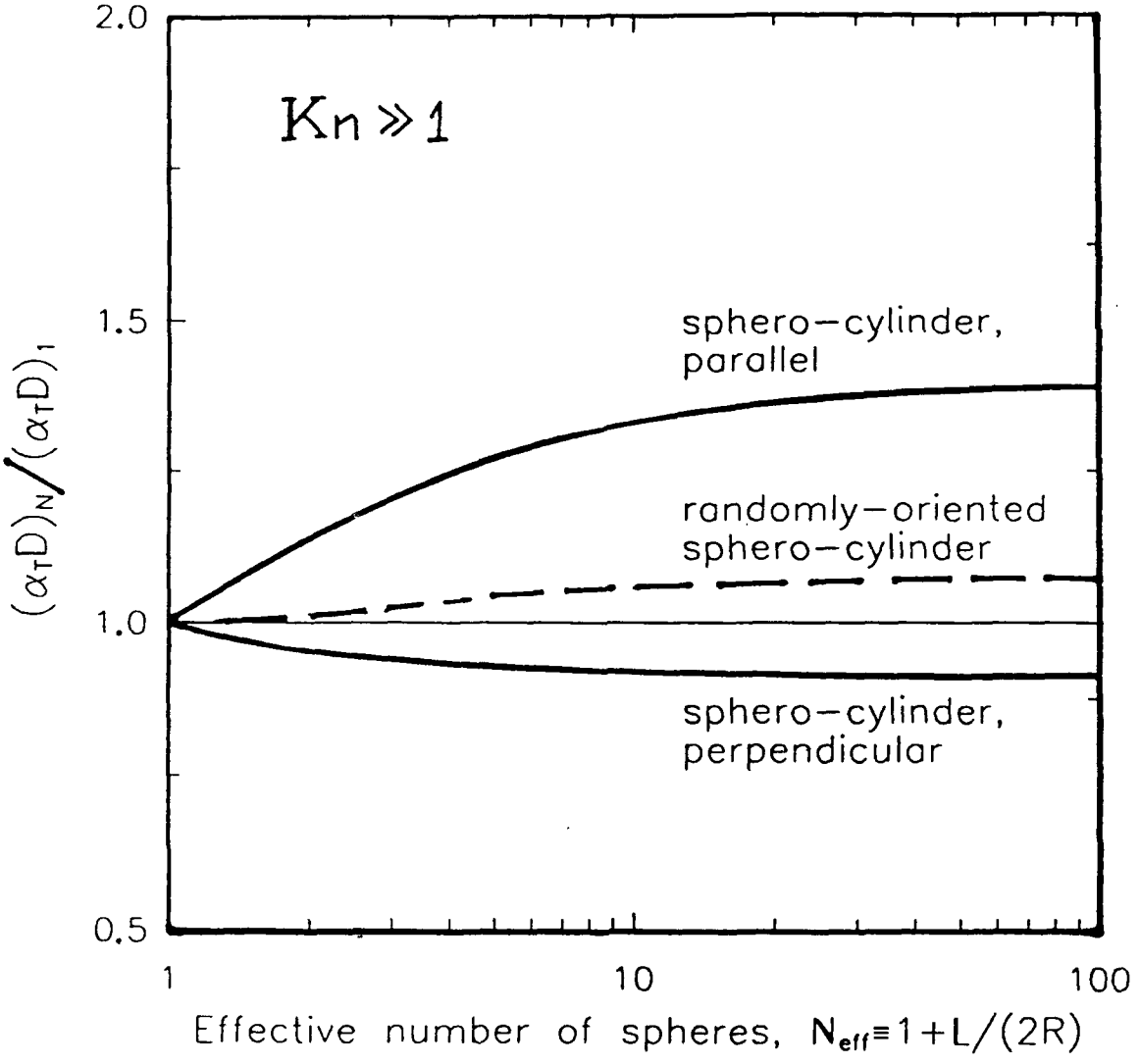

FIGURE 1 Predicted thermophoretic properties of straight chain-like particles in the free-molecule ($Kn \gg 1$) limit, with diffuse reflection ($a \doteq 1$) at the gas/particle interface (after Garcia-Ybarra and Rosner, 1989).

Through the L/R dependence of the diagonal components of $\mathscr{R}$ and $\mathscr{T}$ this relation summarizes the shape (aspect-ratio) effects. Remarkably enough, because of the appearance of $\mathscr{T}_{ii}/\mathscr{R}_{ii}$-ratios, numerical computations show that over the entire range of L/R values, the maximum departures from the spherical value correspond to $a = 1$ and are less than 8%. Figure 1 displays our results for the normalized values of $\langle \alpha_T D \rangle$ as a function of the modified aspect ratio parameter $N_{\text{eff}} = 1 + (L/2R)$. Also shown are the values of this thermophoretical factor for frozen Brownian rotation when **grad** T_g is directed along the sphero-cylinder, $(\alpha_T D)_{par} = (3/4)v\mathscr{T}_{33}/\mathscr{R}_{33}$, and when it is directed perpendicularly, $(\alpha_T D)_{per} = (3/4)v\mathscr{T}_{11}/\mathscr{R}_{11}$.

By way of contrast, for the case of the Brownian diffusion coefficient, we have

$$\langle D \rangle = k_B T \langle b \rangle, \tag{12}$$

where the orientation-averaged mobility $\langle b \rangle$ is obtained exclusively from the inverse resistance matrix $\mathscr{R}^{-1}$ as

$$\langle b \rangle = (N_g \pi R^2 \sqrt{2\pi m k_B T})^{-1} \cdot \tfrac{1}{3} \text{Trace}(\mathscr{R}^{-1}) \tag{13}$$

Equations (12) and (13) show the strong inverse proportional dependence of $\langle D \rangle$ on mean particle cross section for a sphero-cylinder.

Denoting the mobility of a sphere of radius R as:

$$b_{sph} = (N_g \pi R^2 \sqrt{2\pi m k_B T})^{-1} \cdot \frac{3}{8 + a\pi}, \tag{14}$$

then:

$$D_{sph} = k_B T b_{sph}, \tag{15}$$

and the corresponding orientation-averaged Brownian diffusion coefficient, Eq. (12) can be written

$$\frac{\langle D \rangle}{D_{sph}} = \frac{8 + a\pi}{9} \left(\frac{2}{\mathscr{R}_{11}} + \frac{1}{\mathscr{R}_{33}} \right). \tag{16}$$

Introducing the abovementioned values of $\mathscr{R}_{11}$ and $\mathscr{R}_{33}$ we therefore obtain*

$$\frac{\langle D \rangle}{D_{sph}} = \left\{ 1 + \frac{L}{2R} \cdot \frac{1 - \dfrac{6a}{8 + a\pi}\left[1 - \dfrac{3L}{2R} \cdot \left(\dfrac{1}{2} - \dfrac{a}{8 + a\pi}\right)\right]}{1 + \dfrac{L}{2R} \cdot \left(\dfrac{1}{2} + \dfrac{3a}{8 + a\pi}\right)} \right\}^{-1} \tag{17}$$

Numerical estimates from Eq (7) show that in practical situations (with $a = 1$) $\langle D \rangle$ for a sphero-cylinder of length L falls off rapidly as L/R increases (because of the $(\mathscr{R}_{ii})^{-1}$ terms).†

2.2 *Particle Chains and Quasi-Spherical Aggregates in the Near-Continuum Limit*

In the near-continuum flow regime (Kn (based, say, on the inverse of the maximum load surface curvature) $\ll 1$) the thermophoretic motion of a particle of arbitrary shape can, in principle, be obtained through solution of the diffusion (conduction) equation for the fluid and particle temperature, and the creeping flow equations for the fluid velocity (see, *e.g.*, Happel and Brenner, 1965, and Kim and Karrila, 1990). The boundary conditions for these equations must account for the temperature and tangential velocity "jumps" at the surface of the particle, due to the inevitable presence of a Knudsen sublayer, and the thermal "creep" slip flow at the surface arising from a local tangential temperature gradient in the gas (see, *e.g.*, Rosner, 1989a).

For certain particle surfaces conforming to an orthogonal coordinate system, exact solution of the equations is possible. For example, Leong (1984) investigated the

---

*This expression corrects misprints appearing in the corresponding equation of Garcia-Ybarra and Rosner (1989).

†It is interesting to note that this fall off is such that the product of $\langle D \rangle$ and the orientation-averaged cross section, $\pi R^2[1 + (L/2R)]$, remains nearly constant (to within about 25%). However, this approximate dependence on orientation-averaged cross-section fails for small values of a. In fact, for $a = 0$ the cylindrical part would move freely along its axis of revolution and, if, in addition, $L/R \to \infty$, this is the only allowed direction of motion. Yet, the diffusion coefficient does not diverge (nor vanish) but reaches a constant value equal to one third of D_{sph} due to the hemispherical caps at the cylinder ends.

thermophoretic behavior of prolate and oblate spheroids in the continuum ($Kn = 0$) limit and aligned parallel to the temperature gradient. Williams (1987) utilized the bispherical coordinate system to formulate the thermophoretic behavior of a pair of identical spheres. An alternative solution of the two-sphere aggregate problem was obtained by Mackowski (1990), through use of a coupled spherical harmonic technique. The general conclusions of these investigations is that the thermophoretic velocity of an elongated particle, when compared to that of a sphere, is greater when the temperature gradient is parallel to the long axis of the particle, and less when the gradient is perpendicular to this axis. Orientation averaging thus produces an "effective" thermophoretic diffusivity that is not significantly different than the volume-equivalent sphere diffusivity.

Determination of the thermophoretic behavior of more complicated particles than spheroids or binary aggregates would provide more insight into the structure sensitivity of the thermophoretic diffusivity. A particular type of particle that occurs frequently in nature, yet allows for a tractable mathematical analysis, is an aggregate of several spheres. Solution of the conduction and creeping flow equations for such structures can be accomplished using an extension of the coupled spherical harmonics solution. Details of the formulation will be published in a separate paper (Mackowski, 1991), and are simply outlined here.

The analysis is based on the fact that solutions in the spherical coordinate system to the conduction and creeping flow equations can be expressed as infinite series involving spherical harmonics. Specifically, the fluid temperature and velocity fields that satisfy these respective equations and vanish at finite distance from the origin can be written as

$$T_f = \sum_{n=0}^{\infty} \sum_{m=-n}^{n} d_{mn} u_{mn}\{r, \theta, \phi\}, \tag{18}$$

$$\begin{aligned} \mathbf{v} = \sum_{n=0}^{\infty} \sum_{m=-n}^{n} \Bigg\{ & a_{mn} \nabla u_{mn}\{r, \theta, \phi\} \\ & + b_{mn} \left(\frac{1}{n} \mathbf{r} u_{mn}\{r, \theta, \phi\} - \frac{n-2}{2n(2n-1)} \nabla [r^2 u_{mn}\{r, \theta, \phi\}] \right) \\ & + c_{mn} \nabla \times [\mathbf{r} u_{mn}\{r, \theta, \phi\}] \Bigg\}, \end{aligned} \tag{19}$$

where $u_{mn}\{r, \theta, \phi\}$ denotes the solid spherical harmonic:

$$u_{mn}\{r, \theta, \phi\} = r^{-(n+1)} P_n^m \{\cos\theta\} \, e^{im\phi}. \tag{20}$$

The expansion coefficients a_{mn}, b_{mn}, c_{mn} and d_{mn} are specified upon application of the boundary conditions to the solutions.

The governing differential equations and boundary conditions are linear, so a solution valid for a configuration of N spheres can be assembled from the superposition of individual solutions written in spherical coordinates about the origin of each sphere. Added to this solution is the external field (if any) imposed upon the spheres, such as a temperature gradient in the fluid. For the particular problem at

hand, the solution can thus be written

$$T_j = \nabla T_0 \cdot \mathbf{r} + \sum_{i=1}^{N_s} T_j^i \{r_i, \theta_i, \phi_i\}, \tag{21}$$

$$\mathbf{v} = + \sum_{i=1}^{N} \mathbf{v}^i(r_i, \theta_i, \phi_i). \tag{22}$$

To formulate the boundary conditions on the surface of sphere i, the "partial" solutions written about all the other spheres in the configuration must be transformed into solutions written in spherical harmonics about i. This can be accomplished through use of an addition theorem for solid spherical harmonics, which can be written in the form

$$r_j^{-(n+1)} P_n^m \{\cos\theta_j\} e^{im\phi_j} = \sum_{l=0}^{\infty} \sum_{k=-n}^{n} A_{kl}^{mn} r_i^l P_l^k \{\cos\theta_i\} e^{ik\phi_i}, \quad R \geqslant r_i, \tag{23}$$

where the addition coefficient A_{kl}^{mn} is dependent only upon the distance and direction of translation from sphere j to i.

By substituting the addition theorem into the series expressions for the partial field, truncating the series, and applying the boundary conditions at each sphere, a linear relationship among the field expansion coefficients can be obtained. This relationship will be of the general form

$$a^i + \sum_{\substack{j=1 \\ j \neq i}}^{N_s} [\mathbf{T}^{ji}]\mathbf{a}^j = \mathbf{f}^i, \tag{24}$$

where $\mathbf{a}^i$ represents the vector containing the field coefficients (either $(a_{mn}^i, b_{mn}^i, c_{mn}^i)$ or (d_{mn}^i), $\mathbf{T}^{ji}$ is a "translation" matrix from origin j to i, and $\mathbf{f}$ contains the boundary condition and external field information. Equation (24) written for each of the N spheres forms a complete system of linear equations for the field coefficients, which can be solved using appropriate iteration or elimination techniques.

Complete description of the thermophoretic behavior of the sphere configuration begins with the solution of the temperature field for a given external temperature gradient. This solution then supplies the thermal slip boundary condition in the creeping flow problem. The thermophoretic force and torque acting on each sphere, and the agglomerate as a whole, are obtained directly from the degree $n = 1$ expansion coefficients in the velocity field representations. The fluid resistance properties of the aggregate are characterized from the solution of the velocity expansion coefficients with boundary conditions representing aggregate motion and rotation in the fluid.

The thermophoretic behavior of two basic types of aggregates have been investigated using this formulation for the work presented here, namely, straight chains and relatively dense, randomly packed clusters. Results of the computations are summarized in Figure 2, in which $\alpha_T D$, calculated for continuum ($Kn = 0$) conditions and normalized with the value of a single primary sphere, are plotted *vs* the number of spheres in the aggregate, N. The ratio of the particle and gas thermal conductivities, k_g/k_p, was taken to be 0.1 for all calculations. Straight chain results are given for a gas temperature gradient parallel and perpendicular to the chain axis, and the random cluster results represent the average values computed for ten different configurations. The solid fraction of the clusters, based on the smallest sphere completely enclosing the cluster, was between 0.25 and 0.35.

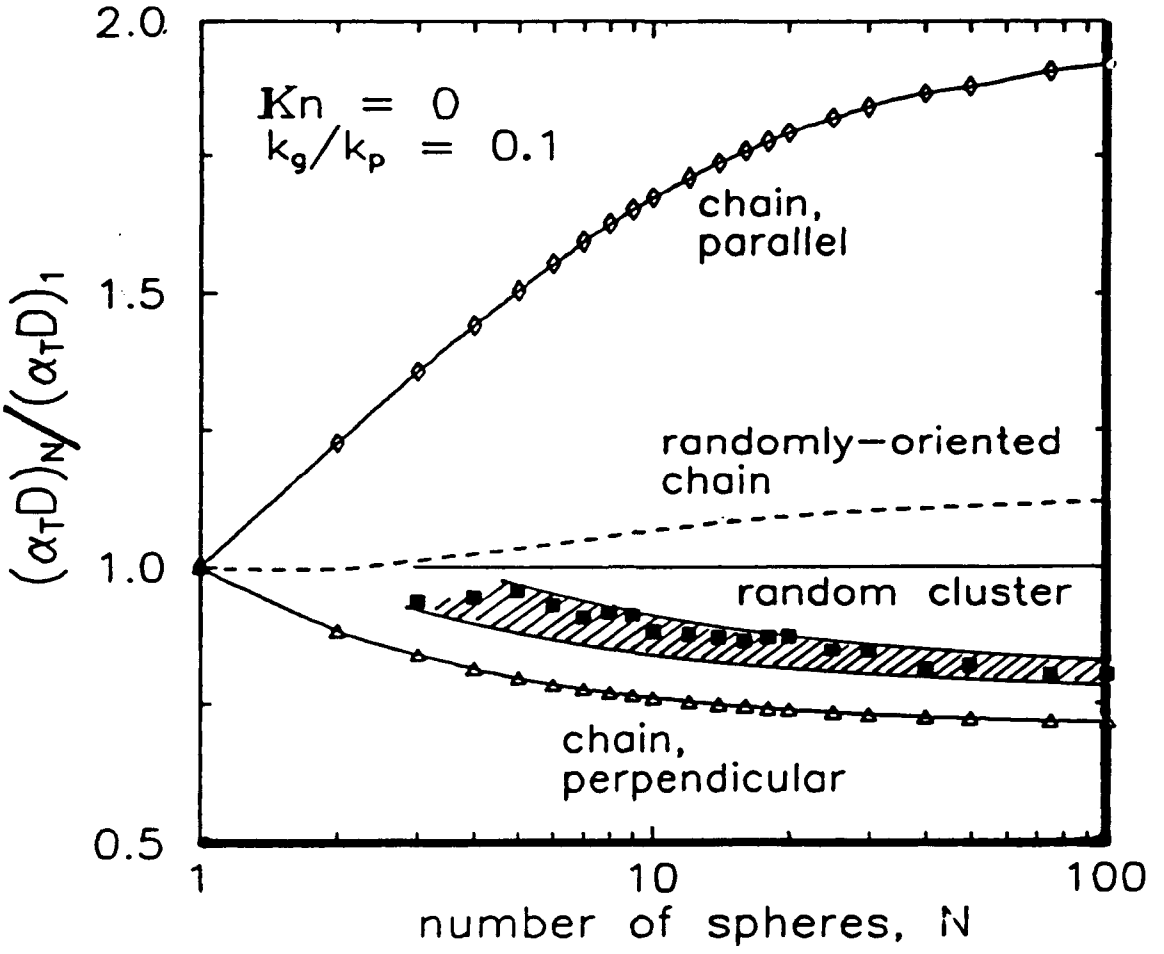

FIGURE 2 Predicted thermophoretic properties of linear- and quasi-spherical aggregated particles containing N primary particles in the continuum ($Kn \ll 1$) limit; thermal conductivity ratio = 0.1 (after Mackowski, 1991).

As expected, the parallel component of the chain $\alpha_T D$ is greater than the perpendicular component. In the limit of infinite chain length, the parallel and perpendicular components asymptote to approximately twice and two-thirds the value of a single sphere, respectively. The random-orientation-averaged value

$$\langle \alpha_T D \rangle = \tfrac{1}{3}(\alpha_T D)_{par} + \tfrac{2}{3}(\alpha_T D)_{per} \tag{25}$$

is thus around 10% larger than the single sphere $\alpha_T D$. The $\langle \alpha_T D \rangle$ values for the random clusters, on the other hand, are approximately 20% smaller than the single sphere results for large N.

It should be cautioned that in many environments *asymmetrical* aggregates will be formed and the assumption of random orientation may not be valid. Recent investigations (Mackowski (1990), Rosner *et al.* (1990)) have indicated that, for small aggregates of *non-identical* spheres, thermophoresis can result in an orienting torque on the aggregate. Such net torques will generally act to align the long axis of a counteracting tendency of Brownian rotation. Consequently, $(\alpha_T D)_N$ for a chain aggregate could be somewhat larger than the random-orientation value given above (*cf.* also, Figure 1, 2; curves marked "parallel orientation"). However, for dense, quasi-spherical aggregates, thermophoretic alignment will have a less significant effect on $\langle \alpha_T D \rangle_N$.

2.3 *Experimental Evidence*

In several experimental studies of organic soot deposition on cooled targets (see, *e.g.*, Eisner and Rosner, 1986, Makel and Kennedy, 1990) from atmospheric pressure flames, it has been reported that the thermophoretically deposition dominated absolute deposition rates were in agreement (say, $\pm$ 10%) with thermophoretic diffusivities estimated from Waldmann kinetic theory for small spherical particles. From our present viewpoint it is significant that this agreement occurs despite the fact that the soot prevailing in these flames, and being captured, was extensively aggregated. Moreover, in very recent experimental studies of the thickness of thermophoretically induced "dust-free" zones in $TiCl_4$-seeded laminar CH_4–N_2–O_2 counterflow diffusion flames (Gomez, and Rosner, 1990) it was concluded that the TiO_2 particles have $\langle \alpha_T D \rangle_N$-values within about 7% of the Waldmann (single sphere, $Kn \gg 1$) values. While the implications of this noteworthy agreement were not really addressed in any of these papers, we now believe that the explanation lies in the insensitivity of $\langle \alpha_T D \rangle_N$ to aggregate size, N, and morphology, which is the focus of this communication.

2.4 *Analogies from the Electrophoresis of Colloidal Particles in Liquid Electrolytes*

In the domain of colloidal particle phoresis in viscous fluids (see, *e.g.*, Anderson, 1989) a noteworthy and interesting "precedent" is the *electrophoretic drift* of a "large" insulating particle in an unbounded Newtonian electrolyte. M. Smoluchowski in 1914 derived an expression for the electrophoretic velocity of an isolated spherical solid particle subjected to an imposed electrical field, and proposed that the result would hold for an insulating body of *arbitrary size and shape* provided that the fluid sublayer of nonzero net charge (the Debye sheath) adjacent to the surface is small on the scale of the local radii of surface curvature. This conjecture was supported by D. C. Henry in 1931, who also treated cylinders, and finally proven by Morrison, 1970. Under these same conditions, Reed and Morrison, 1976, showed that two identical spheres will move with the same velocity as one isolated sphere at all interparticle separations and orientations relative to the electric field. Very recently, Acrivos, *et al.*, 1990, have proven that a "cloud" containing N identical spherical particles of arbitrary concentration but surrounded by an infinite expanse of particle-free liquid will move at the same velocity as a single isolated spherical particle. Moreover, these results also carry over to the surface-tension driven migration of bubbles or immiscible liquid droplets in a non-isothermal Newtonian host liquid. Indeed, from our present viewpoint it is interesting that the abovementioned analyses are based on the nonzero "slip velocity" at the outer edge of the Debye sheath induced by the local electrical field, which plays a role similar to the "thermal creep" velocity appearing in the near-continuum analysis of isolated particle thermophoresis in gases (see, *e.g.*, Brock, 1962 and Mackowski, 1990, 1991). While it should be noted that aggregate particles comprised of *touching* spheres evidently do *not* satisfy the abovementioned local radius of curvature condition, these liquid phase "precedents" help explain the remarkable insensitivity we find of $\langle \alpha_T D \rangle_N$ to size and morphology for aggregates comprised of primary quasi-spherical particles in non-isothermal *gases* at $Kn \ll 1$.

3 ENGINEERING IMPLICATIONS

3.1 *Deposition Rate Predictions*

We have already noted (Section 2.3) that actual soot deposition rates from atmospheric pressure combustion gases to cooled solid targets can be predicted with

remarkable accuracy using the thermophoretic diffusivity expected for the primary particles themselves, even though the actual soot aggregate sizes and morphologies are non-uniform and complex. Indeed, the insensitivity of aggregate $\langle \alpha_T D \rangle$ to size and morphology dramatically simplifies the task of making engineering predictions of soot deposition rates from flowing combustion gases, at least up to the level of shear stress necessary to cause deposited particle "re-entrainment" (Makeh and Kennedy, 1990) or the inability of an arriving particle to "find a stable home" in the deposit (Konstandopoulos and Tassopoulos, 1990, 1991). It is now well known that thermophoretically dominated particle deposition rates from laminar boundary layers (Goren, 1977, Gokoglu and Rosner, 1984, 1986, Batchelor and Shen, 1985) and turbulent boundary layers (see, *e.g.*, Rosner and Fernandez de la Mora, 1982) are nearly proportional to the product $\langle \alpha_T D \rangle$, unless the mainstream particle loading is appreciable (Rosner and Park, 1988). Thus, the abovementioned size/structure insensitivity of the $\langle \alpha_T D \rangle$-value for aggregated particles, especially in the free-molecule limit but even in the near-continuum limit, translates directly into an insensitivity of soot deposition rates to the aggregate size/morphology distribution in the gas mainstream. In contrast, from our previous comments about the Brownian diffusivity $\langle D_N \rangle$ itself, and the fact that convective-diffusion deposition rates are nearly proportional to $\langle D_N \rangle^{2/3}$ in lightly-loaded systems, it follows that one can *not* make accurate predictions of convective diffusion-controlled soot deposition rates (*e.g.*, in nearly isothermal circumstances) without a detailed knowledge of the size- and morphology-distribution of the prevailing aggregated particles (see, *e.g.*, Rosner, 1991, and Rosner *et al.*, 1991). This size/morphology sensitivity will also be true in flow systems for which particle *inertia* plays an important role in determining deposition rates, as in the case of the flow of a particle-laden high speed fluid over solid bodies with streamwise curvature (Israel and Rosner, 1983, and Konstandopoulos and Rosner, 1990) or even turbulent flows over straight surfaces (see, *e.g.*, Rosner and Tassopoulos, 1989). This follows from the Einstein relationship: $\langle D_p \rangle = (k_B T/m_p)\langle t_p \rangle$, where $\langle t_p \rangle$ is the (orientation-averaged) particle stopping time, which plays a decisive role in determining the extent of dynamical non-equilibrium between the suspended particles of mass m_p and the accelerating/decelerating carrier fluid at local temperature T (see, *e.g.*, Rosner, 1986, 1990).

Returning to the case of thermophoretically-dominated aggregate deposition (the focus of the present paper), it should be noted that, whereas total mass deposition rates *can* be accurately estimated without a detailed knowledge of the aggregate size/morphology distribution, it will *not* be possible to predict the *deposit microstructure* (and, hence all microstructurally sensitive transport properties, including the effective thermal conductivity) without this additional information (Tassopoulos, O'Brien, and Rosner, 1989).

3.2 *Capture Efficiency Variations in Soot Particle Sampling*

On the plausible assumption that particle capture efficiency variations would be much smaller for thermophoretic sampling than for capture by Brownian diffusion or inertial impaction, Dobbins and Megaridis, 1987 have recently exploited and recommended this "intrusive" technique as an indispensable aid in studying soot dynamics in hydrocarbon/air flames. They also indicated that their observed morphology distributions were insensitive to probe size. The transport evidence assembled and discussed here confirms their basic assumptions and indicates that relative populations of soot aggregates as seen on a lightly loaded cold electron microscope target cannot be very different from the relative aggregate populations existing in the

combustion gas stream being samples, especially for atmospheric- or subatmospheric-pressure flames. In the near-continuum limit our recent results for the modest size and morphology dependence of $\langle \alpha_T D \rangle$ (Figure 2, Section 2.2) combined with thermophoretic capture theory (see, *e.g.*, Eisner and Rosner, 1986) would begin to allow systematic corrections to be made for the associated capture efficiency variations in the thermophoretic sampling process at higher pressures.

3.3 *Size/Structure Insensitivity of $\langle \alpha_T D \rangle$ Compared to Size/Structure Sensitivity of Aggregate "Optical" Properties*

Non-intrusive "optical" diagnostic techniques based on polarized light scattering and/or extinction are on firm ground in regions where the primary particles are spherical, homogeneous, widely separated and say, log-normally distributed with respect to size. However, in regions where the particles are extensively aggregated the interpretation of extinction and light scattering data becomes problematic, as recently demonstrated by Dobbins, Santoro, and Semerjian, 1990. These authors compared inferred soot area/volume-values based on the isolated sphere theory and a simplified quasi-fractal aggregate theory, revealing local differences of about a factor of three, and much larger differences in the corresponding inferred soot growth/oxidation rates.

Using transient thermocouple response techniques Eisner and Rosner, 1986 demonstrated that in regions free of extensive "vapor growth" or heterogeneous oxidation (gasification) the laws of thermophoresis could be used to infer local soot volume fractions (and, indirectly, local gas temperatures) independent of assumptions regarding particle size spectra or optical properties. It now becomes clear that such local "immersion" methods are largely independent of the size/morphology of inevitable soot aggregates present in these regions, adding considerably to their attractiveness. Nonetheless, it is likely that *combinations* of optical techniques with careful sampling techniques will be necessary, and continue to bear fruit.

3.4 *Consequences for "Dust-Free Zone" Thickness and Brownian Sublayer Thickness*

A corollary of the findings discussed above is that the state of soot aggregation will not appreciably influence the boundary position of the so-called "dust free" zone near a hot solid surface (Park and Rosner, 1987, 1991, Friedlander *et al.*, 1988) or diffusion flame "sheet" (Gomez and Rosner, 1991).* However the thickness and internal structure of such a "front", being dictated by the (distribution of) Brownian diffusivities, *will* change appreciably with the degree of aggregation. Put another way, if one were trying to separate soot aggregates of different sizes and morphologies, thermophoretic means (without asymmetrical particle orientation using electric and/or magnetic fields) would not be particularly effective. The results shown in Sections 2.1–2.2, however, indicate that thermophoretic separation of *oriented* nonspherical aggregated particles, *e.g.* straight chains, remains feasible, and would be most effective in the near-continuum (high pressure) limit.

*Zachariah *et al.* (1989), appear to conclude from their optically inferred silica particle diameter axial profiles that there is a broad spectrum of thermophoretically determined particle stagnation planes, spanning over a 1 mm distance depending upon particle size. This interpretation seems to us to be unlikely for the Knudsen numbers (O(1)) encountered in their silane-seeded hydrogen/oxygen experiments.

3.5 *Conjectures Regarding Polydispersed Primary Particles, Tangential Momentum Accommodation, Particle Thermal Conductivity, and Intermediate Knudsen numbers*

While the size distribution of the primary particles is quite narrow in many laminar systems with negligible backmixing (see, *e.g.*, Megaridis and Dobbins, 1990), in general one might find that the primary particles comprising the aggregates are themselves "polydispersed". This kind of spread is known to influence the drag behavior of linear chains of quasi-spherical primary inorganic particles–indeed, Kops *et al.*, 1975 and G. Kasper, 1982 have provided empirical formulae allowing this effect to be included in the estimation of linear chain aggregate capture by convection-Brownian diffusion or inertia. However, from the aggregate themophoresis results discussed in this paper for several important morphologies we conjecture that $\langle \alpha_T D \rangle$ for aggregates comprised of nonuniform size quasi-spherical particles will also be insensitive to the spread of the primary particle size distribution function, especially in the free-molecule limit. If confirmed by future research this feature will further simplify the engineering prediction of aggregate particle deposition rates in non-isothermal systems characterized by broad distributions of residence times.

Our recent results for the free-molecule limit (Garcia-Ybarra and Rosner, 1989) also suggest that the abovementioned size/structure insensitivity will be further improved when tangential momentum accommodation is *incomplete* upon gas/solid encounters with the primary particles. Indeed, we found that $\langle \alpha_T D \rangle$ is *independent* of sphero-cylinder particle aspect-ratio for the case of purely "specular"* gas molecule reflection. While the factors that determine the scattering properties of primary particle surfaces are not yet well understood (see, *e.g.*, the recent paper of Schaefer and Martin, 1989), it appears that departures from the diffuse reflection limit will favor the size/structure insensitivity of $\langle \alpha_T D \rangle$. In the near-continuum limit, the same can be said for the effects of increasing particle thermal conductivity (Mackowski, 1991).

Finally, while we have not yet studied the intermediate Knudsen number regime, from the well-known size dependence of the single sphere $\alpha_T D$-value, we expect that sufficiently "compact" aggregates will have $\langle \alpha_T D \rangle$-values which fall off appreciably with N. However, it can be conjectured that sufficiently "open" or elongated aggregates will probably also have N-insensitive $\langle \alpha_T D \rangle$-values even when, say, the gas mean-free-path is comparable to the aggregate radius of gyration.

4 CONCLUSIONS, FUTURE WORK

Our recent calculations for a variety of canonical aggregate particle configurations and available experiments on soot transport from/in flames point to the following important simplification in treating the migration of aggregated particles through nonisothermal gases: *Due to a near-cancellation between incremental thermal force and incremental drag the orientation-averaged thermophoretic diffusivity $\langle \alpha_T D \rangle_N$ of aggregates comprised of N uniform sized primary particles is remarkably insensitive to aggregate size, N, and morphology, being within about 8% of the value for a single primary particle in the free-molecule limit and within about 21% of the value for a single*

*Since Waldmann's result for a single spherical particle contains the factor $[1 + (\pi\alpha_{mom}/8)]^{-1}$ it is known that thermophoretic velocities for the case of no tangential momentum accommodation (specular reflection) are greater than for the case of complete tangential momentum accommodation ("diffuse" reflection) by the factor of only $(1 + (\pi/8)) = 1.3927$.

primary particle in the continuum limit. It is reasonable to expect that this result will also hold if the primary particles are themselves not uniform in size, and even in the Knudsen transition regime unless the primary particles are "tightly packed". It follows that the reported size/morphology insensitivity of $\langle \alpha_T D \rangle_N$ will often allow sufficiently accurate engineering predictions of total mass deposition rates (Rosner, 1989) to cooled targets based only on a knowledge of the *total soot volume fraction* in the mainstream; moreover, our present conclusions support the efficacy of thermophoretic soot sampling methods (see, *e.g.*, Dobbins and Megaridis, 1987) and thermophoresis-based probes of local soot volume fraction and gas temperature (Eisner and Rosner, 1986), as well as the inefficiency of aggregate size/morphology separation by thermophoretic means unless the aggregates are asymmetrical and orientation-averaging (*via* Brownian rotation) can be prevented.

Future research will be necessary to better define the limits of validity of these conclusions and conjectures, and extend the presently cited calculations to include other important aggregate morphologies and, ultimately, intermediate Knudsen numbers.

ACKNOWLEDGEMENTS

This research was supported by AFOSR (Grant 89-0223) and DOE-PETC (Grant DE-FG-22-90PC90099) and NATO Collaborative Research Grant (CRG 900615) as well as the 1990–1991 Yale HTCRE Laboratory Affiliates (Shell, DuPont, SCM-Chemicals, Union Carbide). It is a pleasure to acknowledge helpful discussions and/or correspondence with J. Castillo, R. A. Dobbins, J. Fernandez de la Mora, A. Gomez, I. M. Kennedy, A. G. Konstandopoulos, C. M. Megaridis, D. A. Saville, A. Schmidt-Ott, M. Tassopoulos, and M. Zachariah. Correspondence concerning this research should be directed to Professor Rosner, Director Yale HTCRE Lab., at the above address. Dr. Mackowski, formerly Yale HTCRE Lab Postdoctoral Research Engineer, is presently at Auburn Univ., Dept. of Mech Engrg., Auburn, AL.; Dr. Garcia-Ybarra, Yale HTCRE Lab Visiting Scientist, is from UNED, Dept. of Fundamental Physics, Madrid, Spain.

REFERENCES

Acrivos, A., Jeffrey, D. J., and Saville, D. A. (1990). Particle Migration in Suspensions by Thermocapillary or Electrophoretic Motion. *J. Fluid Mechanics* **212**, 95–110.

Anderson, J. L. (1989). Colloid Transport by Interfacial Forces. *Ann. Rev. Fluid Mechanics* **21**, 61–99.

Batchelor, G. K. and Shen, C. J. (1985). *J. Colloid Interface Sci.*, **107**, 21–37.

Brock, J. R. (1962). On the Theory of Thermal Forces Acting on Aerosol Particles. *J. Colloid Sci.* **17**, 768–780.

Dobbins, R. A. and Megaridis, C. M. (1987). Morphology of Flame-Generated Soot As Determined by Thermophoretic Sampling. *Langmuir (ACS)* **3**, 254–259.

Dobbins, R. A. and Megaridis, C. M. (1991). Optical Cross-section of Soot Aggregates. *Applied Optics* (in press).

Dobbins, R. A., Santoro, R. J., and Semerjian, H. G. (1990). Analysis of Light Scattering From Soot Using Optical Cross-Sections for Aggregates. *23rd International Combustion Symposium*, Orleans, France.

Eisner, A. D. and Rosner, D. E. (1985). Experimental Studies of Soot Particle Thermophoresis in Non-Isothermal Combustion Gases Using Thermocouple Response Techniques. *Combustion and Flame* **61**, 153–166.

Eisner, A. D. and Rosner, D. E. (1986). Experimental and Theoretical Studies of Submicron Particle Thermophoresis in Combustion Gases. *J. PhysicoChemical Hydrodynamics* (Pergamon Press), **7**, 91–100.

Friedlander, S. K., Fernandez de la Mora, J., and Gokoglu, S. A. (1988). Diffusive Leakage of Small Particles Across the Dust-Free Layer Near a Hot Wall. *J. Colloid Sci.* **125**, 351–355.

Garcia-Ybarra, P. and Rosner, D. E. (1989). Thermophoretic Properties of Nonspherical Properties and Large Molecules. *AIChE. J.*, **35**, 139–147.

Gokoglu, S. A. and Rosner, D. E. (1984). Correlation of Thermophoretically Modified Small Particle Diffusional Deposition Rates in Forced Convection Systems With Variable Properties, Transpiration Cooling, and/or Viscous Dissipation. *Int. J. Heat Mass Transfer* **27**, 639–645.

Gokoglu, S. A. and Rosner, D. E. (1986). Thermophoretically-Augmented Forced Convection Mass Transfer Rates to Solid Walls Across Non-Isothermal Laminar Boundary Layers. *AIAA J.* **24**, 172–179.

Gomez, A. and Rosner, D. E. (1990). Thermophoretic Effects on Particles in Counterflow Laminar Diffusion Flames. (In preparation).

Goren, S. L. (1977). Thermophoresis of Aerosol Particles in the Laminar Boundary Layer on a Flat Plate. J. Colloid & Interface Sci., **61**, 77–85.

Happel, J. and Brenner, H. (1965). Low Reynolds Number Hydrodynamics. Prentice-Hall, Englewood Cliffs, NJ.

Israel, R. and Rosner, D. E. (1983). Use of a Generalized Stokes Number to Determine the Aerodynamic Capture Efficiency of Non-Stokesian Particles from a Compressible Gas Flow. *J. Aerosol Sci. & Tech. 2, 45–51.*

Kasper, G. (1982). Dynamics and Measurement of Smokes II. The Aerodynamic Diameter of Chain Aggregates in the Transition Regime. Aerosol Sci. Tech. (Elsevier), **1**, 201–215.

Kim, S. and Karrila, S. J. (1990). Microhydrodynamics: Principles and Selected Applications. Butterworths-Heinemann, Stoneham, MA.

Konstandopoulos, A. G. and Rosner, D. E. (1991). Inertial Effects on Thermophoretic Transport of Small Particles to Walls With Streamwise Curvature-I. Experiment, II. Theory. (Prepared for submission to *Int. J. Heat Mass Transfer*).

Konstandopoulos, A. G. and Tassopoulos, M. T. (1990). Simulation of Particle Impaction: Sticking Probability and Microstructure Evolution in the 'Frozen' Deposit Limit. *1990 Annual Meeting of the Amer. Assoc. Aerosol Research*, Philadelphia, PA.

Konstandopoulos, A. G. and Tassopoulos, M. T. (1991). A Kinetic Model of Deposit Growth: I. Characterization of Particle Sticking Probability. *1991 AIChE Annual Meeting*, Los Angeles, CA.

Kops, J., Dibbets, G., Hermans, L., and Van de Vate, J. F. (1975). The Aerodynamic Diameter of "Branched" Chain-Like Aggregates. *J. Aerosol Sci.*, **6**, 329–333.

Leong, K. H. (1984). Thermophoresis and Diffusiophoresis of Large Aerosol Particles of Different Shapes. J. Aerosol Sci., **15**, 511–517.

Mackowski, D. W. (1987). Investigation of the Radiative Properties of Chain-Agglomerated Soot Formed in Hydrocarbon Diffusion Flames, *PhD. Dissertation*, U. Kentucky.

Mackowski, D. W., Altenkirch, R. A. Menguc, M. P., and Saito, K. (1988). Radiative Properties of Chain-Agglomerated Soot Formed in Hydrocarbon Diffusion Flames. *22nd International Combustion Symposium*, The Combustion Institute, 1263–1269.

Mackowski, D. W. (1990). Phoretic Behavior of Asymmetric Particles in Thermal Nonequilibrium with the Gas. *J. Colloid & Interface Sci.* (in press).

Mackowski, D. W. (1991). An analysis of the Thermal and Hydrodynamic Properties of Aggregated Spheres in the Near-Continuum Regime. (To be submitted).

Mackel, D. B. and Kennedy, I. M. (1990). Experimental and Numerical Investigation of Soot Deposition in Laminar Stagnation Point Boundary Layers. *Proc. 23rd International Combustion Symposium*, Orleans, France (in press).

Mason, E. A. (1957). Higher Approximations for the Transport Properties of Binary Gas Mixtures: II. Applications. *J. Chem. Phys.* **27**, 782.

Megaridis, C. M. and Dobbins, R. A. (1990). Morphological Description of Flame-Generated Materials, Combustion Sci. Tech. **71**, 95–109.

Morrison, F. A. (1970). The Electrophoresis of a Particle of Arbitrary Shape. *J. Colloid & Interface Sci. 34, 210–214.*

Reed, L. D. and Morrison, F. A. (1976). Hydrodynamic Interaction in Electrophoresis. J. Colloid & Interface Sci. **54**, 117–133.

Rosner, D. E. and Fernandez de la Mora J. (1982). Small Particle Transport Across Turbulent Non-Isothermal Boundary Layers. *ASME Trans-J. Engrg. for Power*, **104**, 885–894.

Rosner, D. E. (1986, 3rd printing 1990). Transport Processes in Chemically Reacting Flow Systems, Butterworth-Heinemann, Stoneham, MA.

Rosner, D. E. (1989). Total Mass Deposition Rates from "Polydispersed" Aerosols, *AIChE. J.* **35**, 164–167.

Rosner, D. E. (1989a). Side-wall Gas "Creep" and "Thermal Stress Convection" in Microgravity Experiments on Film Growth by Vapor Transport. *Physics Fluids A-Fluid Mechanics* **1**, (11), 1761–1763.

Rosner, D. E. (1991). Particle Size- and Structure-Sensitivity of Total Mass Deposition Rates from Streams Containing Coagulation-Aged Populations of Aggregated Primary Particles. (In preparation).

Rosner, D. E. and Park, H. M. (1988). Thermophoretically Augmented Mass, Momentum and Energy Transfer Rates in High Particle Mass-Loaded Laminar Forced Convection Systems, *Chem. Engrg. Sci.*, **43**, 1497–1508.

Rosner, D. E. and Tassopoulos, M. (1989). Deposition Rates from "Polydispersed" Particle Populations of Arbitrary Spread, *AIChE. J.* **35**, 1497–1508.

Rosner, D. E., Mackowski, D. W., Tassopoulos, M., Castillo, J., and Garcia-Ybarra, P. (1990). Effects of Heat Transfer on the Dynamics and Transport of Small Particles in Gases. Paper 293e Presented at the (S. W. Churchill Birthday) Symposium: *Advances in Rate Processes*. AIChE 1990 Annual Meeting, Chicago IL, November 12, 1990; *Industrial and Engineering Chemistry-Research* (ACS) Special Issue (in press, 1991).

Rosner, D. E., Konstandopoulos, A. G., Tassopoulos, M., and Mackowski, D. W. (1991). Deposition Dynamics of Combustion-Generated Particles: Summary of Recent Research Studies of Particle Transport Mechanisms, Capture Rates and Resulting Deposit Microstructure/Properties, *Proc. Engineering Foundation Conference*: Inorganic Transformations and Ash Deposition During Combustion (in press).

Schaefer, D. W. and Martin, J. E. (1989).

Smoluchowski, M. V. (1914). Handbuch der Elektrizitat und des Magnetismus, (L. Graetz, ed.), Vol. 2, Barth, Leipzig.

Tassopoulos, M., O'Brien, J. A., and Rosner, D. E. (1989). Simulation of Microstructure/Mechanism Relationships in Particle Deposition, *AIChE. J.* 35, 967–980.

Ulrich, G. D. and Riehl, J. W. (1982). Aggregation and Growth of Submicron Oxide Particles in Flames, J. Colloid & Interface Sci., 87, 257.

Ulrich, G. D. and Subramanian, N. S. (1977). Particle Growth in Flames—III. Coalescence as a Rate-Controlling Process. *Comb. Sci. and Tech.*, 17, 119–126.

Waldmann, L. and Schmitt, K. H. (1966). Thermophoresis and Diffusiophoresis of Aerosols, Chap. 6 in *Aerosol Sci.* (C. N. Davies ed.), Academic Press, London, 137–162.

Williams, M. M. R. (1986). Thermophoretic Force Acting on a Spheroid, *J. Physics D, Applied Physics* 19, 1631–1642.

Williams, M. M. R. (1987). The Thermophoretic Forces Acting on a Bispherical System, *J. Physics D,Applied Physics*, 20, 354–359.

Zachariah, M. R., Chin, D., Semerjian, H. G., and Katz, J. L. (1989). Dynamic Light Scattering and Angular Dissymmetry for the *In Situ* Measurement of Silicon Dioxide Particle Synthesis in Flames. *Optics*, 28, 530–536.

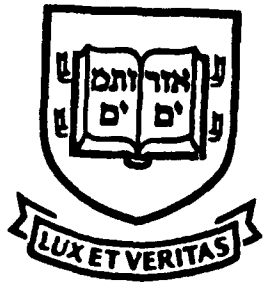

HIGH TEMPERATURE CHEMICAL REACTION ENGINEERING LABORATORY
YALE UNIVERSITY
BOX 2159, YALE STATION
NEW HAVEN, CONNECTICUT 06520 U.S.A.

REPORT DOCUMENTATION PAGE

Form Approved
OMB No. 0704-0188

1. AGENCY USE ONLY (Leave blank)	2. REPORT DATE	3. REPORT TYPE AND DATES COVERED
	1990	Journal publication

4. TITLE AND SUBTITLE
"Phoretic Behavior of Asymmetric Particles in Thermal Non-equilibrium With the Gas: Two-Sphere Aggregates" (U)

5. FUNDING NUMBERS
PE - 61102F
PR - 2308
SA - BS
G - AFOSR 89-0223

6. AUTHOR(S)
Daniel W. Mackowski

7. PERFORMING ORGANIZATION NAME(S) AND ADDRESS(ES)
HIGH TEMPERATURE CHEMICAL REACTION ENGINEERING LABORATORY
YALE UNIVERSITY
BOX 2159, YALE STATION
NEW HAVEN, CONNECTICUT 06520 U.S.A.

8. PERFORMING ORGANIZATION REPORT NUMBER

9. SPONSORING/MONITORING AGENCY NAME(S) AND ADDRESS(ES)
AFOSR/NA
Building 410
Bolling AFB DC 20332-6448

10. SPONSORING/MONITORING AGENCY REPORT NUMBER

11. SUPPLEMENTARY NOTES

12a. DISTRIBUTION/AVAILABILITY STATEMENT
Approved for public release; distribution is unlimited

12b. DISTRIBUTION CODE

13. ABSTRACT (Maximum 200 words)

An investigation into the phoretic behavior arising from thermal slip of an asymmetrical aerosol particle in thermal nonequilibrium with the carrier gas is presented. The asymmetrical particle is modeled as an aggregate of two spheres unequal in size and/or composition, with gas/particle thermal nonequilibrium arising from radiative transfer between the particle and an isotropic background. The particle and gas conduction equations and the creeping flow equation are solved for the binary sphere system using a spherical-harmonics-based method. In high temperature (e.g., combustion) environments, results indicate that the thermal slip forces arising from radiative cooling of an asymmetric aggregate can lead to significant phoretic velocities. The velocity is body-fixed, i.e., directed along the aggregate axis, and in the absence of alignment forces the aggregate motion is stochastic. The "effective" diffusion resulting from this motion can be orders of magnitude larger than ordinary Brownian diffusion for a volume-equivalent sphere. Conventional thermophoresis, resulting from a temperature gradient in the bulk gas, can act to align the aggregate axis with the temperature gradient. Under these conditions, the body-fixed motion of the aggregate will become deterministic, and can lead to a considerable increase or decrease in the "apparent" thermophoretic diffusivity of the aggregate.

14. SUBJECT TERMS
soot, aggregates, Brownian motion, thermophoresis

15. NUMBER OF PAGES
20

16. PRICE CODE

17. SECURITY CLASSIFICATION OF REPORT	18. SECURITY CLASSIFICATION OF THIS PAGE	19. SECURITY CLASSIFICATION OF ABSTRACT	20. LIMITATION OF ABSTRACT
Unclassified	Unclassified	Unclassified	UL

Phoretic Behavior of Asymmetric Particles in Thermal Nonequilibrium with the Gas: Two-Sphere Aggregates[1]

DANIEL W. MACKOWSKI[2]

Yale University, Department of Chemical Engineering, High Temperature Chemical Reaction Engineering Laboratory, New Haven, Connecticut 06520

Received November 27, 1989; accepted March 27, 1990

An investigation into the phoretic behavior arising from thermal slip of an asymmetrical aerosol particle in thermal nonequilibrium with the carrier gas is presented. The asymmetrical particle is modeled as an aggregate of two spheres unequal in size and/or composition, with gas/particle thermal nonequilibrium arising from radiative transfer between the particle and an isotropic background. The particle and gas conduction equations and the creeping flow equation are solved for the binary sphere system using a spherical-harmonics-based method. In high temperature (e.g., combustion) environments, results indicate that the thermal slip forces arising from radiative cooling of an asymmetric aggregate can lead to significant phoretic velocities. The velocity is body-fixed, i.e., directed along the aggregate axis, and in the absence of alignment forces the aggregate motion is stochastic. The "effective" diffusion resulting from this motion can be orders of magnitude larger than ordinary Brownian diffusion for a volume-equivalent sphere. Conventional thermophoresis, resulting from a temperature gradient in the bulk gas, can act to align the aggregate axis with the temperature gradient. Under these conditions, the body-fixed motion of the aggregate will become deterministic, and can lead to a considerable increase or decrease in the "apparent" thermophoretic diffusivity of the aggregate.

NOMENCLATURE

a	sphere radius
A_{mn}, B_{mn}, C_{mn}	gas velocity field expansion coefficients
c_t, c_m, c_s	temperature jump, momentum exchange, and thermal slip coefficients
d_{mn}	particle temperature field expansion coefficients
D	diffusion coefficient
D_{mn}	gas temperature field expansion coefficients
$\mathbf{e}$	unit vector
f	hydrodynamic resistance (force per unit velocity)
F	hydrodynamic force
g	bulk gas temperature gradient
J_n	nth moment of dimensionless internal heat source distribution within a sphere
k	thermal conductivity
k_B	Boltzmann's constant
Kn	Knudsen number $= l/a$
P	pressure
Pe	Peclet number
P_n^m	Legendre function
$\dot{q}_s$	particle thermal energy generation rate
r	radial position
R	sphere separation distance, $=a_1 + a_2$
T	temperature
T_y	y component of hydrodynamic torque
$\mathbf{U}$	velocity at sphere surface
$\mathbf{v}$	gas velocity vector
V	particle velocity

[1] Supported, in part, by the U.S. Department of Energy—Pittsburgh Energy Technology Center under Grant DE-FG-22-86PC90756.

[2] To whom correspondence should be addressed at present address: Department of Mechanical Engineering, Auburn University, AL 36849.

0021-9797/90 $3.00

X_{mn}, Y_{mn}, Z_{mn}	velocity boundary condition expansion coefficients
z_c	center of hydrodynamic stress
α_T	thermophoretic diffusivity factor
ϵ	emissivity
φ	azimuth angle
θ	polar angle
η	gas dynamic viscosity
Ψ	stream function
κ	gas/particle thermal conductivity ratio
μ	$\cos\theta$
ν	gas kinematic viscosity
ρ	gas density
σ	Stephan–Boltzmann constant
σ_t	tangential stress vector
ζ	dimensionless radial position, $=r/a$

Subscripts

b	body-fixed
env	radiation environment
g	gas
p	particle
rot	rotational
T	thermal slip, thermoporetic
v	translational component
x, y, z	cartesian components
r, θ, φ	polar components
ω	rotational component
0	local ambient

1. INTRODUCTION

While its remarkable consequences are often overlooked, a temperature gradient along a macroscopic solid surface can result in a "slip" flow of a gas adjacent to that surface in the direction of the gradient (1). This phenomenon, known as "thermal slip," was first identified by Maxwell in 1879 in his explanation of the "radiometer" effect (2). In the realm of aerosol research, thermal slip over particles in the near-continuum Knudsen number limit is responsible for the transport mechanisms of *thermophoresis* and *photophoresis*. In the former mechanism, the temperature gradient along the surface of the aerosol particle is provided by a gradient in the bulk gas, whereas in the latter the surface temperature gradient arises from the nonuniform absorption of radiation within the particle.

Not surprisingly, most mathematical analyses of thermophoresis (3–5) and photophoresis (6–8) have proceeded from a set of apparently reasonable simplifying assumptions concerning the phenomena. Foremost among these has been the assumption of an isolated spherical particle. Of course, "real" aerosol particles are seldom perfect spheres, yet the mathematical difficulties associated with even moderately nonspherical objects (e.g., ellipsoids) are formidable. Indeed, for many important properties associated with aerosol particles, e.g., mobility and radiative extinction, shape asymmetry typically contributes only higher order effects, and the particle can be considered an "equivalent" sphere having an "effective" diameter.

However, thermo- and photophoresis (combined here into the term *thermal-phoresis*) are essentially related to an asymmetry property of the particle—namely, the asymmetry in the gas temperature distribution adjacent to the particle. For spherical particles with radii considerably larger or smaller than the gas mean-free-path, one can derive the general relationship

$$V \simeq \text{const} \cdot \int_0^{\pi} T_g(r = a, \theta)\cos\theta d\theta = \text{const} \cdot \langle T_g \cos\theta \rangle, \quad [1]$$

where V is the thermal-phoretic velocity of the particle and T_g is the gas temperature extrapolated to the gas/solid surface. The asymmetry factor $\langle T_g \cos\theta \rangle$ typically arises from an asymmetry in the external field—either through a temperature gradient in the bulk gas or from an anisotropic distribution of radiant intensity incident upon the particle.

Intuitively, thermal-phoretic motion could also be significantly affected by *particle* asymmetry. For example, the uniform addition or removal of thermal energy (through chemical reactions or radiative absorption or emission) will produce no phoretic motion for spherical

particles—because the bulk temperature of the particle would be raised or lowered with respect to the gas yet no tangential temperature gradient would be generated at the particle surface. However, for asymmetrical particles this action could result in a nonzero surface temperature gradient. The asymmetrical particle would thus experience a phoretic motion even in the absence of asymmetry in the external field. An interesting and important feature of this motion is that its direction is dependent upon the orientation of the particle, i.e., *body-fixed*, as opposed to *space-fixed* motion encountered in "conventional" thermophoresis and photophoresis (9). The existence of such effects has indeed been recently observed in a series of experiments by Rohatschek (9), who concluded that the photophoretic force on nonspherical, irregularly shaped particles was significantly greater than that predicted for spherical particles.

The general purpose of this paper is to predict the consequences of aerosol particle shape asymmetry on thermal-phoretic motion in the near-continuum flow limit. Specifically, the behavior of an aggregate of two nonidentical spheres is investigated under the conditions of (1) a linear temperature gradient in the bulk gas (conventional thermophoresis) and (2) particle/gas thermal nonequilibrium. This particular model of the aerosol particle was chosen because it represents a commonly occurring shape (such as agglomerated soot), yet allows for a tractable mathematical analysis.

2. MATHEMATICAL MODEL

To simplify the mathematical analysis and yet retain the essential features of the problem, the following assumptions are made:

(1) The aggregate is in thermal nonequilibrium with the gas through radiative transfer from the aggregate to an isotropic background. The radiation transfer is modeled through a volumetric thermal energy generation rate $\dot{q}$, defined for each sphere. In addition, each sphere is taken to be homogeneous in its thermophysical properties, and the ratio of the thermal conductivities between the gas and the spheres is much less than unity.

(2) A steady temperature gradient may exist in the bulk gas. Thermophysical properties of the gas are constant.

(3) The Knudsen numbers characterized by the gas environment of the spheres, Kn_1 and Kn_2, are each significantly less than unity, so that the thermal and fluid dynamic analyses of the particle can be approached from a continuum viewpoint with jump- and slip-corrected boundary conditions.

(4) Both the Peclet and the Reynolds numbers of the spheres are small. Consequently, energy and momentum convection compared to diffusion can be neglected. In addition, the spheres and gas are taken to be in a quasi-steady state.

(5) The area of contact between the two spheres is infinitesimal, and heat transfer between the spheres occurs solely through gas-phase conduction.

The thermophysical-mathematical model defined above is admittedly a simple one, and several of the approximations and assumptions can be readily disputed. For example, the validity of a near-continuum analysis is questionable in the regions between the two spheres close to the point of contact. Furthermore, there will always be some direct heat transfer across the contact area of the spheres. Nevertheless, our goal is to develop a model which is both representative of the key features of the phenomena under investigation (viz., particle/gas thermal nonequilibrium and shape asymmetry) and yet simple enough to utilize analytical mathematical techniques.

Exact solutions of the conduction and creeping-flow equations for two neighboring spheres can be obtained in the bipolar coordinate system (10–12). This technique, however, is limited to two particles and would thus block our future plans to extend the analysis to multiparticle systems. Therefore, the mathematical technique used here involves a spherical-harmonics-based analysis similar to the "method of reflections" developed by

Happel and Brenner (13) for low Reynolds number hydrodynamic interactions between two spheres, and the "coupled spherical harmonics" method developed by Jeffrey (14) for solution of Laplace's equation. Realizing that the equations are linear, solutions valid for the two-sphere system can be obtained from superposition of solutions in spherical coordinates centered about each sphere. The solutions for the separate spheres are coupled in that the field (temperature or velocity) originating about one will appear in the boundary conditions for the other. Details of the method are presented in the following sections covering the conduction and creeping flow equations.

3. THERMAL ANALYSIS

3.1. Solution of the Conduction Equation

Figure 1 illustrates the two spherical coordinate systems employed in the analysis. The fields about sphere 1 and 2 are represented using r_1 and θ_1, and r_2 and θ_2, respectively. As the spheres are aligned on the z-axis, the azimuth angle φ is the same for both systems. Due to the axial symmetry of the model, the temperature gradient in the ambient gas is taken, without loss of generality, to lie in the x–z plane. The gradient is characterized by its x and z components, denoted $g_x = e_x \cdot \nabla T_0$ and $g_z = e_z \cdot \nabla T_0$, respectively.

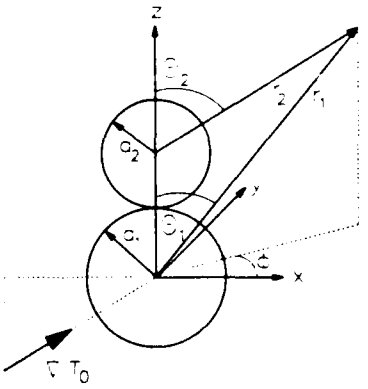

FIG. 1. Two-sphere aggregate model.

Conservation of energy in the gas and in the individual particles is expressed via the PDEs

$$\nabla^2 T_g = 0 \qquad [2]$$

$$\nabla^2 T_{p1} = -\frac{\dot{q}_{s1}(r_1, \theta_1)}{k_{p1}} \qquad [3]$$

$$\nabla^2 T_{p2} = -\frac{\dot{q}_{s2}(r_2, \theta_2)}{k_{p2}}, \qquad [4]$$

where the gas temperature T_g is constructed from contributions expressed in terms of the two coordinate systems, i.e., $T_g = T_{g1}(r_1, \theta_1, \varphi) + T_{g2}(r_2, \theta_2, \varphi)$. The specific nature of the particle heat generation rate $\dot{q}_s$ will be discussed at a later point.

The problem is nondimensionalized by defining the following normalized variables and parameters $\bar{T} \equiv (T - T_0)/T_0$, $\zeta \equiv r/a$, $\kappa \equiv k_g/k_p$, $\bar{q} \equiv a^2 \dot{q}_s / k_p T_0$, $\bar{g}_z = a g_z / T_0$, and $\bar{g}_x = a g_x / T_0$, where T_0 is the local ambient gas temperature. At the surface of sphere i, $i = 1, 2$, the thermal boundary conditions are

$$\kappa_i \frac{\partial}{\partial \zeta_i}(\bar{T}_{g1} + \bar{T}_{g2}) - \frac{\partial \bar{T}_{pi}}{\partial \zeta_i} = 0, \quad \zeta_i = 1 \qquad [5]$$

$$\bar{T}_{g1} + \bar{T}_{g2} - \bar{T}_{pi} = c_t \mathrm{Kn}_i \frac{\partial}{\partial \zeta_i}(\bar{T}_{g1} + \bar{T}_{g2}), \quad \zeta_i = 1. \qquad [6]$$

The first boundary condition represents conservation of energy at the particle/gas interface. Note that the absorption and emission of radiant energy, which is often formulated in the boundary conditions, is more appropriately modeled as a volumetric process for micrometer-sized particles and thermal radiation wavelengths (15). The second boundary condition expresses the familiar temperature "jump" at the particle surface due to the presence of a Knudsen sublayer. For complete thermal accommodation, the value of the dimensionless temperature-jump coefficient c_t has been reported to be 2.16 (5).

For $\zeta \to \infty$, the solution for the gas temperature must also match the ambient gas temperature gradient. This is met by imposing the conditions

$$\bar{T}_{g1}(\zeta_1 \to \infty, \theta_1, \varphi) = \zeta_1(\bar{g}_{z1}\cos\theta_1 + \bar{g}_{x1}\sin\theta_1\cos\varphi) \quad [7]$$

$$T_{g2}(\zeta_2 \to \infty, \theta_2, \varphi) = 0. \quad [8]$$

The solutions for T_{g1} and T_{g2} can thus be written as

$$\bar{T}_{g1} = \sum_{n=0}^{\infty} \zeta_1^{-(n+1)}(D_{0n}^{(1)}P_n(\mu_1) + D_{1n}^{(1)}P_n^1(\mu_1)\cos\varphi) + \zeta_1(g_{z1}P_1(\mu_1) + g_{x1}P_1^1(\mu_1)\cos\varphi) \quad [9]$$

$$\bar{T}_{g2} = \sum_{n=0}^{\infty} \zeta_2^{-(n+1)}(D_{0n}^{(2)}P_n(\mu_2) + D_{1n}^{(2)}P_n^1(\mu_2)\cos\varphi) \quad [10]$$

and the solution for the particle temperature within sphere i can be written (8)

$$\bar{T}_{pi} = \sum_{n=0}^{\infty} \zeta_i^n(d_{0n}^{(i)}P_n(\mu_i) + d_{1n}^{(i)}P_n^1(\mu_i)\cos\varphi) - G_n^{(i)}(\zeta_i)P_n(\mu_i). \quad [11]$$

In the above representations, D_{mn} and d_{mn} are undetermined expansion coefficients, $\mu \equiv \cos\theta$, $P_n(\mu)$, and $P_n^1(\mu)$ are Legendre functions, and

$$G_n^{(i)}(\zeta) = \frac{1}{2}\left\{\zeta^n \int_{\zeta}^{1} t^{1-n} \times \int_{-1}^{1} \bar{q}_i(t,\mu)P_n(\mu)\,d\mu\,dt + \zeta^{-(n+1)} \int_0^{\zeta} t^{n+2} \times \int_{-1}^{1} \bar{q}_i(t,\mu)P_n(\mu)\,d\mu\,dt\right\}. \quad [12]$$

To satisfy the boundary conditions at the surfaces of each sphere, $T_{g1}(\zeta_1, \mu_1, \varphi)$ must be expressed in terms of ζ_2 and μ_2, and likewise for T_{g2}. This is accomplished through application of the addition theorem for solid spherical harmonics (16), which can be expressed as

$$\zeta_2^{-(n+1)}P_n^m(\mu_2) = \left(\frac{R}{a_2}\right)^{-(n+1)}(-1)^{n+m} \times \sum_{\nu=0}^{\infty}\binom{\nu+n}{\nu+m}\left(\frac{R}{a_1}\right)^{-\nu}\zeta_1^{\nu}P_{\nu}^m(\mu_1), \quad \frac{R}{a_1} > \zeta_1 \quad [13]$$

$$\zeta_1^{-(n+1)}P_n^m(\mu_1) = \left(\frac{R}{a_1}\right)^{-(n+1)} \times \sum_{\nu=0}^{\infty}(-1)^{\nu+m}\binom{\nu+n}{\nu+m}\left(\frac{R}{a_2}\right)^{-\nu}\zeta_2^{\nu}P_{\nu}^m(\mu_2), \quad \frac{R}{a_2} > \zeta_2, \quad [14]$$

where

$$\binom{\nu+n}{\nu+m} \equiv \frac{(\nu+n)!}{(n-m)!(\nu+m)!},$$

and R is the center-to-center distance between the two coordinates, which is equal to $a_1 + a_2$ for the two touching spheres. Combining Eqs. [5]–[14] and using the orthogonality of the spherical harmonics yields

$$(n + n(n+1)c_i\mathrm{Kn}_i + (n+1)\kappa_1)D_{0n}^{(1)} = -J_n^{(1)} - n(1 - nc_i\mathrm{Kn}_i - \kappa_1)\left(\frac{R}{a_1}\right)^{-n} \times \left\{\frac{a_2}{\kappa_2 R}J_0^{(2)} + \sum_{\nu=1}^{\infty}(-1)^{\nu}\binom{n+\nu}{n} \times \left(\frac{R}{a_2}\right)^{-(\nu+1)}D_{0\nu}^{(2)}\right\} - (1 - c_i\mathrm{Kn}_i - \kappa_1)\bar{g}_z\delta_{n1}, \quad n = 1, 2, 3, \ldots \quad [15]$$

$$(n + n(n+1)c_i\mathrm{Kn}_i + (n+1)\kappa_1)D_{1n}^{(1)} = -n(1 - nc_i\mathrm{Kn}_i - \kappa_1)\left(\frac{R}{a_1}\right)^{-n} \times \sum_{\nu=1}^{\infty}(-1)^{\nu+1}\binom{n+\nu}{n+1}\left(\frac{R}{a_2}\right)^{-(\nu+1)}D_{1\nu}^{(2)}$$

$$- (1 - c_i \mathrm{Kn}_i - \kappa_i)\bar{g}_x \delta_{n1}, \qquad n = 1, 2, 3, \ldots, \quad [16]$$

where $\delta_{\nu n}$ is the Kroneker delta symbol, and $J_n^{(i)}$ is the nth moment of the heat source distribution in sphere i, defined by

$$J_n^{(i)} = nG_n^{(i)}(1) - G'_n(1) = \frac{2n+1}{2} \int_0^1 \int_{-1}^1 \bar{q}_i(t, \mu) P_n(\mu) t^{n+2} d\mu dt. \quad [17]$$

The equations for sphere 2 are of similar form, with the exception that $(-1)^n$ replaces $(-1)^\nu$ in the summation term.

For $n = 0$, Eq. [15] reduces to $B_{00}^{(i)} = -J_0^{(i)}/\kappa_i$, which is a requirement of energy conservation. The higher-order coefficients are of interest here, since these will account for tangential gas temperature gradients and ultimately be responsible for thermal slip. Equation [15] reveals that, for sphere 1 and $m = 0$, the $n = 1$ and higher coefficients arise from four contributions. The first term on the right-hand-side accounts for nonuniformity in the radiative emission/absorption within sphere 1. The second term represents the field at sphere 1 arising from a source (or sink) of energy of strength $J_0^{(2)}$ located at the origin of sphere 2. The third term represents the perturbation in the field about sphere 1 due to the nonuniformity in the field about sphere 2, and the fourth term superimposes the z-component of the external temperature gradient. For $m = 1$ (Eq. [16]), the field at sphere 1 results only from the perturbation due to the field at 2 and the x-component of the external gradient.

3.2. Radiative Model

An accurate description of the radiative absorption/emission distribution within each sphere would require an electromagnetic analysis of the bispherical system. Fuller and Kattawar (17) have solved the vector wave equations for multiple sphere systems using a superposition technique analogous to (but considerably more complicated than) that described above. The solution is dependent upon the radiative size parameter $x = 2\pi a/\lambda$ (where λ is the radiation wavelength), and refractive index $m = n + ik$ of each sphere in the system, as well as the geometry of the system and direction of incident radiation. For atmospheric pressure, high temperature conditions, and thermal radiation wavelengths, particles large enough to fulfill the near-continuum approximation will also have size parameters in excess of unity. Absorption distributions, which are proportional to the square modulus of the local electric field (15), will be highly nonuniform in this situation. For touching spheres the distributions will be, in addition, strongly dependent upon the angle between the aggregate axis and incident radiation.

In the analysis presented here, however, the nature of the absorption distribution within the spheres will be neglected. Justifications for doing so are, first, the incident radiation is assumed isotropic—which results in a degree of averaging of the absorption distributions with respect to θ. Second, the ratio of the gas and particle thermal conductivities, κ, is assumed to be much less than unity (which is physically often the case). Under these assumptions, the first term on the right-hand side of Eq. [15] (involving $J_n^{(1)}$) will be considerably smaller than the second and third terms. Therefore, to a reasonable approximation, it is necessary to consider only the total rate of radiative energy transfer from each sphere (i.e., J_0) in predicting the gas temperature field. This quantity could be obtained from knowledge of the absorption cross sections of the individual spheres in the agglomerate.

Accurate prediction of the absorption cross sections would in itself require the neighboring-sphere analysis of Ref. (17). Estimation of the individual cross sections from isolated-sphere Lorenz/Mie theory is not justifiable. Rather than employing the neighboring sphere analysis, the radiative properties of the individual spheres will simply be parameterized, in that the rate of radiative transfer from the spheres will be made proportional to a tem-

perature-independent emissivity ϵ having a value between 0 and 1. Because the relative difference between the particle and surrounding gas temperature will be small for micrometer-sized particles, the temperature at which the spheres radiate can be approximated as the local gas temperature T_0, and radiation incident upon the spheres is assumed to originate from a blackbody environment at a temperature T_{env}. With these assumptions, $J_0^{(i)}$ is written

$$J_0^{(i)} = -\frac{a_i \sigma \epsilon_i}{k_{pi} T_0}(T_0^4 - T_{env}^4), \quad i = 1, 2. \quad [18]$$

The above assumptions considerably simplify the radiative exchange process from the aggregate. However, as emphasized before, the aim of this work is to demonstrate that particle asymmetry and thermal nonequilibrium can result in unusual phoretic behavior. The radiative assumptions may limit the ability to quantify the phoretic behavior, but they are not so broad as to invalidate the general conclusions of this investigation.

3.3. Numerical Computation

By truncating the series in Eqs. [15]–[16] after $n = N$ terms, a linear system of $2N$ equations is obtained for the expansion coefficients for each azimuth (m) mode. In matrix form, these equations are expressed

$$[\mathbf{I}]\mathbf{d}_m^{(1)} + [\mathbf{T}_m^{21}]\mathbf{d}_m^{(2)} = \mathbf{f}_m^{(1)}, \quad m = 0, 1 \quad [19]$$

$$[\mathbf{T}_m^{12}]\mathbf{d}_m^{(1)} + [\mathbf{I}]\mathbf{d}_m^{(2)} = \mathbf{f}_m^{(1)}, \quad m = 0, 1, \quad [20]$$

where $[\mathbf{I}]$ is the identity matrix, $[\mathbf{T}_m^{21}]$ and $[\mathbf{T}_m^{12}]$ are fully populated "interaction" matrices for the system 2 to 1 and system 1 to 2, respectively, and $\mathbf{d}_m^{(i)} = [D_{m0}^{(i)}, D_{m1}^{(i)}, \ldots, D_{mN}^{(i)}]$. Equations [19] and [20] can be combined to yield

$$[\mathbf{I} - \mathbf{T}_m^{21}\mathbf{T}_m^{12}]\mathbf{d}_m^{(1)} = \mathbf{f}_m^{(1)} - [\mathbf{T}_m^{21}]\mathbf{f}_m^{(2)}, \quad [21]$$

which results in an uncoupled system of N equations for $\mathbf{d}_m^{(1)}$. Upon solution of Eq. [21], $\mathbf{d}_m^{(2)}$ can be obtained directly from Eq. [20].

The quantity $[\mathbf{T}_m^{12}\mathbf{T}_m^{21}]\mathbf{d}_m^{(1)}$ represents the field at surface 1 arising from the "reflection" of the field originating from 1 off sphere 2. On a physical basis, the spectral radius of $[\mathbf{T}_m^1] \equiv [\mathbf{T}_m^{12}\mathbf{T}_m^{21}]$ must be less than unity, in that $|\mathbf{d}_m^{(1)}|^2 > |[\mathbf{T}_m^1]\mathbf{d}_m^{(1)}|^2$. Therefore, a solution of [18] and [19] can in principle be obtained from the expansion (18)

$$[\mathbf{I} - \mathbf{T}_m^1]^{-1} = [\mathbf{I}] + [\mathbf{T}_m^1] + [\mathbf{T}_m^1]^2 + [\mathbf{T}_m^1]^3 + \cdots. \quad [22]$$

The above formulation is seen to represent the multiple reflections of the field from 1 off of 2. Solution for $\mathbf{d}_m^{(1)}$ using Eq. [22] is equivalent to the *method of reflections* procedure presented in Happel and Brenner (13) for low Re hydrodynamic interactions between neighboring spheres. The convergence of Eq. [22] is very slow for touching spheres. For this situation an accurate and numerically efficient solution is obtained from solution of Eq. [21] with inversion techniques, e.g., LU decomposition (19).

The number of terms used in the series expansions of the temperature fields, N, is somewhat arbitrary. In general, this number was set simply by testing the computed phoretic velocities (discussed in the next section) for convergence. For near-equal sized spheres, typically less than 10 terms were found to be required to ensure acceptable convergence. As the sphere sizes become more disparate, convergence is increasingly slower. Around 25 terms are required for $a_1/a_2 = 4$. For the limiting case of, say, $a_1 \to \infty$ and a_2 finite, the spherical-harmonics method will break down, in that $R/a_1 \to 1$ and the addition theorem, Eq. [13], will not converge. Fortunately, the aims of this work can be obtained without considering spheres of highly dissimilar radii. Recalling assumption 3, if the spheres were of such unequal proportions as to make the method unsuitable for numerical computations, then the Knudsen number of the smaller sphere would invalidate the near-continuum assumption, or the size of the larger sphere would be such to take the model out of the realm of aerosol physics.

4. HYDRODYNAMIC ANALYSIS

4.1. Solution of the Creeping Flow Equation

Assuming Re $\ll$ 1, conservation of fluid momentum reduces to the "creeping-flow" form, i.e.,

$$\nabla^2 \mathbf{v} = \frac{1}{\eta} \nabla P, \qquad [23]$$

where $\mathbf{v}$, η, and P are the velocity vector, dynamic viscosity, and pressure of the fluid, respectively. Using the above equation along with total mass conservation, the solution for the velocity field in spherical coordinates can be obtained in terms of solid spherical harmonics (20). Using the notation of Happel and Brenner (13), the solution is

$$\mathbf{v} = \sum_{n=0}^{\infty} \left(\nabla \times [\mathbf{r}\chi_{-(n+1)}] + \nabla \phi_{-(n+1)} - \frac{n-2}{2n(2n-1)} \nabla [r^2 p_{-(n+1)}] + \frac{1}{n} \mathbf{r} p_{-(n+1)} \right). \qquad [24]$$

where, for the problem at hand, the solid spherical harmonics $\chi_{-(n+1)}$, $\phi_{-(n+1)}$, and $p_{-(n+1)}$ are expressed

$$\phi_{-(n+1)} = \zeta^{-(n+1)} (A_{0n} P_n(\mu) + A_{1n} P_n^1(\mu) \cos \varphi) \qquad [25]$$

$$p_{-(n+1)} = \zeta^{-(n+1)} (B_{0n} P_n(\mu) + B_{1n} P_n^1(\mu) \cos \varphi) \qquad [26]$$

$$\chi_{-(n+1)} = \zeta^{-(n+1)} C_{1n} P_n^1(\mu) \sin \varphi. \qquad [27]$$

For reasons which will become obvious later, the normalized velocity $\bar{\mathbf{v}}$ is defined $\bar{\mathbf{v}} = \mathbf{v}a/\nu$, where ν is the momentum diffusivity (kinematic viscosity). The boundary condition, from which the expansion coefficients A_{mn}, B_{mn}, and C_{mn} are obtained, is basically that the velocity is prescribed on the surface of each sphere, i.e.,

$$(\bar{\mathbf{v}} - c_m \mathrm{Kn} \sigma_t)_{\zeta_i = 1} = \bar{\mathbf{U}}_i(\mu_i, \varphi), \quad i = 1, 2, \qquad [28]$$

where $\bar{\mathbf{U}}_i(\mu_i, \varphi)$ is the specified normalized velocity field on the surface, c_m is the momentum exchange coefficient, and σ_t is the normalized tangential stress vector, given in component form by

$$\sigma_t(\zeta, \mu, \varphi) = \left(\frac{1}{\zeta} \frac{\partial \bar{v}_r}{\partial \theta} + \zeta \frac{\partial}{\partial \zeta} \frac{\bar{v}_\theta}{\zeta} \right) e_\theta + \left(\frac{1}{\zeta \sin \theta} \frac{\partial \bar{v}_\zeta}{\partial \varphi} + \zeta \frac{\partial}{\partial \zeta} \frac{\bar{v}_\varphi}{\zeta} \right) e_\varphi. \qquad [29]$$

The tangential stress term accounts for the "velocity slip" at the surface of the sphere. For complete momentum accommodation, the value of c_m has been given as 1.13 (5).

The procedure for determining the solution valid for the two-sphere system is analogous to that used in the conduction analysis. The velocity field is constructed from components written in terms of the coordinates about each sphere, i.e.,

$$\bar{\mathbf{v}} = \bar{\mathbf{v}}_1(\zeta_1, \theta_1, \varphi) + \bar{\mathbf{v}}_2(\zeta_2, \theta_2, \varphi). \qquad [30]$$

The expansion coefficients for $\mathbf{v}_1$ and $\mathbf{v}_2$ will be denoted by $A_{mn}^{(1)}$, $B_{mn}^{(1)}$, $C_{mn}^{(1)}$ and $A_{mn}^{(2)}$, $B_{mn}^{(2)}$, $C_{mn}^{(2)}$, respectively. The procedure developed by Brenner (21) is used to solve for the coefficients from the boundary condition. Three equations are needed, about each sphere, to solve for the expansion coefficients. Instead of simply matching the normal and tangential components of Eq. [26] (which will not yield equations that can utilize the orthogonality properties of spherical harmonics), the boundary conditions at sphere i are written as

$$\mathbf{e}_{ri} \cdot (\bar{\mathbf{v}}_1 + \bar{\mathbf{v}}_2)_{\zeta_i = 1} = \mathbf{e}_{ri} \cdot \bar{\mathbf{U}}_i = \sum_{n=0}^{\infty} (X_{0n}^{(i)} P_n(\mu_i) + X_{1n}^{(i)} P_n^1(\mu_i) \cos \varphi) \qquad [31]$$

$$-\zeta_i \nabla \cdot (\bar{\mathbf{v}}_1 + \bar{\mathbf{v}}_2 - c_m \mathrm{Kn}_i (\sigma_{t1} + \sigma_{t2}))_{\zeta_i = 1} = -\zeta_i \nabla \cdot \bar{\mathbf{U}}_i = \sum_{n=0}^{\infty} (Y_{0n}^{(i)} P_n(\mu_i) + Y_{1n}^{(i)} P_n^1(\mu_i) \cos \varphi) \qquad [32]$$

$$\mathbf{e}_{ri}\zeta_i \cdot \nabla \times (\bar{\mathbf{v}}_1 + \bar{\mathbf{v}}_2 - c_m \mathrm{Kn}_i(\sigma_{t1} + \sigma_{t2})_{\zeta_i=1} = \mathbf{e}_{ri}\zeta_i \cdot \nabla \times \bar{\mathbf{U}}_i = \sum_{n=0}^{\infty} Z_{in}^{(i)} P_n^1(\mu_i)\sin\varphi. \quad [33]$$

The expansion coefficients $X_{mn}^{(i)}$, $Y_{mn}^{(i)}$, and $Z_{mn}^{(i)}$, $m = 0, 1$, are specified from the particular nature of the velocity field at the surface of each sphere.

The operation of the vector functions in Eqs. [31]–[33] upon the solution for $\bar{\mathbf{v}}$, Eq. [24], will yield results in terms of surface spherical harmonics and is discussed in Brenner (21) and Jeffrey and Onishi (22). The term corresponding to the tangential stress vector σ_t in Eq. [32] can be written

$$-\zeta\nabla \cdot \sigma_t(\zeta = 1) = -\left(\frac{1}{\sin\theta}\frac{\partial}{\partial\theta}\sin\theta\frac{\partial}{\partial\theta} + \frac{1}{\sin^2\theta}\frac{\partial^2}{\partial\varphi^2}\right) \times \bar{v}_r(\zeta = 1) + \left\{\frac{\partial}{\partial\zeta}\frac{1}{\zeta\sin\theta} \times \left(\frac{\partial}{\partial\theta}\sin\theta\bar{v}_\theta + \frac{\partial\bar{v}_\varphi}{\partial\varphi}\right)\right\}_{\zeta=1}, \quad [34]$$

which can be put in a form involving surface spherical harmonics through use of Legendre's equation and the total mass conservation equation. In Eq. [33], the tangential stress term is

$$\mathbf{e}_r\zeta \cdot \nabla \times \sigma_t(\zeta = 1) = \left(\frac{\partial}{\partial\zeta}(\mathbf{e}_r \cdot \nabla \times \bar{\mathbf{v}})\right)_{\zeta=1}. \quad [35]$$

which again only involves surface spherical harmonics.

The formulation of the system of equations for the velocity expansion coefficients is considerably more involved than that for the conduction equation. To construct these equations from Eqs. [24]–[35], it is necessary to employ the following geometrical relations;

$$\mathbf{e}_{r2}\zeta_2 = \mathbf{e}_{r1}\left(\frac{a_1}{a_2}\zeta_1 - \frac{R}{a_2}\cos\theta_1\right) + \mathbf{e}_{\theta 1}\frac{R}{a_2}\sin\theta_2 \quad [36]$$

$$\zeta_2^2 = \left(\frac{a_1}{a_2}\right)^2\zeta_1^2 + \left(\frac{R}{a_2}\right)^2 - 2\frac{a_1}{a_2}\frac{R}{a_2}\zeta_1\cos\theta_1, \quad [37]$$

and the recurrence relations for Legendre functions;

$$(2n + 1)\cos\theta P_n^m(\cos\theta) = (n - m + 1) \times P_{n+1}^m(\cos\theta) + (n + m)P_{n-1}^m(\cos\theta) \quad [38]$$

$$\sin\theta\frac{dP_n^m(\cos\theta)}{d\theta} = n\cos\theta P_n^m(\cos\theta) - (n + m)P_{n-1}^m(\cos\theta). \quad [39]$$

Using the above along with the addition theorems given in Eqs. [13] and [14], and after a considerable amount of algebra, the following equations for the velocity expansion coefficients about sphere 1 can be obtained;

$$2(n + 1)(1 + (2n + 1)c_m\mathrm{Kn}_1)A_{mn}^{(1)} + \left(\frac{R}{a_1}\right)^{-n}\sum_{\nu=1}^{\infty}(-1)^{m+\nu}\binom{n+\nu}{n+m} \times \left(\frac{R}{a_2}\right)^{-(\nu+1)}\left\{n(2n-1)A_{m\nu}^{(2)} + \left(\frac{a_1}{a_2}\right)^2\left(\frac{n(2n+1)}{2(2n+3)}(1 - 2c_m\mathrm{Kn}_1) + \frac{2m^2[n(2-\nu) + 2\nu - 1] - n\nu[n(2\nu-1) + 2 - \nu]}{2\nu(2\nu-1)(n+\nu)}\left(\frac{R}{a_1}\right)^2\right)B_{m\nu}^{(2)} - m(2n-1)\left(\frac{R}{a_2}\right)C_{m\nu}^{(2)}\right\} = [n + 2(n^2 - 1)c_m\mathrm{Kn}_1]X_{mn}^{(1)} + Y_{mn}^{(1)} \quad [40]$$

$$\frac{n+1}{2n-1}(1+(2n+1)c_m\mathrm{Kn}_1)B_{mn}^{(1)}+\left(\frac{R}{a_1}\right)^{-n}\sum_{\nu=1}^{\infty}(-1)^{m+\nu}\binom{n+\nu}{n+m}\left(\frac{R}{a_2}\right)^{-(\nu+1)}$$

$$\times\left\{n(2n+1)(1+2c_m\mathrm{Kn}_1)A_{m\nu}^{(2)}+\left(\frac{a_1}{a_2}\right)^2\left(\frac{n}{2}+(2n+1)(1+2c_m\mathrm{Kn}_1)\right.\right.$$

$$\left.\times\frac{2m^2[n(2-\nu)+2\nu-1]-n\nu[n(2\nu-1)+2-\nu]}{2\nu(2\nu-1)(2n-1)(n+\nu)}\left(\frac{R}{a_1}\right)^2\right)B_{m\nu}^{(2)}-m(2n+1)$$

$$\left.\times(1+2c_m\mathrm{Kn}_1)\left(\frac{R}{a_2}\right)C_{m\nu}^{(2)}\right\}=(n+2)(1+2nc_m\mathrm{Kn}_1)X_{mn}^{(1)}+Y_{mn}^{(1)} \quad [41]$$

$$n(n+1)(1+(n+2)c_m\mathrm{Kn}_1)C_{mn}^{(1)}+[1-(n-1)c_m\mathrm{Kn}_1]\left(\frac{R}{a_1}\right)^{-n}$$

$$\times\sum_{\nu=1}^{\infty}(-1)^{m+\nu}\binom{n+\nu}{n+m}\left(\frac{R}{a_2}\right)^{-(\nu+1)}\left(\frac{a_1}{a_2}\right)\left\{\frac{m}{\nu}\left(\frac{R}{a_2}\right)B_{m\nu}^{(2)}-n\nu C_{m\nu}^{(2)}\right\}=Z_{mn}^{(1)}. \quad [42]$$

When the above equations are written in terms of sphere 2, the subscripts and superscripts denoting spheres 1 and 2 are exchanged, the term $(-1)^{\nu+m}$ is replaced with $(-1)^{n+m}$, and the signs of the $C_{m\nu}$ terms in Eqs. [40]–[41] and the $B_{m\nu}$ term in Eq. [42] are changed. For the zero-slip situation (Kn = 0), Eqs. [40]–[42] reduce exactly to the form presented by Jeffrey and Onishi (22).

Once the boundary conditions (which will be discussed in a subsequent section) are specified the solution procedure for the velocity expansion coefficients is identical to that used in the conduction analysis. The series are truncated after $n = N$ terms, and a system of $(m+2)\cdot N$ linear equations in the form of Eq. [21] is obtained for the expansion coefficients for each azimuth mode.

The hydrodynamic force and torque acting upon each sphere can be obtained directly from the expansion coefficients. The force is conveniently resolved into components acting in the z- and x-directions, and the torque is directed along the y-axis. For the velocity nondimensionalization used here, the force and torque are (21)

$$F_z^{(i)}=-4\pi\rho\nu^2B_{01}^{(i)} \quad [43]$$

$$F_x^{(i)}=-4\pi\rho\nu^2B_{11}^{(i)} \quad [44]$$

$$T_y^{(i)}=-8\pi\rho\nu^2a_iC_{11}^{(i)} \quad i=1,2. \quad [45]$$

4.2. *Thermal Slip and Fluid Resistance*

To characterize the phoretic motion of the particle through the fluid, it is first necessary to solve the hydrodynamic equations with the thermal slip boundary conditions. The nondimensional velocity due to thermal slip at the surface of a sphere can be written

$$\tilde{\mathbf{U}}_T(\theta,\varphi)=c_s(\mathbf{1}-\mathbf{e}_r\mathbf{e}_r)\nabla\tilde{T}_g(\zeta=1,\theta,\varphi), \quad [46]$$

where the subscript T denotes thermal slip and **1** represents the unit tensor. The coefficient of thermal slip c_s has a value, for perfect momentum accommodation, of about 1.14 (5). When put into the form of Eqs. [31]–[33], the boundary condition expansion coefficients are

$$X_{mn,\mathrm{T}}^{(1)}=0, \quad \text{all } m,n. \quad [47]$$

$$Y_{mn,\mathrm{T}}^{(1)}=n(n+1)c_s\left\{D_{mn}^{(1)}+\left(\frac{R}{a_1}\right)^{-n}\right.$$

$$\left.\times\sum_{\nu=0}^{\infty}(-1)^{\nu+m}\binom{n+\nu}{n+m}\left(\frac{R}{a_2}\right)^{-(\nu+1)}D_{m\nu}^{(2)}\right\} \quad [48]$$

$$Z_{mn,\mathrm{T}}^{(1)}=0, \quad \text{all } m,n. \quad [49]$$

In Eq. [48], $D_{mn}^{(1)}$ and $D_{m\nu}^{(2)}$ refer to the expansion coefficients for the gas temperature, Eqs. [9] and [10]. For sphere 2, the sub- and superscripts 1 and 2 in Eq. [48] are exchanged, and the term $(-1)^{\nu+m}$ is replaced by $(-1)^{n+m}$.

Using the above boundary conditions, solution of Eqs. [40]–[42] for the velocity expansion coefficients will yield, via Eqs. [43]–[45], the forces and torque acting on each sphere due to thermal slip. The net thermal-slip force acting on the two-sphere particle is simply the vector sum of the individual sphere forces, i.e.,

$$F_{z,\mathrm{T}} = F_{z,\mathrm{T}}^{(1)} + F_{z,\mathrm{T}}^{(2)} \qquad [50]$$

$$F_{x,\mathrm{T}} = F_{x,\mathrm{T}}^{(1)} + F_{x,\mathrm{T}}^{(2)}. \qquad [51]$$

The net torque in the y-direction at a point a distance z from sphere 1 is due to the torques arising from fluid rotation about the separate spheres and the moment created by the x-directed forces and the distances from the spheres to point z. The net torque due to thermal slip, $T_{y\mathrm{T}}(z)$, is thus

$$T_{y\mathrm{T}}(z) = -zF_{x\mathrm{T}}^{(1)} + (R - z)F_{x\mathrm{T}}^{(2)} + T_{y,\mathrm{T}}^{(1)} + T_{y,\mathrm{T}}^{(2)}. \qquad [52]$$

Thermal slip provides the "motor" to propel the aggregate through the fluid. To compute the resulting velocity and rotation rate of the aggregate, the fluid resistance characteristics of the aggregate as it moves and rotates through the gas are required. This involves determination of the translational resistance components in the z- and x-directions, the center of hydrodynamic stress, and the rotational resistance about the y-axis.

The *translational* resistance components, denoted $f_{z,v}$ and $f_{x,v}$, characterize the drag due to the translation, without rotation, of the aggregate through the gas. They are defined by

$$f_{z,v} = \frac{F_{z,v}}{V_z} \qquad [53]$$

$$f_{x,v} = \frac{F_{x,v}}{V_x}, \qquad [54]$$

where $F_{z,v}$ and $F_{x,v}$ are the components of drag experienced due to velocities V_z and V_x, respectively. Using the reference velocity normalization ν/a, the boundary condition expansion coefficients for motion of the aggregate in the z and x directions become

$$X_{0n,v}^{(i)} = \begin{cases} V_z a_i/\nu, & n = 1 \\ 0, & n \neq 1 \end{cases} \qquad [55]$$

$$X_{1n,v}^{(i)} = \begin{cases} V_x a_i/\nu, & n = 1 \\ 0, & n \neq 1 \end{cases} \qquad [56]$$

$$Y_{mn,v}^{(i)} = Z_{mn,v}^{(i)} = 0, \quad \text{all } m, n, \qquad [57]$$

where $i = 1, 2$. The velocities V_z and V_x are taken in the computations to be unity.

The center of hydrodynamic stress $\mathbf{r}_c$ is the point located such that a force acting through this point will not produce a net torque upon the body (13). By virtue of the symmetry of the aggregate to planes passing through the z-axis, $\mathbf{r}_c$ must be located along the z-axis. Referring to Fig. 2, the distance of $\mathbf{r}_c$ from the center of sphere 1 is denoted z_c. Translation of the aggregate in the x-direction will result in a y-directed torque about each sphere, denoted $T_{yv}^{(1)}$ and $T_{yv}^{(2)}$, due to fluid rotation about the sphere. Because the two spheres are assumed to be rigidly connected, the drag force $F_{xv}^{(2)}$ will also produce a y-directed torque about the center of sphere 1 equal to $R \cdot F_{xv}^{(2)}$, and likewise for $F_{xv}^{(1)}$. The center of hy-

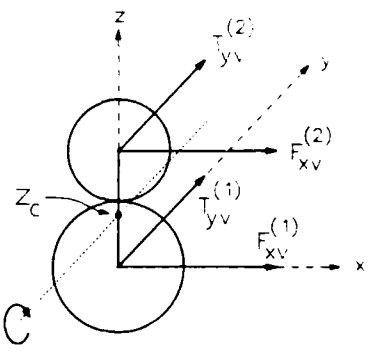

FIG. 2. Hydrodynamic parameters force F_x, torque T_{yv}, center of hydrodynamic stress z_c, and rotation rate ω.

drodynamic stress, z_c, is the point where all of these torques vanish, and is thus given by

$$z_c = \frac{RF_{xr}^{(2)} + T_{yr}^{(1)} + T_{yr}^{(2)}}{F_{xr}^{(1)} + F_{xr}^{(2)}}. \quad [58]$$

Characterization of the *rotational* resistance involves solution of the hydrodynamic equations for rotation of the aggregate about an axis parallel to the y-axis and passing through z_c. Such a rotation would produce no net hydrodynamic force upon the aggregate. Denoting the angular velocity of the aggregate about z_c by ω (Fig. 2), each sphere will undergo the rotation ω along with a translational velocity in the x-direction of $V_{x\omega}^{(1)} = -z_c\omega$ and $V_{x\omega}^{(2)} = (R - z_c)\omega$. Since the z-axis is always taken to be along the line of centers between the two spheres, the spheres experience no z-directed translation due to rotation about z_c. The boundary condition expansion coefficients for this case are

$$X_{0n,\omega}^{(1)} = X_{0n,\omega}^{(2)} = 0 \quad [59]$$

$$X_{1n,\omega}^{(1)} = \begin{cases} -z_c a_1 \omega/\nu, & n = 1 \\ 0, & n \neq 1 \end{cases} \quad [60]$$

$$X_{1n,\omega}^{(2)} = \begin{cases} (R - z_c) a_2 \omega/\nu, & n = 1 \\ 0, & n \neq 1 \end{cases} \quad [61]$$

$$Y_{mn,\omega}^{(1)} = Y_{mn,\omega}^{(2)} = 0, \quad \text{all } m, n \quad [62]$$

$$Z_{1n,\omega}^{(i)} = \begin{cases} 2a_i^2\omega/\nu, & n = 1, \\ 0, & n \neq 1, \end{cases} \quad i = 1, 2. \quad [63]$$

Solution of the hydrodynamic equations for the above boundary conditions will yield the force $F_{x\omega}$ and torque $T_{y\omega}$ on each sphere due to the rotation rate ω. As was the case for the translational resistances, ω is taken to be unity in the computations. The rotational resistance $f'_{y\omega}$, defined as the net torque on the aggregate resulting from a unit rotation rate about z_c, is given by

$$\omega f'_{y\omega} = -z_c F_{x\omega}^{(1)} + (R - z_c) F_{x\omega}^{(2)} + T_{y\omega}^{(1)} + T_{y\omega}^{(2)}. \quad [64]$$

Having characterized the resistance characteristics of the aggregate, the thermal-phoretic velocities in the z- and x-directions and the rotation rate about the y-axis can be obtained. Realizing that the net force and torque due to thermal slip and fluid resistance must be zero, the above quantities are

$$V_{zT} = \frac{F_{zT}}{f_{zv}} \quad [65]$$

$$V_{xT} = \frac{F_{xT}}{f_{xv}} \quad [66]$$

$$\omega_{yT} = \frac{T_{yT}(z_c)}{f'_{y\omega}} = \frac{1}{f'_{y\omega}} (-z_c F_{xT}^{(1)} + (R - z_c) F_{xT}^{(2)} + T_{yT}^{(1)} + T_{yT}^{(2)}). \quad [67]$$

The formulation of the hydrodynamic problem and the numerical computational scheme were tested by comparing the translational resistance behavior with previously published results obtained from the exact bipolar coordinate system method. The quantities used in the comparisons were the correction factors to Stokes drag, Ω_z and Ω_x, defined by

$$F_{zv} = 6\pi\eta a V_z \left(\frac{1 + 2c_m\mathrm{Kn}}{1 + 3c_m\mathrm{Kn}}\right)\Omega_z. \quad [68]$$

For particles in the continuum (i.e., $\mathrm{Kn} \to 0$) regime, the bipolar coordinate system method has been applied to the cases of equal-sized spheres moving parallel to the spheres line of centers (11) and perpendicular to the line of centers (12). The velocity-slip case ($\mathrm{Kn} < 0.1$) has been investigated for motion of equal spheres parallel to their line of centers (23). In all cases the bipolar coordinate system method results and the spherical-harmonics method results were in agreement to five digits. Ten to fifteen terms were required in the velocity expansion to achieve this accuracy.

5. RESULTS

5.1. Thermal-Phoretic Velocity Due to Thermal Nonequilibrium

Examined in this section is the aggregate thermal-phoretic motion in the absence of an

external temperature gradient. The motion is body-fixed in nature (i.e., directed along the aggregate axis) and arises solely from gas/particle thermal nonequilibrium induced by radiative transfer. The phoretic motion predicted in this situation could be classified as a form of photophoresis—since radiative emission/absorption is the "driving force" behind gas/particle thermal nonequilibrium—but will be referred to as thermal-phoresis to emphasize that the driving force need not be radiative in nature.

Results for the body-fixed thermal-phoretic velocity, denoted V_{zb} and calculated for spheres that are identical except for their size, are presented in Fig. 3. The velocities are given as a function of a_1/a_2, with the parameters $\mathrm{Kn}_1 = 0.1$, $\kappa_1 = \kappa_2 = 0.05$, $T_{env} = 1000$ K, and $\epsilon_1 = \epsilon_2 = 1$. The bulk gas temperature T_0 takes on the values 1500, 1800, and 2100 K, and the pressure is constant at one atmosphere.

The thermal-phoretic velocity is zero for $a_1/a_2 = 1$ and, depending upon T_0, attains a maximum value between 0.1 and 0.5 cm/s for a_1/a_2 equal to around 0.5. For a_1/a_2 less than 0.1, V_{zb} is nearly zero. The direction of motion is positive (i.e., directed toward the larger sphere). This is intuitively reasonable because, for radiative cooling ($T_0 > T_{env}$), the larger sphere will be at a lower relative temperature, and one would assume that the slip flow from the colder to the hotter sphere would drive the particle in the direction of the larger (colder) sphere.

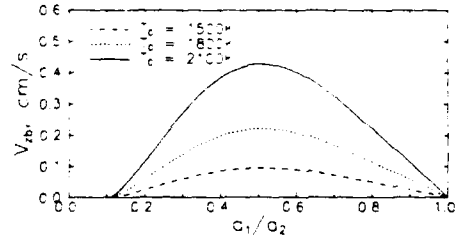

FIG. 3. Body-fixed thermal-phoretic velocity V_{zb} vs sphere radii ratio a_1/a_2, for emissivity $\epsilon_1 = \epsilon_2 = 1$. Sphere 1 Knudsen number $\mathrm{Kn}_1 = 0.1$, gas temperatures $T_0 = 1500$, 1800, and 2100 K, radiation environment temperature $T_{env} = 1000$ K, gas/particle thermal conductivity ratio $\kappa_1 = \kappa_2 = 0.05$, pressure $P = 1$ atm.

Examination of the temperature and velocity fields, however, reveals that the actual situation is considerably more complicated. Presented in Figs. 4–6 are gas and particle isotherms and the stream functions for thermal-slip induced flow, calculated for the equal sphere emissivity case given in Fig. 3 and with $a_1/a_2 = 1.0$, 0.5, and 0.25. The stream function Ψ, which is only definable for axisymmetric cases (i.e., the situation where $g_x = 0$), is given by $\Psi = \Psi^{(1)} + \Psi^{(2)}$, with (13)

$$\Psi^{(i)}(\zeta_i, \theta_i) = \sum_{n=1}^{\infty} \frac{n+1}{2n+1} \zeta_i^{-(n-2)} \times \left(\frac{1}{2(2n-1)} B_{0n}^{(i)} - \zeta_i^{-2} A_{0n}^{(i)} \right) \times (P_{n+1}(\mu_i) - P_{n-1}(\mu_i)), \quad [69]$$

where B_{0n} and A_{0n} are the velocity expansion coefficients obtained from solution of Eqs. [40]–[41] with $m = 0$ and thermal-slip boundary conditions (Eqs. [47]–[49]).

Figures 4–6 indicate that the minimum in the surface temperature occurs in the vicinity of the contact point. Fluid is drawn into this point from regions perpendicular to the aggregate axis, and is "pumped" out both ends of the aggregate. Each sphere is thus "pushed" against its neighbor by the fluid motion. If the spheres were separated this action would draw the spheres together—which would have significant consequences on *particle coagulation rates* (24, 25). The overall motion of the aggregate, however, is governed by the vector sum of the forces on the spheres. In Fig. (4), where the spheres are identical, the forces are equal in magnitude and opposite in direction—resulting in a zero net force upon the aggregate.

Unequal sphere radii produce an asymmetrical flow (Figs. 5 and 6), leading to a net force upon the aggregate. For the particular case chosen, the competition of forces is such that the aggregate moves toward the larger sphere. However, for spheres that are identical except for their size, the *relative* differences in the predicted thermal slip forces between the

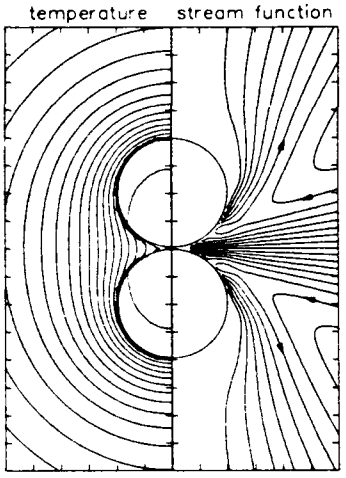

FIG. 4. Isotherms and stream function contours corresponding to Fig. 3 for $a_1/a_2 = 1$, $T_0 = 1800$ K.

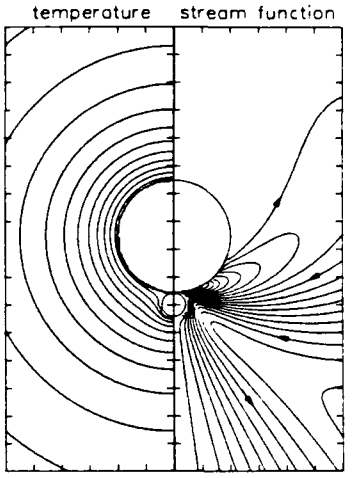

FIG. 6. Isotherms and stream function contours corresponding to Fig. 3 for $a_1/a_2 = 0.25$.

spheres are very small—on the order of 1%. Because the forces are only slightly out of balance, factors which have been neglected in this analysis (such as the distribution of radiant absorption within the spheres) may significantly influence the overall motion of the aggregate.

Particle asymmetry due to differences in the radiative properties of the individual spheres appears to have a more significant effect in determining the direction and magnitude of phoretic motion than asymmetry due to size disparity. Presented in Fig. 7 are thermal-phoretic velocities in which ϵ_2 is fixed at 0.5 and ϵ_1 varies between 0 and 1, with $a_1/a_2 = 1$, 0.5, and 0.25, and $T_0 = 1800$ K. Figure 7 indicates that, for the particular parameters chosen, the direction of aggregate motion is dependent mainly upon the difference in the spheres emissivity. The velocities are also considerably larger than obtained for equal-emissivity spheres.

The dependence of V_{zb} to ϵ_1 is nearly linear, which is to be expected. The force experienced by each sphere due to thermal slip is proportional to the magnitude of the gas temperature

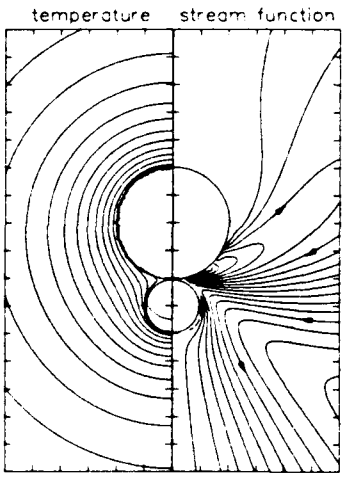

FIG. 5. Isotherms and stream function contours corresponding to Fig. 3 for $a_1/a_2 = 0.5$.

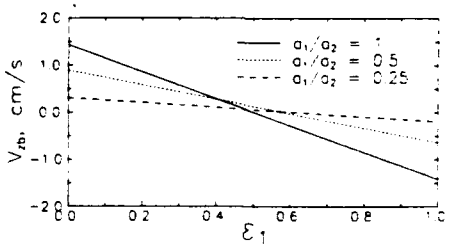

FIG. 7. Body-fixed thermal-phoretic velocity V_{zb} *vs sphere 1 emissivity* ϵ_1, for $a_1/a_2 = 1$, 0.5, and 0.25. Sphere 2 emissivity $\epsilon_2 = 0.5$, $T_0 = 1800$ K, $\kappa_1 = \kappa_2 = 0.05$, $T_{env} = 1000$ K, $P = 1$ atm.

gradient on the sphere's surface. Equation [15] indicates that the gradient "seen" by the spheres is proportional to J_0 (and, accordingly, ϵ) of each sphere. It should be noted, however, that thermal and hydrodynamic interactions between the spheres have a significant effect upon the overall magnitude of the phoretic velocities. Calculations of phoretic velocities in which the thermal and/or hydrodynamic interactions had been neglected (by deleting the summation terms in Eqs. [15], [40], and [41]) produced results appreciably different (typically an order of magnitude greater) than those presented in the previous figures.

Isotherms and stream functions are presented in Fig. 8 for an aggregate having $\epsilon_1 = 0$, $\epsilon_2 = 1$, and $a_1/a_2 = 1$. Extrema in the surface temperature occur in this case only at the ends of the aggregate. The thermal-slip-driven flow is directed from sphere 2 to sphere 1, and the resulting direction of the aggregate motion is unambiguous.

The behavior of V_{zb} vs Kn_1 for fixed a_1/a_2 is presented in Fig. 9. Two sets of curves are presented, corresponding to $\epsilon_1 = 1$ and $\epsilon_1 = 0$, respectively, with $a_1/a_2 = 1$, 0.5, and 0.25 within each set. The ambient temperature T_0 is 1800 K, $\epsilon_2 = 1$, and the remaining parameters are the same as in Fig. (3).

The Kn dependence upon phoretic velocity is seen to be similar to that predicted from the near-continuum analysis of conventional, space fixed thermophoresis and photophoresis (5, 8), in that V_{zb} increases with increasing Kn_1. The velocities predicted for equal sphere emissivities go to zero in the continuum ($\mathrm{Kn}_1 \to 0$) limit (and also go through an interesting reversal in direction), while the nonequal emissivity velocities attain a nonzero constant value in this limit. Additional calculations revealed that the dependence of V_{zb} upon conductivity ratio κ is equally similar in that V_{zb} goes to zero in the continuum regime for highly conductive ($\kappa \to 0$) particles.

In high-temperature environments such as large-scale combustors, the body-fixed thermal-phoretic velocities for micrometer-sized aggregates presented in the previous figures

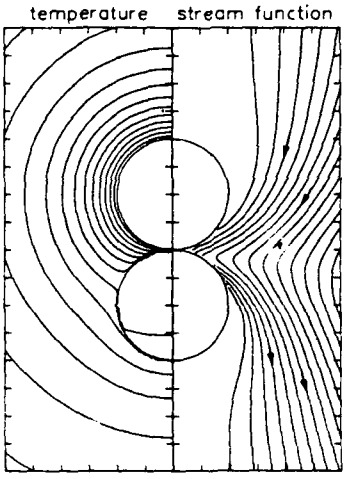

FIG. 8. Isotherms and stream function contours for $\epsilon_1 = 0$, $\epsilon_2 = 1$, $a_1/a_2 = 1$, and the parameters corresponding to Fig. 7.

will be comparable to those associated with conventional, space-fixed thermophoresis and photophoresis (26, 8). However, in the absence of external forces that align the aggregate in space, the body-fixed and space-fixed phoretic mechanisms will yield distinctly different transport behavior of the aggregate. The motion of a cloud of particles acted upon by the latter mechanism will be *deterministic* in that all the particles will be displaced in the same direction. The motion resulting from the former mechanism will always be directed along the aggregate axis. Considering that Brownian rotation will act to randomize the aggregate orientation, the displacement of the aggregate will be *stochastic* in nature. A cloud of particles undergoing this motion would thus appear to an observer to be diffusing.

An estimate of the "effective" diffusion coefficient resulting from body-fixed thermal-phoresis can be obtained from a simple order-of-magnitude analysis. Assume that the aggregate rotates about the y-axis a small angle $\Delta\theta$ in a time step Δt. The mean-square displacement of the aggregate, $\bar{z}^2$, during this time step will be aproximately $(V_{zb}\Delta t)^2$. The effective diffusion coefficient, defined by $D_{\mathrm{eff}} = \bar{z}^2/\Delta t$, would thus be equal to $V_{zb}^2 \Delta t$. The time step

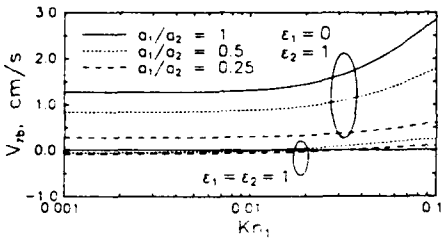

FIG. 9. Body-fixed thermal-phoretic velocity V_{zb} *vs sphere 1 Knudsen number* Kn_1, for $\epsilon_1 = 1$ and $\epsilon_1 = 0$. Radius ratio $a_1/a_2 = 1$, 0.5, and 0.25, $\epsilon_2 = 1$. Other parameters same as Fig. 7.

Δt can be approximated by $1/D_{rot}$, where D_{rot} is the Brownian rotational diffusion coefficient for rotation perpendicular to the aggregate axis. Therefore, the effective diffusion coefficient is

$$D_{eff} = \frac{V_{zb}^2}{D_{rot}}. \qquad [70]$$

The Brownian rotational coefficient can be estimated from equipartition of energy considerations (27) as $D_{rot} = k_B T_0 / f'_{y\omega}$, where k_B is Boltzmann's constant and $f'_{y\omega}$ is the rotational resistance function defined by Eq. [67].

The analysis presented above for the effective "Brownian" diffusion coefficient is at best a zeroth-order approximation, but likely represents the proportionality of D_{eff} to V_{zb} and D_{rot}. Numerical results for D_{eff}, normalized with ν, are presented in Fig. 10 as a function of a_1 with $a_1/a_2 = 0.5$, for the same parameters as in Fig. (9). Also included are results for the translational Brownian diffusion coefficient computed for a sphere having the same volume as the aggregate. As opposed to Brownian diffusion, effective diffusion resulting from body-fixed thermal-phoretic motion *increases* with particle size. For supermicrometer particles D_{eff} is seen to be several orders of magnitude greater than the Brownian counterpart. This behavior, which will be magnified at higher temperatures, could have important consequences on the particle deposition rates onto surfaces (26), as well as on the coagulation rates of particulates (27, 28), in high-gas-temperature environments.

5.2. *Thermophoretic Behavior of the Aggregate*

Investigated in this section is the behavior of the binary aggregate under the influence of a temperature gradient in the bulk gas. In presenting our results, it is convenient to introduce the thermophoretic diffusivity $\alpha_T D$, where α_T is the dimensionless thermal diffusivity factor and D is the Brownian diffusion coefficient. Thermophoretic diffusivity is defined by the equality (29)

$$\mathbf{V}_T = \alpha_T D\left(-\frac{1}{T_g}\nabla T_g\right). \qquad [71]$$

The diffusivity product $\alpha_T D$ does not actually have the same behavior as D itself. The Brownian diffusion coefficient is introduced only to conjure up the notion of thermophoresis as a "diffusion" process driven by a temperature gradient, with α_T playing the role of a dimensionless Soret (thermal diffusion) factor, as in gas diffusion (29).

In general, for nonspherical particles $\alpha_T D$ defined by Eq. [71] is in the form of a dyadic. For the binary agglomerate investigated here, however, the cross-terms of this dyadic are zero in that the component of the temperature gradient in one direction does not contribute to the thermophoretic velocity in a different direction. The two independent components of the thermophoretic diffusivity dyadic are thus denoted $(\alpha_T D)_z$ and $(\alpha_T D)_x$.

Calculations of $(\alpha_T D)_z$ and $(\alpha_T D)_x$ are per-

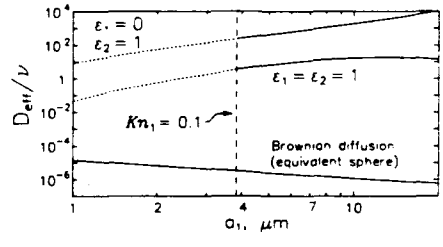

FIG. 10. Effective thermal-phoretic diffusion and Brownian diffusion coefficients, normalized with gas momentum diffusivity ν, vs sphere 1 radius a_1. Sphere 1 emissivity $\epsilon_1 = 0$ and 1, $\epsilon_2 = 1$, and $a_1/a_2 = 0.5$. Other parameters same as Fig. 7.

formed by calculating the thermophoretic velocities for unit temperature gradients in the z- and x-directions with vanishing source terms, i.e., $\epsilon_1 = \epsilon_2 = 0$. Results of the calculations appear in Fig. 11, in which the two components of $\alpha_T D$, normalized with ν, are presented vs a_1/a_2 for $\mathrm{Kn}_1 = 0.1$, $\kappa = 0.05$, and $T_0 = 1800$ K. Note that, for $a_1/a_2 \approx 1$, $(\alpha_T D)_z$ is around 10–20% larger than $(\alpha_T D)_x$. A consequence of this is that the aggregate, when aligned obliquely to the temperature gradient, will not move in precisely the same direction of the gradient. This action is somewhat analogous to the "tacking" of a sailboat against the wind. Previous investigations in this laboratory of the thermophoretic properties of a long cylindrical particle in the free-molecular regime have reported similar findings (30). For a_1/a_2 less than 0.1, the two components of the thermophoretic diffusivity become nearly equal and acquire the value of that of a single sphere having the radius of the larger particle.

It is not clear that the tacking behavior of the aggregate due to the inequality between $(\alpha_T D)_z$ and $(\alpha_T D)_x$ will be of practical importance, especially if $a_1 \neq a_2$. When the sphere radii are not equal, thermophoresis also results in a torque on the aggregate which will tend to align the aggregate with the temperature gradient. The action of the torque is such that the smaller sphere will rotate toward the downstream (or hot) end of the aggregate, and the aggregate moves in the direction of the larger sphere. The torque goes to zero as the aggregate becomes aligned with the gradient—thus the aligned orientation represents the stable configuration of the aggregate in an external temperature gradient.

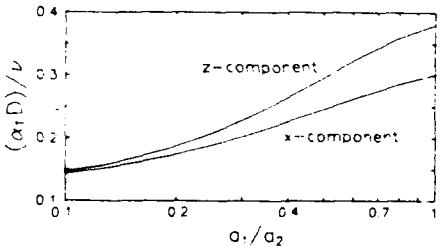

FIG. 11. Directional components of aggregate thermophoretic diffusivity $\alpha_T D$, normalized with ν, vs radius ratio a_1/a_2. Sphere 1 Knudsen number $\mathrm{Kn}_1 = 0.1$.

Of course, the orientation of the aggregate is also subject to the randomizing action of Brownian rotation caused by individual carrier gas molecular impacts. It is of interest to examine the ratio between the stabilizing thermophoretic rotation and the randomizing Brownian rotation; a ratio which can essentially be considered a *thermophoretic rotational Peclet number*, $\mathrm{Pe}_{T\omega}$. This number is defined by

$$\mathrm{Pe}_{T\omega} \equiv \frac{\omega_{yT}}{D_R} = \frac{T_{yT}(z_c)}{k_B T_0}, \qquad [72]$$

where D_R is the rotational Brownian diffusion coefficient and k_B is Boltzmann's constant. The second equality in Eq. [72] follows from the equipartition of energy theory as discussed in the previous section.

The magnitude of $\mathrm{Pe}_{T\omega}$ will reflect upon the relative degree of alignment of the aggregate with respect to the temperature gradient. For $\mathrm{Pe}_{T\omega} \gg 1$ the aggregate is completely aligned, whereas for $\mathrm{Pe}_{T\omega} \ll 1$ the aggregate will have a random orientation. For an aggregate with $a_1/a_2 = 0.5$, $\mathrm{Kn}_1 = 0.1$, and $T_0 = 1800$ K, calculations indicate that $\mathrm{Pe}_{T\omega}$ is of order unity for an external temperature gradient of around 10^4 W/m, and increases with decreasing Kn_1. Temperature gradients encountered in gas-side boundary layers adjacent to heat exchanger surfaces in large-scale combustor environments can easily exceed 10^4 W/m (26). Micrometer-sized aggregates in such environments would thus be substantially aligned with the gradient. Of course, in boundary-layer transport the highest temperature gradients will normally be found where the absolute temperature is lowest—thus strengthening this alignment tendency. In addition, the resulting biased orientation, due to thermophoresis, of aggregates depositing on a surface will have interesting implications for the *microstructure* of such deposits (31).

5.3. *Combined Body-Fixed Thermal-Phoresis and Thermophoresis*

The alignment action of space-fixed thermophoresis obviously has important consequences on the body-fixed thermal-phoretic motion of the asymmetrical binary aggregate. In a sufficiently strong external temperature gradient the body-fixed motion will become space-fixed and, depending upon the nature of the asymmetry, either add to or subtract from the thermophoretic velocity. Both cases appear equally likely because, from the discussion in Section 5.1, the direction of body-fixed thermal-phoresis is dependent more upon differences in particle radiative properties than differences in particle size. The net motion of the aggregate would be thermophoretic in nature—i.e., directed with a temperature gradient, but characterized by an anomalously large or small "apparent" thermophoretic diffusivity, as defined by Eq. [71]. Indeed, in situations where the body-fixed force is directed toward the smaller sphere and exceeds the thermophoretic force, the aggregate would move *up* the temperature gradient—resulting in a *negative* apparent thermophoretic diffusivity.

Rohatschek (9) came to somewhat similar conclusions in interpretation of experimental results in which measured photophoretic velocities of irregular particles were found to be both positive and negative (i.e., with and against the incident radiation) and three to four orders of magnitude greater than that predicted by "conventional" photophoresis. He concluded that nonuniformities in the thermal accommodation coefficient on the particle were responsible for a body-fixed force that was the dominant mode of "propulsion" of the particle through the gas. However, the conventional photophoretic force and torque, arising from nonuniform illumination of the particle, resulted in a space-fixed alignment of the particle. The body-fixed force, coupled with the alignment, resulted in the significant deterministic particle motion observed in experiment.

To illustrate the effect of body-fixed motion upon conventional thermophoresis, the "effective" thermophoretic diffusivity of an asymmetrical aggregate is presented in Fig. 12, in which $(\alpha_T D)_{eff}$ has been defined from Eq. [71], but the velocity is now taken to be the sum of the thermophoretic and body-fixed components. The results are presented as a function of T_0 for an aggregate with $a_1/a_2 = 0.5$ and the three cases of (1) $\epsilon_1 = \epsilon_2 = 1$, (2) $\epsilon_1 = 0$, $\epsilon_2 = 1$, and (3) $\epsilon_1 = 1$, $\epsilon_2 = 0$. Also given is the curve corresponding to "pure" thermophoresis, i.e., no body-fixed aggregate motion. The body-fixed phoretic motion predicted for equal sphere emissivities results in a doubling of the effective diffusivity at high temperatures. When one of the spheres is nonabsorbing (cases 2 and 3) the effect upon $(\alpha_T D)_{eff}$ is much more extreme. The body-fixed component in these cases will dominate the aggregate motion at moderate temperatures, and result in positive and negative effective diffusivities that exceed the conventional diffusivity by over an order of magnitude.

The results in Fig. 12 corresponding to an absorbing/nonabsorbing pair represent the most extreme case of aggregate asymmetry. The behavior of aggregates possessing more moderate asymmetries will fall between these two curves. Nevertheless, asymmetry due to size alone (which corresponds to the smallest degree of body-fixed motion) has, for the given

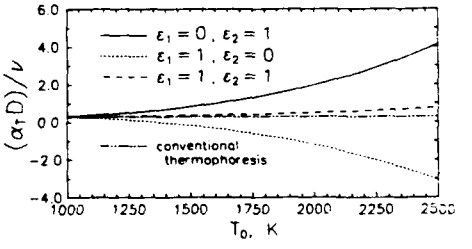

FIG. 12. Effective thermophoretic diffusivity under body-fixed aggregate motion $(\alpha_T D)_{eff}$, normalized with ν, vs gas temperature T_0, for sphere emissivities $\epsilon_1 = \epsilon_2 = 1$, $\epsilon_1 = 0$, $\epsilon_2 = 1$, and $\epsilon_1 = 1$, $\epsilon_2 = 0$. Gas temperature gradient $g_s = 10^5$ K/m, $Kn_1 = 0.1$, $a_1/a_2 = 0.5$.

conditions, a considerable effect upon the effective thermophoretic diffusivity. This behavior can have significant implications on the deposition rates of micrometer-sized, combustion-generated particles onto heat exchanger surfaces. Thermophoresis has been recognized as an important contributor to particle deposition in such situations (32). However, under the condition of gas/particle thermal nonequilibrium and heat transfer asymmetry, thermophoresis could actually impede the deposition of certain aggregates, while considerably accelerating the deposition rate of others.

6. CONCLUSIONS

The focus of this theoretical investigation has been upon the thermal-phoretic behavior of asymmetrical two-sphere aggregates in thermal nonequilibrium with the surrounding gas. Several potentially important conclusions can be drawn from this study:

(1) A mathematical method based upon spherical-harmonic expansions of the temperature and velocity fields about each sphere provides solutions to the conduction and creeping-flow equations that are in excellent agreement with exact, bipolar-coordinate-system methods. The present method has the significant advantage over the latter in that it can be extended to systems involving more than two spheres.

(2) In high-temperature environments, radiative cooling or heating of the aggregate will, in general, result in a tangential gas temperature gradient on the particle surface. The gradient will drive a slip-flow of gas over the aggregate and, for nonidentical spheres, will lead to a body-fixed thermal-phoretic motion of the aggregate through the gas. The velocities attained by micrometer-sized aggregates can be in excess of thermophoretic velocities arising from typical gas temperature gradients encountered in large-scale combustor environments.

(3) For the axisymmetric two-sphere aggregates investigated here, the action of body-fixed thermal-phoresis produces no torque upon the aggregate. In the absence of external alignment forces, the displacement of the aggregate due to body-fixed thermal-phoresis will be stochastic in nature. For micrometer-sized particles, the effective diffusion of the aggregate due to thermal-phoresis can be significantly larger than ordinary Brownian diffusion.

(4) The "conventional" thermophoretic diffusivity of the binary aggregate in the z-direction, $(\alpha_T D)_z$, can be up to 20% larger than the x-direction component. For aggregates of equal-sized spheres the direction of the thermophoretic motion will, in general, be nonparallel to the gas temperature gradient.

(5) When the sphere radii are dissimilar, thermophoresis produces a torque on the aggregate which will tend to align the aggregate such that the larger sphere is directed down the gas temperature gradient. The alignment forces produced on micrometer-sized aggregates by typical gas temperature gradients in combustors (10^5 K/m) will be significantly larger than the randomizing actions of Brownian rotation.

(6) The body-fixed thermal-phoretic velocities, coupled with the alignment action of thermophoresis, can result in positive or negative "effective" thermophoretic diffusivities with magnitudes considerably larger than conventional thermophoretic diffusivities.

This investigation indicates that the "thermal-phoretic" behavior of particles can be significantly influenced by the combination of particle asymmetry and gas/particle thermal nonequilibrium. In view of the fact that the vast majority of industrial and naturally occurring particulates possess some degree of asymmetry, the present results are likely to have important implications for the transport and deposition of such particles in high-temperature environments. Our current efforts in this field involve extension of the thermophysical model to aggregates of three or more primary spheres, and investigation of the ef-

fects on coagulation and deposition rates and deposit microstructure.

ACKNOWLEDGMENTS

It is a pleasure to acknowledge the DOE-PETC and the Yale HTCRE Laboratory Industrial Affiliates (Shell, ACVO-Lycoming, SCM-Chemicals) for the financial support which made this research and its publication possible. The author has benefited from helpful discussions with D. E. Rosner, P. L. Garcia-Ybarra, A. G. Konstandopoulous, and M. T. Tassopoulos.

REFERENCES

1. Rosner, D. E., *Phys. Fluids A (Fluid Mech.)* **1,** 1761 (1989).
2. Maxwell, J. C., *Philos. Trans. R. Soc. London* **170,** 231 (1879). See, also, "The Scientific Papers of James Clerk Maxwell," Vol. 2, p. 681. Dover, New York, 1962.
3. Waldmann, L., and Schmidt, K. H., *in* "Aerosol Science" (C. N. Davies, Ed.), Chap. 6. Academic Press, New York, 1966.
4. Brock, J. R., *J. Colloid Sci.* **17,** 768 (1962).
5. Talbot, L., Cheng, R. K., Schefer, R. W., and Willis, D. R., *J. Fluid Mech.* **101,** 737 (1980).
6. Yalamov, Yu. I., Kutukov, V. B., and Shchukin, E. R., *J. Colloid Interface Sci.* **57,** 564 (1976).
7. Akhtaruzzaman, A. F. M., and Lin, S. P., *J. Colloid Interface Sci.* **61,** 171 (1977).
8. Mackowski, D. W., *Int. J. Heat Mass Transfer* **32,** 843 (1989).
9. Rohatschek, H., *J. Aerosol Sci.* **16,** 29 (1985).
10. Morse, P. M., and Feshbach, H., "Methods of Theoretical Physics," Part II. McGraw-Hill, New York, 1953.
11. Stimson, M., and Jeffery, G. B., *Proc. R. Soc. A* **111,** 110 (1926).
12. Goldman, A. J., Cox, R. G., and Brenner, H., *Chem. Eng. Sci.* **21,** 1151 (1966).
13. Happel, J., and Brenner, H., "Low Reynolds Number Hydrodynamics." Prentice-Hall, Englewood Cliffs, NJ, 1965.
14. Jeffrey, D. J., *Proc. R. Soc. London A* **335,** 355 (1973).
15. Dusel, P. W., Kerker, M., and Cooke, D. D., *J. Opt. Soc. Amer.* **69,** 55 (1979).
16. Hobson, E. W., "The Theory of Spherical and Ellipsoidal Harmonics," Chap. 4. Cambridge Univ. Press, Cambridge 1931.
17. Fuller, K. A., and Kattawar, G. W., *Opt. Lett.* **13,** 90 (1988).
18. Atkinson, K. E. "An Introduction to Numerical Analysis," Chap. 7. Wiley, New York, 1978.
19. Press, W. H., Flannery, B. P., Teukolsky, S. A., and Vetterling, W. T., "Numerical Recipes," Chap. 2. Cambridge Univ. Press, Cambridge, 1986.
20. Lamb, H., "Hydrodynamics," Chap. 11. Dover, New York, 1945.
21. Brenner, H., *Chem. Eng. Sci.* **19,** 519 (1964).
22. Jeffrey, D. J., and Onishi, Y., *J. Fluid Mech.* **139,** 261 (1984).
23. Reed, L. D., and Morrison, F. A., Jr., *J. Aerosol Sci.* **5,** 175 (1974).
24. Mackowski, D. W., Rosner, D. E., and Tassopoulos, M., "Effect of Thermophoretic Attraction and Repulsion between Particles on Coagulation Rates." In preparation (1989).
25. Rosner, D. E., Mackowski, D. W., Tassopoulos, M., Castillo, J., and Garcia-Ybarra, P., "Effect of Heat Transfer on Small-Particle Coagulation and Transport Rates." To be presented at the Ninth International Heat Transfer Conference, Jerusalem, Israel, July 1990 (1989).
26. Rosner, D. E., and Fernandez de la Mora, J., *J. Eng. Power* **104,** 885 (1982).
27. Friedlander, S. K., "Smoke, Dust, and Haze—Fundamentals of Aerosol Behavior." Wiley, New York, 1977.
28. Park, H. M., and Rosner, D. E., *Chem. Eng. Sci.* **44,** 2225 (1989).
29. Rosner, D. E., "Transport Processes in Chemically Reacting Flow Systems." Butterworths, Stoneham, MA, 1986.
30. Garcia-Ybarra, P., and Rosner, D. E., *AIChE J.* **35,** 139 (1989).
31. Tassopoulos, M., O'Brien, J. A., and Rosner, D. E., *AIChE J.* **35,** 967 (1989).
32. Rosner, D. E., and Park, H. M., *Chem. Eng. Sci.* **43,** 2689 (1988).
33. Mackowski, D. W., and Rosner, D. E., "Contribution of Body-Fixed Phoretic Motion to Particle Deposition Rates Across Laminar Boundary Layers. In preparation (1989).

REPORT DOCUMENTATION PAGE

Form Approved
OMB No. 0704-0188

1. AGENCY USE ONLY (Leave blank)	2. REPORT DATE	3. REPORT TYPE AND DATES COVERED
	1989	Journal Publication

4. TITLE AND SUBTITLE
"Thermophoretic Properties of Nonspherical Particles and Large Molecules" (U)

5. FUNDING NUMBERS
PE - 61102F
PR - 2308
SA - BS
G -AFOSR 89-0223

6. AUTHOR(S)
Pedro Garcia-Ybarra and Daniel E. Rosner

7. PERFORMING ORGANIZATION NAME(S) AND ADDRESS(ES)
HIGH TEMPERATURE CHEMICAL REACTION ENGINEERING LABORATORY
YALE UNIVERSITY
BOX 2159, YALE STATION
NEW HAVEN, CONNECTICUT 06520 U.S.A.

8. PERFORMING ORGANIZATION REPORT NUMBER

9. SPONSORING/MONITORING AGENCY NAME(S) AND ADDRESS(ES)
AFOSR/NA
Building 410
Bolling AFB DC 20332-6448

10. SPONSORING/MONITORING AGENCY REPORT NUMBER

11. SUPPLEMENTARY NOTES

12a. DISTRIBUTION/AVAILABILITY STATEMENT
Approved for public release; distribution is unlimited

12b. DISTRIBUTION CODE

13. ABSTRACT (Maximum 200 words)

The $Kn_p \gg 1$ gas-kinetic approach of Waldmann (1959, 1961) is extended to predict the thermophoretic properties of nonspherical aerosol *particles*, and massive nonspherical gas *molecules*. Calculations are presented for sphero-cylindrical particles (molecules) of arbitrary aspect ratio, L/R, predicting that in a local temperature gradient ***grad T*** they will thermophoretically drift: i) more rapidly when their major axis is aligned with $-$***grad T***; ii) at a velocity different from that of a sphere of radius R equal to the cylinder radius; iii) at an angle with respect to $-$***grad T*** when their major axis is not parallel to, nor perpendicular to, $-$***grad T***; and iv) *without* a net torque tending to orient the particle with respect to $-$***grad T***. Important corollaries are that nonspherical particles in a temperature gradient should also experience new thermophoretically-induced coagulation mechanisms. We predict that the orientation-averaged thermal diffusion factor α_T should increase approximately linearly with particle (molecule) length.

14. SUBJECT TERMS
nonspherical particles, soot, macro-molecules, Soret effect, thermophoresis

15. NUMBER OF PAGES
9

16. PRICE CODE

17. SECURITY CLASSIFICATION OF REPORT	18. SECURITY CLASSIFICATION OF THIS PAGE	19. SECURITY CLASSIFICATION OF ABSTRACT	20. LIMITATION OF ABSTRACT
Unclassified	Unclassified	Unclassified	UL

Reprinted from AICHE JOURNAL, January 1989

Thermophoretic Properties of Nonspherical Particles and Large Molecules

The $Kn_p \gg 1$ gas-kinetic approach of Waldmann (1959, 1961) is extended to predict the thermophoretic properties of nonspherical aerosol *particles*, and massive nonspherical gas *molecules*. Calculations are presented for sphero-cylindrical particles (molecules) of arbitrary aspect ratio, L/R, predicting that in a local temperature gradient ***grad T*** they will thermophoretically drift: i) more rapidly when their major axis is aligned with $-$***grad T***; ii) at a velocity different from that of a sphere of radius R equal to the cylinder radius; iii) at an angle with respect to $-$***grad T*** when their major axis is not parallel to, nor perpendicular to, $-$***grad T***; and iv) *without* a net torque tending to orient the particle with respect to $-$***grad T***. Important corollaries are that nonspherical particles in a temperature gradient should also experience new thermophoretically-induced coagulation mechanisms. We predict that the orientation-averaged thermal diffusion factor α_T should increase approximately linearly with particle (molecule) length.

Pedro Garcia-Ybarra
Daniel E. Rosner
High Temperature Chemical Reaction Engineering Laboratory
Department Chemical Engineering
Yale University
New Haven, CT 06520

Introduction

The importance of thermal diffusion *mass* transport in gases (Soret effect for vapors, and "thermophoresis" for submicron aerosol particles) in many technologies has been recently discussed (*e.g.*, Rosner, 1980). In addition, its decisive influence on the appearance of several kinds of combustion wave instabilities has been recently studied (Garcia-Ybarra *et al.*, 1984). But in all areas, accurate predictions require a knowledge of the *thermal diffusion factor* α_T of the transported species in the prevailing gaseous mixture. Although theoretical and experimental values of the other transport coefficients are readily available in the literature (*e.g.*, Galloway and Sage, 1967) little is known about the thermal diffusion coefficient of, say, long-chain paraffin hydrocarbons and other gaseous fuels. Theoretically, the difficulty comes from the great complexity of available kinetic theory when one must take into account the "nonspherical" nature of the intermolecular potential, as well as the effects of internal degrees of freedom. Molecules of the usual fuels and adduct intermediates formed from them are complex enough to make both effects nonnegligible.

A classical kinetic theory for a gas of rigid sphero-cylinders has been elaborated by Curtiss and his coworkers (Curtiss, 1956; Curtiss and Muckenfuss, 1957; Muckenfuss and Curtiss, 1958). Based on the Wang Chang-Uhlenbeck-de Boer semiclassical treatment of polyatomic gases, expressions for the transport coefficients have been obtained (Monchick *et al.*, 1963, 1968) even for the case of slightly nonspherical molecules (Matzen and Hoffman, 1975). Nevertheless, for many practical purposes, such expressions are too complicated and a more tractable approach is needed. For spherical potentials, Fristrom and Monchick (1988) have recently suggested a phenomenological relationship to easily compute the thermal diffusion factor of molecules having internal degrees of freedom, but the case of highly nonspherical polyatomic molecules seems to be out of the realm of practical applicability *via* gas kinetic theory. The alternative pursued here is based on one used by Waldmann (1959, 1968) in problems related to aerosol *particle* diffusion. The method, initially developed to interpret Millikan's oil drop experiment (Epstein, 1924), considers the carrier gas to be in a nonequilibrium state in which the scale Λ of the thermodynamic inhomogeneities (*e.g.*, gradient of temperature) is very large compared with the gas mean-free path l. The corresponding carrier gas Knudsen number $Kn = l/\Lambda$ is a small parameter and the results of the Enskog-Chapman theory apply to the corresponding distribution function for the molecule velocities. Immersed in this carrier gas a very heavy particle is assumed to be in local thermal equilibrium with its neighborhood and to have a size R very small compared to the gas mean-free path, in such a way

P. Garcia-Ybarra is a visiting scholar, Yale HTCRE Laboratory. His permanent address is U.N.E.D. Dpto. Fisica Fundamental, Apdo.60141, Madrid 28080, Spain
Correspondence concerning this paper should be addressed to D. E. Rosner.

that the associated particle Knudsen number $Kn_p = l/(2R)$ is a *large* parameter. In these circumstances, the "hydrodynamic" (continuum) limit fails and a "free-molecule" flow approach is adopted to calculate the force on the particle by adding all of the impulses transferred to it by the colliding gas molecules. In addition, an effective spherical shape for the particle was assumed by Epstein and Waldmann and the effects arising from its complex local and internal structure were summarized in a single parameter: the fraction of the colliding molecules diffusely reflected, a. Results of this theory have been tested by comparison with the corresponding ones obtained from the kinetic theory of polyatomic gases under suitable assumptions (Mason and Chapman, 1962; Monchick *et al.*, 1963), *i.e.*, in the quasi-Lorentzian or "dusty-gas" model (Mason, 1957; Fernandez de la Mora and Mercer, 1982) and excellent agreement has been found.

A more general criterion for the applicability of Waldmann's approach and one which motivates our extensions from aerosol *particles* to heavy vapor *molecules* can be obtained by imposing the condition that the displacement of the "particle" during a time of the order of the characteristic time τ between gas/particle collisions must be small compared to its own dimensions. For the illustrative case of a large sphere of radius R, this condition is simply $V\tau \ll 2R$, V being the particle velocity. Now the mean momentum transferred to the particle per collision with the gas molecules is of the order $MV \sim (\pi/2)m\bar{c}$, where $\bar{c}$ is the mean gas molecule velocity, and M and m are the particle and molecule masses, respectively. Moreover, the time τ may be roughly estimated as $\tau \sim 4/(\pi R^2 N\bar{c})$, N being the number of molecules per unit volume. Therefore, this criterion can be written:

$$8\pi\sqrt{2}\cdot\frac{m}{M}\cdot\left(\frac{r_g}{R}\right)^2\cdot Kn_p \ll 1 \qquad (1)$$

where we used $l = (4\sqrt{2}\pi N r_g^2)^{-1}$ for the gas mean-free path, and r_g is the gas molecule radius.

With respect to particle rotations, if I is the particle moment of inertia, ω is its angular velocity and $F \cdot R$ the torque due to a collision, we have $I\omega \sim \int FR dt$ but $I \sim MR^2$ and $\int F dt \sim m\bar{c}$, then the inverse of the characteristic rotation time of the particle is given by $\omega \sim m\bar{c}/MR$. Thus, we find that criterion 1 is equivalent to $\omega\tau \ll 1$, which indicates that the particle does not appreciably rotate between successive molecular impacts. These conditions can also be satisfied for sufficiently small *nonspherical* aerosol particles and even sufficiently large vapor molecules in a "light" carrier gas. In general, the nonsphericity of a particle should play an important role in determining its transport characteristics, and it will *not* be sufficient to assume an effective spherical shape for a particle, hoping to include "nonsphericity effects" in the diffuse reflection coefficient, a. Rather, one must consider the actual overall particle shape and retain this coefficient only to account for the more localized effects of internal degrees of freedom. Fortunately, the Waldmann approach, as described below, provides the means to predict such "shape" effects.

Since we need $Kn_p \gg 1$ to use results valid in the free-molecule flow limit, condition 1 imposes an important restriction to the theory. Its range of validity can be roughly estimated from Figure 1, where we have plotted the dimensionless group appearing in Eq. 1 and the particle Knudsen number as functions of the particle size R (we have, for this illustration only, assumed spherical shapes and equal mass densities, with $r_g = 1.6$ Å for the gas molecule radius). Evidently, for the nominal conditions $p \approx 1$ atm, $T \approx 1{,}000$ K, one can expect the present theory to be valid for small particles or giant molecules in the approximate range: 10–100 Å in size.

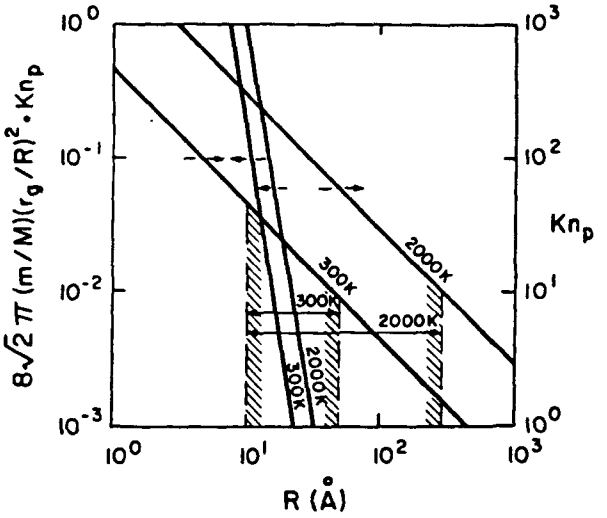

Figure 1. Knudsen number Kn_p and group $8\pi\sqrt{2}\,(m/M)\cdot(r_g/R)^2\cdot Kn_p$ as functions of the effective aerosol particle radius R.

The shaded regions show the regime of validity of the present approach for $p \approx 1$ atm, $T \approx 300$ and 2,000 K.

Recapitulating, the idea developed in this introductory paper is to apply the Waldmann approach to investigate the thermal diffusion of heavy nonspherical *molecules* (*e.g.*, paraffin hydrocarbons) in low molecular weight atmospheres, although our results also apply, of course, to the very important thermophoretic properties of small nonspherical "aerosol" particles such as "soot" aggregates formed in combustion (Rosner, 1986). In the following sections, we therefore extend Waldmann's theory to nonspherical particles and then particularize our results to spherocylinders as an approximation to the effective shape of paraffin molecules.

Method of Calculation

We proceed here by first evaluating the thermophoretic and resistance forces on a particle of convex (but otherwise arbitrary) shape, using Waldmann's theory.

Let us consider a gas subjected to a temperature gradient in such a way that its linearized distribution function for molecular velocities, as given by the Enskog-Chapman first-order approximation, is (*e.g.*, Chapter 5 of Ferziger and Kaper, 1972):

$$f = f_M\cdot(1+\phi) \qquad (2)$$

where f_M is the local Maxwellian distribution function:

$$f_M = N\left(\frac{m}{2\pi k_B T}\right)^{3/2}\cdot\exp\left(-\frac{mC^2}{2k_B T}\right) \qquad (3)$$

and ϕ is the correction due to each of the prevailing gradients, *i.e.*:

$$\phi = -\frac{3\mu}{2Nk_BT}\cdot\left(\frac{mC^2}{2k_BT}-\frac{5}{2}\right)\boldsymbol{C}\cdot\boldsymbol{grad}\ln T - \frac{m\mu}{Nk_B^2T^2}\cdot\left(\boldsymbol{CC}-\frac{1}{3}C^2\boldsymbol{I}\right):\boldsymbol{grad}\,\boldsymbol{v} \tag{4}$$

Here N is the local molecular number density, m the molecular mass, k_B the Boltzmann constant, T the absolute temperature, $\boldsymbol{C}$ the molecular velocity, μ the dynamic viscosity coefficient, $\boldsymbol{I}$ the unit matrix, and $\boldsymbol{v}$ the macroscopic gas velocity.

The relative importance of the temperature and velocity gradient terms in ϕ is:

$$\frac{\boldsymbol{C}\cdot\boldsymbol{grad}\ln T}{\boldsymbol{CC}:\boldsymbol{grad}\,\boldsymbol{v}}\sim\frac{1}{Ma}\gg 1 \quad \text{iff} \quad \frac{\delta_h}{\delta_{mom}}\sim O(1) \tag{5}$$

where $Ma \approx v/C \ll 1$, is the local Mach number, and δ_h and δ_{mom} are the thermal and momentum boundary layer thickness, respectively. Since we will restrict our attention to subsonic flows, in what follows we will disregard the contribution of velocity gradients to ϕ.

Let us assume that the particle is moving with respect to the gas with a constant velocity $\boldsymbol{V}$ small in magnitude compared with the average gas molecular velocity. Then, written in a frame attached to the particle and neglecting second order terms, the distribution function is:

$$f^- \simeq N\left(\frac{h}{\pi}\right)^{3/2}\cdot e^{-hc^2}\cdot\left[1-2h\boldsymbol{c}\cdot\boldsymbol{V}-3\nu h\left(hc^2-\frac{5}{2}\right)\boldsymbol{c}\cdot\boldsymbol{grad}\ln T\right] \tag{6}$$

where $\boldsymbol{c} = \boldsymbol{C} - \boldsymbol{V}$ is the molecule velocity relative to the moving particle,

$$h \equiv \frac{m}{2k_BT} \tag{7}$$

and

$$\nu \equiv \frac{\mu}{Nm} \tag{8}$$

is the momentum diffusivity ("kinematic viscosity" coefficient).

Let $d^2\Sigma$ be an element of the particle surface and $\boldsymbol{n}$ the exterior normal unit vector that forms with the tangential vectors $\boldsymbol{t}_1$ and $\boldsymbol{t}_2$ a local orthogonal system. The number of molecules striking per unit time on $d^2\Sigma$ with velocities between $\boldsymbol{c}$ and $\boldsymbol{c}+d^3\boldsymbol{c}$ is $-f^-(\boldsymbol{c}\cdot\boldsymbol{n})d^3\boldsymbol{c}d^2\Sigma$, where attention must be restricted to $(\boldsymbol{c}\cdot\boldsymbol{n})<0$. Then the force $d\boldsymbol{F}_I$ exerted on $d^2\Sigma$ by the impinging molecules is:

$$d\boldsymbol{F}_I = -d^2\Sigma\, m\int_{\boldsymbol{c}\cdot\boldsymbol{n}<0}\boldsymbol{c}(\boldsymbol{c}\cdot\boldsymbol{n})f^-\,d^3\boldsymbol{c} \tag{9}$$

Projecting in the normal and tangential directions and performing the indicated integral, we find:

$$\boldsymbol{n}\cdot d\boldsymbol{F}_I = -\frac{mN}{\sqrt{\pi h}}\cdot\left(\frac{1}{4}\sqrt{\frac{\pi}{h}}+\boldsymbol{n}\cdot\boldsymbol{V}+\frac{3\nu}{4}\boldsymbol{n}\cdot\boldsymbol{grad}\ln T\right)d^2\Sigma \tag{10}$$

$$\boldsymbol{t}_i\cdot d\boldsymbol{F}_I = -\frac{mN}{2\sqrt{\pi h}}\cdot\left(\boldsymbol{t}_i\cdot\boldsymbol{V}+\frac{3\nu}{4}\boldsymbol{t}_i\cdot\boldsymbol{grad}\ln T\right)d^2\Sigma \quad (i=1,2) \tag{11}$$

To take into account inelastic collisions, it is assumed that a fraction a of the total number of molecules impinging per unit time undergoes diffuse (nonspecular) reflection and is therefore scattered with a Maxwellian distribution function f^+, that is:

$$f^+ = N_D\left(\frac{h}{\pi}\right)^{3/2}\cdot\exp(-hc^2) \tag{12}$$

where the coefficient N_D must be chosen such that the total number per unit time of molecules diffusively reflected equalizes the fraction a of the impinging molecules. This condition leads to:

$$N_D = aN\cdot(1+\sqrt{\pi h}\,\boldsymbol{V}\cdot\boldsymbol{n}) \tag{13}$$

Once f^+ is known we can evaluate the corresponding force $d\boldsymbol{F}_{DR}$ on the surface element $d^2\Sigma$, which is given by:

$$d\boldsymbol{F}_{DR} = -d^2\Sigma m\int_{\boldsymbol{c}\cdot\boldsymbol{n}>0}\boldsymbol{c}(\boldsymbol{c}\cdot\boldsymbol{n})f^+\,d^3\boldsymbol{c} \tag{14}$$

After projecting in the normal and tangential directions, and evaluating the indicated integrals, we find:

$$\boldsymbol{n}\cdot d\boldsymbol{F}_{DR} = -d^2\Sigma\frac{amN}{4}\sqrt{\frac{\pi}{h}}\cdot\left(\frac{1}{\sqrt{\pi h}}+\boldsymbol{V}\cdot\boldsymbol{n}\right) \tag{15}$$

$$\boldsymbol{t}_i\cdot d\boldsymbol{F}_{DR} = 0 \qquad (i=1,2) \tag{16}$$

The remaining fraction $1-a$ of the colliding molecules is assumed to be specularly reflected (without tangential momentum transfer) in such a way that if the velocity of a molecule was $\boldsymbol{c}$ then its velocity after reflection must be $\boldsymbol{c}-2(\boldsymbol{c}\cdot\boldsymbol{n})\boldsymbol{n}$. So the force produced will be:

$$d\boldsymbol{F}_{SR} = d^2\Sigma\, m(1-a)\cdot\int_{\boldsymbol{c}\cdot\boldsymbol{n}<0}[\boldsymbol{c}-2(\boldsymbol{c}\cdot\boldsymbol{n})\boldsymbol{n}](\boldsymbol{c}\cdot\boldsymbol{n})f^-\,d^3\boldsymbol{c} \tag{17}$$

which leads to the projections:

$$\boldsymbol{n}\cdot d\boldsymbol{F}_{SR} = (1-a)\boldsymbol{n}\cdot d\boldsymbol{F}_I \tag{18}$$

$$\boldsymbol{t}_i\cdot d\boldsymbol{F}_{SR} = -(1-a)\boldsymbol{t}_i\cdot d\boldsymbol{F}_I \tag{19}$$

Then, by addition, we find the total force in the normal and tan-

gential directions:

$$\boldsymbol{n} \cdot d\boldsymbol{F} = -d^2\Sigma \frac{mN}{\sqrt{\pi h}} \cdot \left\{ \frac{1}{2}\sqrt{\frac{\pi}{h}} + \left[2 - a\left(1 - \frac{\pi}{4}\right)\right](\boldsymbol{n} \cdot \boldsymbol{V}) + (2 - a)\frac{3\nu}{4}(\boldsymbol{n} \cdot \boldsymbol{grad} \ln T) \right\} \quad (20)$$

$$\boldsymbol{t}_i \cdot d\boldsymbol{F} = d^2\Sigma \frac{am\sqrt{}}{2\sqrt{\pi h}} \cdot \left(\boldsymbol{t}_i \cdot \boldsymbol{V} + \frac{3\nu}{4} \boldsymbol{t}_i \cdot \boldsymbol{grad} \ln T \right), (i = 1, 2) \quad (21)$$

Finally, the total force $\boldsymbol{F}$ on the particle would be the integral of the elementary forces $d\boldsymbol{F}$ over the total particle surface Σ,

$$\boldsymbol{F} = \int_{\Sigma} d\boldsymbol{F} \quad (22)$$

where $d\boldsymbol{F}$ is obtained from the projections (Eqs. 20 and 21) as:

$$d\boldsymbol{F} = (\boldsymbol{n} \cdot d\boldsymbol{F})\boldsymbol{n} + (\boldsymbol{t}_1 \cdot d\boldsymbol{F})\boldsymbol{t}_1 + (\boldsymbol{t}_2 \cdot d\boldsymbol{F})\boldsymbol{t}_2 \quad (23)$$

A similar result, but for the diffusiophoresis phenomenon, has been obtained by Yalamov et al. (1979).

We will now apply these results to a "sphero-cylindrical" particle: i.e., a cylinder of length L and radius R with hemispherical caps at both ends, Figure 2.

Due to the linearity of the calculation, the force on a sphero-cylinder can be obtained by addition of the forces on its spherical and cylindrical parts. A straightforward computation leads to:

$$\boldsymbol{F} = -\frac{mN}{\sqrt{h}} \cdot \pi R^2 \cdot \left\langle \left[\frac{8}{3}\left(1 + a\frac{\pi}{8}\right) + \frac{2L}{R}\left(1 + a\frac{\pi - 2}{8}\right)\right] \boldsymbol{V}_y + \frac{3\nu}{4}\left[\frac{8}{3} + \frac{2L}{R}\left(1 - \frac{a}{4}\right)\right]\frac{\partial \ln T}{\partial y}\boldsymbol{e}_y + \left\{ \left[\frac{8}{3}\left(1 + a\frac{\pi}{8}\right) + \frac{L}{R}a\right] \boldsymbol{V}_z + \frac{3\nu}{4}\left(\frac{8}{3} + \frac{L}{R}a\right)\frac{\partial \ln T}{\partial z}\right\}\boldsymbol{e}_z \right\rangle \quad (24)$$

where $\boldsymbol{e}_y$ and $\boldsymbol{e}_z$ are unit vectors along the y and z axis. Taking advantage of the axial symmetry of the sphero-cylinder without loss of generality, it has been assumed that it was aligned in the $\boldsymbol{e}_z$ direction and that both $\boldsymbol{V}$ and $-\boldsymbol{grad}\ T$ lie in the yz plane, as shown in Figure 2.

When we pass to the limit $L/R \to 0$ (*i.e.*, the spherical case), Eq. 24 reduces to Waldmann's result. In the opposite limit $L/R \to \infty$ (*i.e.*, the cylindrical case) a partial check can be obtained by noting that Eq. 24 specializes to a previous result of Dahneke (1973) for the drag force, $\boldsymbol{F} \cdot \boldsymbol{V}/V$, in a constant temperature environment: *i.e.*, $-\boldsymbol{grad}\ T = 0$.

As shown by Eq. 24, when $a = 0$ (pure specular reflection) the cylindrical surfaces themselves experience thermophoretic and resistance forces along a direction normal to its axis of revolution, these forces being proportional to the corresponding components of $-\boldsymbol{grad}\ T$ and $\boldsymbol{V}$ along the same direction, in such a way that if these two vectors are directed along the cylinder axis of revolution no thermophoresis nor resistance force exist. When we "close" both ends of the cylinder with hemispherical caps, we must add to the previous forces new ones directed along $-\boldsymbol{grad}\ T$ and $\boldsymbol{V}$ (just the thermophoretic drift and the resistance force corresponding to a sphere). If $a \neq 0$ (diffuse reflection also occurs, implying tangential momentum transfer), the situation is somewhat more complex but, in any case, the resulting thermophoretic (*cf.* resistance) force does not coincide with the direction of $-\boldsymbol{grad}\ T$ and, as a consequence, the nonspherical shape leads to a "lift" in the resistance force as well as to a force normal to $-\boldsymbol{grad}\ T$ in the thermophoretic force. So, in general, when a stationary motion is attained (and $\boldsymbol{F} = 0$) the vectors $\boldsymbol{V}$ and $-\boldsymbol{grad}\ T$ will have different directions: *i.e.*, the giant elongated molecule does not drift "down" the temperature gradient. Equating both components of $\boldsymbol{F}$ to zero, we obtain two equations that allow us to calculate both components of $\boldsymbol{V}$. If the sphero-cylinder is aligned in the $\boldsymbol{e}_z$ direction and β is the angle between $\boldsymbol{e}_z$ and $\boldsymbol{grad}\ T$, then the magnitude V and the angle α between $\boldsymbol{e}_z$ and $\boldsymbol{V}$ (see Figure 2) are given, respectively, by:

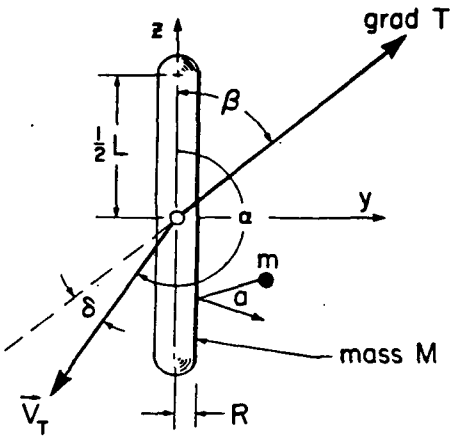

Figure 2. Sphero-cylindrical particle in a nonuniform temperature gas showing the choice of coordinates and notation.

$$V = -\frac{\cos\beta}{\cos\alpha} \cdot A\nu \cdot |\boldsymbol{grad} \ln T| \quad (25)$$

with

$$A = \frac{3}{4\left[1 + \dfrac{a\pi/3}{(8/3) + (aL/R)}\right]} \quad (26)$$

and

$$\tan\alpha = B \tan\beta \quad (27)$$

with

$$B = \frac{3}{4A \cdot \left[1 + \dfrac{a\pi/8}{1 - \dfrac{aL/2R}{(8/3) + (2L/R)}}\right]} \quad (28)$$

The behavior predicted by Eq. 25 and the deviation angle $\delta = \pi + \beta - \alpha$ for a very long particle ($L/R \to \infty$) are depicted in Figures 3 and 4, respectively, which summarize the "shape effects" of greatest interest. Figure 3 shows that, provided the impinging gas molecules can transport tangential momentum (*i.e.* are not fully specularly reflected, we have chosen $a = 0.8$), a long sphero-cylindrical particle with a major axis aligned with the direction of $-\boldsymbol{grad}\ T$ will thermophoretically drift approximately 31% *faster* down the temperature gradient than a sphere of radius R (equal to the cylindrical radius), whereas a long spherocylindrical particle with its major axis perpendicular to $-\boldsymbol{grad}\ T$ will thermphoretically drift approximately 6% *slower* than a sphere of radius R in the same local environment. An important corollary of this orientation dependence of the thermophoretic velocity is a "new" mechanism of coagulation for nonspherical particles in a temperature gradient (*i.e.*, particles of one orientation are able to "overtake" particles of another orientation). Since, when $Kn_p \gg 1$, the thermophoretic velocity of a sphere is size-*independent*, this result also implies that a noncoalescing liquid (or solid) aerosol in a temperature gradient will coagulate faster than a coalescing one. A somewhat subtler mechanism of coagulation, also new and associated with thermophoresis, is implied in Figure 4. It shows that the direction of thermophoretic drift of "nonaligned" (neither parallel nor perpendicular) particles departs (by as much as 12°) from the direction of $-\boldsymbol{grad}\ T$. The stochastic effect of such "lateral" displacements for particles which are experiencing Brownian rotation will be to introduce a "thermo-Brownian" contribution to the coagulation rate for nonspherical particles in a temperature gradient. These particle coagulation implications of the results displayed in Figures 3 and 4 will be pursued elsewhere.

Due to Brownian rotatory motion, after a very long time compared to the rotation time, the giant molecule will go through all possible orientations. Then, if all orientations were equiprobable, the orientation-averaged thermophoretic velocity $\langle V_T \rangle$, in the direction of $-\boldsymbol{grad}\ T$, would be:

$$\langle V_T \rangle = \frac{1}{2}\int_0^{\pi} V \cos\delta \sin\beta \, d\beta$$

$$= \frac{1}{3} A(1 + 2B)\, \nu \cdot |\boldsymbol{grad} \ln T| \quad (29)$$

In the equivalent result of kinetic theory, the proportionality factor between the thermophoretic velocity and the gradient $\boldsymbol{grad} \ln T$ is usually written as the product $\alpha_T D$ of the binary thermal diffusion factor α_T and the binary diffusion coefficient D. For a quasi-Lorentzian gas of hard spheres, the kinetic theory gives the result (Mason, 1957):

$$[\alpha_T D]_{QL} = (3/4)\nu \quad (30)$$

which reduces to the following result of Waldmann (1961) when only "specular" collisions occur ($a = 0$):

$$[\alpha_T D]_{a} = \frac{[\alpha_T D]_{QL}}{1 + (a\pi/8)} \quad (31)$$

This result predicts a decrease in the thermophoretic drift velocity when inelastic collisions occur ($a > 0$) but contains no information about shape effects. In the quasi-Lorentzian and

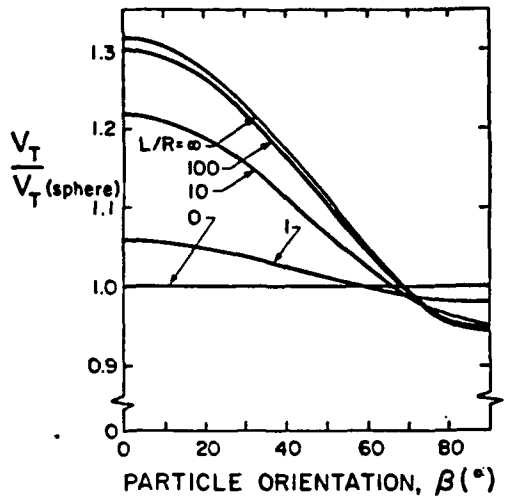

Figure 3. Normalized magnitude of the thermophoretic velocity for a sphero-cylindrical particle as a function of particle orientation β (diffuse fraction $a = 0.8$).

Waldmann model, the shape dependence of the thermal diffusion factor is contained in the ratio $Sc = \nu/D$, known as the Schmidt number (see, *e.g.*, Israel, 1983). Then our results (Eq. 29) can be written as:

$$\langle \alpha_T D \rangle = \tfrac{4}{9} A(1 + 2B)[\alpha_T D]_{QL} \quad (32)$$

where the brackets indicate the orientation-averaged value.

Figure 5 shows the dependence of $\langle \alpha_T D \rangle$ on shape for a sphero-cylinder compared with a sphere at the same a (diffuse fraction) value. It is interesting to note that $\langle \alpha_T D \rangle$ would be rel-

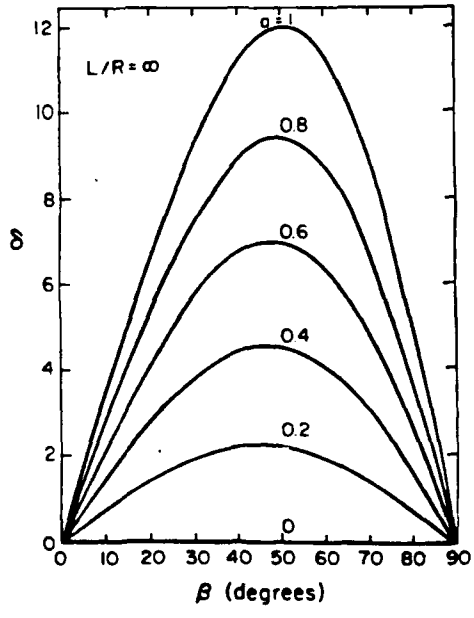

Figure 4. Deviation angle δ (drift direction with respect to $-\boldsymbol{grad}\ T$) for an infinite cylinder ($L/R \to \infty$) as function of cylinder orientation β with respect to $-\boldsymbol{grad}\ T$.

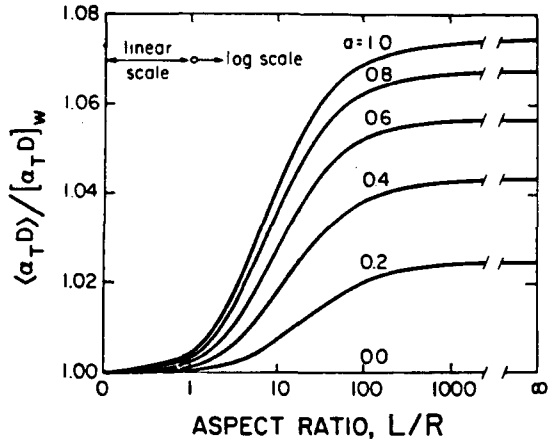

Figure 5. Values of $\langle \alpha_T D \rangle$ for a sphero-cylinder normalized with the corresponding Waldmann result for a *sphere* at the same diffuse-fraction *a* value.

Dependence on aspect ratio L/R and diffuse-fraction coefficient a.

evant for high Schmidt number, thermophoretically-dominated particle transport across continuum thermal boundary layers because Brownian rotation would not be "frozen" on the (transit-) time scale $\delta_h/\langle V_T \rangle$. Further implications of this shape dependence are discussed in the next section.

Using Eq. 24 the thermophoretic torque τ on the "particle" may be evaluated by integration of the torque $d\tau$ on each elemental surface $d^2\Sigma$, over the whole particle surface. That is:

$$\tau = \int_\Sigma d\tau = \int_\Sigma r \times dF \tag{33}$$

where r is the position vector of the surface points. Calculation shows that, for the chosen spherocylindrical model, there is no net torque on the particle. This is a consequence of the particular shape symmetry. In fact, *any* particle (molecule) having three mutually perpendicular planes of symmetry would experience zero net torque. Moreover, it can be shown that translation and rotation are uncoupled. This is a well known result for the low Reynolds number continuum regime (Happel and Brenner, 1965) that can be "verbatim" translated to the free molecule regime whenever a convex body is considered, due to the formal analogy between both theories (Rohatschek and Zulehner, 1987).

Discussion

If all collisions were specular ($a = 0$), our result corresponds to the quasi-Lorentzian gas in the hard-sphere limit (Eq. 30). On the other hand, in the limit of a very long particle, $L/R \to \infty$, the result (Eq. 32) is:

$$\langle \alpha_T D \rangle_\infty = \frac{1 + [(\pi/3) - 2]a/8}{1 + (\pi - 2)a/8} \cdot [\alpha_T D]_{QL} \tag{34}$$

so the ratio $\langle \alpha_T D \rangle / [\alpha_T D]_{QL}$ is always smaller than unity, taking its minimum value when all collisions are "diffuse" ($a = 1$). In other words, as shown by Waldmann's sphere result, Eq. 31, *inelastic* collisions ($a > 0$) *decrease* thermophoretic drift velocity, despite the fact that an elongated shape reduces this tendency (cf. Figure 5).

Evaluation of the thermal diffusion factor α_T from Eq. 32 requires computation of the binary diffusion coefficient D. This can be done by using Einstein's relation:

$$D = k_B T b \tag{35}$$

where the "mobility" b is obtained from the principal values c_1, c_2, c_3, of the resistance coefficient matrix as (see, *e.g.*, the book of Landau and Lifshitz, 1975, p. 228):

$$b = \frac{1}{3}\left(\frac{1}{c_1} + \frac{1}{c_2} + \frac{1}{c_3}\right) \tag{36}$$

In our case, due to the special choice of coordinate frame along the symmetry axis of the sphero-cylinder, the resistance matrix obtained from Eq. 24 is diagonal and $c_1 = c_2 = c_y$, $c_3 = c_z$, where:

$$c_y = \frac{mN}{\sqrt{\pi h}} \cdot \pi R^2 \cdot \left[\frac{8}{3}\left(1 + a\frac{\pi}{8}\right) + 2\frac{L}{R}\left(1 + a\frac{\pi - 2}{8}\right)\right] \tag{37}$$

$$c_z = \frac{mN}{\sqrt{\pi h}} \cdot \pi R^2 \cdot \left[\frac{8}{3}\left(1 + a\frac{\pi}{8}\right) + \frac{L}{R}a\right] \tag{38}$$

By denoting

$$b_W = \frac{3\sqrt{\pi h}}{8mN\pi R^2(1 + a\pi/8)} \tag{39}$$

the corresponding Waldmann mobility for a sphere of radius R and using Eq. 37 and 38 in Eq. 36 the mobility of a sphero-cylinder can be written:

$$b = E b_W \tag{40}$$

where

$$E = \frac{1}{1 + \frac{L}{2R} \cdot \frac{1 + \frac{L}{R}\frac{a}{1 + a\pi/8}\left(\frac{3}{2} - \frac{a}{1 + a\pi/8}\right)}{1 + \frac{L}{2R}\left(\frac{1}{2} + \frac{a}{1 + a\pi/8}\right)}} \tag{41}$$

Let

$$D_W = k_B T b_W \tag{42}$$

be the diffusion coefficient of a sphere of radius R, and

$$D_{QL} = k_B T \cdot \frac{3\sqrt{\pi h}}{8mN\pi R^2} \tag{43}$$

be the diffusion coefficient of the analogous "quasi-Lorentzian" gas of hard spheres. Then our result can be written:

$$D = E D_W = \frac{E}{1 + a\pi/8} \cdot D_{QL} \tag{44}$$

This expression gives the diffusion coefficient of a sphero-cylinder as a function of three parameters: L, R and a. These parameters must be adjusted to fit experimental values of D. It is noteworthy that in the case of paraffin hydrocarbons diffusing in nitrogen, such agreement is attained with reasonable values of these three parameters. The special choices $R = 2$ Å, and $L = (n-1)R$, n being the number of carbons in the paraffin, are compared with the experimental measurements in Figure 6 (Galloway and Sage, 1967), which reveals gradually better agreement upon increasing the number of carbons of the paraffin (as the criterion 1 is more accurately fulfilled).

Now we can use Eq. 32 to compute the values of the thermal diffusion factor:

$$\alpha_T = \frac{4A(1+2B)}{9E} \cdot \left(1 + a\frac{\pi}{8}\right) \cdot \alpha_{T_{QL}} \tag{45}$$

where we have used Eq. 44 and $\alpha_{T,QL} = 3\nu/(4D_{QL})$ is the thermal diffusion factor of the associated quasi-Lorentzian gas. This factor is intimately related to the relative size of the "particle," R, and the surrounding gas r_g, (Eisner and Rosner, 1985) because using Eq. 43 and the hard-sphere kinetic theory to determine ν, we find $\alpha_{T,QL} = [5/(4\sqrt{2})](R/r_g)^2$. Note that we have defined $\alpha_T = \langle \alpha_T D \rangle / D$ because this is the parameter obtained from steady-state experiments in which concentration-(Brownian or Fick) diffusion counterbalances Soret diffusion. In Figure 7 we have plotted the values obtained from Eq. 45 corresponding to our computed values of D plotted in Figure 6.

Incidentally, we have also displayed the values given by the kinetic theory for a binary mixture of hard spheres where one of the species is highly diluted. This last approach then assumes spherical shape and variable mass for the diluted species (the praffin) and should be a good approximation for the light paraffins. The present theory assumes a very large mass for the paraffin but variable nonspherical shape, thereby giving a better description of the heavy paraffin behavior. Figure 7 shows a rather encouraging matching of both descriptions in the intermediate region. This figure also shows the limit of expression 45

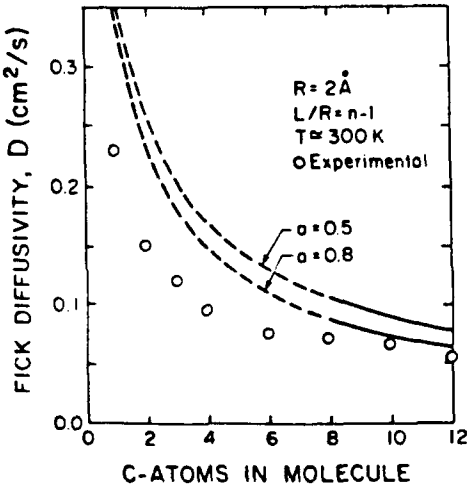

Figure 6. Experimental and predicted diffusion coefficients D for paraffin hydrocarbons as function of the number of C atoms in the molecule.

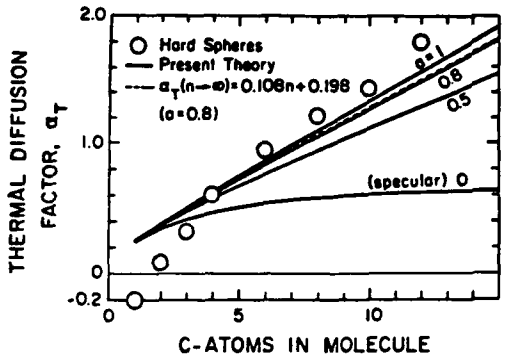

Figure 7. Predicted values for the dimensionless thermal diffusion factor α_T for paraffin hydrocarbons as function of the number of C atoms in the molecule.

for large values of n, whose analytical form is:

$$\alpha_{T\infty} = [\alpha_T D]_{QL} \cdot \frac{2(a/a_0)(3/8 - a/4a_0)}{k_B T b_W (1/4 + a/2a_0)} \cdot \frac{1 + (\pi/6 - 1)a/4}{1 + (\pi/2 - 1)a/4} n \cdot \left\{1 + \frac{(\pi a^2/4) - \pi[1 + (\pi/2 - 1)a/4]^2}{3n[1 + (\pi/2 - 1)a/4][3 + (\pi/2 - 3)a/4]} - \frac{1 - (a_0/a) + [1/(1/4 + a/2a_0)]}{n} + O(n^{-2})\right\} \tag{46}$$

where $a_0 = (8 + a\pi)/3$ and we have assumed that $L/R = n - 1$. Then we predict a straight line for the dependence of α_T on n when $n \to \infty$. Figure 7 reveals that this limit is in fact reached quickly, even for moderate values of n.

Conclusions

The formalism used by Epstein (1924) and Waldmann (1959, 1968) to study the dynamics of small spherical particles in a nonisothermal gas is here shown to be useful to investigate not only the behavior of small *nonspherical* particles, but also the behavior of "giant" nonspherical molecules.

Interesting results of this analysis include the predictions that, provided gas molecule reflection is not completely specular, sphero-cylindrical particles in a local temperature gradient ***grad T*** will thermophoretically drift: (i) more rapidly when their major axis is aligned with ***-grad T*** than when perpendicular to ***-grad T*** (by about 48% for the limiting case $L/R \to \infty$, $a = 1$); (ii) at a different velocity (depending upon particle orientation and L/R) than that of a sphere of radius R equal to the cylinder radius, (iii) at an angle (up to 12°) with respect to ***-grad T*** when their major axis is not parallel to, or perpendicular to, ***grad T***, (iv) *without* a net torque tending to orient the particle with respect to ***-grad T***. Important corollaries of these findings, now under quantitative investigation, are that nonspherical particles in a temperature gradient should also experience new thermophoretically-induced coagulation mechanisms, and that thermophoretically augmented coagulation rates in the presence of rapid coalescence should be slower than those in the absence of rapid coalescence (*i.e.*, when nonspherical aggregates form).

In the case of sphero-cylindrical "particles" studied here, we find that there is no net thermophoretically oriented *torque* so that the only particle rotation would be the rotational Brownian motion. This would be also the case for other differently shaped particles which possess the same symmetry: all axisymmetric nonspherical bodies with a plane of symmetry normal to the axis of revolution, like cylinders and discs. In fact, this result can be generalized further to bodies possessing three mutually perpendicular planes of symmetry (see, *e.g.*, Davies, 1979, for particle dynamics in the continuum limit). However, in general, the thermophoretic torque on the particle will be nonzero, leading either to nonspherical particle alignment or continuous rotation, depending on the particle symmetry. These implications of our present work, when applied to unsymmetrical nonspherical particles or heavy molecules, are currently under investigation. However, as a particular result for sphero-cylindrical "particles" we have estimated the thermophoretic velocity of the paraffin hydrocarbons, modelled as sphero-cylinders. Our formulae depend on three parameters associated with the molecular geometry and structure, but additional experimental information will be required before assigning precise values to them.

This asymptotic kinetic theory approach is now also being used to predict the behavior of molecules with flat nonaxisymmetric structures, such as benzene and anthracene, of great current importance in hydrocarbon fuel and coal processes.

It should be noted that particle shape effects on thermophoretic behavior have recently been investigated in the opposite limit of *small* particle Knudsen number by several authors (Leong, 1984; Reed, 1971). Although an exhaustive study of particle orientation implications is still lacking in this "near-continuum" limit, it has been shown that in this case also the particle thermophoretic drift is strongly dependent of both shape and relative orientation. Results, however, depend on the ratio of the *thermal conductivity* of the particle to the gas, whereas in the present ($Kn_p \gg 1$) case they depend on the momentum accommodation coefficient a. But, despite the fact that in both limiting cases ($Kn_p \ll 1$, $Kn_p \gg 1$) thermophoretic drift is "caused" by different phenomena (thermal "slip," and momentum transfer, respectively), we can state in general that an elongated particle will thermophoretically drift faster than a sphere when it is oriented parallel to $-\boldsymbol{grad}\ T$. Also, flattened particles behave qualitatively in a similar manner: they drift faster when they have either major axis parallel to $-\boldsymbol{grad}\ T$, although, while the lowest drift velocity in the limit of vanishing thickness vanishes for a 'large' particle, it remains nonzero for a small particle. Our present interest in the $Kn_p \gg 1$ limit is, of course, motivated by the realization that results in this limit will often be applicable to 'heavy molecules', rather than just "true particles." This important hypothesis will be tested further for both long (paraffin-like) or platelet (polycycle aromatic) molecules in our follow-on studies.

Acknowledgments

This research was supported in part by the U.S. Air Force Office of Scientific Research (Grant AFOSR-84-0034) and the U.S. Dept. of Energy (Contract DE-AC21-85MC22075 and DE-FG22-86PC90756).

The authors have benefited from discussions with Drs. J. Castillo, J. Fernandez de la Mora and with I. Gallily, deceased July 31, 1988, to whose memory this paper is dedicated.

We are also particularly indebted to Dr. A. Eisner for his critical review and suggestions on a preliminary draft (P. G-Y., 1985) of this paper, and for presenting it to stimulate discussion at the annual conference of the American Association for Aerosol Research, Nov. 18–22, 1985, Albuquerque, NM.

Notation

A = parameter
a = diffusively reflected gas molecule fraction
B = parameter
b = particle mobility
C = sound velocity
c_y, c_z = principal values of the resistance matrix
C = molecular velocity
c = relative molecular velocity
$\hat{c}$ = mean gas molecule velocity
D = particle diffusion coefficient
E = parameter
e_y, e_z = unit vectors along y and z axis
F = total force on the particle
f^+ = diffusively reflected gas velocity distribution function
f^- = gas velocity distribution function
F_{DR} = force due to the diffusively reflected molecules
F_I = force due to the impinging molecules
F_{SR} = force due to the specularly reflected molecules
f_M = Maxwellian distribution function
$h = m/2k_BT$
I = particle moment of inertia
I = unit matrix
k_B = Boltzmann constant
Kn = gas Knudsen number
Kn_p = particle Knudsen number
L = cylinder length
l = gas mean-free path
M = particle mass
m = gas molecule mass
N = gas molecule number per unit volume
N_D = coefficient in f^+
n = number of C atoms
n = normal unit vector
R = particle radius
r = position vector
r_g = gas molecule radius
T = absolute temperature
t_1, t_2 = tangential unit vectors
V = particle velocity
v = macroscopic gas velocity
V_T = thermophoresis velocity

Greek letters

α = angle between e_z and V
α_T = thermal diffusion factor
β = angle between e_z and $\boldsymbol{grad}\ T$
$\delta = \pi + \beta - \alpha$
δ_h = thermal boundary layer thickness
δ_{mom} = momentum boundary layer thickness
ϕ = gradient correction to the distribution function
Λ = macroscopic gradient scale
μ = dynamic viscosity coefficient
ν = momentum diffusivity
Σ = particle surface
τ = torque on particle
τ = gas-particle collision time
ω = particle angular velocity

Subscripts

QL = quasi-Lorentzian
W = Waldmann
∞ = infinitely long particle

Literature Cited

Curtiss, C. F., "Kinetic Theory of Nonspherical Molecules," *J. Chem. Phys.*, **24**, 225 (1956).

Curtiss, C. F., and C. Muckenfuss, "Kinetic Theory of Nonspherical Molecules-II," *J. Chem. Phys.*, *26, 1619 (1957).*

Dahneke, B. E., "Slip Correction Factors for Nonspherical Bodies-II Free Molecule Flow," *Aerosol Sci. and Technol.*, **4**, 147 (1973).
Davies, C. N., "Particle-Fluid Interaction," *J. Aerosol Sci.* **10**, 477 (1979).
Eisner, A. D. and D. E. Rosner, "Experimental Studies of Soot Particle Thermophoresis in Nonisothermal Combustion Gases Using Thermocouple Response Techniques," *Comb. and Flame*, **61**, 153 (1985).
Epstein, P. S., "On the Resistance Experienced by Spheres in Their Motion Through Gases," *Phys. Rev.*, **23**, 710 (1924).
Fernandez de la Mora, J., and J. M. Mercer, "Modified Fokker-Planck Equation for the Motion of Brownian Particles in a Nonuniform Gas," *Phys. Rev.*, **A26**, 2178 (1982).
Ferziger, J. H., and H. G. Kaper, *Mathematical Theory of Transport Processes in Gases*, North-Holland Publishing Co. (1972).
Fristrom, R. M., and L. Monchick, "Two Simple Approximations to the Thermal Diffusion Factor and their Applications to Flame Studies," *Comb. and Flame*, **71**, 89 (1988).
Galloway, T. R., and B. H. Sage, "Prediction of the Transport Properties of Paraffin Hydrocarbons," *Chem. Eng. Sci.*, **22**, 979 (1967).
Garcia-Ybarra, P., C. Nicoli, and P. Clavin, "Soret and Dilution Effects on Premixed Flames," *Comb. Sci. and Technol.*, **42**, 87 (1984).
Happel, J., and H. Brenner, *Low Reynolds Number Hydrodynamics*, Prentice-Hall, Englewood Cliffs, NJ (1965).
Israel, R., *Thermal Diffusion Effects on Fuel Vapor Mass Transport across Non-Isothermal Boundary Layers in Surface-Catalyzed Combustion*, PhD Diss., Chemical Engineering Department, Yale University (1983).
Landau, L., and Lifchitz, *Fluid Mechanics*, Pergamon Press (1975).
Leong, K. H., "Thermophoresis and Diffusiophoresis of Large Aerosol Particles of Different Shapes," *J. Aerosol Sci.*, **15**(4), 511 (1984).
Mason, E. A., "Higher Approximation for the Transport Properties of Binary Gas Mixtures: II. Applications," *J. Chem. Phys.*, **27**, 782 (1957).
Mason, E. A., and S. Chapman, "Motion of Small Suspended Particles in Nonuniform Gases," *J. Chem. Phys.*, **36**, 627 (1962).
Matzen, M. K., and D. K. Hofman, "Thermal Diffusion in Isotropic Mixtures of Polyatomic Gases: I. The Thermal Diffusion Coefficient," *J. Chem. Phys.*, **62**, 500 (1975).
Monchick, L., K. S. Yun, and E. A. Mason, "Formal Kinetic Theory of Transport Phenomena in Polyatomic Gas Mixtures," *J. Chem. Phys.*, **39**, 654 (1963).
Monchick, L., S. I. Sandler, and E. A. Mason, "Thermal Diffusion in Polyatomic Gases: Nonspherical Interactions," *J. Chem. Phys.*, **49**, 1178 (1968).
Muckenfuss, C., and C. F. Curtiss, "Kinetic Theory of Nonspherical Molecules-III," *J. Chem. Phys.*, **29**, 1257 (1958).
Reed, L. D., "A Continuum Slip Flow Analysis of Steady and Transient Thermophoresis," M.S. Thesis, University of Illinois, Urbana-Champaign (1971).
Rohatscheck, H., and W. Zulehner, "The Resistance Force on Nonspherical Bodies in the Free Molecule Regime," *J. Colloid Interf. Sci.*, **119**, 378 (1987).
Rosner, D. E., "Thermal (Soret) Diffusion Effects on Interfacial Mass Transport Rates," *Phys.-Chem. Hydrody.*, **1**, 159 (1980).
Rosner, D. E., *Transport Processes in Chemically Reacting Flow Systems*, Butterworths, Stoneham, MA (1986, 1988).
Waldmann, L., "On the Motion of Spherical Particles in Nonhomogeneous Gases," *Rarefied Gas Dynamics*, ed., L. Talbot, Academic Press, 323 (1961); *Z. Naturforsch.*, 14a, 589 (1959).
Yalamov, Y. I., M. N. Gaidukov, and V. B. Redchits, "Diffusiophoresis of Nonspherical Aerosol Particles in a Free Molecular Flow," *Sov. Phys. Tech. Phys.*, **24**, 731 (1979).

Manuscript received Apr. 3, 1987, and revision received Aug. 15, 1988.

REPORT DOCUMENTATION PAGE

Form Approved
OMB No. 0704-0188

1. AGENCY USE ONLY (Leave blank)	2. REPORT DATE	3. REPORT TYPE AND DATES COVERED
	1990	Journal Publication

4. TITLE AND SUBTITLE
"Photophoretic Modification of the Transport of Absorbing Particles Across Combustion Gas Boundary Layers" (U)

5. FUNDING NUMBERS
PE - 61102F
PR - 2308
SA - BS
G - AFOSR 89-0223

6. AUTHOR(S)
Jose L. Castillo, Daniel W. Mackowski, Daniel E Rosner

7. PERFORMING ORGANIZATION NAME(S) AND ADDRESS(ES)
HIGH TEMPERATURE CHEMICAL REACTION ENGINEERING LABORATORY
YALE UNIVERSITY
BOX 2159, YALE STATION
NEW HAVEN, CONNECTICUT 06520 U.S.A.

8. PERFORMING ORGANIZATION REPORT NUMBER

9. SPONSORING/MONITORING AGENCY NAME(S) AND ADDRESS(ES)
AFOSR/NA
Building 410
Bolling AFB DC 20332-6448

10. SPONSORING/MONITORING AGENCY REPORT NUMBER

11. SUPPLEMENTARY NOTES

12a. DISTRIBUTION/AVAILABILITY STATEMENT
Approved for public release; distribution is unlimited

12b. DISTRIBUTION CODE

13. ABSTRACT (Maximum 200 words)

Abstract—Since radiation energy fluxes can be comparable to or even dominate 'convective' (Fourier) fluxes in large fossil-fuel-fired power stations and furnaces, we examine particle drift ('phoresis') induced by the nonuniform photon-produced heating of particles in a 'host' gas. Our analysis of the resulting photophoretic particle velocity shows that photophoresis is a significant transport mechanism for micron-sized absorbing particles in high radiative transfer combustion environments, with equivalent photophoretic diffusivity ratios (dimensionless photophoretic velocities) being as large as 10% of the better-known thermophoretic diffusivity. Since previous experimental results demonstrated that thermophoresis causes over a 3-decade increase in small particle deposition rates by convective diffusion, clearly, for small, absorbing particles, photophoresis will also be an important contributor to observed deposition rates. Accordingly, we present predicted dimensionless mass transfer coefficients for particle transport across non-isothermal laminar gaseous boundary layers, including the simultaneous effects of both particle thermophoresis and photophoresis. It is also shown that our earlier 'additive suction velocity' prediction/correlation scheme successfully anticipates the present numerical (large Schmidt number, laminar boundary layer) results for radiative/conductive flux ratios encountered in practice.

14. SUBJECT TERMS	15. NUMBER OF PAGES
photophoresis, soot, mass transport, aerosols, boundary layers	8
	16. PRICE CODE

17. SECURITY CLASSIFICATION OF REPORT	18. SECURITY CLASSIFICATION OF THIS PAGE	19. SECURITY CLASSIFICATION OF ABSTRACT	20. LIMITATION OF ABSTRACT
Unclassified	Unclassified	Unclassified	UL

Prog. Energy Combust. Sci. 1990. Vol. 16, pp. 253–260
Printed in Great Britain.

0360-1285/90 $0.00 + .50

#171

PHOTOPHORETIC MODIFICATION OF THE TRANSPORT OF ABSORBING PARTICLES ACROSS COMBUSTION GAS BOUNDARY LAYERS

JOSE L. CASTILLO,* DANIEL W. MACKOWSKI† and DANIEL E. ROSNER‡

Yale University, Department of Chemical Engineering, High Temperature Chemical Reaction Engineering Laboratory, New Haven, CT 06520, U.S.A.

Abstract—Since radiation energy fluxes can be comparable to or even dominate 'convective' (Fourier) fluxes in large fossil-fuel-fired power stations and furnaces, we examine particle drift ('phoresis') induced by the nonuniform photon-produced heating of particles in a 'host' gas. Our analysis of the resulting photophoretic particle velocity shows that photophoresis is a significant transport mechanism for micron-sized absorbing particles in high radiative transfer combustion environments, with equivalent photophoretic diffusivity ratios (dimensionless photophoretic velocities) being as large as 10% of the better-known thermophoretic diffusivity. Since previous experimental results demonstrated that thermophoresis causes over a 3-decade increase in small particle deposition rates by convective diffusion, clearly, for small, absorbing particles, photophoresis will also be an important contributor to observed deposition rates. Accordingly, we present predicted dimensionless mass transfer coefficients for particle transport across non-isothermal laminar gaseous boundary layers, including the simultaneous effects of both particle thermophoresis and photophoresis. It is also shown that our earlier 'additive suction velocity' prediction/correlation scheme successfully anticipates the present numerical (large Schmidt number, laminar boundary layer) results for radiative/conductive flux ratios encountered in practice.

CONTENTS

1. INTRODUCTION

A key ingredient in the prediction of deposition rates in combustion environments is an understanding of the mechanisms involved in transporting particles across gaseous boundary layers and onto heat exchanger surfaces. Brownian diffusion is a major contributor to deposition for ultra-small (*ca* $10^{-2}\,\mu$m) particles (and heavy vapors) whereas inertial impaction becomes dominant for relatively large particles (*ca* $10\,\mu$m for gas velocities typical in large-scale furnaces).[1–5]

Thermophoresis, or the drift of aerosol particles down a temperature gradient, becomes a significant transport mechanism for intermediate-sized particles. This is a consequence of the very steep gas temperature gradients produced within the boundary layers adjacent to heat exchanger surfaces. Previous investigations[2,3] have demonstrated the importance of thermophoresis for particle deposition to a cooled surface. Indeed, experimental observations[6] indicate that thermophoresis can cause over a 3-decade increase in small particle deposition rates over that by convective diffusion alone.

A transport mechanism which has not received previous attention by engineers is photophoresis. Photophoresis is similar to thermophoresis in that the particle motion results from a temperature-gradient-induced gas flow (thermal creep) adjacent to the particle surface. In thermophoresis, the temperature gradient exists in the bulk gas, whereas in photophoresis the temperature gradient is localized about the particle and is the result of nonuniform absorption of radiation within the particle. Considering that *radiative* transport is typically the dominant mode of energy transfer in large, pulverized-coal furnaces,[7] the 'driving force' for photophoresis is certainly significant.

* Professor and Head, Depto. Fisica Fundamental, U.N.E.D., Madrid, Spain.

† Postdoctoral Research Associate, Yale University, Chemical Engineering Dept., HTCRE Laboratory; Present address: Dept Mech. Eng., Auburn Ui, Auburn AL 38649-5341.

‡ Professor of Chemical Engineering, Yale University, Chemical Engineering Dept.; Director, HTCRE Laboratory; to whom inquiries concerning this research should be directed.

Accurate analysis, however, of the photophoretic velocity v_{ph} of a particle having arbitrary size and radiative properties is made difficult by the complicated nature of the radiative absorption process within the particle, and only recently have solutions for v_{ph} been obtained even for homogeneous spherical particles.[8-10] Diffusivity ratios (or dimensionless velocities) for micrometer-sized, radiatively-absorbing spherical particles can be of the order of 10% of the better-known thermophoretic diffusivities ratios.[11-13] Since radiative energy fluxes actually dominate 'convective-diffusion' energy fluxes in many applications, this conclusion indicates that photophoresis can be an important contributor to the observed deposition rates of absorbing particles in high radiative transfer environments, especially for particle sizes just below the onset of inertial impaction.

The investigation presented here focuses on the effect of photophoresis upon the deposition rate of intermediate-sized particles—i.e., small enough to preclude inertial impaction, and yet large enough to exhibit negligible Brownian diffusivity. Indeed, it is in this intermediate size range (typically having diameters between ca 10^{-1} and 10 μm) that we expect the most important influence of photophoresis upon particle deposition rates. Even in cases where most of the mainstream particle mass loading is due to larger particles, the photophoretic effect can still exert a considerable influence on system performance since the intermediate size particles (often droplets) could serve as a 'glue' to assist the capture of still larger impacting 'solid' particles[14] or alter the conditions of (underlying) metal corrosion (e.g. associated with the collection of 'soot' particles).

2. PHOTOPHORETIC AND THERMOPHORETIC PARTICLE 'DIFFUSIVITIES'

The local thermophoretic velocity (i.e., the terminal velocity reached for an isolated particle in a gas with a locally constant temperature gradient) is normally written in the form:

$$v_T = \alpha_T D_p \cdot [-(\text{grad } T)/T] \tag{1}$$

where α_T is the dimensionless *thermal diffusion factor* and D_p the Brownian diffusion coefficient of the particles. Actually, D_p is included here just to emphasize the similarity between v_T and a diffusion velocity, but the value of the *thermophoretic diffusivity* $\alpha_T D_p$ does not really depend on D_p (which, in fact, will be taken to be zero in our present asymptotic analysis). For spherical particles in the near-continuum (or slip-flow) regime (i.e., the particle radius, a, is much larger than the gaseous mean-free path, l), $\alpha_T D_p$ can be obtained from solution of the conduction and creeping-flow equations with slip-corrected boundary conditions.[15-17] This analysis yields:

$$\alpha_T D_p = \frac{2c_s \nu \left(\frac{k_g}{k_p} + c_t \frac{l}{a}\right)\left[1 + \frac{l}{a}(A + Be^{-Ca/l})\right]}{\left(1 + 3c_m \frac{l}{a}\right)\left(1 + 2\frac{k_g}{k_p} + 2c_t \frac{l}{a}\right)} \tag{2a}$$

where ν is the gas momentum diffusivity (kinematic viscosity), k_g and k_p are the thermal conductivities of the gas and particle*, respectively; and $l \approx 2\nu/\bar{c}$, with $\bar{c} = (8RT/\pi M_g)^{1/2}$. The parameters in the Cunningham correction factor have the approximate values $A = 1.20$, $B = 0.41$, $C = 0.88$. The coefficients of thermal slip, momentum exchange, and temperature jump have values (for perfect accommodation) of $c_s = 1.17$, $c_m = 1.14$, and $c_t = 2.18$, respectively. In the free-molecular limit, i.e. $a \ll l$, the analysis of Waldmann for perfect accommodation yields:[16,18,19]

$$\alpha_T D_p = 0.54\nu \tag{2b}$$

In view of the fact that Eq. (2a), evaluated at the limit $l \gg a$, yields the numerical factor 0.56, Talbot *et al.*[14] suggested that Eq. (2a) should provide a useful approximation for $\alpha_T D_p$ in the transition regime ($l \approx a$).

By analogy,[10] the corresponding *photophoretic velocity* for an isolated particle will be written

$$v_{ph} = \alpha_{ph} D_p \cdot \frac{\dot{q}''_R}{k_g T} \tag{3}$$

where $\alpha_{ph} D_p$ is the *photophoretic diffusivity* and $\dot{q}''_R$ the local radiative heat flux. The photophoretic diffusivity can be obtained in the slip-flow and free-molecular regimes from an analysis to that for the thermophoretic diffusivity, with the exception that the absorption of radiation within the particle is now included in the particle conduction equation. In the slip flow regime, this analysis yields[10]

$$\alpha_{ph} D_p = -\frac{2c_s \nu J_1}{3} \cdot \frac{1 + \frac{l}{a}(A + Be^{-Ca/l})}{\left(1 + 3c_m \frac{l}{a}\right) \cdot \left(1 + 2c_t \frac{l}{a} + 2\frac{k_g}{k_p}\right)} \tag{4}$$

whereas, in the free-molecular limit, the corresponding expression is (for perfect accommodation):

$$\alpha_{ph} D_p = -0.14 \nu J_1 \cdot (a/l) \tag{5}$$

Here, J_1 is the photophoretic asymmetry factor and represents a weighted integration of the absorption of radiant energy over the particle volume. For spherical, homogeneous particles and monochromatic radiation, J_1 has been obtained from Lorenz-Mie

* For particles in the size range of interest here there is no appreciable error in neglecting the heat transport effects of the rotation that particles would inevitably experience in a 'vortical' boundary layer flow.

theory as a function of the particle radiative size parameter $x = 2\pi a/\lambda$, where λ is the radiation wavelength, and the complex index of refraction $m = n + ik$. An exact, series-expansion expression for J_1 has been derived which is analogous to the expressions for the radiative cross sections.[10]

As its name implies, J_1 reflects the asymmetry in the distribution of energy absorption within the particle. As the particle dimensions become much smaller than the wavelength of the radiation ($x \ll 1$), the energy absorption within the particle becomes uniform and J_1 rapidly goes to zero. On the other hand, absorption for particles having $x \gg 1$ takes place essentially at the surface facing the radiation source. For this case J_1 approaches the limiting minimum value of -0.5. It is interesting to note that J_1 can, in general, be negative or positive. A positive J_1 implies that radiation absorption is weighted towards the side of the particle facing away from the radiation source, leading to v_{ph} directed towards the radiation. Physically, this situation arises for relatively weakly-absorbing particles (such as fly ash) having size parameters x of the order of 1–10.

For spectrally-distributed radiation (such as thermal radiation), J_1 is obtained from integration of its monochromatic value over the prevailing wavelength distribution. In the examples below, it will be assumed that the incident radiation can be approximated by a blackbody spectrum characterized by a radiation temperature T_R and that the refractive index m of the particle is wavelength-independent. Under this approximation, the wavelength-integrated J_1 can be expressed as a function of a thermal radiation size parameter, $x = 2\pi a/\lambda_{max}$, where λ_{max} corresponds to the wavelength of maximum emission at temperature T_R, i.e. $\lambda_{max} = 2898\,\mu m\,K/T_R$.

Unfortunately, there have been very few experimental investigations of photophoresis, but several studies involving spherical particles (such as droplets) have resulted in a good agreement between measurements and theory.[20,21] Interestingly, in a recent investigation by Rohatschek,[22] the photophoretic velocities of irregularly-shaped particles were found to be well in excess of the theoretical predictions for 'equivalent' spherical particles. In view of the fact that photophoresis is ultimately the result of an asymmetric property of the particle (e.g. asymmetry in the absorption of radiation), it is reasonable to expect that particles having an inherent asymmetry in their shape will experience a larger photophoretic velocity than spherical particles.[39]

3. UNDERLYING ASSUMPTIONS AND FORMULATION OF PARTICLE DEPOSITION RATE THEORY

To simplify the problem of predicting particle photophoretically-modified deposition rates, without losing its essential features, the following defensible assumptions will be made:

(1) Flow within the boundary layer (BL) is steady and laminar (L). The usual LBL approximations will be adopted and self-similarity assumed (see, e.g., Schlichting).[23]

(2) Aerosol particles are present not only at low volume fractions but also at small *mass* fractions, so that the prevailing mixture velocity and temperature fields are not significantly affected by their presence.

(3) All thermophysical properties of the host gas will be considered constant and taken to be equal to the values for the carrier gas at mainstream conditions. Photophoretic and thermophoretic transport properties for the dispersed particles will also be taken to be constant. Lastly, the mixture will be considered effectively incompressible, i.e., the density will be assumed to be constant.

(4) Aerosol particles do not appreciably diffuse as a result of their Brownian motion (i.e. $Sc \equiv \nu/D_p \gg 1$). Therefore, at each position, the (deterministic) velocity of the particles is taken to be the gas velocity plus the thermophoretic and photophoretic velocities, with these velocities being those corresponding to an isolated particle in a locally uniform gas with the same temperature gradient and radiant energy flux. The direction of the radiative flux will be taken to be normal to the solid collecting surface.

The accuracy of most of these assumptions has been discussed elsewhere[24,25] and these restrictions can readily be relaxed in sufficiently extreme cases.[26–28]

Because of its relevance to the forward stagnation region of a heat exchanger tube in cross-flow, we consider the two-dimensional stagnation point (Hiemenz) flow. This corresponds to a steady flow which arrives from the direction of the y-axis, impinges on a (locally) flat solid wall placed at $y = 0$, where it divides into two streams near the wall, leaving in both ($\pm$) x-directions. The external (inviscid) tangential velocity distribution in the neighborhood of the symmetrical forward stagnation 'point' (at $x = y = 0$) is given[23] by:

$$u_e(x) = \left(\frac{du_e}{dx}\right)_{x=0} \cdot x \qquad (6)$$

For this high Reynolds number laminar stagnation region flow of a constant property Newtonian fluid, the local velocity and temperature fields are well-known functions of only the 'stretched' distance, η, from the wall, where

$$\eta \equiv y \cdot \left[\frac{1}{\nu}\left(\frac{du_e}{dx}\right)_{x=0}\right]^{1/2} \qquad (7)$$

and can be expressed via the dimensionless stream (Blasius) function $f(\eta)$.[23]

Our interest is now focused on the motion of the small suspended particles in this local flow field, under the simultaneous influence of host gas convection, particle thermophoresis and particle photophoresis. Suppose, for simplicity, that in the mainstream there

are $N_{p,\infty}$ particles per unit volume, each with radius, a_∞. In the absence of particle coagulation or break-up, the local number density of particles, N_p, satisfies the partial differential (conservation) equation[4]

$$\mathrm{div}\{v_p N_p\} = 0. \tag{8}$$

Under assumption (4), the local particle velocity is given by the vector sum:

$$v_p = v + v_{ph} + v_T \tag{9}$$

with v_{ph} and v_T given by Eq. (3) and Eq. (1), respectively. Defining $n \equiv N_p/N_{p,\infty}$, the first order linear ODE for n takes the simple form:

$$A\frac{dn}{d\eta} + Bn = 0 \tag{10}$$

where we have introduced the dimensionless functions:

$$A\{\eta\} \equiv f\{\eta\} + \left(\beta + \alpha\frac{d\theta}{d\eta}\right), \tag{11}$$

$$B\{\eta\} \equiv \alpha\frac{d^2\theta}{d\eta} = \alpha Prf\frac{d\theta}{d\eta}, \tag{12}$$

$$\theta\{\eta; Pr\} \equiv T/T_\infty \tag{13}$$

where $Pr \equiv [\nu/(k/\rho c_p)]_g$ is the gas Prandtl number (momentum/heat diffusivity ratio). Two important dimensionless parameters are:

$$\alpha \equiv (\alpha_T D_p)/\nu \quad \text{(thermophoretic)}, \tag{14}$$

$$\beta \equiv \frac{\alpha_{ph} D_p(-q''_{R,y})}{k_g T_\infty}\cdot\left[\nu\left(\frac{du_e}{dx}\right)_{x=0}\right]^{-1/2}$$

(photophoretic) (15)

where $q''_{R,y}$ is the normal (y) component of the radiative flux.

4. RESULTS

The solution of Eq. (1), with the single boundary condition $n = 1$ @ $y = \infty$, can be written in the form of a 'quadrature':

$$n\{\eta\} = \exp\left[\int_\eta^\infty \frac{B\{\varphi\}}{A\{\varphi\}}\,d\varphi\right] \tag{16}$$

which allows the straightforward numerical calculation of $n\{0\} \equiv n_w = N_{p,w}/N_{p,\infty}$ (as required below).

The normal velocity of particles within the boundary layer is given by

$$v_p = v + v_T + v_{ph} = -\left[\nu\left(\frac{du_e}{dx}\right)_{x=0}\right]^{1/2}\cdot\left[f + \alpha\left(\frac{d\theta}{d\eta}\right) + \beta\right] \tag{17}$$

which is negative for particles approaching the wall.

Under some circumstances, the particles cannot reach the wall ($\eta = 0$) and a 'dust-free' region (sublayer) appears inside the boundary layer.[5] The separation line $\eta = \eta_{sl}$ between the dust-laden region and the 'dust-free' region is located at the value of η where $v_p = 0$; that is, where

$$A \equiv f + \left(\beta + \alpha\frac{d\theta}{d\eta}\right) = 0. \tag{18}$$

In most engineering applications, both transport mechanisms 'cooperate' in bringing particles *toward* the wall. However, when they 'compete' (oppose one another) the dust free zone exists only when

$$-\beta \geq \frac{\alpha}{\delta}(1 - \theta_w) \text{ for } \beta < 0 \text{ and } \theta_w < 1 \tag{19}$$

or

$$\frac{\alpha}{\delta}(\theta_w - 1) \geq \beta \quad \text{for } \beta > 0 \text{ and } \theta_w > 1$$

('hot wall' case) (20)

where the dimensionless thermal diffusion BL thickness $\delta\{Pr\} = 2.0167$ for $Pr = 0.7$. Note that when both transport velocities oppose each other and are exactly equal in magnitude at the wall (i.e., when the equal sign is attained in the above inequalities) the separation line coincides with the wall; that is, particle deposition vanishes even when the particles are to be found everywhere inside the boundary layer. In this very particular case, however, some deposition will occur due to non-zero Brownian diffusion.[20] Not surprisingly, when thermophoresis and photophoresis both force the particles *away* from the wall, that is, when $\theta_w > 1$ and $\beta < 0$, the 'dust-free' zone will exist for any value of β and θ_w and particles will not be collected by the solid surface.

Focusing now on cases when none of the above inequalities holds, the particle deposition rate will be given by:

$$N_{p,w}\cdot(-v_{p,w}) = \left[\nu\left(\frac{du_e}{dx}\right)_{x=0}\right]^{1/2}\cdot N_{p,\infty} n_w \cdot \left[\beta + \frac{\alpha}{\delta}(1 - \theta_w)\right]. \tag{21}$$

Thus, the *dimensionless* deposition rate coefficient, S, of particles will be:

$$S \equiv \frac{N_{p,w}\cdot(-v_{p,w})}{N_{p,\infty}\left[\nu\left(\frac{du_e}{dx}\right)_{x=0}\right]^{1/2}} = n_w\cdot\left[\beta + \frac{\alpha}{\delta}(1 - \theta_w)\right]. \tag{22}$$

The dimensionless deposition rate, S, is closely related to the transfer coefficient: $St_\infty \cdot Re^{1/2}$ often used in reporting mass transfer rates across laminar forced-

convection boundary layers.[4] For perhaps the case of greatest practical interest, viz., the forward stagnation region of an 'isolated' cylinder of diameter d_w in high Reynolds number crossflow, it is easy to show that $St_m \cdot Re^{1/2} = 2 \cdot S\{\theta_w, \alpha, \beta; Pr\}$ where $Re \equiv U_\infty d_w/\nu_g$ and St_m is defined such that the local mass deposition flux is $(\rho U \omega_p)_\infty \cdot St_m$.

If one is interested in the corresponding *mass* deposition rate (instead of particle *number* deposition rate), the appropriate dimensionless transfer coefficient is:

$$J_m \equiv \frac{1}{\rho \omega_{p,\infty}} \left[\nu \left(\frac{du_t}{dx} \right)_{x=0} \right]^{-1/2} \cdot (-j''_{m,w}) \quad (23)$$

where $\omega_{p,\infty}$ is the mass fraction of particles in the mainstream and $-j''_{m,w}$ is the total mass deposition flux at the wall. It is easy to see that, for the case of single-size particles, $J_m = S$. But when we consider the generally encountered case of a distribution of particle sizes and intrinsic particle density $\tilde{\rho}_p\{a\}$ in the mainstream[30] the definition (23) can be retained, but we readily find that the total mass transfer coefficient, J_m, is obtained from the following 'weighting' of $S\{a\}$:

$$J_m = \frac{\int n_\infty\{a\} \tilde{\rho}_p\{a\} a^3 S\{a\} \, da}{\int n_\infty\{a\} \tilde{\rho}_p\{a\} a^3 da} \quad (24)$$

where $n_\infty\{a\} \equiv dN_{p,\infty}/da$ and $S\{a\}$ is given by Eq. (22), with n_w, β being functions of the particle radius a.

5. DISCUSSION OF EFFECTS OF SIMULTANEOUS PHOTOPHORESIS AND THERMOPHORESIS

Figure 1 presents the predicted dimensionless transfer coefficient, S, as a function of the wall temperature ratio T_w/T_∞, for particles having a thermophoretic coefficient $\alpha = 0.5$ (a value close to that corresponding to the free-molecular limit). The curve labelled $\beta = 0$ corresponds to 'pure' thermophoretic deposition with negligible photophoretic particle transport. In that previously well-studied case, particles are captured only by 'cold' surfaces (i.e. when $T_w/T_\infty < 1$) and as previously shown[5,6,26] the deposition rate increases as the wall temperature *decreases*. When photophoresis acts to drive the particles *toward* the surface (i.e. when $\beta > 0$), it produces two effects: on one hand, it can cause the capture of particles even for 'overheated' surfaces ($T_w/T_\infty > 1$). More commonly, it can noticeably increase the dimensionless deposition rate S for given 'cold-wall' values of the ratio T_w/T_∞. The opposite is true for negative values of β (which need not correspond to an outward radiation flux since α_{ph} can be negative; see Fig. 3 discussed below), the range of temperatures over which deposition occurs is diminished as well as the deposition rate for a given surface temperature. Analogous results are obtained for the lower thermophoretic parameter $\alpha = 0.1$ (Fig. 2) although, of course, the relative importance of photophoresis (cf. thermophoresis) is then greater. Thus, for $\beta = -10^{-1}$, no deposition occurs for the entire range of surface temperature ratios considered.

From Eq. (15), it can be seen that the photophoretic parameter β can be re-expressed:

$$\beta = \frac{1 - \theta_w}{\delta} \cdot \left(\frac{\dot{q}''_R}{\dot{q}''_F} \right) \cdot \alpha F \quad (25)$$

where $\dot{q}''_F$ is the conductive (Fourier) heat flux *at the solid surface*, and F is the ratio ν_{ph}/ν_T computed for equal $\dot{q}''_R$ and $\dot{q}''_F$. For particles in the slip-flow regime ($l/a < 1$), F can be expressed[10]

$$F = \frac{J_1 k_g}{3k_p \cdot \left(\frac{k_g}{k_p} + c_t \frac{l}{a} \right)} \quad (26)$$

Numerical results of F for carbonaceous char and fly ash particles with $k_g/k_p \approx 0.1$, exposed to a black body radiation spectrum at $T_{Rad} = 1800$ K originally presented by Mackowski[10] are reproduced in Fig. 3. Note that because of the nature of radiative heating of

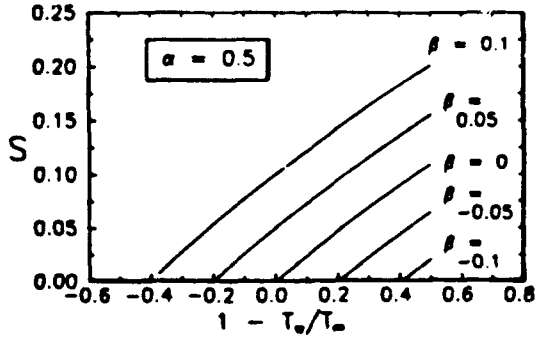

FIG. 1. Predicted dimensionless deposition rates, S, of particles as a function of the temperature contrast parameter $1 - (T_w/T_\infty)$, for a constant thermophoretic coefficient $\alpha = 0.5$ (Eq. (14)) and different values of the photophoretic coefficient β (Eq. (15)). Laminar two-dimensional stagnation point boundary layer flow of a 'dusty' gas with Prandtl number $Pr \approx 0.7$.

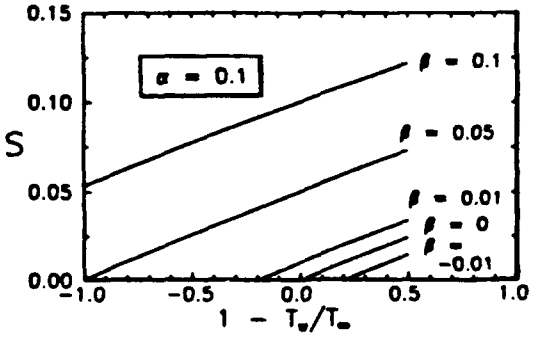

FIG. 2. Predicted dimensionless deposition rates, S, of particles as a function of the temperature contrast parameter $1 - (T_w/T_\infty)$, for a constant thermophoretic coefficient $\alpha = 0.1$ (Eq. (14)) and different values of the photophoretic coefficient β (Eq. (15)).

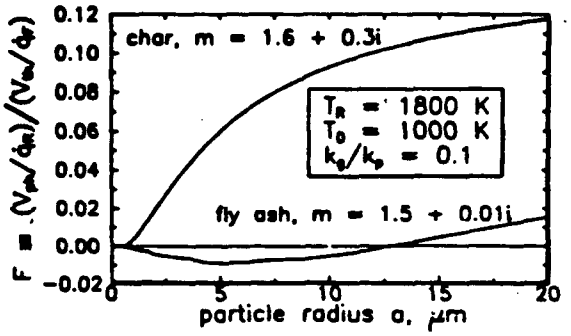

FIG. 3. Predicted[10] photophoretic-to-thermophoretic particle velocity ratio, F, for equal radiative and conductive heat flux for carbonaceous char and fly ash particles, as a function of particle radius. Radiation temperature $T_{R,\infty}$ = 1800 K.

small silica-like particles, (small) negative values of F can be achieved. This means that a radiative flux *toward* the wall will *inhibit* the deposition rate of sufficiently small silica-like particles, but accelerate the deposition of larger particles. For particles with 'char-like' absorption characteristics this interesting 'reversal' situation does not occur and the values of the phoretic velocity ratio, F, are seen to be considerably larger.

By using the above expression for β together with the values of F indicated in Fig. 3, the deposition rate of char-like (absorbing) particles has been predicted and it is represented in Fig. 4 for the fixed value $T_w/T_\infty = 0.7$ and different $\dot{q}''_R/\dot{q}''_F$ ratios. For vanishing radiative fluxes the larger char particles are somewhat less efficiently captured due to their smaller thermophoretic coefficient a (obtained from Eq. (2)). If the radiative heat flux were directed *from* the solid surface towards the bulk (i.e., when $\dot{q}''_R > 0$), the char particles would be rejected by photophoresis and the deposition rate would decrease. Note that for very large outward radiative fluxes, photophoresis would preclude the thermophoretic capture of char particles larger than a given size. Ultimately, however, *inertial* effects (not considered here) would set in and dominate the rate of larger particle collection.[1,31-33]

Lastly, it is of interest to ask if a simple 'additive suction velocity' prediction/correlation scheme of the type introduced earlier[11,34,35] and currently under further development, can be used to estimate deposition rates under the combined influences of forced convection, thermophoresis and photophoresis. In the present cases, we find that this scheme leads us to expect:

$$S\{a\} \approx [S\{a\}]_{\dot{q}''_R/\dot{q}''_F=0} \cdot \left\{1 + \text{const} \cdot \left(\frac{\dot{q}''_R}{\dot{q}''_F}\right) \cdot F\left\{\left(\frac{a}{l}, \frac{2\pi a}{\lambda}, \ldots\right)\right\}\right\} \quad (27)$$

where 'const.' is a Pr-dependent constant near unity for $Pr \approx 0.7$.

The relative error between Eq. (27) and the exact results presented in Fig. 4 is less than 5% for all $|\dot{q}''_R/\dot{q}''_F|$ ratios and particle radius values. The 'additive suction velocity' scheme is quite successful and, hence, promising for engineering design purposes.

6. CONCLUSIONS, IMPLICATIONS

A number of interesting conclusions can be drawn even from this preliminary investigation of the role of *photophoresis* in altering the deposition rate of absorbing particles on solid surfaces exposed to moving 'dusty' gases:

(1) For intermediate size absorbing particles the recent *photophoretic* predictions of Mackowski[10] lead us to expect a noticeable (ca 10%) increase in particle deposition rates to heat exchanger surfaces exposed to incident radiative fluxes comparable to 'convective' (local conductive) fluxes. For environments in which the radiative flux *dominates* convection the photophoretic influence on the deposition rates of such absorbing particles thus takes on engineering importance.

(2) In the case of 'intermediate' size particles for which $v/D_p \gg 1$ and yet *inertia* is negligible[31-34] it is possible to make generalized (dimensionless) predictions of the photophoretically modified (augmented or reduced) particle deposition rate across laminar non-isothermal forced convection boundary layers.

(3) Even at the radiative/conductive flux ratios achieved in ordinary engineering practice (in, say, pulverized coal power stations and furnaces) photophoretic deposition effects are expected to be negligible for very small particles (say, $d_p \ll 1\,\mu$m) and for particles large enough to be strongly influenced by their inertia (say, $d_p \gg 10\,\mu$m).[31-34] The effects for intermediate size particles are also diminished if the particles are highly thermally conductive.

(4) An 'additive suction velocity' scheme for conveniently calculating/correlating particle deposition rates in flow systems under the simultaneous influence of several mechanisms, currently under development at this laboratory[34,35] successfully describes the present high Sc LBL-results for all $\dot{q}''_R/\dot{q}''_F$ ratios of current practical interest.

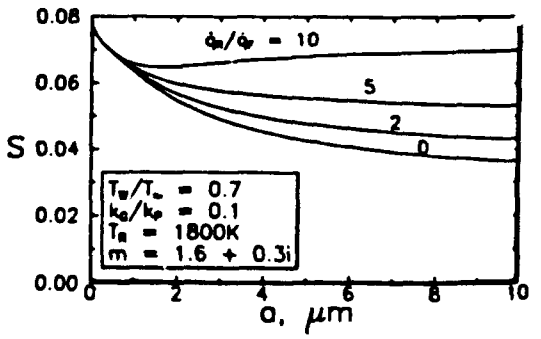

FIG. 4. Predicted dimensionless deposition rates, S, for char-like particles as a function of the particle size (radius) a, for a heat exchanger surface maintained at $T_w/T_\infty = 0.7$ and different ratios of the radiative to conductive heat flux at the surface.

(5) Size- and wavelength-dependent photophoretic control of the local deposition rate of (partially) absorbing particles from hot 'dusty' gases could be exploited using intense laser sources, perhaps for research purposes.

While we have here explicitly considered *laminar* (stagnation region) boundary layer flows it should be realized that because of the existence of rate-limiting-viscous sublayers near the solid surface of sufficiently smooth surfaces,[1,4,23,28] even *turbulent* BL particle transport will exhibit many of the characteristics exhibited above. Regarding photophoretic influences away from the foward stagnation 'point', it seems clear that the (locally) *normal (y-) component* of radiative energy fluxes will remain decisive. Indeed, it will be of interest to test the conjecture that at any position x along an immersed body:

$$St_m \cong (St_m)_{q_R=0} \cdot \left\{1 + \text{const.} \cdot \frac{\dot{q}''_{R,y}(x)}{\dot{q}''_{F,y}(x)} \cdot F\left(\frac{a}{l}, \frac{2\pi a}{\lambda}, \ldots\right)\right\} \quad (28)$$

where, for a circular cylinder in crossflow, the calculation of local values of $(St_m Re^{1/2})_{q_R=0}$ prior to transition to turbulence (and for $Sc \gg 1$) has been previously performed.[36-38]

Our results have implications beyond those associated with 'fouling' in particle-laden systems. For example, in *aerosol sampling* applications, it is evident from these illustrative cases that the combination of photophoresis and thermophoresis induces changes in the inferred particle size distribution in the mainstream through the dependence of α and β on particle size. Indeed, by an appropriate combination of radiative and conductive fluxes, particle sizes larger than a given value could be avoided in a deposit and, for particles which present an extreme in the function $F(a/l, 2\pi a/\lambda, \ldots)$ (as is the case for fly ash particles) using appropriate radiative fluxes only a narrow width of particle sizes could be 'selected' to deposit. It may be possible to exploit photophoretic control to reduce or eliminate particle contamination in technologies such as semiconductor fabrication processes.[27,29] As discussed elsewhere[40] radiation heating or cooling of particles also influences the coagulation dynamics of aerosol populations, especially in the near-continuum (high pressure) regime. Finally, since *asymmetries* will be common in combustion-generated particles (e.g., aggregates) the 'anomalous' photophoresis and Brownian diffusivity of such particles requires further study.[39]

The insights obtained from the present deliberately simplified analysis are expected to provide useful background in developing necessary extensions for particular technologies. In this way we hope the present theory and illustrative results systematically contribute to the understanding and ultimate control of undesirable or desirable particle deposition phenomena encountered in many energy conversion applications and in the materials processing industries.

Acknowledgements—It is a pleasure to acknowledge the financial support of DOE-PETC (under grant DE-FG22-86PC90756) and the U.S. AFOSR (under grant AFOSR-89-0223) as well as the related support of the Yale HTCRE Laboratory by our current Industrial Affiliates: Shell, General Electric, Textron-Lycoming and SCM-Chemicals. The authors have benefited from the perceptive comments of J. Fernandez de la Mora, M. Tassopoulos, M. Sitarski, A. Konstandopoulos, and P. Garcia-Ybarra.

REFERENCES

1. Friedlander, S. K., *Smoke, Dust and Haze—Fundamentals of Aerosol Behavior*, J. Wiley, New York (1977).
2. Fernandez de la Mora, J. and Rosner, D. E., Inertial deposition of particles revisited and extended: Eulerian approach to a traditionally langrangian problem, *J. Physico Chem. Hydrodynamics* **2**, 1–21 (1981).
3. Fernandez de la Mora, J. and Rosner, D. E., Effects of inertia on the diffusional deposition of small particles to spheres and cylinders at low Reynolds numbers, *J. Fluid Mech.* **125**, 379–395 (1982).
4. Rosner, D. E., *Transport Processes in Chemically Reacting Flow Systems*, Butterworths, Stoneham, MA (1986); second printing (1988).
5. Goren, S. L., Thermophoresis of aerosol particles in the laminar boundary layer on a flat plate, *J. Colloid Interf. Sci.* **61**, 77–85 (1977).
6. Rosner, D. E. and Kim, S. S., Optical experiments on thermophoretically augmented submicron particle deposition from 'dusty' high temperature gas flows, *Chem. Engng J.* **29**, 3, 147–157 (1984).
7. Viskanta, R., and Menguc, M. P., Radiation heat transfer in combustion systems, *Prog. Energy Combust. Sci.* **13**, 97–160 (1987).
8. Yalamov, Yu., Kutukov, V. B. and Shchukin, E. R., Theory of the photophoretic motion of the large-size volatile aerosol particle, *J. Colloid Interf. Sci.* **57**, 564–571 (1976).
9. Akhtaruzzaman, A. F. M. and Lin, S. P., Photophoresis of absorbing particles, *J. Colloid Interf. Sci.* **61**, 171–182 (1977).
10. Mackowski, D. W., Photophoresis of aerosol particles in the free-molecular and slip-flow regimes, *Int. J. Heat Mass Transfer* **32**, 843–854 (1989).
11. Rosner, D. E., Thermal (Soret) diffusion effects on interfacial mass transport rates, *J. Physico Chem. Hydrodynamics* **1**, 159–185 (1980).
12. Rosner, D. E., Mass transfer across gas thermal boundary layers—power production and materials processing implications, *Heat Transfer in Fire and Combustion Systems* HTD 45, ASME, N.Y. 3–8 (1985).
13. Rosner, D. E. and Fernandez de la Mora, J., Small particle transport across turbulent non-isothermal boundary layers, ASME Trans., *J. Engng Power* **104**, 885–894 (1982).
14. Rosner, D. E. and Nagarajan, R., Toward a mechanistic theory of net deposit growth from ash-laden flowing combustion gases: self-regulated sticking of impacting particles and deposit erosion in the presence of vapor 'glue', Proc. 24th National Heat Transfer Conference, *A.I.Ch.E. Symposium Series* **83**, R. W. Lyczkowski (Ed.) (257), pp. 289–296 (1987).
15. Brock, J. R., On the theory of thermal forces acting on aerosol particles, *J. Colloid Sci.* **17**, 768–780 (1962).

16. TALBOT, L., CHENG, R. K., SCHEFER, R. W. and WILLIS, D. R., Thermophoresis of particles in a heated boundary layer, *J. Fluid Mech.* **101**, 737–758 (1980).
17. TALBOT, L., Thermophoresis—a review, *Rarefied Gas Dynamics*, Part 1, S. S. Fisher (Ed.), *Prog. Astronaut. Aeronaut.* **74**, 467–488 (1981).
18. WALDMANN, L., *Rarefied Gas Dynamics*, L. Talbot (Ed.), p. 323, Academic Press (1961).
19. GARCIA-YBARRA, P. and ROSNER, D. E., Thermophoretic properties of nonspherical particles and large molecules *A.I.Ch.E. Jl* **35**, (1) 139–147 (1989).
20. ARNOLD, S., AMANI, Y. and ORENSTEIN, A., Photophoretic spectrometer, *Rev. Sci. Instrum.* **51**, 1202–1204 (1980).
21. ARNOLD, S. and LEWITTES, M., Size dependence of the photophoretic force, *J. Appl. Phys.* **53**, 5314–5319 (1982).
22. ROHATSCHEK, H., Direction, magnitude, and causes of photophoretic forces, *J. Aerosol Sci.* **16**, 29–42 (1985).
23. SCHLICHTING, H., *Boundary Layer Theory*, McGraw-Hill (6th edn) (1968).
24. CASTILLO, J. L. and ROSNER, D. E., Nonequilibrium theory of surface deposition from particle-laden, dilute condensible vapor-containing stream, allowing for particle thermophoresis and vapor scavenging within the laminar boundary layer, *Int. J. Multiphase Flow* **14** (1) 99–120 (1988).
25. CASTILLO, J. L. and ROSNER, D. E., Theory of surface deposition from a unary dilute vapor containing stream allowing for condensation within the laminar boundary layer, *Chem. Engng Sci.* **44** (4) 925–937 (1989).
26. GOKOGLU, S. A. and ROSNER, D. E., Thermophoretically-augmented forced convection mass transfer rates solid walls across non-isothermal laminar boundary layers, *AIAA J.* **24**, (1) 172–179 (1986).
27. GOKOGLU, S. A. and ROSNER, D. E., Prediction and rational correlation of thermophoretically reduced particle mass transfer to hot surfaces across laminar or turbulent forced-convection gas boundary layers, *Ch.E. Commun.* **44**, 107–119 (1986).
28. ROSNER, D. E. and PARK, H. M., Thermophoretically augmented mass, momentum and energy transfer rates in high particle mass-loaded laminar forced convection systems, *Chem. Engng Sci.* **43** (10) 2689–2704 (1988).
29. FRIEDLANDER, S. K., FERNANDEZ DE LA MORA, J. and GOKOGLU, S. A., Diffusive leakage of small particles across the dust-free layer near a hot wall, *J. Colloid Interf. Sci.* **125**, 351–355 (1988).
30. ROSNER, D. E., Total mass deposition rates from 'polydispersed' aerosols, *A.I.Ch.E. Jl* **35**, (1) 164–167 (1989).
31. ISRAEL, R. and ROSNER, D. E., Use of a generalized Stokes number to determine the aerodynamic capture efficiency of non-Stokesian particles from a compressible gas flow, *Aerosol Sci. Technol.* **2**, 45–51 (1983).
32. WESSEL, R. A. and RIGHI, J., Generalized correlations for inertial impaction of particles on a circular cylinder, *Aerosol Sci. Technol.* **9**, (1) 29–60 (1988).
33. WANG, H. C., Theoretical adhesion efficiency for particles impacting a cylinder at high Reynolds number, *J. Aerosol Sci.* **17**, 827–837 (1986).
34. ROSNER, D. E., ISRAEL, R. and ZYDNEY, A., Effect of thermophoresis on minimum aerosol diffusional deposition rate before the onset of inertial impaction, presented at the *ACS/IEC-81 Winter Symposium on Aerosol Systems*, Tucson, AZ, 26–28 (1981).
35. GOKOGLU, S. A. and ROSNER, D. E., Correlation of thermophoretically-modified small particle diffusional deposition rates in forced convection systems with variable properties, transpiration cooling and/or viscous dissipation, *Int. J. Heat Mass Transfer* **27**, 639–645 (1984).
36. WALKER, K. L., HOMSY, G. M. and GEYLING, F. T., Blasius series for thermophoretic deposition of small particles, *J. Colloid Interf. Sci.* **83**, 495–501 (1981).
37. BATCHELOR, G. K. and SHEN, C., Thermophoretic deposition of particles in gas flowing over cold surfaces, *J. Colloid Interf. Sci.* **107**, 21–37 (1985).
38. SHEN, C., Thermophoretic deposition of particles onto cold surfaces of bodies in two-dimensional and axisymmetric flows, *J. Colloid Interf. Sci.* **127**, (1) 104–115 (1989).
39. MACKOWSKI, D. W., Phoretic behavior of asymmetric particles in thermal non-equilibrium with the gas: two sphere aggregates, *J. Colloid Interf. Sci.* (in press, 1990).
40. ROSNER, D. E., MACKOWSKI, D. W., TASSOPOULOS, M., CASTILLO, J.L. and GARCIA-YBARRA, P., Effects of heat transfer on the dynamics and transport of small particles in gases, *Ninth Int. Heat Transfer Conf.*, Poster OPF II-18, August 23, 1990 Jerusalem, Israel; I/EC-Research (ACS) (submitted, 1990).

HIGH TEMPERATURE CHEMICAL REACTION ENGINEERING LABORATORY
YALE UNIVERSITY
BOX 2159, YALE STATION
NEW HAVEN, CONNECTICUT 06520 U.S.A.

REPORT DOCUMENTATION PAGE

Form Approved
OMB No. 0704-0188

1. AGENCY USE ONLY (Leave blank)	2. REPORT DATE	3. REPORT TYPE AND DATES COVERED
	1989	Journal Publication

4. TITLE AND SUBTITLE

"Total Mass Deposition Rates from 'Polydispersed' Aerosols" (U)

5. FUNDING NUMBERS

PE - 61102F
PR - 2308
SA - BS
G - AFOSR 89-0223

6. AUTHOR(S)

Daniel E. Rosner

7. PERFORMING ORGANIZATION NAME(S) AND ADDRESS(ES)

HIGH TEMPERATURE CHEMICAL REACTION ENGINEERING LABORATORY
YALE UNIVERSITY
BOX 2159, YALE STATION
NEW HAVEN, CONNECTICUT 06520 U.S.A.

8. PERFORMING ORGANIZATION REPORT NUMBER

9. SPONSORING/MONITORING AGENCY NAME(S) AND ADDRESS(ES)

AFOSR/NA
Building 410
Bolling AFB DC 20332-6448

10. SPONSORING/MONITORING AGENCY REPORT NUMBER

11. SUPPLEMENTARY NOTES

12a. DISTRIBUTION/AVAILABILITY STATEMENT

Approved for public release; distribution is unlimited

12b. DISTRIBUTION CODE

13. ABSTRACT (Maximum 200 words)

We consider particle deposition rates from "coagulation-aged" aerosol-containing streams. For high Schmidt number-low mass loading convective-diffusion we prove that, to a first approximation, total mass deposition rates will be about 90 percent of the values corresponding to a hypothetical 'monodispersed' aerosol (with all particles having the *mean* particle volume ϕ_p/N_p) under otherwise identical fluid dynamic and geometric conditions. To within about +/- 2 percent these simple results are shown to be insensitive to the fluid dynamic state of the boundary layer (laminar or turbulent), particle Knudsen number, and even apply to "open" (fractal) quasi-spherical agglomerates.

14. SUBJECT TERMS

deposition, coagulation, convective-diffusion, polydispersed aerosols, eddy impaction

15. NUMBER OF PAGES

4

16. PRICE CODE

17. SECURITY CLASSIFICATION OF REPORT	18. SECURITY CLASSIFICATION OF THIS PAGE	19. SECURITY CLASSIFICATION OF ABSTRACT	20. LIMITATION OF ABSTRACT
Unclassified	Unclassified	Unclassified	UL

Reprinted from AICHE JOURNAL, January 1989

Total Mass Deposition Rates from "Polydispersed" Aerosols

Daniel E. Rosner
High Temperature Chemical Reaction
Engineering Laboratory
Department of Chemical Engineering
Yale University
New Haven, CT 06520

Research in the last two decades has led to a greatly improved understanding of the nature of particle size *distributions* resulting from the various coagulation mechanisms (see, for example, the review of Friedlander, 1977, in Chapter 7), as well as of the laws governing single-sized particle deposition across gaseous boundary layers Rosner (1986). Quantitative information from both of these areas is, of course, needed to predict total mass deposition rates from "polydispersed" aerosols in engineering applications. In the present paper we demonstrate that, over a rather wide range of important conditions, total mass deposition rates from polydispersed aerosols resulting from coagulation, can be readily calculated from the corresponding deposition rate from a hypothetical "monodispersed" aerosol in which all particles have the prevailing average size (volume) $\bar{v}(=\phi_p/N_p)$. We illustrate our approach for the frequently encountered case of high-Peclet-number convective diffusion across nearly isothermal boundary layers, obtaining results that are remarkably insensitive to fluid dynamic conditions [laminar or turbulent boundary layer (BL)], particle Knudsen number (free-molecule or continuum Brownian diffusion) or particle morphology (dense spherical particles or low-density agglomerates). Generalizations with respect to particle deposition mechanism and shape of the particle size distribution are then indicated, along with potential engineering applications.

Convective-Diffusion Mass Deposition Rates from Particle Size Distributions

Suppose the particle size distribution at the outer edge of a gaseous boundary layer is $n\{v\}$; defined such that the total particle mass fraction is:

$$\omega_p = \frac{1}{\rho} \cdot \int_0^\infty \tilde{\rho}_p\{v\} \cdot v \cdot n\{v\}\, dv \qquad (1)$$

where v is the individual particle volume (treated here as a continuous variable), ρ is the mixture density and $\tilde{\rho}_p\{v\}$ is the intrinsic density of a particle of volume v. If the local dimensionless mass transfer coefficient (Stanton number) is written $St_m\{v, \ldots\}$, then the total mass deposition rate can be formally written:

$$-\dot{m}_p'' = U \cdot \int_0^\infty St_m\{v, \ldots\} \cdot \tilde{\rho}_p\{v\} \cdot v \cdot n\{v\}\, dv \qquad (2)$$

showing that $-\dot{m}_p''$ is proportional to the integral of the particle size distribution function after "weighting" by the function: $St_m\{v, \ldots\} \cdot \tilde{\rho}_p\{v\} \cdot v$. In the cases examined explicitly, Figure 1, we assume:

1. $St_m \sim Sc^{-b}$ where, for high Peclet number transport, $b = \frac{2}{3}$ for laminar BLs, and 0.701 for turbulent BLs (Friedlander, 1977; Rosner, 1986). [High *Pe* behavior even applies to *low* Reynolds number flows because of the largeness of the particle Schmidt number (smallness of the particle Brownian diffusivity compared to the host gas momentum diffusivity, ν) (Friedlander, 1977; Fernandez de la Mora and Rosner, 1982).]
2. $n\{v\}$ is "self-preserving" in the sense that $n\bar{v}/N_p = \Psi$ is a calculable function of $v/\bar{v} = \eta$ (Friedlander, 1977; Friedlander and Wang, 1966; Lai *et al.*, 1977)
3. $\tilde{\rho}_p\{v\}$ is a constant independent of v
4. Further coagulation within the fluid-dynamic boundary layer is neglected (for a discussion of coagulation in thermophoretically-dominated situations, see Park and Rosner, 1988)

Here *Sc*, the particle Schmidt number, is the diffusivity ratio ν/D_p, where D_p is the particle Brownian diffusivity in the prevailing gas; and $\bar{v}$ is the mean particle volume defined by ϕ_p/N_p, where:

$$\phi_p = \int_0^\infty v n\{v\}\, dv \quad \text{(total particle volume fraction)} \qquad (3)$$

$$N_p = \int_0^\infty n\{v\}\, dv \quad \text{(total particle number density)} \qquad (4)$$

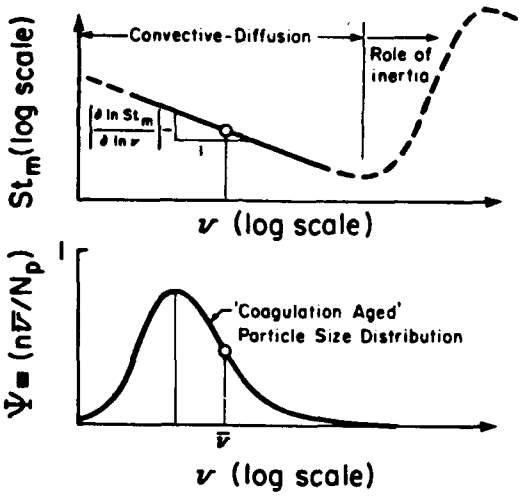

Figure 1. Behavior of the dimensionless mass transfer coefficient, St_m, and dimensionless aerosol particle size distribution, Ψ, as a function of the logarithm of the particle volume.

The purpose of this note is to compare the total mass deposition rate computed from Eq. 2 with the appropriate *reference* value:

$$-\dot{m}''_{p,\text{ref}} = U \cdot St_m\{\bar{v}\} \cdot \hat{\rho}_p\{\bar{v}\} \cdot \bar{v} N_p \tag{5}$$

or, the corresponding mass deposition rate from a hypothetical "monodispersed" aerosol comprised particles each having the volume $\bar{v}$. [For the special case of $Sc \gg 1$ deposition of dense spherical particles from a turbulent dusty gas flow in a circular duct, Friedlander (1977) has made a similar type of calculation, but using a rather different value of $-\dot{m}''_{p,\text{ref}}$, based on the deposition rate of the "monomer" (vapor) from which the particles were presumably formed, a choice which is not of the same order of magnitude as $-\dot{m}''_{p,\text{actual}}$.]

For dense spheres, two limiting cases are of special interest, *viz.* Knudsen ("free-molecule") diffusion, in which case:

$$D_p \sim v^{-2/3} \tag{6}$$

and Stokes-Einstein ("continuum") diffusion, in which case:

$$D_p \sim v^{-1/3} \tag{7}$$

For quasispherical agglomerates comprised primary particles which sum to v, the interesting recent work of Mountain, Mulholland, and Baum (1986) indicates that Eqs. 6 and 7 generalize these proportionalities to:

$$D_p \sim v^{-2/D} \quad \text{(Knudsen)} \tag{8}$$

and:

$$D_p \sim v^{-1/D} \quad \text{(Stokes-Einstein)} \tag{9}$$

where the "fractal" dimension (near 1.8) replaces 3 in the indicated exponents. Combining these laws reveals that in each of the abovementioned cases:

$$\frac{-\dot{m}''_{p,\text{actual}}}{-\dot{m}''_{p,\text{ref}}} = \int_0^\infty \eta^k \cdot \Psi\{\eta\} d\eta \equiv \mu_k \tag{10}$$

for some appropriate value of k calculated from the exponent b, the diffusion regime, and the fractal "dimension" D. Accordingly, calculation of the total mass deposition rate from such polydispersed aerosols reduces to a computation of $-\dot{m}''_{p,\text{ref}}$ (based on all particles of size $\bar{v}$), corrected only by an appropriate (dimensionless) "moment" of the self-preserving size distribution function. The required correction factors are readily estimated below by interpolating between the selected moments numerically computed earlier by Wang and Friedlander (1967), and Lai, Friedlander, Pich and Hidy (1972). It should be remarked that, as a consequence of the definitions of Ψ and η and Eqs. 3 and 4, both the zeroth moment and first moment of $\Psi\{\eta\}$ must be unity.

Required "Moments" for Convective Diffusion

Table 1 collects the resulting values of the exponent k in Eq. 10 for each of the particle deposition cases considered here, as well as the corresponding estimated moments μ_k, Figure 2. It is interesting to note that these k-values fall between 0.218 and 0.778 and, as shown in Figure 2, between $k = 0$ and 1, both Knudsen-$\Psi\{\eta\}$ and the continuum-$\Psi\{\eta\}$functions have moments which exhibit a very shallow minimum near $k = 1/2$. [Until reliable $\Psi\{\eta\}$ and μ_k-values become available for the two $D = 1.8$ cases, these particular estimates (especially for the Knudsen diffusion case) should be viewed as tentative.] As a consequence of this property, and of the abovementioned requirements $\mu_0 = 1$, $\mu_1 = 1$, all of the inferred μ_k-values (cf. Eq. 10) fall in a remarkably narrow band between 0.88 and 0.92. This leads to a

Table 1. Parameter Values, Required Moments, and Predicted Ratios, of $-\dot{m}''_p$ (Polydispersed)/$-\dot{m}''_p$ (Monodispersed with $v = \bar{v}$) for High-Peclet-Number Convective Diffusion of Dense Particles and Agglomerates from Coagulation-Aged Aerosols

Case		Knudsen Diffusion		Continuum Diffusion	
Sc-Exponent (b)	Fractal Dimension (D)*	Relevant Moment (k)	Moment Value (μ_k)	Relevant Moment (k)	Moment Value (μ_k)
2/3 (LBL)	3 (dense)	0.5556	0.888	0.7778	0.924
2/3 (LBL)	1.8 (agglom.)	0.2593	0.901*	0.6296	0.901*
0.704 (TBL)	3 (dense)	0.5307	0.902	0.7653	0.922
0.704 (TBL)	1.8 (agglom.)	0.2178	0.919*	0.6089	0.899*

*Values of μ_k for the $D = 1.8$ (fractal agglomerate cases) should be considered tentative estimates (especially for Knudsen diffusion) pending numerical calculations of $\Psi\{\eta\}$ for the relevant collision kernels.

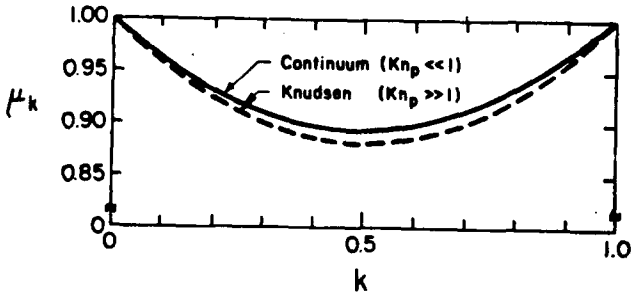

Figure 2. Behavior of the moments of the self-preserving size distribution functions $\Psi\{\eta\}$ for Knudsen diffusion ($Kn_p \gg 1$, dashed line) and continuum diffusion ($Kn_p \ll 1$) for k values between zero and unity.

Compare with Eq. 2, ($k = 1 + (\partial \ln St_m/\partial \ln v)$.

simplification of potential conceptual and engineering utility—namely, *to a first approximation, total mass deposition rates by convective-diffusion from "coagulation-aged" aerosol population distributions will be about 90% of the values corresponding to a hypothetical "monodispersed" aerosol [with all particles having the mean particle size (volume) $\bar{v}(\equiv \phi_p/N_p)$] under otherwise identical fluid dynamic and geometric conditions.* To within about ±2%, these results are insensitive to the fluid dynamic state of the boundary layer, particle Knudsen number (ratio of gas mean free path to particle diameter) and, evidently, even apply to "open" agglomerates.

Generalizations and Implications

It can be seen from the abovementioned formulation that the following conditions will lead to $-\dot{m}''_p/-\dot{m}''_{p,ref}$ ratios *even closer to unity:*

1. The simultaneous role of particle *thermophoresis*, which is known to reduce the absolute value of $\partial \ln St_m/\partial \ln v$ when the target is cooler than the gas stream (see Rosner, 1980; 1986)

2. Mainstream particle size distributions which are *narrower* than those corresponding to coagulation-aged aerosols, *i.e.*, narrower than the "self-preserving" distributions $\Psi\{\eta\}$, or their near-"log-normal" equivalents (with $\sigma_g \approx 1.32$–1.35) (Lee, 1983; Lee *et al.*, 1984)

Of course, in general, $St_m\{v\}$ is not a simple power law over the *entire* particle size range, Figure 1, but we can verify that a "local" power-law approximation is adequate by expanding $\ln St_m$ *vs* $\ln v$ *in* a Taylor series about $\ln \bar{v}$, *i.e.*:

$$\ln St_m \simeq (\ln St_m)_{v=\bar{v}} + \left(\frac{\partial \ln St_m}{\partial \ln v}\right)_{v=\bar{v}} \cdot \ln\left(\frac{v}{\bar{v}}\right) + \frac{1}{2!}\left(\frac{\partial^2 \ln St_m}{\partial \ln v^2}\right)_{v=\bar{v}} \cdot \left(\ln \frac{v}{\bar{v}}\right)^2 + \cdots \quad (11)$$

Inserting Eq. 11 into Eq. 2 and introducing the definitions of Ψ and η, one can show that the power-law approximation is adequate provided:

$$\left|\frac{1}{2} \cdot \left(\frac{\partial^2 \ln St_m}{\partial \ln v^2}\right)_{v=\bar{v}}\right| \cdot \frac{1}{\mu_k} \cdot \int_0^\infty (\ln \eta)^2 \cdot \eta^k \cdot \Psi\{\eta\} \cdot d\eta \ll 1 \quad (12)$$

where, as before:

$$k = 1 + \left(\frac{\partial \ln St_m}{\partial \ln v}\right)_{v=\bar{v}} \quad (13)$$

and μ_k is defined by Eq. 10.

It is known that the value of $(\partial \ln St_m/\partial \ln v)_{v=\bar{v}}$ will increase with the onset of particle "inertia" effects at the larger particle sizes. Of course, this will increase μ_k and, ultimately, drive $-\dot{m}''_p/-\dot{m}''_{p,ref}$ above unity. For example, the phenomenon called "eddy impaction" causes $St_m/(C_f/2)^{1/2}$ for turbulent flow through smooth circular ducts to increase like $(t_p^+)^2$ over an approximately 2.5 decade range of t_p^+, (see, e.g., Papavergos and Hedley, 1984), where:

$$t_p^+ \equiv \frac{u_*^2 t_p}{\nu} \quad (14)$$

Here u_* is the "friction velocity" $(\bar{\tau}_w/\rho)^{1/2}$, and t_p the characteristic particle "stopping" time. Under continuum ($Kn_p \ll 1$) conditions, $t_p \sim d_p^2 \sim v^{2/3}$ so that, over nearly a 2-decade range of v, this corresponds to:

$$\frac{\partial \ln St_m}{\partial \ln v} = +\frac{4}{3} \quad (15)$$

and hence, $k = 7/3 = 2.333$. Interpolating, using values of μ_2 and μ_3 reported earlier by Wang and Friedlander (1967), we find $\mu_{7/3} \approx 2.9$ under such "eddy-impaction" conditions. While it is true that jet impaction situations (as in a "cascade impactor") can lead to still larger local values of $\partial \ln St_m/\partial \ln v$, for most external- and internal-flow situations μ_k will fall between the abovementioned limits of *ca.* 0.9 (convective diffusion) and *ca.* 2.9 (eddy impaction-modified turbulent transport). Accordingly, $-\dot{m}''_p/-\dot{m}''_{p,ref}$ will normally fall between these same limits for a wide class of more general $St_m\{v\}$ functions, *including the now-classical "capture efficiency" correlations* for steady inviscid flow past isolated cylinders or spheres, (Rosner, 1986; Israel and Rosner, 1983; Friedlander, 1977).

Acknowledgments

It is a pleasure to acknowledge the financial support of DOE-PETC *via* Grant No. DE-FG22-86PC90756 and the US AFOSR *via* Grant No. AFOSR-84-0034, as well as the related support of the Yale HTCRE Laboratory by our current industrial affiliates: Shell Foundation, AVCO-Lycoming-Textron, and SCM-Chemicals. In this research, the author has benefited from helpful discussions with Professors J. Fernandez de la Mora and J. O'Brien, as well as his current and former graduate students.

The author wishes to dedicate this paper to the memory of aerosol dynamics researcher, Prof. Isaiah Gallily (Hebrew U.), who died on July 31, 1988.

Literature Cited

Fernandez de la Mora, J., and D. E. Rosner, "Effects of Inertia on the Diffusional Deposition of Small Particles to Spheres and Cylinders at Low Reynolds Numbers," *J. Fluid Mechanics*, **125**, 379 (1982).

Friedlander, S. K., *Smoke, Dust and Haze-Fundamentals of Aerosol Behavior*, Wiley, New York (1977).

Friedlander, S. K., and C. S. Wang, "The Self-Preserving Particle Size Distribution for Coagulation by Brownian Motion," *J. Colloid & Interf. Sci.*, **22**, 126 (1966).

Lai, F. S., S. K. Friedlander, J. Pich, and G. M. Hidy, "The Self-Preserving Particle Size Distribution for Brownian Coagulation in the

Free-Molecule Regime," *J. Colloid. & Interf. Sci.*, **39**(2), 395 (May 1972).
Lee, K. W., "Change of Particle Size Distribution during Brownian Coagulation," *J. Colloid & Interf. Sci.*, **92**, 315 (1983).
Lee, K. W., H. Chen, and J. A. Gieseke, "Log-Normal Preserving Size Distribution for Brownian Coagulation in the Free-Molecule Regime," *Aerosol Sci. & Tech.*, **3**, 53 (1984).
Mountain, R. D., G. W. Mulholland, and H. Baum, "Simulation of Aerosol Agglomeration in Free-Molecular and Continuum Flow Regimes," *J. Colloid & Interf. Sci.*, **114**(1), 67 (1986).
Papavergos, P. G., and A. B. Hedley, "Particle Deposition Behavior from Turbulent Flows," *Chem. Eng. Res. Dev.*, British Inst. Chem. Engs., **62**, 275 (1984).
Park, H. M., and D. E. Rosner, "Effect of Coagulation in the Boundary Layer on the Size Distribution of Thermophoretically Deposited Particles," *Chem. Eng. Sci.* (in press); Appendix 5 of D. E. Rosner and H. M. Park, "Thermophoretically Augmented Mass-, Momentum- and Energy-Transfer Rates in High Particle Mass-Loaded Laminar Forced Convection Systems," *Chem. Eng. Sci.*, **43**, 2689 (1988).
Rosner, D. E., "Thermal (Soret) Diffusion Effects on Interfacial Mass Transport Rates," *J. Phys. Chem. Hydrody.*, **1**, 159 (1980).
Rosner, D. E., *Transport Processes in Chemically Reacting Flow Systems*, Butterworth, Stoneham, MA (1986); second printing, (1988).
Wang, C. S., and S. K. Friedlander, "The Self-Preserving Particle Size Distribution for Coagulation by Brownian Motion," *J. Colloid & Interf. Sci.*, **24**, 170 (1967).

Manuscript received May 2, 1988, and revision received Aug. 9, 1988.

REPORT DOCUMENTATION PAGE

Form Approved
OMB No. 0704-0188

1. AGENCY USE ONLY (Leave blank)	2. REPORT DATE	3. REPORT TYPE AND DATES COVERED
	1989	Journal Publication

4. TITLE AND SUBTITLE
"Deposition Rates From Polydispersed Particle Populations of Arbitrary Spread" (U)

5. FUNDING NUMBERS
PE - 61102F
PR - 2308
SA - BS
G - AFOSR 89-0223

6. AUTHOR(S)
Daniel E. Rosner and Menelaos Tassopoulos

7. PERFORMING ORGANIZATION NAME(S) AND ADDRESS(ES)
HIGH TEMPERATURE CHEMICAL REACTION ENGINEERING LABORATORY
YALE UNIVERSITY
BOX 2159, YALE STATION
NEW HAVEN, CONNECTICUT 06520 U.S.A.

8. PERFORMING ORGANIZATION REPORT NUMBER

9. SPONSORING/MONITORING AGENCY NAME(S) AND ADDRESS(ES)
AFOSR/NA
Building 410
Bolling AFB DC 20332-6448

10. SPONSORING/MONITORING AGENCY REPORT NUMBER

11. SUPPLEMENTARY NOTES

12a. DISTRIBUTION/AVAILABILITY STATEMENT
Approved for public release; distribution is unlimited

12b. DISTRIBUTION CODE

13. ABSTRACT (Maximum 200 words)

For particle deposition from log-normal polydispersed aerosol streams by one or more of several mechanisms described by piece-wise-power-law mass transfer coefficients, we derive useful relations between actual total mass deposition rates and the 'reference' rate one would calculate by imagining that all particles in the mainstream population had the average particle volume $\bar{v}(-\phi_\rho / N_\rho)$. Included here are diffusion or inertial mechanisms for laminar- or turbulent-boundary layers, free-molecular or continuum diffusion at high Peclet numbers of dense spherical particles, or fractal agglomerates. The mainstream particle volume distribution is considered to be log-normal with arbitrary 'spread' parameter, thereby generalizing earlier results for "coagulation-aged" (self-preserving) distributions. Further generalizations include transitions between important particle transport mechanisms, opening the way to efficient, finite-analytic methods for predicting mass deposition rates for arbitrary, size-dependent particle capture efficiencies.

14. SUBJECT TERMS
deposition, suspensions, aerosols, coagulation, mass transfer, convective-diffusion, Brownian motion, aggregates

15. NUMBER OF PAGES
12

16. PRICE CODE

17. SECURITY CLASSIFICATION OF REPORT	18. SECURITY CLASSIFICATION OF THIS PAGE	19. SECURITY CLASSIFICATION OF ABSTRACT	20. LIMITATION OF ABSTRACT
Unclassified	Unclassified	Unclassified	UL

Reprinted from AICHE JOURNAL, September 1989

Deposition Rates from Polydispersed Particle Populations of Arbitrary Spread

For particle deposition from log-normal polydispersed aerosol streams by one or more of several mechanisms described by piecewise-power-law mass transfer coefficients, we derive useful relations between actual total mass deposition rates and the 'reference' rate one would calculate by imagining that all particles in the mainstream population had the average particle volume $\bar{v}(=\phi_p/N_p)$. Included here are diffusion or inertial mechanisms for laminar- or turbulent-boundary layers, free-molecular or continuum diffusion at high Peclet numbers of dense spherical particles, or fractal agglomerates. The mainstream particle volume distribution is considered to be log-normal with arbitrary 'spread' parameter, thereby generalizing earlier results for "coagulation-aged" (self-preserving) distributions. Further generalizations include transitions between important particle transport mechanisms, opening the way to efficient, finite-analytic methods for predicting mass deposition rates for arbitrary, size-dependent particle capture efficiencies.

Daniel E. Rosner
Menelaos Tassopoulos
Yale University
Department of Chemical Engineering
High Temperature Chemical Reaction
Engineering Laboratory
New Haven, CT 06520

Introduction

Background and motivation

It is well known that the ability of an immersed surface to capture particles present in a "dust-laden" mainstream is quite particle-size-dependent, reflecting the mechanism (diffusion, inertia, . . .) of transport (Fuchs, 1964; Friedlander, 1977; Rosner, 1988, 1989). Moreover, in most environments the particle-size distribution (PSD) in the mainstream is itself quite broad, reflecting, of course, the mechanism(s) of particle formation (see, e.g., Flagan and Friedlander, 1978.) Thus, to calculate total mass deposition rates, one must sum (integrate) over both capture efficiency $\eta_{cap}\{v\}$ and the *mass* distribution function $\tilde{\rho}_p\{v\} \cdot v \cdot n\{v\}$, where $n\{v\}dv$ is the particle *number* density between particles of volume v and $v + dv$, with the particle volume treated as a continuous variable (Rosner, 1989).

As in the kinetic theory of gases, it would be useful if the results of greatest engineering interest could be expressed in terms of certain averages characterizing the distribution such as the reference deposition rate, if all particles had the *mean* particle volume: $\bar{v} = \phi_p/N_p$, where ϕ_p is the particle volume fraction (first moment of the distribution). [Recall the utility of such kinetic theory concepts as the *mean* thermal speed (Bernoulli, Maxwell; see, e.g., Garber et al., 1986) and the *mean*-free path (Clausius, Maxwell, and Reynolds).]

$$\phi_p = \int_0^\infty v \cdot n\{v\}dv \equiv \mu_1 \tag{1}$$

and N_p is the total particle number density (zeroth moment):

$$N_p = \int_0^\infty n\{v\}dv \equiv \mu_0 \tag{2}$$

This suggests the following practical approach to estimating total particle mass deposition rates. First, using $\eta_{cap}\{v\}$, one calculates the expected (reference) mass deposition flux $-\dot{m}''_{p,ref}$ if all particles in the mainstream had the same volume $\bar{v}$. Then, one corrects this reference deposition rate by a factor (often quite near unity, see below) which is expected to depend on the "shapes" of the functions $\eta_{cap}\{v\}$ and the PSD $n\{v\}$.

Recent results

For the commonly encountered situation that $\eta_{cap}\{v\}$ or its Stanton number counterpart can be adequately represented by a simple power law and $n\{v\}$ is "self-preserving" (as in "coagula-

tion-aged" aerosols, see, e.g., Friedlander and Wang, 1966; Lai et al., 1977; Friedlander, 1977), we recently presented simple results for $-\dot{m}''_p/(-\dot{m}''_{p,ref})$ (Rosner, 1989). [Since we frequently must deal with targets that present zero projected (frontal) area, it is more useful to adopt here the dimensionless mass transfer coefficient, St_m, defined by $-\dot{m}''_p/(\rho_p U_\infty)$ (see, e.g., Rosner, 1988).] The results show that the quantities of interest could be obtained directly by merely interpolating previously calculated dimensionless fractional moments of $\psi\{v/\bar{v}\} \equiv n\bar{v}/N_p$ to determine the moment μ_k corresponding to:

$$k = 1 + \left(\frac{\partial \ln St_m}{\partial \ln v}\right) \tag{3}$$

In this way, it was possible to show (Rosner, 1989) that, for say $Pe \gg 1$, convective-diffusion $-\dot{m}''_p/(-\dot{m}''_{p,ref}) \simeq 0.90 \pm 0.02$ irrespective of turbulence in the boundary layer, particle Knudsen number (Kn_p) and even quasispherical particle morphology (dense vs. fractal agglomerates). [For particle transport in gases, one finds that the Schmidt number $Sc \equiv \nu/D_p$ is quite often so large that large Peclet numbers ($Pe = Re \cdot Sc$) are achieved even when the Reynolds number is *small* (see, e.g., Friedlander, 1977; Fernandez de la Mora and Rosner, 1982).] Particle *inertial* effects were shown to increase $-\dot{m}''_p/(-\dot{m}''_{p,ref})$ above unity, yielding values near 2.9 for the eddy impaction of $Kn_p \ll 1$ dense spherical particles.

Objectives and outline

It would be valuable to extend these results in two respects. First, we wish to calculate deposition rates from mainstream particle-size distributions which may be much broader or narrower than those pertaining to "coagulation-aged" distributions. Quite often actual aerosol particle populations, generated under a variety of conditions, can be approximated by log-normal distributions (Aitchison and Brown, 1969; Raabe, 1971; Fuchs, 1964 and its references). Furthermore, self-preserving distributions themselves are not very different from log-normals of a specific geometric standard deviation (Lee, 1983; Lee et al., 1984; Ali and Zollars, 1988, for self-preserving distributions due to shear coagulation). Second, we wish to calculate and present useful results for commonly-encountered $St_m\{v\}$ functions that are more complex than a single power law.

This path inevitably leads to a simple, computationally-efficient "finite-analytic" method for calculating total mass deposition rates for the general case of *arbitrary* $St_m\{v\}$ and *arbitrary* PSD $n\{v\}$ by suitably combining our results for "piecewise"-power-law $St_m\{v\}$ functions and log-normal PSD's of arbitrary spread. But perhaps more important than such an "algorithm" is the conceptual content of the results to be presented: i.e., the insight they provide into the factors governing total deposition rates from "polydispersed"-flowing dust-laden fluids. Moreover, we also calculate and present "once-and-for-all" results that enable the rapid estimation of particle mass deposition rates in a rather wide variety of commonly-encountered engineering situations, with the conclusions and implications discussed in the last section.

Table 1. Exponent b: Power-Law Dependence of $St_m(v)$ on Particle Volume, v

Sc Exponent	Fractal Dimension (D)*	Knudsen Diffusion	Continuum Diffusion	Eddy Impaction
2/3 (LBL)	3 (dense)	−0.4444	−0.2222	—
2/3 (LBL)	1.8 (aggreg.)	−0.7407	−0.3704	—
0.704 (TBL)	3 (dense)	−0.4693	−0.2347	—
0.704 (TBL)	1.8 (aggreg.)	−0.7822	−0.3911	—
—	3 (dense)	—	—	1.3333

*Here we take $D_p \sim v^{-3/D}$ or $-v^{-1/D}$ for free-molecular and continuum diffusion, respectively (Mountain et al., 1986). D is the fractal dimension, equal to 3 for dense particles and equal to about 1.8 for diffusion-limited aggregates (Meakin, 1983).

Deposition from Log-Normal Distributions When $St_m\{v\}$ Is a Power Law

Consider an aerosol with particle-size distribution function, $n\{v\}$, outside the gaseous boundary layer. In terms of the dimensionless mass transfer Stanton number $St_m\{v, \ldots\}$ (Rosner 1988, 1989), the total mass deposition rate is given by:

$$-\dot{m}''_p = U \cdot \int_0^\infty St_m\{v, \ldots\} \cdot \tilde{\rho}_p \cdot v \cdot n\{v\}\, dv \tag{4}$$

where U is the gas-free stream velocity, and $\tilde{\rho}_p$ is the intrinsic particle density, assumed to be independent of particle size. As already indicated, we will focus attention on the comparison between the total mass deposition rate $-\dot{m}''_p$ and the *reference* deposition rate, $-\dot{m}''_{p,ref}$, from a hypothetical monodispersed population comprising particles, each having the size (volume) $\bar{v}$; i.e.,

$$-\dot{m}''_{p,ref} \equiv U \cdot St_m\{\bar{v}\} \cdot \tilde{\rho}_p \cdot \bar{v} N_p \tag{5}$$

If we further denote by R the deposition rate ratio that we seek, then

$$R \equiv \frac{-\dot{m}''_p}{-\dot{m}''_{p,ref}} = \int_0^\infty \frac{St_m\{v\}}{St_m\{\bar{v}\}} \cdot \frac{v \cdot n\{v\}\, dv}{\bar{v} N_p} \tag{6}$$

As noted earlier (Rosner, 1989), if deposition occurs due to *either* convective Brownian diffusion *or* eddy impaction alone, then we may take $St_m \sim v^b$ throughout the particle volume range of interest; for example, we may assume a power-law form for the dependence of the local mass Stanton number on particle volume, where b is determined by the nature of the deposition mechanism, Knudsen number, and fractal dimension of the particles. In Table 1, we give some typical values for the exponent b for each of the above-mentioned cases. Substituting the power-law form for St_m into Eq. 6, we obtain

$$R = \int_0^\infty \left(\frac{v}{\bar{v}}\right)^{1+b} \cdot \frac{n\{v\}}{N_p}\, dv \tag{7}$$

From Eq. 7, we see that at least for the case of deposition in a regime over which $St_m\{v\}$ has a single-power-law dependence, in order to obtain R, we simply have to evaluate an appropriate moment $k(=1+b)$ of the mainstream aerosol PSD.

Assuming a log-normal aerosol PSD at the outer edge of the gaseous boundary layer, we may write $n\{v\} = N_p \cdot C_1\{v\}$, with

$C_1\{v\}$ the normalized log-normal particle-size (volume) distribution function defined by

$$C_1\{v\} = \frac{1}{v \ln \sigma_g \sqrt{2\pi}} \exp\left[-\frac{\ln^2\{v/v_g\}}{2 \ln^2 \sigma_g}\right] \quad (0 < v < \infty) \quad (8)$$

where v_g is the median volume of the distribution (or geometric mean) and σ_g is the corresponding geometric standard deviation of the distribution. [The PSD function based on particle radius (here we assume spherical particles), say $C_1\{r\}$, is also log-normal, with median r_g determined through $v_g = (4/3)\pi r_g^3$ and standard deviation equal to $\sigma_g^{1/3}$.] The arithmetic mean of $C_1\{v\}$, written $\bar{v}$ and chosen as our reference particle dimension, is related to the median v_g which appears explicitly in Eq. 8 through (see, e.g., Raabe, 1971):

$$\bar{v} = v_g \exp\{\tfrac{1}{2} \ln^2 \sigma_g\} \quad (9)$$

Combining now Eq. 7, 8 and 9, we find

$$R = \left(\frac{v_g}{\bar{v}}\right)^{1+b} \cdot \int_0^\infty v_*^{1+b} C_1\{v_*\}\, dv_* = \exp\left(-\frac{1+b}{2} \ln^2 \sigma_g\right) \cdot \int_0^\infty v_*^{1+b} C_1\{v_*\}\, dv_* \quad (10)$$

where $v_* = v/v_g$ and $C_1\{v_*\}$ is a log-normal distribution with median equal to unity and standard deviation equal to σ_g. Equation 10 can be simplified further, if we note that the kth moment of any log-normal function can be expressed in terms of another log-normal with the same standard deviation and a different median, v_k (Raabe, 1972). Specifically, if we take the original log-normal to be $C_1\{v\}$ as defined in Eq. 5, then one can show that:

$$v^k C_1\{v\} dv = \exp\left[k \ln v_g + \frac{k^2}{2} \ln^2 \sigma_g\right] \cdot \left\{\frac{1}{(v/v_k) \ln \sigma_g \sqrt{2\pi}} \exp\left[-\frac{\ln^2\{v/v_k\}}{2 \ln^2 \sigma_g}\right]\right\} d\left(\frac{v}{v_k}\right) \quad (11)$$

where the new median v_k is determined by:

$$\ln v_k = \ln v_g + k \ln^2 \sigma_g \quad (12)$$

Making use of these relationships and further noting the normalization condition:

$$\int_0^\infty C_1\{v\}\, dv = 1$$

we finally obtain the remarkably simple result:

$$R = \exp\left[\frac{b(1+b)}{2} \cdot \ln^2 \sigma_g\right] \quad (13)$$

Thus, when the mass transfer coefficient $St_m\{v\}$ can be represented by a single power law ($\sim v^b$), Eq. 13 gives the total mass deposition rate compared to the corresponding deposition rate for a hypothetical monodispersed population of particles of individual volume $\bar{v}$, in terms of the actual deposition mechanism (consistent with the choice of b), and the standard deviation (spread) of the depositing aerosol main-stream particle-size distribution.

In Figure 1 we plot the deposition rate ratio R vs. the standard deviation of the aerosol PSD, σ_g, for *continuum* diffusion of dense or fractal particles through laminar (LBL) or turbulent boundary layers (TBL). For the exact "order" $k[(=1 + b)$ in Eq. 13] of the corresponding moments, see Table 1. In Figure 1, we also mark the σ_g value at which the log-normal and the self-preserving distributions are approximately the same. [Lee (1983) reports that a log-normal particle-size distribution that is based on *linear* size, such as the particle radius, is similar to the self-preserving distribution for $\sigma_g \simeq 1.32 - 1.35$. We use a PSD based on particle volume, and hence the corresponding standard deviation at which it will become similar to the self-preserving one is for $\sigma_g \simeq 1.35^3 = 2.46$, as mentioned previously.] Note the fair agreement between the self-preserving PSD results of Rosner (1989) for R and our present results for the nearest log-normal PSD.

Figure 2 shows the corresponding total deposition rate ratios R vs. σ_g for Knudsen ($Kn_p \gg 1$) diffusion. It is interesting to note that while in continuum diffusion and for a PSD of arbitrary σ_g, dense particles deposit at higher normalized rates than fractal aggregates, in the free molecular regime the opposite occurs. It is straightforward to explain this behavior if we realize that $R(b)$ (Eq. 13) has a local minimum at $b = \frac{1}{2}$. In the continuum regime as we go from dense to fractal particles, the order of the relevant moment decreases from 0.78 for LBL and dense particles to 0.61 for TBL and fractal aggregates, thus making the corresponding deposition rate ratio decrease too. On the other hand, for Knudsen diffusion, dense particles correspond to moments of order 0.56–0.53 (Table 1), e.g., close to the regime where the minimum of R lies, while fractal particles with

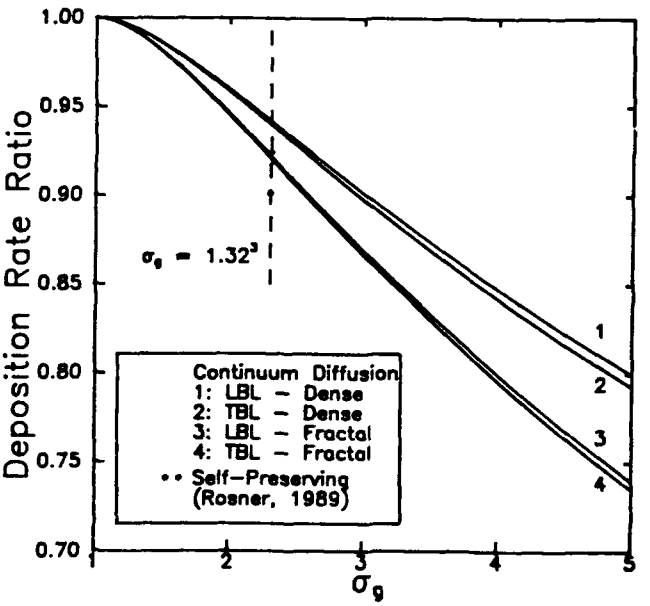

Figure 1. Deposition rate ratio, R, vs. the standard deviation, σ_g, of the aerosol PSD for *continuum* diffusion of dense or fractal particles through laminar or turbulent boundary layers.

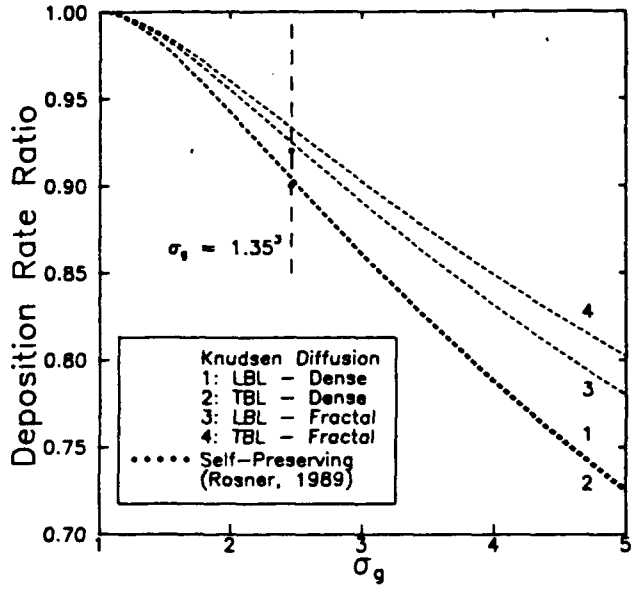

Figure 2. Deposition rate ratio, R, vs. the standard deviation, σ_g, of the aerosol PSD, for *Knudsen* diffusion of dense or fractal particles through laminar or turbulent boundary layers.

required moments in the range of 0.26–0.22 yield higher deposition rate ratios.

In Figure 3 we plot deposition rate ratio against the standard deviation of the log-normal distribution for eddy impaction in the $(t_p^+)^2$ regime (see also Table 1). Since higher σ_g values result in a larger fraction of the total aerosol mass associated with large particles, in this regime the relative deposition rate is an increasing function of σ_g.

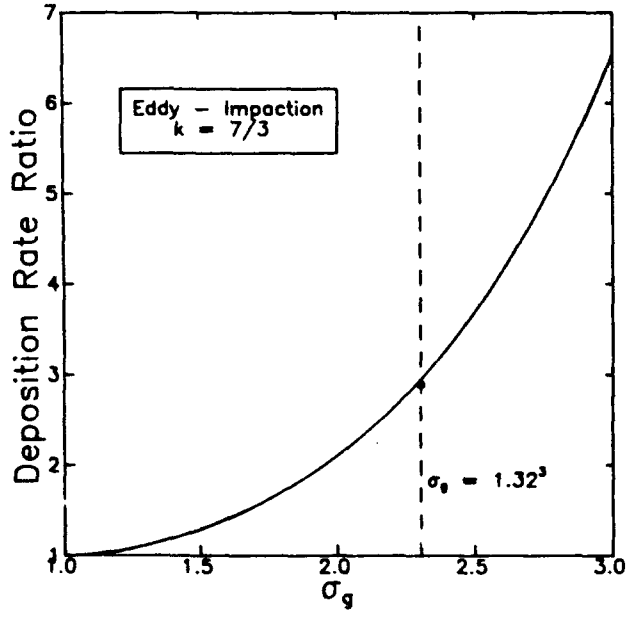

Figure 3. Deposition rate ratio, R, vs. the standard deviation of the aerosol PSD, σ_g, for eddy impaction of dense particles.

Deposition from Log-Normal Distributions When $St_m(v)$ Is a Piecewise Power-Law

In most situations of practical interest one cannot assume a single deposition mechanism: i.e., $St_m\{v\}$ is not a simple power law throughout the relevant range of particle sizes, especially if the particle-size distribution of the depositing aerosol is rather broad. On the other hand, quite often $St_m\{v\}$ is well-approximated by a piecewise power law, as in the case of turbulent deposition in duct flow systems (McCoy and Hanratty, 1977; Papavergos and Hedley, 1984). In particular, if we consider turbulent deposition in the absence of appreciable particle sedimentation effects, there is both experimental (McCoy and Hanratty, 1977) and theoretical evidence for the case of convective diffusion (e.g., Friedlander, 1977) that:

$$\frac{St_m}{\left(\frac{1}{2}C_f\right)^{1/2}} \simeq \begin{cases} 0.086\,(Sc)^{-0.701} & \text{for } t_p^+ \le t_{p,1}^+\{Sc\} \\ 3.25\times 10^{-4}(t_p^+)^2 & \text{for } t_{p,1}^+\{Sc\} \le t_p^+ \le 22.9 \\ 0.17 & \text{for } t_p^+ \ge 22.9 \end{cases} \quad (14)$$

where C_f is the nondimensional wall-friction coefficient, Sc is the particle Schmidt number ($= \nu/D_p \sim v^{+1/3}$ for continuum diffusion), and t_p^+ the dimensionless particle stopping time, defined by:

$$t_p^+ = \frac{u_*^2 t_p}{\nu}$$

u_* is the so-called friction velocity $(\bar{\tau}_w/\rho)^{1/2}$, and t_p the characteristic particle stopping time ($= [\bar{\rho}_p d_p^2/(18\mu)] \sim v^{2/3}$). In Eq. 14, $t_{p,1}^+\{Sc\}$ denotes the dimensionless particle stopping time which marks the transition from a convective-diffusion to an eddy-impaction transport mechanism, clearly a function of the particle Schmidt number (see Eq. 17; Rosner, 1988). A typical value for $t_{p,1}^+$ is about 0.2 (McCoy and Hanratty, 1977), and further let $v_{crit,1}$ denote the particle size corresponding (in the prevailing environment) to this dimensionless relaxation time, e.g., the particle size at which the deposition mechanism is assumed to change abruptly from convective diffusion to eddy impaction. Similarly, let $v_{crit,2}$ denote the particle size at which the particle/fluid decoupling (inertial cut-off) occurs, and define

$$r = \frac{v_{crit,2}}{v_{crit,1}} \simeq \left(\frac{22.9}{0.2}\right)^{3/2} = 1{,}225 \quad (15)$$

where r reflects the extent of the particle-size range that deposits due to the eddy-impaction mechanism. Equation 14 can now be rewritten in terms ov v and r as follows:

$$St_m \sim \begin{cases} v_{crit,1}^{0.2337}\, v^{-0.2337} & \text{for } 0 < v \le v_{crit,1} \\ v_{crit,1}^{-1.3333}\, v^{1.3333} & \text{for } v_{crit,1} \le v \le v_{crit,2} \\ r^{1.333} & \text{for } v_{crit,2} \le v < \infty \end{cases} \quad (16)$$

where we req[illegible] $St_m\{v\}$ to be a continuous function of v. The piecewise power law dependence of the dimensionless mass transfer coefficient on the particle size is clearly shown in Figure

4, where we plot $St_m/(\frac{1}{2}C_f)^{1/2}$ vs. the dimensionless particle stopping time, t_p^+. The experimental data in this figure have been compiled by McCoy and Hanratty (1977), and Ganic and Mastanaiah (1981).

In their review papers, both McCoy and Hanratty (1977), and Papavergos and Hedley (1984) imply that the dimensionless particle relaxation time at which the deposition mechanism changes from convective diffusion to eddy impaction is constant (specifically independent of particle Schmidt number) and equal to about 0.2 (cf. Eq. 14). Using their data, we estimated r (Eq. 15) to be equal to about 1,225. However, in order to obtain the general dependence of r on the particle Schmidt number, we use the fact that $St_m\{v\}$ is a continuous function of v. By equating the mass Stanton number that one predicts for convective diffusion at $v_{crit,1}$ to the eddy impaction $St_m\{v_{crit,1}\}$ we find:

$$0.086[Sc\{v_{crit,1}\}]^{-0.701} = 3.25 \times 10^{-4}[t_p^+\{v_{crit,1}\}]^2$$

or

$$t_p^+\{v_{crit,1}\} = 16.27[Sc\{v_{crit,1}\}]^{-0.35} \sim v_{crit,1}^{-0.12}$$

Using the last equation we find for r (see also Eq. 15) that

$$r = \left(\frac{22.9}{16.27[Sc\{v_{crit,1}\}]^{-0.35}}\right)^{3/2} = 1.67[Sc\{v_{crit,1}\}]^{-0.53} \sim v_{crit,1}^{-0.18}, \quad (17)$$

for example, the regime over which eddy impaction is important as parameterized here by r varies approximately with the inverse of the square root of the particle Schmidt number.

In order to calculate the deposition rate ratio R, it is useful to break the v space in three regimes, one for each mode of deposition, that is

$$R = \frac{\int_0^{v_{crit,1}} St_m\{v\}vC_1\{v\}\,dv}{St_m\{\bar{v}\}\bar{v}} + \frac{\int_{v_{crit,1}}^{v_{crit,2}} St_m\{v\}vC_1\{v\}\,dv}{St_m\{\bar{v}\}\bar{v}} + \frac{\int_{v_{crit,2}}^{\infty} St_m\{v\}vC_1\{v\}\,dv}{St_m\{\bar{v}\}\bar{v}} \quad (18)$$

In Appendix A we show that the partial moment of any log-normal distribution can be expressed in terms of error functions as follows:

$$\int_a^b v^q C_1\{v\}\,dv = \frac{1}{2}\exp\left[q\ln v_g + \frac{1}{2}q^2\ln^2\sigma_g\right] \cdot \left\{\mathrm{erf}\left[\frac{\ln\left(\frac{\beta}{v_g}\exp\{-q\ln^2\sigma_g\}\right)}{\sqrt{2}\ln\sigma_g}\right] - \mathrm{erf}\left[\frac{\ln\left(\frac{\alpha}{v_g}\exp\{-q\ln^2\sigma_g\}\right)}{\sqrt{2}\ln\sigma_g}\right]\right\} \quad (19)$$

Using Eqs. 18 and 19, and after some algebra, we can determine R for any log-normal distribution with arithmetic mean $\bar{v}$ (see Eq. 9 for the relationship between $\bar{v}$ and v_g), and standard deviation σ_g. We define here $\xi = \bar{v}/v_{crit,1}$, and for brevity we also introduce the function $E\{P, x\}$, such that:

$$E\{P, x\} = \mathrm{erf}\left[\frac{\ln\left\{P \cdot \exp\left\{-\frac{1+2x}{2}\ln^2\sigma_g\right\}\right\}}{\sqrt{2}\ln\sigma_g}\right] \quad (20)$$

If we denote by a, b, and c the exponents that characterize the dependence of St_m on particle volume in the convective diffusion, eddy-impaction and inertial cut-off regimes, respectively, (e.g., $a = -0.701$, $b = 1.3333$, and $c = 0$; see Eq. 18), then we find that for $v \le v_{crit,1}$ or equivalently for $\xi \le 1$

$$R = \frac{1}{2}\exp\left[\frac{a(a+1)}{2}\ln^2\sigma_g\right]\cdot\left\{E\left\{\frac{1}{\xi}, a\right\} + 1\right\} + \frac{1}{2}\xi^{b-a}\exp\left[\frac{b(b+1)}{2}\ln^2\sigma_g\right]\cdot\left\{E\left\{\frac{r}{\xi}, b\right\} - E\left\{\frac{1}{\xi}, b\right\}\right\} + \frac{1}{2}\xi^{c-a}r^{b-c}\exp\left[\frac{c(c+1)}{2}\ln^2\sigma_g\right]\cdot\left\{1 - E\left\{\frac{r}{\xi}, c\right\}\right\} \quad (21a)$$

For $v_{crit,1} \le \bar{v} \le v_{crit,2}$, or $1 \le \xi \le r$, we find

$$R = \frac{1}{2}\xi^{a-b}\exp\left[\frac{a(a+1)}{2}\cdot\ln^2\sigma_g\right]\cdot\left\{E\left\{\frac{1}{\xi}, a\right\} + 1\right\} + \frac{1}{2}\exp\left[\frac{b(b+1)}{2}\ln^2\sigma_g\right]\cdot\left\{E\left\{\frac{r}{\xi}, b\right\} - E\left\{\frac{1}{\xi}, b\right\}\right\} + \frac{1}{2}\xi^{c-b}r^{b-c}\exp\left[\frac{c(c+1)}{2}\ln^2\sigma_g\right]\cdot\left\{1 - E\left\{\frac{r}{\xi}, c\right\}\right\} \quad (21b)$$

And finally for $r \le \xi < \infty$, we find

$$R = \frac{1}{2}\xi^{a-c}r^{c-b}\exp\left[\frac{a(a+1)}{2}\ln^2\sigma_g\right]\cdot\left\{E\left\{\frac{1}{\xi}, a\right\} + 1\right\} + \frac{1}{2}\xi^{b-c}r^{c-b}\exp\left[\frac{b(b+1)}{2}\ln^2\sigma_g\right]\cdot\left\{E\left\{\frac{r}{\xi}, b\right\} - E\left\{\frac{1}{\xi}, b\right\}\right\} + \frac{1}{2}\exp\left[\frac{c(c+1)}{2}\ln^2\sigma_g\right]\cdot\left\{1 - E\left\{\frac{r}{\xi}, c\right\}\right\} \quad (21c)$$

In Figure 5, we plot deposition rate ratio, R, vs. $\xi = v/v_{crit,1}$, for different values of σ_g, and for $r = 1{,}225$ (Eq. 15). For $\xi \ll 1$, deposition occurs primarily due to convective diffusion, and indeed the deposition rates we compute here are identical to the deposition rates found earlier for the case of a single transport mechanism (see, e.g., previous two sections and Figure 1). As ξ increases and becomes closer to unity, R increases for two reasons:

- A greater fraction of the large particles and hence a greater fraction of the aerosol mass deposits due to an eddy-impaction mechanism
- At the same time the reference deposition rate, $-\dot{m}''_{p,ref}\{\bar{v}\}$, decreases, until for ξ equal to unity R obtains its maximum value.

Note also, that the higher the standard deviation of the PSD, the earlier, with respect to ξ values, the deposition rate ratio starts increasing. As ξ increases further above unity, R

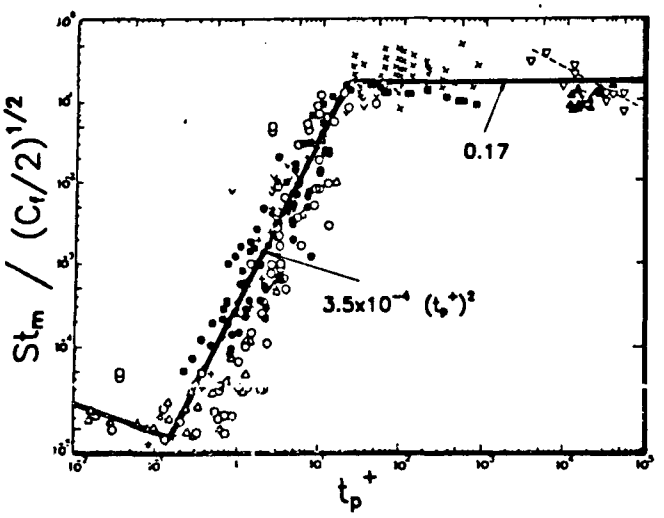

Figure 4. Literature deposition data for fully-developed duct flow in the absence of appreciable sedimentation effects.

Piecewise power law dependence of the dimensionless mass transfer coefficient on the particle stopping time.
Source: McCoy and Hanratty (1977), and Ganic and Mastanaiah (1981).

decreases towards a steady value that corresponds to deposition due to a purely eddy-impaction mechanism (compare with Figure 3). The small decrease of R, which occurs for ξ slightly larger than unity, is due primarily to an increase of the reference deposition rate in this region. Finally, as the mean volume of the distribution increases further and approaches the critical volume above which capture becomes independent of particle size (inertial cut-off), the deposition rate ratio begins to decrease, goes through a local minimum at $\bar{v} = v_{crit,2}$, or equivalently at $\xi = r$ (which we can rationalize with arguments similar to the ones we used for $\xi = 1$), and then, as expected, approaches unity. A rather interesting general implication of the local extremum exhibited by the total deposition rate ratio, $-\dot{m}_p''/-\dot{m}_{p,ref}''$, for particle sizes that correspond to a transition in the deposition mechanism, is that *R will not necessarily fall between the limits obtained for either of the two mechanisms acting alone.* In the present case, the deviations are quite small (for, say, convective diffusion/eddy impaction, and $\sigma_g = 1.35$, the deviation is less than 10%); but under different deposition conditions (cf. convective diffusion and inertial impaction on a cylinder in cross flow), they can become very large. In such situations, one should exercise caution when basing total mass deposition predictions exclusively on the reference deposition rate, which (by definition) is based on a single mechanism.

In Figure 6, we plot again the deposition rate ratio vs. $\xi = v/v_{crit,1}$, for $\sigma_g = 2.5$ and different values of $r = v_{crit,2}/v_{crit,1}$. As expected, the closer the two transition volumes $v_{crit,1}$ and $v_{crit,2}$ are, or equivalently for smaller r's, the importance of the eddy-impaction mechanism decreases. Note that this effect will become even more pronounced as the standard deviation, σ_g of the PSD of the depositing aerosol increases.

An examination of Figure 5, suggests that an aerosol with unimodal PSD of typical spread (σ_g of about 2.0 to 3.0) and under typical deposition conditions, say, $r = O(10^3)$, will "experience" a single or at most a combination of two transport mechanisms, that is, convective-diffusion/eddy-impaction or eddy-impaction/inertial deposition, regardless of where the mean of the particle-size distribution is located with respect to the sizes that mark the transition between the various mechanisms. On the other hand, if the PSD is bimodal or even multimodal, like, for example, in the case of supermicron particle deposition in the presence of condensible vapors (a problem of great practical interest; Rosner and Nagarajan, 1987), then all three transport mechanisms will have to be considered simultaneously.

Limiting ourselves to distributions with a single mode, we

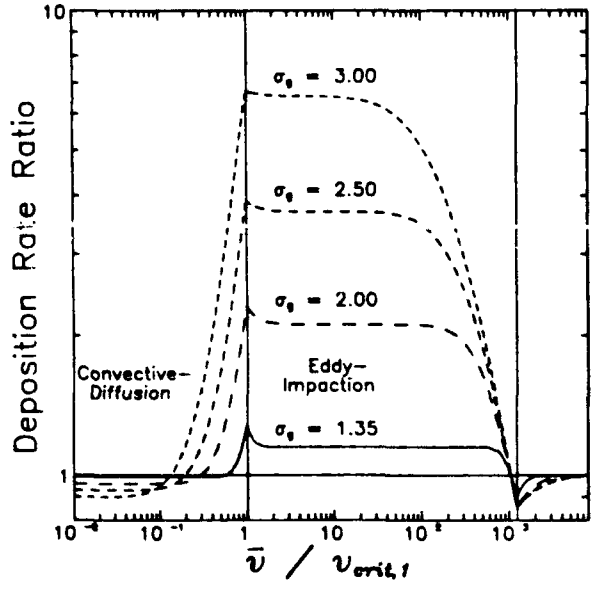

Figure 5. Deposition rate ratio R vs. dimensionless mean size of particle size distribution for various values of PSD standard deviation.

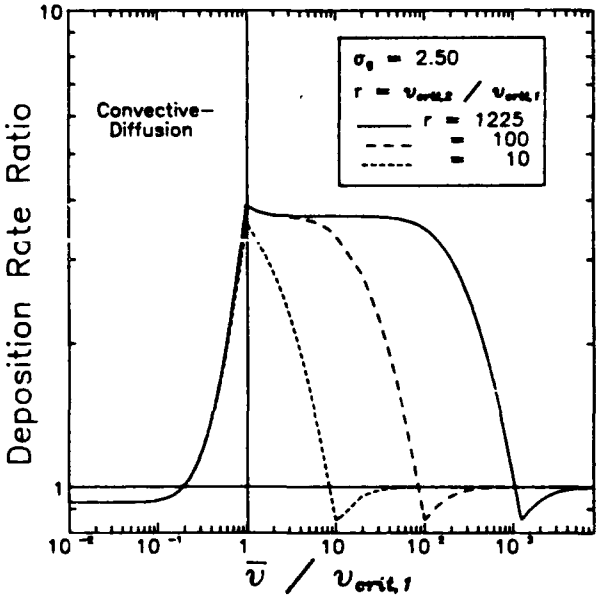

Figure 6. Effect of the extent of the eddy-impaction regime, as determined by r, on the deposition rate ratio R for a PSD with $\sigma_g = 2.5$.

present in Figure 7 curves of constant deposition rate ratio R on a σ_g vs. $\bar{v}/v_{crit}$ plot for the case of deposition due to convective-diffusion and eddy-impaction. This figure is a cross plot of the left half of Figure 5 and can be readily used to determine the deposition rate ratio as a function of the location of the PSD mean with respect to v_{crit} as determined by the local conditions and the PSD standard deviation. Thus, for $(\bar{v}/v_{crit}, \sigma_g)$ pairs that lie in the shaded region (region II), both mechanisms have to be considered. In this case, a first estimate of the deposition rate ratio can be obtained from the given iso-R curves. If, on the other hand, the pairs lie in regions I or III, then the deposition is determined primarily by a single mechanism, and so Eq. 13 can be used with an expected accuracy of ±3%. A similar plot for eddy impaction/inertial deposition is given in Figure 8. In region I Eq. 13 may again be used, but in region III the deposition rate ratio is equal to unity.

Generalizations

Finite-analytic procedure for calculating total deposition rates

In this section, we outline a "finite-analytic" method that allows us to compute total mass deposition rates in the general case where $St_m\{v\}$ is an arbitrary function of particle volume. The basic idea is simple indeed: since log (St_m) vs. log $\{v\}$ can be approximated to any desired degree of accuracy by a series of straight line segments, St_m can be always reduced to a piecewise power law. But, recall that for this case we already have an analytic solution (cf. previous two sections). In Appendix B, we give an expression for

$$R = \frac{-\dot{m}''_{p,tot}}{-\dot{m}''_p\{\bar{v}\}} = \frac{\sum_{i=1}^{N} \int_{v_{i-1}}^{v_i} St_{m,i} v C_1\{v\}\, dv}{St_{m,k}\{\bar{v}\}\bar{v}} \qquad (21)$$

for the case of St_m consisting of say N discrete power-law segments, and the *arithmetic mean volume* of the aerosol population $\bar{v}$ lying in the kth interval In Eq. 21, we assume that $v_1 = 0$ and $v_N = \infty$.

Clearly in implementing this method, one should approximate St_m by a *larger* number of *shorter* straight line segments wherever the curvature is higher. In order to test whether in any given particle volume regime, (v_{k-1}, v_k), the power-law approximation is adequate we propose the following simple criterion (Rosner, 1989). By expanding ln $St_m(\bar{v})$ vs. ln v in a Taylor series around $\bar{v}$ and inserting into Eq. 21, we find that this approximation is acceptable provided:

$$\frac{\sum_{i=1}^{N} \int_{v_{i-1}}^{v_i} \frac{1}{2!}\left(\frac{\partial^2 \ln St_m}{\partial (\ln v)^2}\right)_{v=\bar{v}} \left(\ln \frac{v}{\bar{v}}\right)^2 v C_1\{v\}\, dv}{R \cdot \left[(\ln St_m)_{v=\bar{v}} + \left(\frac{\partial \ln St_m}{\partial \ln v}\right)_{v=\bar{v}} \cdot \left(\ln \frac{v}{\bar{v}}\right)\right] \cdot \bar{v}} \ll 1 \qquad (22)$$

This criterion can be readily introduced into a general-purpose code, so that the number and location of the straight line segments that are needed to approximate a given capture efficiency curve is optimal. In the present illustrative calculations (cf. Figures 9 and 10), however, we simply increased the number of Δ (ln v) segments until the computed R values acceptably converged

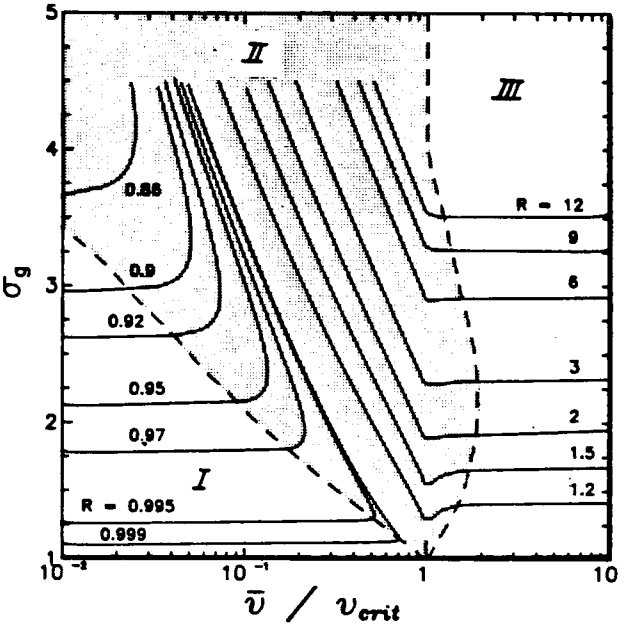

Figure 7. Constant deposition rate ratio R on σ_g vs. (log) $\bar{v}/v_{crit}$ plot for the case of deposition due to convective diffusion and eddy impaction.
In regions I and III, Eq. 13 is valid, and it is only in the shaded regime where both mechanisms must be considered simultaneously.

Convective diffusion and inertial impaction on a cylinder in cross flow

We will demonstrate the application of our method for the case of convective diffusion and inertial impaction on a cylinder in cross flow, perhaps the most important example from an engineering point of view. We will assume that the Reynolds number, Re, based on cylinder diameter, d_w, is large ($Re^{1/2} \gg 1$) and that the interception parameter, d_p/d_w, is small (at least for the particle sizes that deposit due primarily to Brownian diffusion) so that we can neglect deposition due to interception. For this simplified case, it is well known that the convective-diffusion capture efficiency, η_{cap}, defined as the fraction of the particles collected from the fluid volume swept by the cylinder, is given by (see, e.g., the Nusselt number correlations in Eckert and Drake, 1981; Perry and Chilton, 1973):

$$\eta_{cap} = 2 \cdot \left(\frac{\overline{Nu}_m}{Re \cdot Sc}\right) \simeq 0.054\, Re^{-0.195} Sc^{-2/3} \qquad (23)$$

Note that, in this regime, the particle capture fraction depends on the collector-based Reynolds number and the particle Schmidt number.

In the case of "pure" inertial deposition, the capture efficiency of the cylinder depends on the particle Stokes number, Stk and, for non-Stokesian particles (because the velocity of the flow field is high and/or because the particles are large) it will also depend on a Reynolds number, Re_p, based on particle diameter and the free-stream velocity. For a potential flow field approximation to the carrier fluid motion around the collector, the collection efficiency has been calculated numerically (Brun et al., 1955) and has been also correlated in terms of an effective

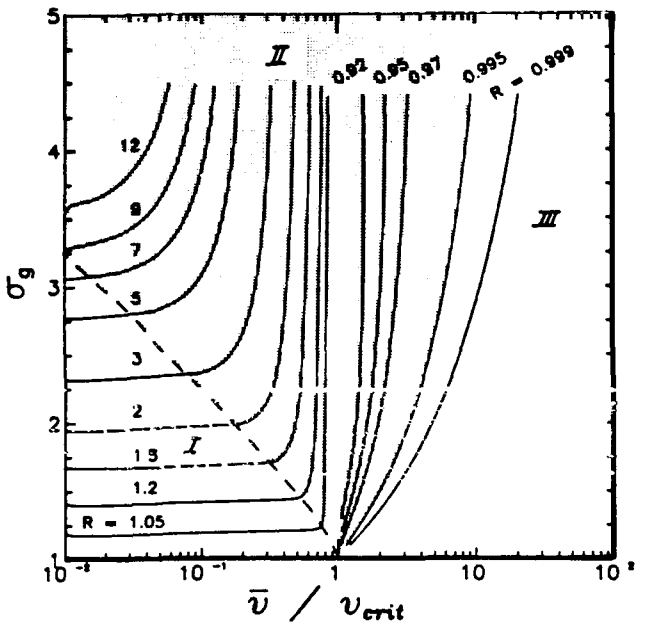

Figure 8. Constant deposition rate ratio R on a σ_g vs. (log) $\bar{v}/v_{crit}$ plot for the case of capture due to eddy impaction and inertial deposition.

In region I, Eq. 13 is valid, in the shaded area both mechanisms must be considered; in region III, the deposition rate ratio can be taken equal to unity.

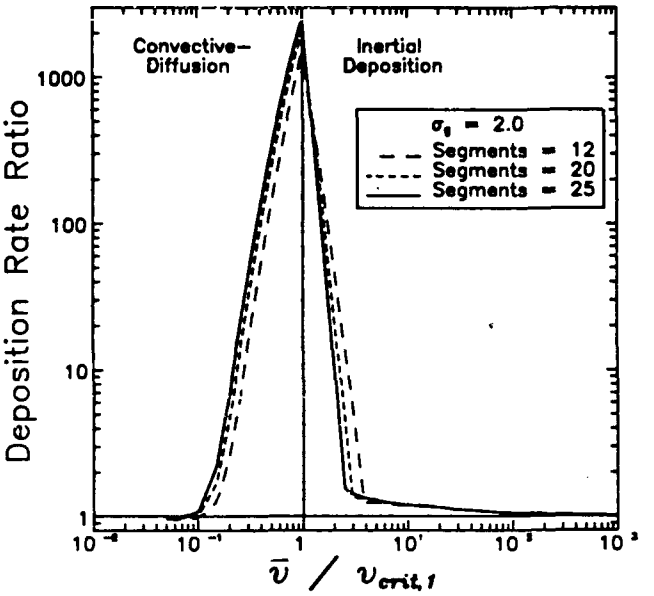

Figure 10. Convergence of the deposition rate ratio R as the number of power-law segments (used to approximate the capture efficiency curve of Figure 8) increases.

Stokes number (Israel and Rosner, 1983) which accounts for the above-mentioned parameters. For these reasons Israel and Rosner (1983) introduced a generalized Stokes number:

$$Stk_{eff} = \Psi\{Re_p\} \cdot Stk \tag{24}$$

where for our purposes Stk is the conventionally-defined Stokes number $[=\tilde{\rho}_p d_p^2 U/(18\mu)]$ and $\Psi\{Re_p\}$ a correction factor to account for non-Stokesian behavior, i.e.:

$$\Psi\{Re_p\} = \frac{24}{Re_p} \cdot \int_0^{Re_p} \frac{dRe'}{C_D\{Re'\}Re'} \tag{25}$$

Integrating Eq. 25 for a quasisteady drag coefficient, C_D of the commonly used approximate form

$$C_D\{Re\} = \frac{24}{Re}(1 + 0.158Re^{2/3})$$

one readily finds

$$\Psi\{Re_p\} \simeq \frac{3}{0.0628Re_p} \cdot [(0.0628Re_p)^{1/3} - \tan^{-1}\{(0.0628Re_p)^{1/3}\}] \tag{26}$$

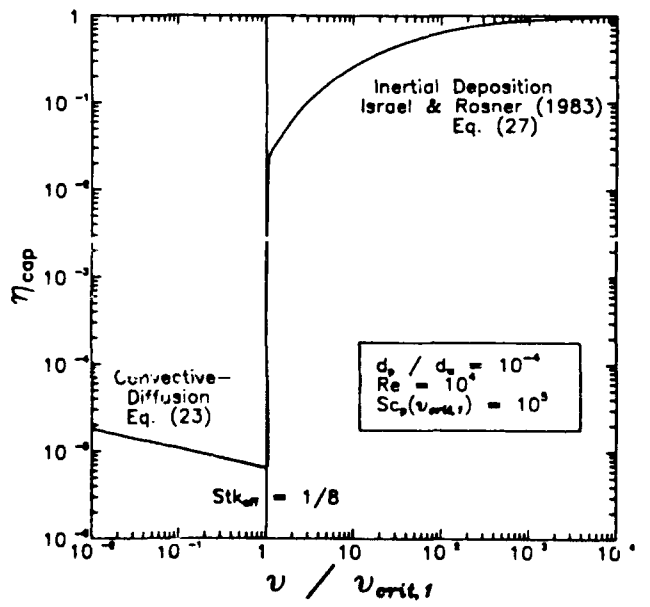

Figure 9. Typical behavior of the efficiency curve for particle capture on a circular cylinder in cross-flow in the high Reynolds number limit ($Re^{1/2} \gg 1$).

For a circular cylinder collection geometry and $Stk_{eff} > 0.14$, Israel and Rosner (1983) recommend the following correlation for the capture fraction (if each impacting particle "sticks"):

$$\eta_{cap}\{Stk_{eff}\} \simeq \left[1 + 1.25\left(Stk_{eff} - \frac{1}{8}\right)^{-1} - 1.4 \times 10^{-2} \cdot \left(Stk_{eff} - \frac{1}{8}\right)^{-2} + 0.058 \times 10^{-4}\left(Stk_{eff} - \frac{1}{8}\right)^{-3}\right]^{-1} \tag{27}$$

although equally acceptable alternatives are given by Wessel and Righi (1988), and Wang (1986).

At this point, we are not aware of any correlation for $\eta_{cap}\{Stk_{eff}\}$ in the near-critical range of Stk_{eff} (from 0.125 to 0.14),

and so for that range we simply take:

$$\eta_{cap} \simeq A \cdot \left(Stk_{eff} - \frac{1}{8}\right)^d \tag{28}$$

[In the spirit of earlier calculations of the critical Stokes number (Friedlander, 1977), such a near-Stk_{crit} relation can be derived by using a second-order expansion of the flow field in the vicinity of the forward stagnation point.] Equation 28 does exhibit the proper limiting behavior as Stk_{eff} approaches Stk_{crit}, but other than that is not based on any physical grounds. By matching Eq. 27 to Eq. 24 for $Stk_{eff} = 0.14$ and further requiring the first derivative of $\eta_{cap}\{v\}$ with respect to v to be also continuous, we estimate the two constants appearing in Eq. 28:

$$\eta_{cap} \simeq 0.043 \left(Stk_{eff} - \frac{1}{8}\right)^{0.11} \tag{29}$$

In Figure 9, we give a typical capture efficiency curve that encompasses both the convective diffusion and inertial deposition regimes. Note that, since in the convective-diffusion regime η_{cap} is already a power law, we can analytically integrate this entire size range ([0, 1] in dimensionless volume units) in one "giant" step, thus saving computational time. [If we neglect the effect of Kn_p, i.e., within the confines of continuum ($Kn_p \ll 1$) diffusion.] In Figure 10, we show the dependence of the deposition rate R on $\bar{v}/v_{crit,1}$ for a log-normal mainstream particle-size distribution that has $\sigma_g = 2.0$ and that deposits according to η_{cap} as depicted in Figure 11. Note that if we "fit" the inertial deposition part of the (log) η_{cap} vs. log $(v/\bar{v})$ curve with about 20 linear segments R converges. Finally, in Figure 11, we show the dependence of the total mass deposition rate ratio on the dimensionless mean size of the aerosol population for different values of the standard deviation of the PSD.

From Figures 10 and 11, it is clear that, in the case of deposition on a cylinder in cross flow, the total mass deposition rate ratio is a very sensitive function of the relative location of the mean particle size, $\bar{v}$, with respect to the particle size at which transition occurs from deposition due to convective diffusion to an inertial mechanism. This is another example where one should avoid basing deposition calculations on a single regime, since in this case the total deposition rate can be severely underpredicted. From a mathematical point of view, R almost diverges in the neighborhood of $\bar{v}/v_{crit} \simeq 1$, because in this regime there is a great difference of order $O(10^3)$ between the magnitude of the actual total mass deposition rate and the reference deposition rate.

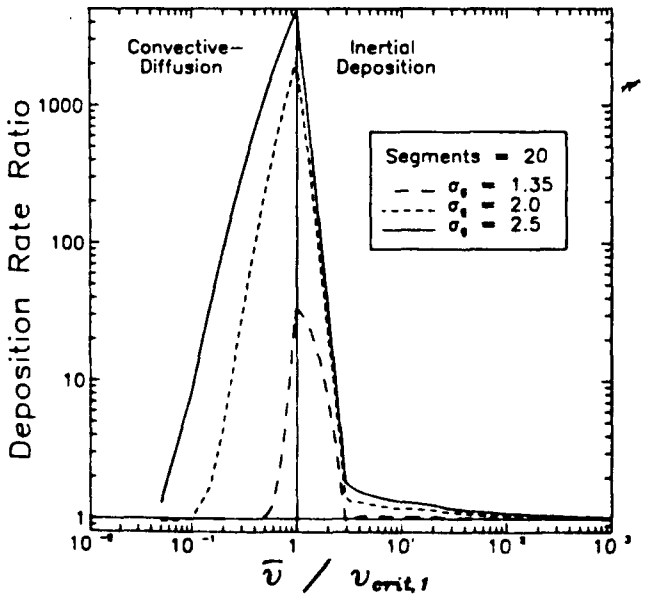

Figure 11. Dependence of the total mass deposition rate ratio on the dimensionless average size of aerosol population for different values of the PSD standard deviation.

Variance of non-log-normal single-mode distributions

In this paper we deliberately cast our results in terms of the particle arithmetic mean size (volume), $\bar{v}$, and the standard deviation, σ_g, of the aerosol PSD. We decided to use the average particle size of the population, rather than the distribution median, v_g, because the former has also a simple physical significance, despite the fact that, if we had used v_g, some of our analytical expressions would have been simplified. By the same token, we have here used σ_g to quantify the spread of the (log-normal) distribution, a natural choice from a mathematical point of view, while we could also have used the square root of the dimensionless variance of the PSD, here denoted simply by σ and defined as

$$\sigma \equiv \left[\frac{1}{\bar{v}} \cdot \int_0^\infty (\bar{v} - v)^2 C_1\{v\}\, dv\right]^{1/2} = [\exp\{\ln^2\sigma_g\} - 1]^{1/2} \tag{30}$$

Since not all single-mode PSD's are "log-normal," we conjecture that, if our present results were recast in terms of the square root of the variance σ, then they would (approximately) apply to a wide variety of single-mode distributions.

Conclusions

For commonly encountered engineering applications, in which total mass deposition rates are required from fluid streams containing suspended particles distributed near "log-normally," we have developed and presented simple results for piecewise-power-law mass transfer coefficients (e.g., turbulent convective diffusion and eddy impaction) (including an inertial decoupling "cut-off"). Thus, we have shown that, whenever we may assume a simple power-law dependence of $St_m\{v\}$ on the size of the depositing particles, the total mass deposition rate ratio, R, is given analytically by a very simple expression that involves only the exponent that describes the dependence of the mass Stanton number on particle volume and the spread of the aerosol PSD, σ_g (cf. Eq. 13). We further obtained analytical expressions (in terms of error functions) for R in the case of piecewise-power-law mass transfer coefficients, St_m, (Eq. 21 and Appendix B) which can be readily used in computations and have also provided graphs (Figures 7 and 8) from which one can directly obtain the local deposition rate ratio for the commonly-encountered case of deposition due to a combination of convective-diffusion/eddy-impaction or eddy-impaction/inertial mechanism.

These results/plots, which generalize the recent conclusions of Rosner (1989) for power-law capture from coagulation-aged (self-preserving shape) aerosols, reduce the general problem of

computing actual deposition rates to the straightforward one of first calculating the (reference) deposition rate if all particles in the population had the same (average) volume and then correcting this result by a ratio R calculated here for several commonly-encountered mechanistic combinations over a range of aerosol PSD "spread" parameters. Apart from their direct engineering utility and conceptual value, our viewpoint and procedures are shown to open the way to computationally-efficient finite-analytic methods for computing total mass deposition rates from aerosol population distributions of *arbitrary* shape, captured in accord with an efficiency function of *arbitrary* shape. [Indeed, this strategy could clearly be adopted to compute many other properties of aerosol populations which require the integral of a product of the particle-size distribution function and some other particle size dependent quantity, e.g., light scattering efficiency (Buckius and Hwang, 1980).]

It would be prudent to recall the most important assumption which underlies our present methods and predictions: viz., *each particle size class does not influence the deposition rate of other size classes*. In practice, we know that this assumption would have to be relaxed whenever:

- The diffusional capture of small particles influences the inertial capture (via sticking probability) of larger particles (see, e.g., Rosner and Nagarajan, 1987)
- Appreciable particle-particle coagulation occurs in the immediate vicinity of the collector (see, e.g., Park and Rosner, 1988a; Biswas, 1988)
- A portion of the preexisting aerosol population coupled with the host fluid flow to modify the transfer coefficient of the smaller particles (see, e.g., Park and Rosner, 1988b, 1989)
- The depositing particles scavenge an appreciable mass of coexisting vapor within the thermal boundary layer adjacent to the collector (see, e.g., Castillo and Rosner, 1988)
- Appreciable particle production (from a supersaturated vapor) occurs within the thermal boundary layer adjacent to the collector (see, e.g., Castillo and Rosner, 1989; Liang et al., 1989).

However, even in most of these more complex (coupled) cases, it will still be useful and instructive to compare actual rates to those expected based on the simple procedure outlined in this paper.

Finally, it should be recognized that in many current and future applications, in addition to predicting the total deposit mass, it will be necessary to have a quantitative understanding of the *deposit microstructure* and, of course, microstructure-sensitive deposit properties (see, e.g., Tassopoulos et al., 1989). This is clearly a more ambitious goal of deposition rate theory, but one which can no longer be postponed

Acknowledgment

It is a pleasure to acknowledge the financial support of DOE-PETC via Grant No. DE-FG22-86PC90756 and the U.S. AFOSR via Grant No. AFOSR 84-0034, 89-0223, as well as the related support of the Yale HTCRE Laboratory by our current Industrial Affiliates: Shell Foundation, Lycoming-Textron, and SCM-Chemicals. In this research, the authors have benefited from helpful discussions with Professors J. Fernandez de la Mora and J. O'Brien, Dr. D. W. Mackowski, as well as A. G. Konstandopoulos.

Notation

b = exponent characterizing dependence of St_m on particle volume v
C_f = nondimensional wall-friction coefficient; $=\bar{\tau}_w/(\frac{1}{2}\rho U^2)$
C_D = quasisteady particle drag coefficient
$C_f\{v\}$ = normalized log-normal distribution function, Eq. 8
d_p = particle diameter
d_w = circular cylinder (target) diameter
D_p = particle Brownian diffusion coefficient
$E\{P, x\}$ = function, Eq. 20
k = "order" of PSD moment
Kn_p = particle Knudsen number, l/d_p
l = gas-mean-free path
$-\dot{m}_p''$ = total mass deposition rate, Eq. 4
$-\dot{m}_{p,ref}''$ = reference mass deposition rate, Eq. 5
$n\{v\}$ = particle number density function
N_p = particle number density, Eq. 1
P = dummy variable, Eq. 20
Pe = Peclet number for particle diffusion
q = "order" of partial moment of log-normal distribution, Eq. 19
r = parameter reflecting extent of the particle size range over which eddy impaction is the predominant deposition mechanism
R = deposition rate ratio, Eq. 6
Re = Reynolds number based on cylinder diameter
Re_p = Reynolds number based on particle diameter
Sc = particle Schmidt number
St_m = dimensionless mass transfer coefficient
Stk = particle Stokes number
Stk_{eff} = effective particle Stokes number, Eq. 24
t_p = characteristic particle stopping time
t_p^+ = dimensionless particle stopping time, $u_*^2 t_p/\nu$
$t_{p,1}^+$ = dimensionless particle stopping time marking transition from convective-diffusion to eddy-impaction deposition
u_* = friction velocity; $(C_f/2)^{1/2}U$
U = gas-free-stream velocity
v = particle size (volume)
$\bar{v}$ = mean particle volume; ϕ_p/N_p
v_{crit} = particle size marking a transition in deposition mechanism
$v_{crit,1}$ = particle size marking transition from a convective-diffusion to eddy-impaction deposition mechanism; Figure 4
$v_{crit,2}$ = particle size marking transition from eddy-impaction to size-insensitive deposition; Figure 4
v_g = median volume of log-normal distribution
v_i = critical particle size marking beginning of the $(i+1)$ deposition regime
v_k = median volume of a particular log-normal distribution function, Eq. 11
v_* = dimensionless particle size $(=v/v_g)$
x = dummy variable, Eq. 20

Greek letters

α = lower limit of partial moment of log-normal distribution, Eq. 19
β = upper limit of partial moment of log-normal distribution, Eq. 19
η_{cap} = capture fraction
μ = gas dynamic viscosity
ν = gas momentum diffusivity (kinematic viscosity)
ξ = dimensionless mean particle size $(=\bar{v}/v_{crit})$
ρ = gas density
$\tilde{\rho}_p$ = intrinsic particle density
σ^2 = dimensionless variance of log-normal distribution, Eq. 30
σ_g = geometric standard deviation of log-normal distribution
ϕ_p = particle volume fraction, Eq. 1
Ψ = self-preserving distribution function
Ψ = correction factor accounting for non-Stokesian drag behavior of particles, Eqs. 24, 25

Literature Cited

Ali, S. I., and R. L. Zollars, "Generation of Self-Preserving Particle Size Distributions during Shear Coagulation," *J. Coll. Interf. Sci.*, **126**, 377 (1988).

Aitchison, J., and J. A. C. Brown, *The Log-Normal Distribution*, Cambridge University Press (1969).

Biswas, P., "Differential Impaction of Aerosols," *J. Aerosol Sci.*, **19**, 603 (1988).
Brun, R. J., W. Lewis, P. J. Perkins, and J. S. Serafini, "Impingement of Cloud Droplets on a Cylinder and Procedure for Measuring Liquid-Water Content and Droplet Sizes in Supercooled Clouds by Rotating Multicylinder Method," NACA Rep. 1215 (1955).
Buckius, R. O., and D. C. Hwang, "Radiation Properties for Polydispersions: Application to Coal," *ASME J. Heat Transfer*, **102**, 99 (1980).
Castillo, J. L., and D. E. Rosner, "Nonequilibrium Theory of Surface Deposition from Particle-Laden, Dilute Condensible Vapor-Containing Stream, Allowing for Particle Thermophoresis and Vapor Scavenging within the Laminar Boundary Layer," *Int. J. Multiphase Flow*, **14**(1), 99 (1988).
Castillo, J. L., and D. E. Rosner, "Theory of Surface Deposition from a Binary Dilute Vapor-Containing Stream, Allowing for Equilibrium Condensation within the Laminar Boundary Layer," *Int. J. Multiphase Flow*, **15**(1), 97 (1989).
Eckert, E. R. G., and R. M. Drake, Jr., *Heat and Mass Transfer*, R. E. Krieger, FL (1981).
Fernandez de la Mora, J., and D. E. Rosner, "Effects of Inertia on the Diffusional Deposition of Small Particles to Spheres and Cylinders at Low Reynolds Numbers," *J. Fluid Mech.*, **125**, 379 (1982).
Flagan, R., and S. K. Friedlander, *Recent Developments in Aerosol Science*, J. Davis, ed., Wiley, New York, 25 (1978).
Friedlander, S. K., *Smoke, Dust and Haze-Fundamentals of Aerosol Behavior*, Wiley, New York (1977).
Friedlander, S. K., and C. S. Wang, "The Self-Preserving Particle Size Distribution for Coagulation by Brownian Motion," *J. Coll. Interf. Sci.*, **22**, 126 (1966).
Fuchs, N. A., *Mechanics of Aerosols*, Pergamon, New York (1964).
Ganic, E. N., and K. Mastanaiah, "Investigation of Droplet Deposition from a Turbulent Gas Stream," *Int. J. Multiphase Flow*, **7**, 401 (1981).
Garber, E., S. G. Brush, and C. W. F. Everitt, *Maxwell on Molecules and Gases*, MIT Press, Cambridge, MA (1986).
Israel, R., and D. E. Rosner, "Use of a Generalized Stokes Number to Determine the Aerodynamic Capture Efficiency of Non-Stokesian Particles from a Compressible Gas Flow," *Aerosol Sci. Tech.*, **2**, 45 (1983).
Lai, F. S., S. K. Friedlander, J. Pich, and G. M. Hidy, "The Self-Preserving Particle Size Distribution for Brownian Coagulation in the Free-Molecule Regime," *J. Coll. Interf. Sci.*, **39**(2), 395 (1972).
Lee, K. W., "Change of Particle Size Distribution during Brownian Coagulation," *J. Coll. Interf. Sci.*, **92**, 315 (1983).
Lee, K. W., H. Chen, and J. A. Gieseke, "Log-Normal Preserving Size Distribution for Brownian Coagulation in the Free-Molecule Regime," *Aerosol Sci. Tech.*, **3**, 53 (1984).
Liang, B., A. Gomez, J. L. Castillo, and D. E. Rosner, "Experimental Studies of Nucleation Phenomena within Thermal Boundary Layers—Influence on Chemical Vapor Deposition Rate Processes," *Chem. Eng. Comm.*, in press (1989).
McCoy, D. D., and T. J. Hanratty, "Rate of Deposition of Droplets in Annular Two-Phase Flow," *Int. J. Multiphase Flow*, **3**, 319 (1977).
Meakin, P., "Diffusion-Controlled Cluster Formation in 2-6-Dimensional Space," *Phys. Rev. A*, **27**, 1495 (1983).
Mountain, R. D., G. W. Mulholland, and H. Baum, "Simulation of Aerosol Agglomeration in Free-Molecular and Continuum Flow Regimes," *J. Coll. Interf. Sci.*, **114**(1), 67 (1986).
Papavergos, P. G., and A. B. Hedley, "Particle Deposition Behavior from Turbulent Flows," *Chem. Eng. Res. Des.*, **62**, 275 (1984).
Park, H. M., and D. E. Rosner, "Boundary Layer Coagulation Effects on the Size Distribution of Thermophoretically Deposited Particles," *Chem. Engrg. Sci.*, in press (1988).
———, "Combined Inertial and Thermophoretic Effects on Particle Deposition Rates in Highly Loaded Dusty Gas Systems," *Chem. Eng. Sci.*, in press (1989).
Perry, R. H., and C. H. Chilton, *Chemical Engineers' Handbook*, McGraw Hill, New York (1971).
Raabe, O. G., "Particle Size Analysis Utilizing Grouped Data and the Log-Normal Distribution," *J. Aerosol Sci.*, **2**, 289 (1971).
Rosner, D. E., "Total Mass Deposition Rates from Polydispersed Aerosols," *AIChE J.*, **35**, 164 (Jan., 1989).
———, *Transport Processes in Chemically Reacting Flow Systems*, 2nd Printing, Butterworth, Stoneham, MA (1988).
Rosner, D. E., and H. M. Park, "Thermophoretically Augmented Mass-, Momentum-and Energy-Transfer Rates in High Particle Mass-Loaded Laminar Forced Convection Systems," *Chem. Eng. Sci.*, **43**(10), 2689 (1988).
Rosner, D. E., and R. Nagarajan, "Toward a Mechanistic Theory of Net Deposit Growth from Ash-Laden Flowing Combustion Gases: Self-Regulated Sticking of Impacting Particles and Deposit Erosion in the Presence of Vapor Glue," *AIChE Symp. Ser.*, **83**(257), R. W. Lyczkowski, ed., 289 (1987).
Tassopoulos, M., J. A. O'Brien, and D. E. Rosner, "Simulation of Microstructure/Mechanism Relationships in Deposition," *AIChE J.*, **35**, 967 (June, 1989).
Wang, C. S., and S. K. Friedlander, "The Self-Preserving Particle Size Distribution for Coagulation by Brownian Motion," *J. Coll. Interf. Sci.*, **24**, 170 (1967).
Wang, H. C., "Theoretical Adhesion Efficiency for Particles Impacting a Cylinder at High Reynolds Number," *J. Aerosol Sci.*, **17**, 827 (1986).
Wessel, R. A., and J. Righi, "Generalized Correlations for Inertial Impaction of Particles on a Circular Cylinder," *Aerosol Sci. Tech.*, **9**, 29 (1988).

Appendix A: Partial Moments of Log-Normal Distribution

The log-normal particle-size distribution is given by:

$$C_1(v) = \frac{1}{v \ln \sigma_g \sqrt{2\pi}} \exp\left[-\frac{\ln^2 (v/v_g)}{2 \ln^2 \sigma_g}\right] \qquad (0 < v < \infty) \quad \text{(A1)}$$

The partial moment, μ_q, of order q, in the range say α to β, is defined here by:

$$\mu_q = \int_\alpha^\beta v^q C_1(v) dv \qquad \text{(A2)}$$

Note further that for any log-normal distribution (Raabe, 1972)

$$v^q C_1(v) = \exp\left[q \ln v_g + \frac{q^2}{2} \ln^2 \sigma_g\right] \cdot \left\{\frac{1}{v \ln \sigma_g \sqrt{2\pi}} \exp\left[-\frac{\ln^2 (v/v_q)}{2 \ln^2 \sigma_g}\right]\right\} \qquad \text{(A3)}$$

where

$$\ln v_q = \ln v_g + q \ln^2 \sigma_g \qquad \text{(A4)}$$

From Eqs. A1, A2 and A3, we obtain for the partial moment

$$\mu_q = \exp\left[q \ln v_g + \frac{q^2}{2} \ln^2 \sigma_g\right] \cdot \int_\alpha^\beta \frac{1}{v \ln \sigma_g \sqrt{2\pi}} \exp\left[-\frac{\ln^2 (v/v_q)}{2 \ln^2 \sigma_g}\right] dv \qquad \text{(A5)}$$

with the distribution in the definite integral of Eq. A5 another log-normal. Noting also that in general the log-normal is defined as a distribution of sizes whose logarithms are normally distributed, it becomes apparent that the required definite integral can be expressed in terms of the well-known error function. Specifi-

cally, we have

$$\int_\alpha^\beta \frac{1}{v \ln \sigma_g \sqrt{2\pi}} \exp\left[-\frac{\ln^2(v/v_g)}{2 \ln^2 \sigma_g}\right] dv = \int_{\ln(\alpha/v_q)/\ln\sigma_g}^{\ln(\beta/v_q)/\ln\sigma_g} \frac{1}{\sqrt{2\pi}} \exp\left[-\frac{1}{2}\left(\frac{\ln(v/v_q)}{\ln\sigma_g}\right)^2\right] d\left(\frac{\ln(v/v_q)}{\ln\sigma_g}\right)^2 = \frac{1}{2} \cdot \int_{\ln(\alpha/v_q)/\sqrt{2}\ln\sigma_g}^{\ln(\beta/v_q)/\sqrt{2}\ln\sigma_g} \frac{2}{\sqrt{\pi}} \exp - t^2\, dt \quad \text{(A6)}$$

Combining now Eqs. A4 and A6, while substituting for v_q from Eq. A4, we obtain for the partial moment of order q:

$$\mu_q \int_\alpha^\beta v^q C_i(v)\, dv = \frac{1}{2} \exp\left[q \ln v_g + \frac{1}{2} q^2 \ln^2 \sigma_g\right] \cdot \left\{\operatorname{erf}\left[\frac{\ln\left(\frac{\beta}{v_g} \exp(-q \ln^2 \sigma_g)\right)}{\sqrt{2} \ln \sigma_g}\right] - \operatorname{erf}\left[\frac{\ln\left(\frac{\alpha}{v_g} \exp(-q \ln^2 \sigma_g)\right)}{\sqrt{2} \ln \sigma_g}\right]\right\} \quad \text{(A7)}$$

that is, Eq. 19.

Appendix B: Analytic Expression for Total Mass Deposition Rate Ratio When $St_m(v)$ Is a Piecewise Power-Law

Suppose that the mass Stanton number, $St_m(v)$, consists of N discrete power-law segments, and that the arithmetic mean of the aerosol particle-size distribution, $\bar{v}$, lies in the kth (power-law) segment. In this case, the total mass deposition rate ratio, R, is defined here by:

$$R = \frac{-\dot{m}''_{p,\text{tot}}}{-\dot{m}''_p(\bar{v})} = \frac{\sum_{i=1}^{N} \int_{v_{i-1}}^{v_i} St_{m,i} v C_i(v)\, dv}{St_{m,k}(\bar{v})\bar{v}} \quad \text{(B1)}$$

where $St_{m,i}$ denotes the Stanton mass number in the ith interval. Here we also take $v_0 = 0$ and $v_N = \infty$. If $v_{\text{crit},i}$ is the particle size (volume) that marks the transition from the ith to the $i + 1$ deposition mechanism, let

$$r_i = \frac{v_{\text{crit},i}}{v_{\text{crit},1}} \quad \text{for} \quad i = 2, N - 1 \quad \text{(B2)}$$

Since $St_m(v)$ is a continuous function of the particle size, v, it is straightforward to show that the Stanton number in the ith interval is given by

$$St_{m,i} \sim \left(\prod_{j=1}^{i-2} r_j^{b_{j+1}-b_{j+2}}\right) \cdot \xi^{b_i} \quad \text{(B3)}$$

where ξ is the dimensionless mean particle size, $\xi = \bar{v}/v_{\text{crit},1}$.

If we substitute now into Eq. B1 and use the expression for the partial moment of a log-normal distribution (Appendix A), after some algebraic manipulation one finds that

$$R = \frac{1}{2} \sum_{i=1}^{N} \frac{St_{m,i}}{St_{m,k}} \cdot \exp\left[\frac{b_i(b_i+1)}{2} \ln^2 \sigma_g\right] \cdot \left\{E\left(\frac{r_{i-1}}{\xi}, b_i\right) - E\left(\frac{r_{i-2}}{\xi}, b_i\right)\right\} \quad \text{(B4)}$$

where E is a function introduced here for brevity, defined by Eq. 20.

Manuscript received Feb. 28, 1989, and revision received June 20, 1989.

REPORT DOCUMENTATION PAGE

Form Approved
OMB No. 0704-0188

1. AGENCY USE ONLY (Leave blank)	2. REPORT DATE	3. REPORT TYPE AND DATES COVERED
	1989	Journal Publication

4. TITLE AND SUBTITLE

COMBINED INERTIAL AND THERMOPHORETIC EFFECTS ON PARTICLE DEPOSITION RATES IN HIGHLY LOADED DUSTY-GAS SYSTEMS† (U)

5. FUNDING NUMBERS

PE - 61102F
PR - 2308
SA - BS
G - AFOSR 89-0223

6. AUTHOR(S)

H.M.Park and D.E.Rosner

7. PERFORMING ORGANIZATION NAME(S) AND ADDRESS(ES)

HIGH TEMPERATURE CHEMICAL REACTION ENGINEERING LABORATORY
YALE UNIVERSITY
BOX 2159, YALE STATION
NEW HAVEN, CONNECTICUT 06520 U.S.A.

8. PERFORMING ORGANIZATION REPORT NUMBER

9. SPONSORING/MONITORING AGENCY NAME(S) AND ADDRESS(ES)

AFOSR/NA
Building 410
Bolling AFB DC 20332-6448

10. SPONSORING/MONITORING AGENCY REPORT NUMBER

11. SUPPLEMENTARY NOTES

12a. DISTRIBUTION/AVAILABILITY STATEMENT

Approved for public release; distribution is unlimited

12b. DISTRIBUTION CODE

13. ABSTRACT (Maximum 200 words)

Abstract – Little is yet known (theoretically or experimentally) about the simultaneous effects of particle inertia, particle thermophoresis and high mass loading on the important engineering problem of predicting deposition rates from flowing "dusty" gases. For this reason, we investigate the motion of particles present at nonnegligible mass loading in a flowing nonisothermal gaseous medium and their deposition on strongly cooled or heated solid objects by examining the instructive case of steady axisymmetric "dusty-gas" flow between two infinite disks: an inlet (porous) disk and the impermeable "target" disk—a flow not unlike that encountered in recent seeded-flame experiments. Since this stagnation flow/geometry admits interesting self-similar solutions at all Reynolds numbers, we are able to predict laminar flow mass-, momentum- and energy-transfer rate coefficients over a wide range of particle mass loadings, dimensionless particle relaxation times (Stokes numbers), dimensionless thermophoretic diffusivities, and gas Reynolds numbers. As a by-product, we illustrate the accuracy and possible improvement of our previous "diffusion model" for tightly coupled dusty-gas systems. Moreover, we report new results illustrating the dependence of the important "critical" Stokes number (for incipient particle impaction) on the particle mass loading and the wall gas temperature ratio for dust-laden gas motion towards "overheated" solid surfaces. The present formulation and resulting transport coefficients should not only be useful in explaining/predicting recent deposition rate trends in "seeded"-flame experiments, but also highly mass loaded systems of technological interest, such as the deposition of opto-electronic materials by jet impingement, and fouling layers from ash-laden fossil fuel combustion products.

14. SUBJECT TERMS

soot, mass transport, thermophoresis, inertia, stagnation flow, deposition, high mass loading

15. NUMBER OF PAGES

12

16. PRICE CODE

17. SECURITY CLASSIFICATION OF REPORT	18. SECURITY CLASSIFICATION OF THIS PAGE	19. SECURITY CLASSIFICATION OF ABSTRACT	20. LIMITATION OF ABSTRACT
Unclassified	Unclassified	Unclassified	UL

Chemical Engineering Science, Vol. 44, No. 10, pp. 2233–2244, 1989
Printed in Great Britain

0009-2509/89 $3.00 + 0.00

COMBINED INERTIAL AND THERMOPHORETIC EFFECTS ON PARTICLE DEPOSITION RATES IN HIGHLY LOADED DUSTY-GAS SYSTEMS†

H. M. PARK‡ and D. E. ROSNER§
Department of Chemical Engineering, Yale University, New Haven, CT 06520, U.S.A.

(*Accepted in revised form* 10 *March* 1989)

Abstract—Little is yet known (theoretically or experimentally) about the simultaneous effects of particle inertia, particle thermophoresis and high mass loading on the important engineering problem of predicting deposition rates from flowing "dusty" gases. For this reason, we investigate the motion of particles present at nonnegligible mass loading in a flowing nonisothermal gaseous medium and their deposition on strongly cooled or heated solid objects by examining the instructive case of steady axisymmetric "dusty-gas" flow between two infinite disks: an inlet (porous) disk and the impermeable "target" disk—a flow not unlike that encountered in recent seeded-flame experiments. Since this stagnation flow/geometry admits interesting self-similar solutions at all Reynolds numbers, we are able to predict laminar flow mass-, momentum- and energy-transfer rate coefficients over a wide range of particle mass loadings, dimensionless particle relaxation times (Stokes numbers), dimensionless thermophoretic diffusivities, and gas Reynolds numbers. As a by-product, we illustrate the accuracy and possible improvement of our previous "diffusion model" for tightly coupled dusty-gas systems. Moreover, we report new results illustrating the dependence of the important "critical" Stokes number (for incipient particle impaction) on the particle mass loading and the wall gas temperature ratio for dust-laden gas motion towards "overheated" solid surfaces. The present formulation and resulting transport coefficients should not only be useful in explaining/predicting recent deposition rate trends in "seeded"-flame experiments, but also highly mass loaded systems of technological interest, such as the deposition of opto-electronic materials by jet impingement, and fouling layers from ash-laden fossil fuel combustion products.

1. INTRODUCTION

Transport phenomena involving the motion of small particles suspended in gaseous media and their deposition on immersed or containment solid surfaces occur often in industry and nature [see for example, Friedlander (1977) and Hidy (1984)]. Indeed, a wide variety of technologies, including the fabrication of optical waveguides and semiconductor devices, process gas cleaning, corrosion/fouling/erosion of combustion turbine and fossil-fuel-fired boiler components, etc., require an ability to predict the transport rates of aerosol particles, often submicrometer in size. Depending on the context, interest may be in accelerating or suppressing particle deposition rates and or achieving a prescribed deposit uniformity and microstructure.

Each of the abovementioned "dusty-gas" examples involves a two-phase flow system with a very small *volume* fraction of particles, but often with a significant *mass* fraction of particles (Rosner and Park, 1988). Despite the chemical engineering importance of highly (mass-)loaded aerosol systems, the literature of this branch of aerosol dynamics can be said to be still in its infancy, so that reliable, versatile engineering prediction/correlation techniques are not yet available. In principle, for many applications the information sought is the collective motion of the particle "phase" relative to the carrier (host) fluid, especially in the immediate vicinity of solid surfaces. In such cases, it is convenient to view the particle "phase" as a continuum having its own local densities of momentum, mass and energy. Eulerian partial differential equations for each phase can then be written which account for all important interactions between the phases through the interfacial exchange of momentum, mass and energy [see, for example, Marble (1970), Boure and Delhaye (1977), Fernandez de la Mora and Rosner (1982) and Rosner (1986)]. In this way, it should be possible to provide a theoretical understanding of the coupled effects of particle inertia, thermophoresis and convection in highly mass loaded systems. The present work describes our first steps in this direction.

As is well known, a dusty-gas flow can be treated as single-phase flow if the suspended particles "track" the host fluid sufficiently closely. The relevant dimensionless criterion is the Stokes number (for interphase linear momentum exchange) defined by

$$Stk_{mom} \equiv t_{mom}/t_{flow} \tag{1-1}$$

where t_{mom} is the so-called "particle stopping time" [see, for example, Friedlander (1977)], and t_{flow} is a characteristic flow (transit or deceleration) time.

†Originally submitted March 1987 to *Chemical Engineering Science*. Based, in part, on H. M. Park's PhD dissertation, Department of Chemical Engineering, Yale University (1987).

‡Graduate Research Assistant, High Temperature Chemical Reaction Engineering Laboratory, Yale University. Present address: Center for Fluid Mechanics, Brown University, Providence, RI 02912, U.S.A.

§Director, High Temperature Chemical Reaction Engineering Laboratory, and Professor, Chemical Engineering Department, Yale University. Author to whom correspondence should be addressed.

Chemical engineers will note that this is a sort of inverse Damköhler number governing *dynamical* non-equilibrium (Rosner, 1986). If the Stokes number (for linear momentum exchange) is larger, one must usually resort to a "multi-fluid" model (i.e. with each phase governed by its own momentum, energy and species mass balance equations). At the other extreme (very small Stokes numbers) one can explicitly neglect the dynamics of particle phase by treating the particle phase motion as "nearly the same" as that of the host fluid (the so-called "diffusion limit"). It can be shown that this is a kind of singular perturbation problem [see, for example, Van Dyke (1969)] with the diffusion limit corresponding to the so-called "outer" solution (Marble, 1970).

In our previous work, motivated in part by the current processes for depositing optical waveguide glass (Rosner and Park, 1988; Park and Rosner, 1989a, b), we considered applications of the "diffusion model" for nonisothermal dusty gas mixtures *with appreciable submicron particle mass loading* but negligible "inertial effects".† In this paper, we consider for the first time more general balance equations governing the motion of a highly loaded "dusty" nonisothermal gas mixture ("two-fluid" model) in the presence of appreciable inertial effects. One of our goals is to investigate the limitations and possible systematic improvements of the previously explored "diffusion model". Another important goal is to illustrate for the first time the coupled effects of high particle mass loading, particle (momentum and thermal) *inertia* and particle *thermophoresis*. This approach also opens the way toward the numerical investigation of non-self-similar two-dimensional geometries encountered in recent experiments (Rosner and Kim, 1984; Kim and Kim, 1986, 1988). Ultimately, based in part on the results of physical and numerical experiments, we hope to develop rational yet tractable correlation schemes which will allow straightforward engineering estimates in convective flow systems characterized by this cluster of thermophysical phenomena [extending the approach exploited in, for example, Gökoğlu and Rosner (1984a, b), Rosner *et al.* (1983), Israel and Rosner (1983), Rosner and Park (1988) and Castillo *et al.* (1989)].

Generally speaking, while multi-fluid models are powerful (versatile) for highly interactive multiphase continuum flows, it is not trivial to solve numerically even two-fluid model equations. In adopting two-fluid models the number of differential equations to be solved, of course, nearly doubles. However, perhaps the most severe difficulty is the "stiffness" of the problem due to the interaction ("source") terms in the momentum, energy and species mass balance equations, especially when the relevant Stokes numbers are small (Rosner and Park, 1988). Because of these difficulties there are not yet many cases where two-fluid model equations for highly loaded dusty-gas systems have been solved "completely" [see, for example, Zung (1969)]. For lightly loaded systems the computational problems become somewhat more tractable—for a recent two-dimensional application of the present approach, see, for example, Kim and Kim (1988). Our purpose here is to initiate the study of more physically complex systems, using a particularly tractable geometry having many features in common with geometries encountered in practice or in the laboratory.

One flow configuration that permits a relatively simple, yet highly instructive analysis is the steady axisymmetric dusty-gas flow between two infinite‡ stationary "disks", one being porous (through which the "dusty gas" is "injected") and the other ("target") nonporous (see Fig. 1). Except for the absence of rotation, this laminar stagnation flow is a generalization of the "flow induced by an infinite rotating disk" (von Karman, 1921), which, for a dusty gas, admits an interesting self-similar solution (Zung, 1969). Moreover, as noted above, this steady flow exhibits most features of the "low" Reynolds number stagnation region† flows generated in recent flat flame-seeded burner laboratory experiments (Rosner and Kim, 1984; Eisner and Rosner, 1985; Kim and Kim, 1988). A variant of this flow (i.e. the stagnation region of opposed jets) has also been fruitfully used to study coal-dust/air combustion phenomena (Graves and Wendt, 1982). Here, we consider highly loaded dusty-gas flow with an arbitrary (but subsonic) injection rate of dusty gas. Adapting Batchelor's analysis of von

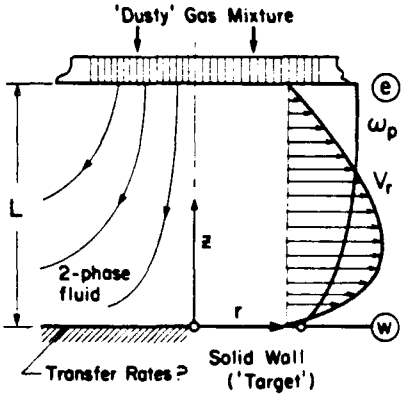

Fig. 1. Steady axisymmetric stagnation flow of a "dusty gas" toward a solid cooled (heated) target; configuration and nomenclature.

†Ironically, Gourdin and Andrejco (1982) explicitly neglected high mass loading effects and suggested that the general form of impingement-type ("vapor-axial") deposits was determined by inertial (Stokes) forces on the suspended particles. However, under their experimental conditions it appears that the dimensionless particle stopping time, Stk_{mom}, was too small [$O(10^{-4})$] to support this contention. Indeed, it will be shown below that such situations fall well within the domain of our diffusion model.

‡We anticipate that the effects of finite dimension will be negligible if the axial gap, L, is comparatively small. Nevertheless, L is assumed to be very large compared to the mean free path in the gas, and the suspended particle diameters.

Karman's flow problem (Batchelor, 1951), we have employed a somewhat simpler similarity transformation than that of Zung (1969).

In what follows, we formulate two-fluid model conservation equations for this prototypical system (Section 2), and then outline the derivation of simplified forms of these balance equations valid in the limit of small Stokes number (Section 3). In Section 4 we predict/present/discuss representative results for the various dimensionless *wall transfer coefficients* of maximum engineering interest for such systems and, in Section 5, we summarize our principal conclusions on the simultaneous deposition rate effects of high particle mass loading, particle *thermophoresis* and particle *inertia*.

2. TWO-FLUID MODEL

Consider the steady, axisymmetric flow of a "dusty" gas, composed of a compressible viscous Newtonian fluid (here a "perfect" gas) and suspended small spherical particles, between two infinite disks (cf. Fig. 1). The lower (target) disk is here considered nonporous, while the upper disk through which the "dusty" gas of prescribed velocity, temperature and dust mass fraction is injected (Fig. 1) is porous.

In accord with our research objectives, we consider a (pseudo-) single-component gas and neglect the thermal effects of the rate of viscous dissipation associated with particle "slip"[†] and the thermal effects of $\mathbf{v}_g \cdot \mathbf{grad}\, p$ work. We also neglect the (nonlocal) thermal effects of radiative *energy* transport between particles of different temperature, presuming instead that the dominant energy transfer mechanism is local conduction from the particles to the surrounding gas (or *vice versa*). The particles are assumed here to be "identical" upon injection and to remain constant in diameter (and mass), implying (among other things) that the effects of coagulation due to Brownian- motion and/or gas shear, thermophoresis[‡] are negligible. Quantitative criteria for the neglect of boundary layer coagulation process in such systems are given in Rosner and Park (1988) and Park and Rosner (1989b). Because they are not so easily satisfied in systems with high particle mass loading and nonnegligible inertia, the present theory should be generalized in the future to include the systematic effects of particle–particle encounters in highly-loaded systems, especially where the mainstream ("injected") particles are not all of the same size. As in our earlier study of small-particle transport phenomena relevant to the deposition of optical waveguide "preforms" (Rosner and Park, 1988) the suspended particles are taken to be large enough so that their Brownian diffusion can be neglected compared to their thermophoretic drift in the prevailing local temperature gradient [see also Goren (1977)]. However, in our present extensions into the domain of nonnegligible particle *inertia* we also neglect the drift produced by gas vorticity-induced "lift" forces [see, for example, Saffman (1965)] compared to the prevailing thermophoretic drift velocities across streamlines.[§] In our numerical illustrations the "slip" velocities will be assumed to be small enough to allow the use of linear laws for interphase momentum and energy transfer—i.e. the characteristic times t_{mom} and t_h introduced below will be taken to be insensitive to the local "slip" velocity $|\mathbf{v}_p - \mathbf{v}_g|$.

For an axisymmetric flow in cylindrical coordinates (r, z) the Eulerian continuum balance equations for this steady dusty-gas flow system are:

Gas (carrier fluid) phase:

Mass conservation:

$$\frac{1}{r}\frac{\partial}{\partial r}(r\rho_g u_g)+\frac{\partial}{\partial z}(\rho_g v_g)=0 \tag{2-1}$$

r-Momentum balance:

$$\rho_g\left(u_g\frac{\partial u_g}{\partial r}+v_g\frac{\partial u_g}{\partial z}\right)=-\frac{\partial p}{\partial r}+\frac{\partial}{\partial r}\left[\frac{4}{3}\mu_g\frac{\partial u_g}{\partial r}-\frac{2}{3}\mu_g\frac{u_g}{r}-\frac{2}{3}\mu_g\frac{\partial v_g}{\partial z}\right]+\frac{\partial}{\partial z}\left[\mu_g\left(\frac{\partial u_g}{\partial z}+\frac{\partial v_g}{\partial r}\right)\right]+\frac{2\mu_g}{r}\left(\frac{\partial u_g}{\partial r}-\frac{u_g}{r}\right)+\rho_p\frac{u_p-u_g}{t_{mom}}-\rho_p\frac{\alpha_T D_p}{t_{mom}}\frac{\partial \ln T_g}{\partial r} \tag{2-2}$$

z-Momentum balance:

$$\rho_g\left(u_g\frac{\partial v_g}{\partial r}+v_g\frac{\partial v_g}{\partial z}\right)=-\rho_g g-\frac{\partial p}{\partial z}+\frac{\partial}{\partial z}\left[\frac{4}{3}\mu_g\frac{\partial v_g}{\partial z}-\frac{2}{3}\mu_g\frac{\partial u_g}{\partial r}-\frac{2}{3}\mu_g\frac{u_g}{r}\right]+\frac{1}{r}\frac{\partial}{\partial r}\left[\mu_g r\left(\frac{\partial u_g}{\partial z}+\frac{\partial v_g}{\partial r}\right)\right]+\rho_p\frac{v_p-v_g}{t_{mom}}-\rho_p\frac{\alpha_T D_p}{t_{mom}}\frac{\partial \ln T_g}{\partial z} \tag{2-3}$$

[†] An order of magnitude estimate reveals that this assumption will be self-consistent provided the combination $(\rho_g/\bar{\rho}_p)\,\omega_{p,e}\,Stk^2\,Re^{\frac{1}{2}}(\Delta T/T_e)^{-1}$ is small compared to unity. For the cases discussed below this number is at most of order 10^{-2}.

[‡] Normally thermophoresis alone in a system with "initially" uniform size (hence $\alpha_T D_p$) will not bring about encounters [see, for example, Rosner and Park (1988)]. However, due to the thermal boundary layers around large particles for which $T_p \neq T_g$, the Brownian coagulation rate is modified [see Mackowski and Rosner (1989)]

[§] This can be shown to be valid if a dimensionless group of the form

$$(d_p/L)\,Stk_{mom}\,Re^{\frac{1}{2}}(\Delta T/T_\infty)^{-1}$$

is sufficiently small. For the cases treated here thermophoretic drift is expected to dominate shear-induced particle drift by more than two orders of magnitude. One can also show that since the particle rotational relaxation time is of the same order of magnitude as the abovementioned (translational) relaxation time, then particle rotational inertia will not influence our $(d_p \ll L)$ particle transport rate predictions.

Energy balance:†

$$\rho_g c_{p,g}\left(u_g\frac{\partial T_g}{\partial r}+v_g\frac{\partial T_g}{\partial z}\right)=\frac{1}{r}\frac{\partial}{\partial r}\left(rk_g\frac{\partial T_g}{\partial r}\right)+\frac{\partial}{\partial z}\left(k_g\frac{\partial T_g}{\partial z}\right)+\rho_p c_{p,p}\frac{T_p-T_g}{t_h} \quad (2\text{-}4)$$

Particle (aerosol) phase:

Mass balance:

$$\frac{1}{r}\frac{\partial}{\partial r}(r\rho_p u_p)+\frac{\partial}{\partial z}(\rho_p v_p)=0 \quad (2\text{-}5)$$

r-Momentum balance:

$$\rho_p\left(u_p\frac{\partial u_p}{\partial r}+v_p\frac{\partial u_p}{\partial z}\right)=-\rho_p\frac{u_p-u_g}{t_{mom}}+\rho_p\frac{\alpha_T D_p}{t_{mom}}\frac{\partial \ln T_g}{\partial r} \quad (2\text{-}6)$$

z-Momentum balance:

$$\rho_p\left(u_p\frac{\partial v_p}{\partial r}+v_p\frac{\partial v_p}{\partial z}\right)=-\rho_p\frac{v_p-v_g}{t_{mom}}+\rho_p\frac{\alpha_T D_p}{t_{mom}}\frac{\partial \ln T_g}{\partial z} \quad (2\text{-}7)$$

Energy balance:

$$\rho_p c_{p,p}\left(u_p\frac{\partial T_p}{\partial r}+v_p\frac{\partial T_p}{\partial z}\right)=-\rho_p c_{p,p}\frac{T_p-T_g}{t_h} \quad (2\text{-}8)$$

where all field densities, thermophysical properties and coordinates are defined in the Notation.

Following von Karman (1921), we now seek solutions such that $v, f[\equiv u(r,z)/r]$ and T for each phase are functions of z only, and, using the $(Ma)^2 \ll 1$ analysis [cf. Batchelor (1951)], we can simplify this PDE set to the following coupled ODE set:

Gas mass balance:

$$\frac{d}{dz}(\rho_g v_g)+2\rho_g f_g=0 \quad (2\text{-}9)$$

Gas r-momentum balance (differentiated in z-direction):

$$\frac{d^2}{dz^2}\left(\mu_g\frac{df_g}{dz}\right)-\frac{d}{dz}\left[\rho_g\left(f_g^2+v_g\frac{df_g}{dz}\right)\right]+\frac{d}{dz}\left[\frac{\rho_p(f_p-f_g)}{t_{mom}}\right]=0 \quad (2\text{-}10)$$

Gas energy balance:

$$\frac{d}{dz}\left(k_g\frac{dT_g}{dz}\right)-\rho_g c_{p,g}v_g\frac{dT_g}{dz}+\rho_g c_{p,p}\frac{T_p-T_g}{t_h}=0 \quad (2\text{-}11)$$

Particle mass balance:

$$\frac{d}{dz}(\rho_p v_p)+2\rho_p f_p=0 \quad (2\text{-}12)$$

Particle r-momentum balance:

$$v_p\frac{df_p}{dz}+f_p^2+\frac{f_p-f_g}{t_{mom}}=0 \quad (2\text{-}13)$$

Particle z-momentum balance:

$$v_p\frac{dv_p}{dz}+\frac{v_p-v_g}{t_{mom}}-\frac{\alpha_T D_p}{t_{mom}}\frac{d\ln T}{dz}=0 \quad (2\text{-}14)$$

Particle energy balance:

$$\rho_p c_{p,p}v_p\frac{dT_p}{dz}+\rho_p c_{p,p}\frac{T_p-T_g}{t_h}=0 \quad (2\text{-}15)$$

Gas equation of state:

$$\rho_g=\frac{pM_g}{RT} \quad (2\text{-}16)$$

where

$$f_g(z)\equiv u_g/r \quad \text{and} \quad f_p(z)\equiv u_p/r. \quad (2\text{-}17)$$

For our present purposes the boundary conditions of greatest interest can be summarized as follows:

at Ⓦ ($z=0$): $v_g=0, f_g=0, T_g=T_w$

at Ⓒ ($z=L$): $v_g=v_{g,e}, v_p=v_{p,e}, f_g=0, f_p=0$

$T_g=T_p=T_e, \omega_p=\omega_{p,e}$ (specified).

Physically, these correspond, respectively, to the conditions [at $z=0$ (cf. Fig. 1)] of no gas suction (or blowing) and no tangential *gas* "slip", and (at $z=L$) specified gas/particle injection velocities, no tangential "slip" for gas and particles, and specified (equal) gas and particle temperatures.

Our interest is to some extent on the coexisting local "fields" of gas and particle velocity, temperature and concentration, but mainly on the corresponding *wall* ($z=0$) *fluxes* of momentum, energy and particle mass (i.e. deposition rates). These fluxes can be computed from the properties of the fields at, and in the immediate vicinity of, station Ⓦ ($z=0$) and will be reported in the form of certain *dimensionless transfer coefficients* (Rosner, 1986) defined in Section 4.

There are many numerical algorithms for solving this kind of nonlinear two-point boundary value problem. We adopted Keller's "box scheme" (Keller, 1974), a finite-difference method which has an accuracy of $O(h^2)$. The number of mesh point used was 800, which, for the two-fluid model, imposes a limit on the lowest value of the Stokes number that can accurately be solved numerically (*ca* 10^{-2}).

3. DIFFUSION MODEL AND HIGHER-ORDER DIFFUSION MODEL

As mentioned previously, if the Stokes numbers (dimensionless momentum and thermal relaxation times) are very small, the set of eqs (2-9)–(2-17) becomes "stiff" and difficult to solve numerically. Not surprisingly, we can use perturbation techniques to

†In view of our neglect of the $(v_g\partial p/\partial z)+\ldots$ terms and our subsequent suppression of $p(z)$ from the momentum eq. (2-10), one additional constraint that must be satisfied is $(Ma)^2 \ll 1$, but, for the parameter range of primary interest to us, this "subsonic" flow condition is realistic.

circumvent this difficulty.[†] However, to apply perturbation analysis it is more convenient (and conventional) to use mixture conservation equations rather than the individual fluid phase balance equations. For this purpose we define the following mixture field densities:

Mixture mass:

$$\rho \equiv \rho_p + \rho_g \tag{3-1}$$

Mixture momentum:

$$\rho v \equiv \rho_p v_p + \rho_g v_g \tag{3-2}$$

$$\rho f \equiv \rho_p f_p + \rho_g f_g \tag{3-3}$$

Mixture sensible energy:

$$\rho c_p T \equiv \rho_p c_{p,p} T_p + \rho_g c_{p,g} T_g \tag{3-4}$$

where $\rho c_p = \rho_p c_{p,p} + \rho_g c_{p,g}$.

With these definitions of "mixture variables" and the corresponding balance equations for the particle phase and fluid phase we can derive the following governing equations for the present flow configuration:

Mixture mass balance:

$$\frac{d}{dz}(\rho v) + 2\rho f = 0 \tag{3-5}$$

Mixture momentum balance:

$$\frac{d^2}{dz^2}\left(\mu_g \frac{df_g}{dz}\right) \quad \frac{d}{dz}(\rho f^2) \quad \frac{d}{dz}\left(\mu \frac{df}{dz}\right)$$

$$-\frac{d^2}{dz^2}[\rho_p(f_p - f)(v_p - v)]$$

$$-\frac{d^2}{dz^2}[\rho_f(f_g - f)(v_g - v)] - \frac{d}{dz}[\rho_p(f_p - f)(f_p - f)]$$

$$-\frac{d}{dz}[\rho_g(f_g - f)(f_g - f)] = 0 \tag{3-6}$$

Mixture energy equation:

$$\frac{d}{dz}\left(k_g \frac{dT}{dz}\right) - \rho c_p v \frac{dT}{dz} - \rho(v_p - v)(c_{p,p} - c_{p,g})\frac{dT}{dz}$$

$$+ \rho c_p v \frac{dT}{dz} + \rho_p(v_p - v)(c_{p,p} - c_{p,g})\frac{dT}{dz}$$

$$- \rho_g c_{p,g} v_g \frac{dT_g}{dz} - \rho_p c_{p,p} v_p \frac{dT_p}{dz} = 0. \tag{3-7}$$

The remaining equations necessary to "close" the system are the particle phase conservation eqs (2-12)–(2-15). Next, the dependent variables are separated into two groups, i.e. "fast" variables and "slow" variables. (For a linear uncoupled system, the *time constant* of "fast" variables is very small compared with that of "slow" variables.) For the present system, we tentatively identify f_p, v_p and T_p as "fast" variables with the remaining field variables being classified as "slow". We then simply assume the following regular perturbation scheme to suppress the dynamics of "fast" variables

$$\begin{bmatrix} v_p \\ f_p \\ T_p \end{bmatrix} = \sum_{k=0}^{\infty} \varepsilon^k \begin{bmatrix} v_{p,k} \\ f_{p,k} \\ T_{p,k} \end{bmatrix} \tag{3-8}$$

where $\varepsilon \equiv t_{mom}/t_{flow}$. Upon substituting eq. (3-8) into eqs (2-13)–(2-15) and collecting terms of the same order in ε, the following set of algebraic "constitutive" equations is obtained for the "fast" variables (retaining up to first-order terms in ε):

$$f_p = f_g - t_{mom}\left[f_g^2 + \left(v_g - \alpha_T D_p \frac{d\ln T_g}{dz}\right)\frac{df_g}{dz}\right] \tag{3-9}$$

$$v_p = \left(v_g - \alpha_T D_p \frac{d\ln T_g}{dz}\right) - t_{mom}\left(v_g - \alpha_T D_p \frac{d\ln T_g}{dz}\right)\frac{d}{dz}$$

$$\times\left(v_g - \alpha_T D_p \frac{d\ln T_g}{dz}\right) \tag{3-10}$$

$$T_p = T_g - t_{mom}\frac{1}{R}\left(v_g - \alpha_T D_p \frac{d\ln T_g}{dz}\right)\frac{dT_g}{dz} \tag{3-11}$$

where the particle characteristic time *ratio*, $R\ (\equiv t_{mom}/t_h)$ is usually of order unity [see Appendix 1 in Rosner and Park (1988)].

If, alternatively, only the zeroth expansion of the "fast" variables is retained the resulting ODEs are as follows.[‡] Hereafter, we call this simplified set of ODEs the diffusion model (limit) for the present system.

Diffusion model

Mixture mass balance:

$$\frac{d}{dz}(\rho v) + 2\rho f = 0 \tag{3-12}$$

Mixture momentum balance:

$$\frac{d^2}{dz^2}\left(\mu_g \frac{df}{dz}\right) - \frac{d}{dz}\left[\rho\left(f^2 + v\frac{df}{dz}\right)\right] = 0 \tag{3-13}$$

Mixture energy balance:

$$\frac{d}{dz}\left(k_g \frac{dT}{dz}\right) - \rho c_p v \frac{dT}{dz} + \rho \alpha_T D_p \omega_p (1 - \omega_p)\frac{d\ln T}{dz}$$

$$\times (c_{p,p} - c_{p,g})\frac{dT}{dz} \tag{3-14}$$

[†]Note, for example, that the well-known Enskog–Chapman solution of the Boltzmann equation, compatible with the Navier–Stokes equations of continuum fluid mechanics (employed here), is itself the (outer) solution of a singular perturbation problem, where the small parameter can be identified as the Knudsen number.

[‡]Interestingly enough, the same set of equations can be derived by assuming that the suspended particles simply act as "gigantic" molecules in a disparate molecular weight "gas" mixture (Rosner and Park, 1988) implying, among other things, that particle transport by Brownian motion can be neglected compared with thermophoresis {i.e. $\alpha_T D_p \gg D_p$ and $v/D_p \gg 1$ [see, for example, Goren (1977)]}.

Particle mass balance:

$$\rho v\frac{d\omega_p}{dz}-\frac{d}{dz}\left[\rho\alpha_T D_p\omega_p(1-\omega_p)\frac{d\ln T}{dz}\right]=0 \quad (3\text{-}15)$$

where $\omega_p\equiv\rho_p/\rho$ (particle mass fraction).

The diffusion model can describe the system very well at extremely small Stokes numbers [cf., for example, Rosner and Park (1988)]. However, for the range of small Stokes numbers in which it is difficult to solve two-fluid model equations and yet there are nonnegligible particle inertia effects, we retain up to first-order terms in eqs (3-9), (3-10) and (3-11). The resulting set of equations will be called a "higher-order diffusion model". For brevity we omit the detailed equations governing this model, but it may be worthwhile to state that whenever derivative terms arise which are higher order than the original equation, they are reduced to lower-order derivative terms using the diffusion model. One important defect of this "higher-order diffusion model" is that it cannot accommodate arbitrary initial conditions, or "memory" effects, which become significant as the Stokes numbers increase. These considerations establish an upper limit on the Stokes number for the applicability of this higher-order diffusion model (or, more generally, the "outer" solution of this singular perturbation problem).

4. RESULTS AND DISCUSSION

To summarize the results of principal engineering interest we define the following *dimensionless wall transfer coefficients* [see, for example, Rosner (1986) and Rosner and Park (1988)], considering first the "diffusional" mechanisms:

Radial momentum:

$$C_{f,\mathrm{diff}}\equiv\frac{\left(\mu_g\frac{du_g}{dz}\right)_w}{\frac{1}{2}\rho_{g,e}v_{g,e}^2} \quad (4\text{-}1)$$

Energy:

$$St_{h,\mathrm{diff}}\equiv\frac{\left(k_g\frac{dT_g}{dz}\right)_w}{\rho_{g,e}(-v_{g,e})(h_{g,e}-h_{g,w})} \quad (4\text{-}2)$$

Mass:

$$St_{m,\mathrm{diff}}\equiv\frac{\left(\rho\alpha_T D_p\omega_p\frac{d\ln T_g}{dz}\right)_w}{\rho_{g,e}(-v_{g,e})\omega_{p,e}} \quad (4\text{-}3)$$

where

$-v_{g,e}\equiv$ injection velocity of gas,
$h_{g,e}\equiv$ specific enthalpy of injected gas (at the porous disk),
$h_{g,w}\equiv$ specific enthalpy of gas at the "target" disk,
$\omega_{p,e}\equiv$ mass fraction of the particle phase in the injected stream.

Additionally, we define the following "inertial" transfer coefficients (associated with the particle *impaction* contribution if no particles "reflect"):

$$C_{f,\mathrm{inertia}}\equiv\frac{\rho_{p,w}u_{p,w}(-v_{p,w})}{\frac{1}{2}\rho_{g,e}v_{g,e}^2} \quad (4\text{-}4a)$$

$$St_{h,\mathrm{inertia}}\equiv\frac{\rho_{p,w}(-v_{p,w})c_{p,p}(T_{p,w}-T_w)}{\rho_{g,e}(-v_{g,e})(h_{g,e}-h_{g,w})} \quad (4\text{-}4b)$$

$$St_{m,\mathrm{inertia}}\equiv\frac{\rho_{p,w}(-v_{p,w})-\left(\rho\alpha_T D_p\omega_p\frac{d\ln T_g}{dz}\right)_w}{\rho_{g,e}(-v_{g,e})\omega_{p,e}} \quad (4\text{-}4c)$$

where

$u_{p,w}\equiv$ tangential velocity of particles arriving at the target wall,
$v_{p,w}\equiv$ normal velocity of particles at the target wall.

Note that in defining $C_{f,\mathrm{inertia}}$ we are explicitly accounting for the nonzero particle slip velocity at the wall ($u_{p,w}\neq 0$). Moreover, in defining $St_{h,\mathrm{inertia}}$ we are not counting separately a contribution associated with the (usually small) translational kinetic energy of the arriving particles—i.e. $\rho_{p,w}(-v_{p,w})(v_{p,w}^2/2)$. Finally, note that $St_{m,\mathrm{inertia}}$ pertains to the inertial contribution to the net deposition rate only if every impacting particle is "captured" [cf., for example, Rosner and Nagarajan (1987)]. Clearly, if one is only interested in the *total* particle deposition rate (i.e. deposition as a result of both thermophoretic drift *and* inertial impaction) then it is the *sum* $St_{m,\mathrm{diff}}+St_{m,\mathrm{inertia}}$ which is needed. Thus, actual (dimensional) particle mass fluxes can be calculated from the abovementioned sum, $St_{m,\mathrm{diff}}+St_{m,\mathrm{inertia}}$, by simple multiplication with the *reference* mass flux, $\rho_{g,e}(-v_{g,e})\omega_{p,e}$, in the application of interest. Based on the abovementioned definitions similar statements can be made for the total tangential momentum flux and the total heat flux to the wall. However, in the figures below we have deliberately "decomposed" these totals because each contribution varies with system parameters (e.g. Stk_{mom}) in its own (instructive) way.

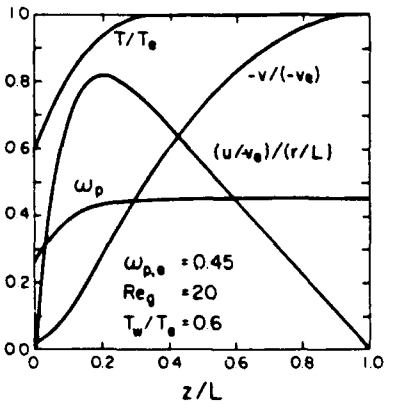

Fig. 2. Typical computed dimensionless velocity and temperature profiles from the "diffusion model" ($Re_g=20$, $\omega_{p,e}=0.45$, $T_e=0.6$).

In our illustrative numerical integrations, we assumed constant thermophysical property *ratios* (i.e. $Pr_g = 0.7$, $c_{p,p}/c_{p,g} = 0.65$) and used the interpolation formula of Talbot (1981) for estimating local particle thermophoretic factors.† Since our primary concern is with parametric trends, computations were carried out by simply covering interesting ranges of the (assumed independent‡) governing dimensionless parameters $\omega_{p,e}$, T_w/T_e, $(\alpha_T D_p/\nu_g)$, Re_g and Stk_{mom}.

Typical predicted profiles for velocities, temperatures and particle concentration are shown in Fig. 2 for the "diffusion" model ($Stk_{mom} \ll 1$) at a Reynolds number of 20. As noted above, in the diffusion model, one cannot take account of arbitrary initial conditions for the particles, so it is implicitly assumed that $v_{p,e} = v_{g,e} - (\alpha_T D_p \, d \ln T/dz)_e$. To make the results of both models consistent with each other we choose the same boundary condition for v_p (particle injection velocity) in the full two-fluid model, with illustrative results included below.

Figure 3 gives a comparison between the "diffusional" particle mass-transfer results of the diffusion model, the higher-order diffusion model and the full two-fluid model. Note that for a range of small Stokes numbers with nonnegligible inertial effects (up to a doubling of St_m) the higher-order diffusion model yields nearly the same results as those of the two-fluid model (which is "exact"). Note that in such (cold-wall) cases there is no threshold ("critical") Stokes number below which inertial effects vanish.

Figure 4 shows the effect of the momentum Stokes number on all dimensionless wall transfer coefficients for the particular case of $\omega_{p,e} = 0.3$, $Re_g = 1$. For zero Stokes number the results are from the "diffusion model" [cf. Rosner and Park (1988)] and for $0 < Stk < 5 \times 10^{-2}$ the results are obtained using the "higher-order diffusion model". The remaining range

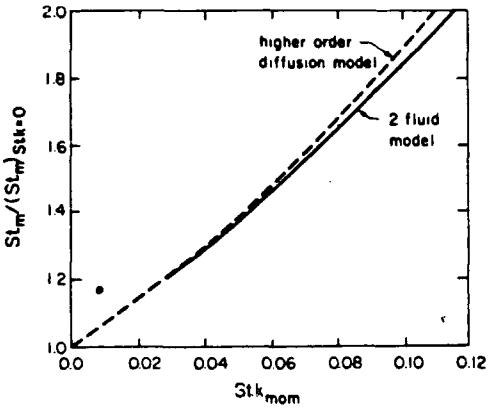

Fig. 3. Comparison of the "higher-order diffusion model" with the "two-fluid model" for the "diffusional" (thermophoretic) *mass*-transfer Stanton number ($Re_g = 5$, $\omega_{p,e} = 0.3$, $T_w/T_e = 0.6$).

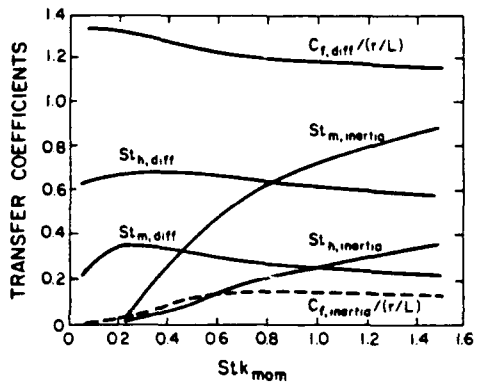

Fig. 4. Variation of all predicted dimensionless momentum-, heat-, and mass-transfer coefficents with Stokes number ($Re_g = 5$, $\omega_{p,e} = 0.3$, $T_w/T_e = 0.6$).

†Incidentally, despite the fact that we are considering flow with the nonzero vorticity (ζ_g) and spherical particles large enough to experience translational (and, hence, rotational) *inertial* effects, it is easy to show that the conductivity ratios k_p/k_g are too small for particle rotation to appreciably alter the predicted thermophoretic forces and corresponding drift velocities under the conditions explored here.

‡Of course, in practice, (e.g. a particular set of experiments) these parameters may not be "independent". Thus, if an investigator changes Stk_{mom} by changing the injection velocity ($-v_{g,e}$), this will normally be associated with a corresponding change in the system Reynolds number. Alternately, if Stk is changed by changing the diameter of the particles suspended in a gas this will generally (unless $d_p \ll l$) produce a change in the dimensionless particle thermophoretic diffusivity ($\alpha_T D_p \nu_g$). Even if Stk_{mom} is changed by "merely" changing the intrinsic density of particles of fixed size, there could be nonnegligible associated changes in Stk_h and $\alpha_T D_p/\nu_g$. These possible *interdependencies* must be kept in mind in the interpretation of any particular set of experiments, or in making engineering predictions. However, in no way does this mitigate the value of using the dimensionless groups Stk, Re and $\alpha_T D_p \nu_g$ to economically summarize results of the present (or future) work (see, for example, Rosner and Fernandez de la Mora (1984) and Chap. 7 of Rosner (1986)].

of "large" Stokes numbers is covered by the "two-fluid model". Here, the "inertial" transfer coefficients $C_{f,\text{inertia}}$, $St_{h,\text{inertia}}$, and $St_{m,\text{inertia}}$ increase monotonically as the Stokes number increases. However, $C_{f,\text{diff}}$, $St_{h,\text{diff}}$ and $St_{m,\text{diff}}$ (the corresponding "diffusional" transfer coefficients) first increase and attain maxima before decreasing to their ultimate values (NB: as $Stk \to \infty$, the phases become completely uncoupled). Initial increases in the values of these transfer coefficients are associated with the "accumulation" of particles near the wall (i.e. ω_p increases near the "target" disk) as the Stokes number increase from 0 to 0.1 or 0.2 [see, also the discussion of particle phase "compressibility" in Fernandez de la Mora and Rosner (1981, 1982)]. Note that the momentum and thermal interaction terms in the fluid r-momentum and fluid energy equations are, respectively:

$$\frac{\frac{d}{dz}[\rho_p(f_p - f_g)]}{t_{mom}} \quad \text{and} \quad \frac{\rho_p c_{p,p}(T_p - T_g)}{t_h}$$

The trend is such that $\rho_{p,w}$ increases as Stk increases from zero to *ca* 0.2 (after this value $\rho_{p,w}$ decreases) but $(f_p - f_g)$ and $(T_p - T_g)$ continue to increase as Stk increases. Thus, for small values of Stokes number, these interaction terms increase and this causes derivatives $(\hat{c}u/\hat{c}z)_w$ and $(\hat{c}T/\hat{c}z)_w$ at the wall to increase. However, for sufficiently large values of Stk (e.g. large values of t_{mom} and t_h) these interaction terms ultimately *decrease*, causing reductions from the peak "diffusional" transfer coefficients achieved at intermediate Stk values (see Figs 4–7). Returning to the *inertial* (contribution to) C_f, St_h and St_m, one can show from their definitions and the boundary conditions at e that, as $Stk \to \infty$, they should ultimately approach 0, $(c_{p,p}/c_{p,g})\omega_{p,e}(1-\omega_{p,e})^{-1}$ and $(1-\omega_{p,e})^{-1}$, respectively. These limits follow from the fact that the particle "state" (momentum, energy) upon impact will be uninfluenced by the host gas within $0 \leqslant z \leqslant L$ in this $(Stk \to \infty)$ limit.

Figures 5–10 are the corresponding three-dimensional plots ("surfaces") of the various dimensionless transfer coefficients to illustrate the combined effects of Stokes number and particle mass loading. The particle mass loading effects shown in the limit of $Stk_{mom} \to 0$ (diffusion limit) are qualitatively consistent with the "suction" effects displayed and correlated for high-Re LBL flow in Rosner and Park (1988). It is

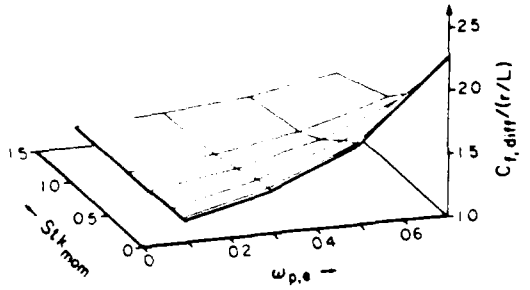

Fig. 5. Variation of the predicted dimensionless "diffusive" *tangential momentum* transfer coefficient with particle mass loading and Stokes number ($Re_g = 5$, $T_w/T_e = 0.6$, $\alpha_T D_p/\nu_g = 0.5$).

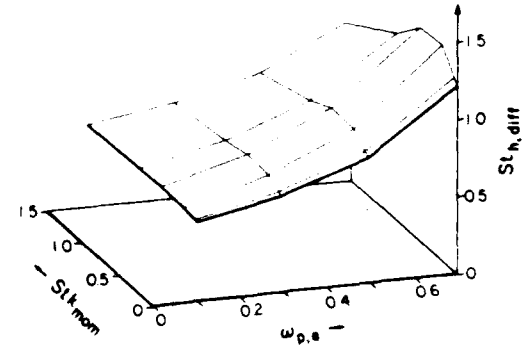

Fig. 6. Variation of the predicted dimensionless "diffusive" *heat*-transfer coefficient, $St_{h,diff}$, with particle mass loading and Stokes number ($Re_g = 5$, $T_w/T_e = 0.6$).

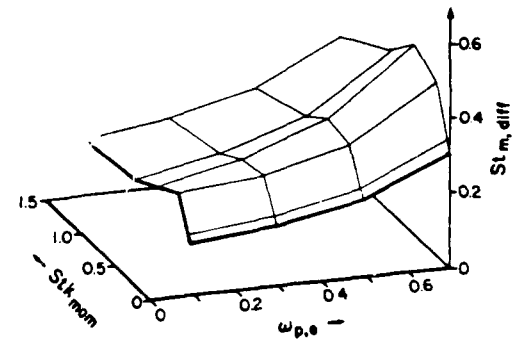

Fig. 7. Variation of the predicted dimensionless "diffusive" *mass*-transfer coefficient, $St_{m,diff}$, with particle mass loading and Stokes number ($Re_g = 5$, $T_w/T_e = 0.6$).

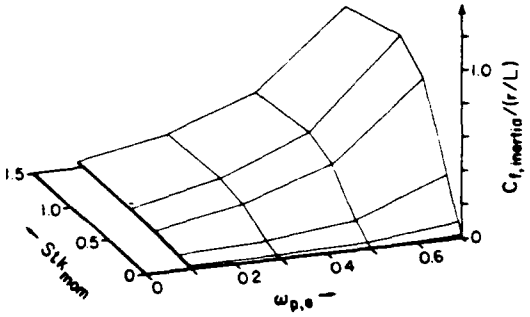

Fig. 8. Variation of the predicted dimensionless inertial *tangential momentum* transfer coefficient with particle mass loading and Stokes number ($Re_g = 5$, $T_w/T_e = 0.6$).

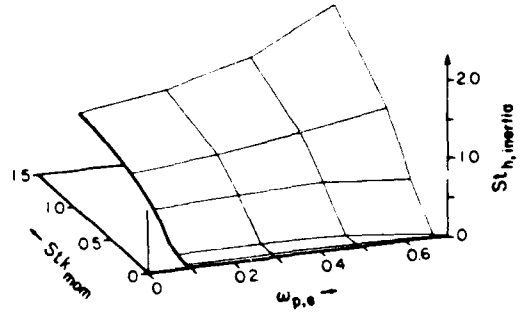

Fig. 9. Variation of the predicted dimensionless inertial *heat*-transfer coefficient with particle mass loading and Stokes number ($Re_g = 5$, $T_w/T_e = 0.6$).

significant that the inertial effect on the thermophoretic mass transfer coefficient $St_{m,diff}$ set in at lower particle mass loadings than for the corresponding heat-transfer coefficient $St_{h,diff}$—a phenomenon that can be attributed to the above-mentioned "accumulation" (on inertially produced enrichment) of particles near the wall. While the effects of particle inertia on the diffusional heat and momentum transfer coefficient are somewhat smaller, an interesting corollary of the observed behavior of the "diffusive" (gas-transmitted) *heat* transfer coefficient $St_{h,diff}(\omega_{p,e}, Stk)$ and also $C_{f,diff}(\omega_{p,e}, Stk)$ is

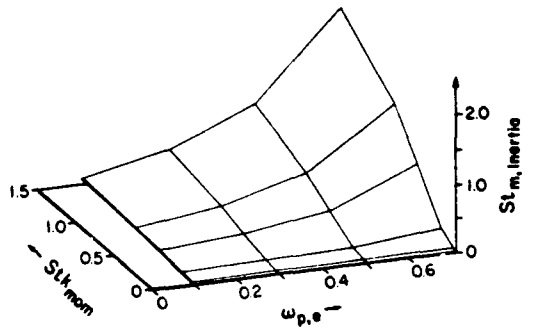

Fig. 10. Variation of the predicted dimensionless inertial *mass*-transfer coefficient with particle mass loading and Stokes number ($Re_d = 5$, $T_w/T_e = 0.6$).

that in highly particle loaded gaseous systems we would expect Stk to have a similar influence on the convective diffusion (mass) transport of a "nonparticipating" dilute *vapor* also present in the mainstream. This is one of several possible influences that the presence/deposition of suspended particles can have on the simultaneous deposition of, say, an important condensible vapor [see also Castillo and Rosner (1988), Rosner and Liang (1988) and Park and Rosner (1989c)]. In future studies it will also be interesting to explore the preliminary observation that some "high particle mass loading" transport effects become important when the *product* $\omega_{p,e}Re^{1/2}$ is nonnegligible. Thus, in high-Re systems of primary engineering importance it is not necessary that the particle mass fraction, $\omega_{p,e}$, *itself* be appreciable to encounter "high particle mass loading" effects.

Recalling that the prediction of the *total* wall fluxes of (tangential) momentum, energy and particle mass will require (respectively) the *sums* $C_{f,\text{diff}} + C_{f,\text{inertia}}$, $St_{h,\text{diff}} + St_{h,\text{inertia}}$ and $St_{m,\text{diff}} + St_{m,\text{inertia}}$ we note from Figs 5–10 that, at nonnegligible mass loadings, the diffusional and inertial contributions are often of comparable magnitude, especially for momentum Stokes' numbers of order unity.

While it is beyond our purpose here to discuss factors governing impacting particle "sticking" coefficients [see, for example, Rosner and Nagarajan (1987)] it is interesting to note that nonzero $St_{h,\text{inertia}}$ values [cf. Figs 4 and 9, and eq. (4-4b)] imply that the particles striking the surface are systematically hotter than the surface itself (and the adjacent gas mixture). Clearly, this would be particularly important if the surface were maintained *below* the freezing point and the mainstream was *above* the freezing point of the suspended particulate matter, in which case *latent heat* transport effects would also have to be included.

Finally, we briefly consider the interesting case of a "hot target" in the presence of particle *inertia* effects. If the target is maintained at a temperature higher than that of the inlet mixture stream, the thermophoretic force acts to *repel* particles from the wall [(see, for example, Gökoğlu and Rosner (1986), Friedlander *et al.* (1988), Park and Rosner (1989c) and Stratman *et al.* (1988)] and the only mechanism contributing to particle deposition is the inertial "drift" (Fernandez de la Mora and Rosner, 1981, 1982).† In such cases a "*critical*" *Stokes number* can be defined such that, if the Stokes number is smaller than Stk_{crit}, particles cannot reach the target disk. Figures 11 and 12 show the dependence of this critical Stokes number on the particle mass loading, $\omega_{p,e}$, and the wall temperature ratio, T_w/T_e. It is quite interesting that high particle mass loading noticeably increases Stk_{crit} (cf. Fig. 12)—"delaying" the onset of particle impaction.

5. CONCLUSIONS

To shed light on challenging dusty-gas deposition problems now of industrial interest we have investigated theoretically the transport and deposition of small particles in flowing nonisothermal gaseous media, simultaneously including for the first time the interacting effects of high particle mass loading, particle "inertia" (momentum and thermal), and particle thermophoresis. By exploiting the fact that the full Navier–Stokes equations for the gas phase and Eulerian conservation equations for the particle phase can be reduced to a coupled set of ODEs for steady axisymmetric stagnation flow (between two infinite parallel disks), we have formulated and solved both the "two-fluid" model and a "higher-order diffusion" model for this instructive class of "dusty" gas systems and obtained the important dimensionless coefficients describing the diffusive and inertial heat-, mass- and momentum-transfer rates to the solid wall over a wide range of particle Stokes numbers and mass loadings. While only selected (illustrative) results are included here, and much remains to be done to develop generally useful, rational correlation techniques based, in part, on these new results, certain important trends are already apparent. For example, as expected, the "inertial" heat- and mass-transfer coefficients [eqs (4-4)] increase monotonically with increasing Stokes number. However, for each value of the feed stream particle mass loading there is a local maximum in each of "diffusive" transfer coefficients [eqs (4-1)–(4-3)] at some intermediate momentum Stokes numbers, corresponding to the maximum coupling effects of the interphase momentum and energy exchange terms. Our results for this interesting and experimentally realizable axisymmetric stagnation flow field, which permit very simple analysis and computation, suggest rational and flow field independent procedures for generalizing our previous treatments (diffusion model) for small particle transport in nonisothermal laminar boundary layer flows (Rosner and Park, 1988; Park and Rosner, 1989a, b) to embrace cases in which the

†In the presence of appreciable radiation energy fluxes photophoretic ("radiometric") effects can also become important for intermediate size absorbing particles. As shown in Castillo *et al.* (1989), this effect, like inertia, can drive particles onto an "overheated" surface.

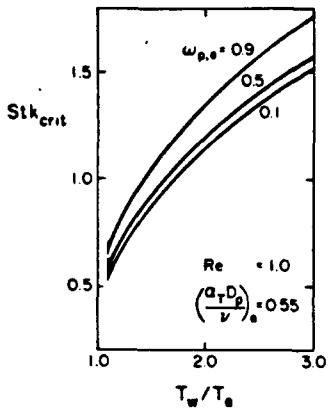

Fig. 11. Variation of the critical Stokes number for particle impaction with "overheat" temperature ratio, T_w/T_e, at several feed stream particle mass loadings, $\omega_{p,e}$ [$Re_e = 1$, $(\alpha_T D_p / \nu_g)_e = 0.55$].

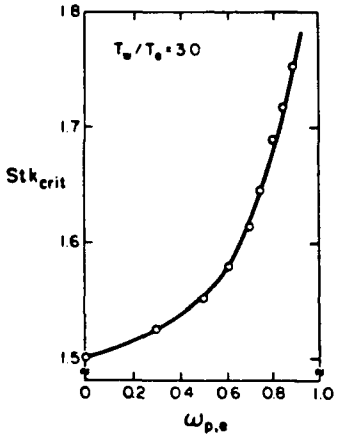

Fig. 12. Predicted increase of critical Stokes number for particle impaction with particle mass loading [at fixed "overheat" temperature ratio, $T_w/T_e = 3$ ($Re_e = 1$)].

Stokes numbers become nonnegligible (e.g. due to larger particle sizes).

In this connection, it should be remarked that, recently, Kim and Kim (1986, 1988) have repeated and extended (to larger particle sizes) the low mass loading thermophoretic deposition experiments of Rosner and Kim (1984) using atmospheric pressure seeded premixed gas flames. For the case of very low Stokes numbers (negligible inertial effects), the deposition rate trends they report are evidently compatible with the results of our earlier experiments and theoretical ("diffusion") model. However, at the higher Stokes numbers (when particle inertia plays an important role over the broad range of particle sizes simultaneously introduced into the flame), quantitative tests of the present theory are, as yet, incomplete. Certainly, additional controlled experiments in which these transport mechanisms (inertia, thermophoresis, convection) participate would be timely, even for lightly loaded [illegible], along with extended computations patterned after those introduced here but including other commonly encountered geometries.

The fact that most systems of technological interest inevitably involve a *distribution* of particle sizes [see, for example, Rosner (1989)] and, hence, a distribution of particle relaxation times, suggests the importance of being able to extend the present treatment in this direction. From the multiphase continuum viewpoint of this paper, in effect, this can be dealt with by treating each "size class" as a distinct particle "phase" governed by a set of Eulerian balance equations of forms (2-5)–(2-8). Not only would each particle size class experience "two-way" interactions with the host carrier gas, this would also increase the importance of particle–particle interactions [e.g. leading to coagulation and possible coalescence [see, for example, Park and Rosner (1988b) and Biswas (1988)] or, in principle, encounters leading to particle break-up]. In accord with the observations on particle–gas momentum and energy coupling effects above, even if the mass fraction of particles with $Stk = O(10^{-1}–10^{0})$ were small, measurable coupling effects could result at high enough Reynolds numbers. These potentially important phenomena, beyond the scope of this introductory paper, are certainly now amenable to systematic study. Also of engineering interest would be extensions of earlier research on suspended particle/vapor (interphase *mass* transfer) interactions [see, for example, Castillo and Rosner (1988), Rosner and Liang (1988) and Park and Rosner (1989a)] into the domain of appreciable particle "phase" *inertia*.

In closing, we remark that this axisymmetric stagnation flow configuration is also proving to be convenient for studying the interesting phenomenon of local phase separation (i.e. the existence of a "dust-free" sublayer bounded by a "thermophoretic shock") near "overheated" (solid or gas flame) surfaces (Park and Rosner, 1989c; Stratman *et al.*, 1988) and its possible exploitation for particle thermophoretic diffusivity (property) determinations (Gomez *et al.*, 1988) and practical "gas cleaning" in an otherwise awkward particle size range—i.e the continuous removal of submicron particles (Park and Rosner, 1989b). Also of considerable practical interest (e.g. combustion turbine technology), and currently under investigation for this flow (and closely related) configuration(s), is the effect of dust-free gas injection through Ⓦ (i.e. "transpiration" protection [see, for example, Gökoğlu and Rosner (1984)] on the critical Stokes number for inertial impaction, and total particle deposition rates above Stk_{crit}. It is hoped that the insights and engineering correlations ultimately derivable from such theoretical studies will, in the near future, reduce the cost of developing and optimizing equipment operating in such particle-laden hot gas convective environments.

Acknowledgements—It is a pleasure to acknowledge the financial support of Department of Energy-Pittsburgh Energy Technology Center (under Grant DE-FG22-86PC90756) and the U.S. Air Force Office of Scientific Research (under Grant 84-0034), as well as the related

support of the Yale High Temperature Chemical Reaction Engineering Laboratory by our current industrial affiliates (Shell Foundation, Textron-Lycoming and SCM Chemicals). We are also grateful to Drs B. T. Chu and J. Fernandez de la Mora (Yale), J. L. Castillo and P. Garcia-Ybarra (UNED, Madrid, Spain), S. S. Kim (KAIST, Seoul, South Korea), and A. G. Konstandopoulos (Yale HTCRE Laboratory) for helpful discussions and suggestions.

NOTATION

C_f	tangential momentum transfer ("friction") coefficient
$c_{p,g}$	gas heat capacity
$c_{p,p}$	particle heat capacity
D_p	particle Brownian diffusivity ($\ll v_g$)
d_p	particle diameter
f	z-dependent part of radial velocity $[u(r, z)/r]$
g	gravitational body force per unit mass (g_z)
h	specific enthalpy
h	step-size in finite-difference (numerical) method
$j''_{p,w}$	particle diffusion flux at the wall
k_g	gas phase thermal conductivity
L	gap width (Fig. 1) (z_e)
M	molecular weight
Ma	Mach number (of inlet gas)
p	local thermodynamic (static) pressure
Pr	Prandtl number (momentum/heat diffusivity ratio) for gas
R	universal gas constant
R	ratio t_{mom}/t_h for particle "relaxation"
r	radial coordinate in axisymmetric geometry (Fig. 1)
Re_g	Reynolds number based on carrier gas properties $[(-v_{g,e})L/v_{g,e}]$
Sc	Schmidt number (v_g/D_p) (assumed large)
St_h	heat transfer Stanton number
Stk	Stokes number $\{t_{mom}/[L/(-v_{g,e})]\}$
St_m	mass-transfer Stanton number
T	mixture temperature
t_{flow}	characteristic flow time $[L/(-v_{z,ge})]$
T_g	gas temperature
t_h	particle heat transfer relaxation time [eq. (2-4)]
t_h	particle thermal relaxation time [eq. (2-8)]
t_{mom}	particle momentum relaxation time [eq. (2-2)]
T_p	particle temperature
u	r-directional velocity (v_r)
v	z-directional velocity (v_z)
$\mathbf{v}_g$	gas phase (mass-averaged) velocity vector
$\mathbf{v}_p$	particle phase (mass-averaged) velocity vector
z	distance normal to the solid wall (Fig. 1)

Greek letters

α_T	thermal diffusion factor for particles
ε	perturbation parameter (t_{mom}/t_{flow})
ζ_θ	θ-component of fluid vorticity
μ_g	dynamic (Newtonian) viscosity of gas phase
ν_g	gas momentum diffusivity (kinematic viscosity) (μ_g/ρ_g)
ρ	mass density
$\tilde{\rho}_p$	intrinsic density (of an individual particle)
ω_p	particle mass fraction in mixture

Subscripts

crit	critical (singular) value
diff	diffusional (contribution)
e	at upstream (permeable wall) (Fig. 1)
g	gas phase
h	heat (energy) transfer
inertia	inertial (contribution)
m	mass transfer
mom	momentum transfer
p	particle phase
w	at the impermeable wall (Fig. 1)

Abbreviations

ODE	ordinary differential equation
PDE	partial differential equation

Operators

Δ	change in ($\Delta T \equiv T_e - T_w$)
$O(\ )$	order (of magnitude)

REFERENCES

Batchelor, G. K., 1951, Note on a class of solutions of the Navier–Stokes equations representing steady rotationally-symmetric flow. *Q. Jl Mech. appl. Math.* **44**, 29–41.

Biswas, P., 1988, Differential impaction of aerosols. *J. Aerosol Sci.* **19**, 603–610.

Boure, J. A. and Delhaye, M., 1982, General equations and two-phase flow modeling, in *Handbook of Multiphase Systems* (Edited by G. Hetsroni), Section 1.2, pp. 1-36–1-95. Hemisphere–McGraw-Hill, New York.

Castillo, J. L., Mackowski, D. W. and Rosner, D. E., 1989, Photophoretic modifications of the transport of absorbing particles across combustion gas boundary layers. Presented at the ACS 197th Annual Meeting—Symposium on Ash Deposition, Dallas, TX (6–10 April 1989). To appear in *Prog. Energy Combust. Sci.*

Castillo, J. L. and Rosner, D. E., 1988, Nonequilibrium theory of surface deposition from particle-laden, dilute condensible vapor-containing stream, allowing for particle thermophoresis and vapor scavenging within the laminar boundary layer. *Int. J. Multiphase Flow* **14**, 99–120.

Eisner, A. D. and Rosner, D. E., 1986, Experimental and theoretical studies of submicron particle thermophoresis in combustion gases. *Physicochem. Hydrodynamics* **7**, 91–100.

Fernandez de la Mora, I. and Rosner, D. E., 1981, Inertial deposition of particle revisited and extended: Eulerian approach to a traditionally Lagragian problem. *Physicochem. Hydrodynamics* **2**, 1–21.

Fernandez de la Mora, J. and Rosner, D. E., 1982, Effects of inertia on the diffusional deposition of small particles to spheres and cylinders at low Reynolds numbers. *J. Fluid Mech.* **125**, 379–395.

Friedlander, S. K., 1977, *Smoke, Dust and Haze—Fundamentals of Aerosol Behavior*. J. Wiley, New York.

Friedlander, S. K., Fernandez de la Mora, J. and Gökoğlu, S. A., 1988, Diffusive leakage of small particles across the dust-free layer near a hot wall. *J. Colloid Interface Sci.* **125**, 351–355.

Gökoğlu, S. A. and Rosner, D. E., 1984a, Correlation of thermophoretically-modified small particle diffusional deposition rates in forced convection systems with variable

properties, transpiration cooling and/or viscous dissipation. *Int. J. Heat Mass Transfer* **27**, 639–645.

Gökoğlu, S. A. and Rosner, D. E., 1984b, Effect of particle thermophoresis in reducing the fouling rate advantages of effusion-cooling. *Int. Heat Fluid Flow* **5**, 37–41.

Gökoğlu, S. A. and Rosner, D. E., 1986, Prediction and rational correlation of thermophoretically reduced particle mass transfer to hot surfaces across laminar or turbulent forced convection gas boundary layers. *Chem. Engng Commun.* **44**, 107–119.

Goren, S. L., 1977, Thermophoresis of aerosol particles in the laminar boundary layer on flat plate. *J. Colloid Interface Sci.* **61**, 77–85.

Gourdin, W. H. and Andrejco, M. J., 1982, Particle deposition in a burner. *J. Appl. Phys.* **53**, 5920–5925.

Graves, D. B. and Wendt, J. O. L., 1982, Flammability characteristics and structure of a pulverized coal, laminar opposed jet diffusion flame, in *Proceedings of the 19th Symposium (International) on Combustion*, pp. 1189–1196. Combustion Institute, Pittsburgh, PA.

Hidy, G. M., 1984, *Aerosols—an Industrial and Environmental Science*. Academic Press, New York.

Israel, R. and Rosner, D. E., 1983, Use of a generalized Stokes number to determine the aerodynamic capture efficiency of non-Stokesian particles from a compressible gas flow. *J. Aerosol Sci. Technol.* **2**, 45–51; see also Wessel, R. A. and Righi, J., 1988, Generalized correlations for inertial impaction of particles on a circular cylinder. *Aerosol Sci. Technol.* **9**, 29–60.

Keller, H. B., 1974, Accurate difference methods for nonlinear two-point boundary value problems. *SIAM J. numerical Analysis* **11**, 305–320.

Kim, S. S. and Kim, Y. J., 1986, Experimental studies of particle deposition by thermophoresis and inertial impaction from particulate-laden high temperature gas flow, in *Proceedings of the 4th Miami International Symposium on Multiphase Transport*. Hemisphere, Washington, DC.

Kim, Y. J. and Kim, S. S., 1988, Experimental and numerical investigations of particle size effects of particle deposition from non-isothermal stagnation point flows, in *Proceedings of the 1st KSME–JSME Thermal and Fluids Engineering Conference*, Vol. 2, pp. 2-177–2-182.

Mackowski, D. W. and Rosner, D. E., 1989, Thermophoretic modification of the scavenging rate of small particles by large particles in combustion gases. In preparation.

Marble, F. E., 1970, Dynamics of dusty gases, in *Annual Reviews of Fluid Mechanics*, Vol. 2, pp. 397–446. Annual Reviews, Palo Alto, CA.

Park, H. M. and Rosner, D. E., 1989a, Multiphase continuum theory of dopant redistribution across aerosol-laden laminar nonisothermal boundary layers. *Chem. Engng Sci.* **44**, 603–617.

Park, H. M. and Rosner, D. E., 1989b, Boundary layer coagulation effects on the size distribution of thermophoretically deposited particles. *Chem. Engng Sci.* **44**, 2225–2231.

Park, H. M. and Rosner, D. E., 1989c, Thermophoretically induced phase-separation in highly mass-loaded dusty gas mixtures. High Temperature Chemical Reaction Engineering Laboratory Publication No. 162 (prepared for submission to *A.I.Ch.E. J.*).

Rosner, D. E., 1986, *Transport Processes in Chemically Reacting Flow Systems*. Butterworths, Stoneham, MA. Second printing 1988.

Rosner, D. E., 1989, Total mass deposition rates from 'polydispersed' aerosols. *A.I.Ch.E. J.* **35**, 164–167; see also Rosner, D. E. and Tassopoulos, M., 1989, Mass deposition rates from streams containing 'polydispersed' particle populations of arbitrary spread. Submitted to *A.I.Ch.E. J.*

Rosner, D. E. and Fernandez de la Mora, J., 1984, Boundary layer effects on particle impaction and capture. *A.S.M.E. Trans. J. Fluids Engng* **106**, 113–114.

Rosner, D. E., Gökoğlu, S. A. and Israel, R., 1983, Rational engineering correlations of diffusional and inertial particle deposition behavior in non-isothermal forced convection environments, in *Fouling of Heat Exchanger Surfaces* (Edited by R. Bryers), pp. Engineering Foundation, NY, 235–256.

Rosner, D. E. and Kim, S. S., 1984, Optical experiments on thermophoretically augmented submicron particle deposition from 'dusty' high temperature gas flows. *Chem. Engng J.* **29**, 147–157.

Rosner, D. E. and Liang, B., 1988, Experimental studies of deposition rates in the presence of alkali sulfate vapor scavenging by submicron particles in combustion gas boundary layers. *Chem. Engng Commun.* **64**, 27–46.

Rosner, D. E. and Nagarajan, R., 1987, Toward a mechanistic theory of net deposit growth from ash-laden flowing combustion gases: self-regulated sticking of impacting particles and deposit erosion in the presence of vapor 'glue'. *A.I.Ch.E. Symp. Ser.* **83**(257), 289–296.

Rosner, D. E. and Park, H. M., 1988, Thermophoretically augmented mass-, momentum- and energy-transfer rates in high particle mass loaded laminar forced convection systems. *Chem. Engng Sci.* **43**, 2689–2704 [NB add exponent -1 to expression for t_{coag} in eqs (A5-1) and (A5-3)].

Saffman, P. G., 1965, The lift on a small sphere in a slow shear flow. *J. Fluid Mech.* **22**, 385–400.

Stratman, F., Fissan, H., Papperger, A. and Friedlander, S. K., 1988, Suppression of particle deposition to surfaces by the thermophoretic force. *Aerosol Sci. Technol.* **9**, 115–121.

Talbot, L., 1981, Thermophoresis—a review, in *Rarefied Gas Dynamics, Part I* (Edited by S. S. Fisher). *Prog. Astronaut. Aeronaut.* **74**, 467–488.

Van Dyke, M., 1969, *Perturbation Methods in Fluid Dynamics*. Academic Press, New York.

von Kármán, T. 1921, Laminare und Turbulent Reibung. *Z. angew. Math. Mech.* **1**, 233–251 [see also NACA TM 1092 (1946)].

Zung, L. B., 1969, Flow induced in fluid–particle suspension by an infinite rotating disk. *Phys. Fluids* **12**, 18–23.

REPORT DOCUMENTATION PAGE

Form Approved
OMB No. 0704-0188

1. AGENCY USE ONLY (Leave blank)	2. REPORT DATE	3. REPORT TYPE AND DATES COVERED
	1989	Journal Publication

4. TITLE AND SUBTITLE
THEORY OF SURFACE DEPOSITION FROM A UNARY DILUTE VAPOR-CONTAINING STREAM ALLOWING FOR CONDENSATION WITHIN THE LAMINAR BOUNDARY LAYER (U)

5. FUNDING NUMBERS
PE - 61102F
PR - 2308
SA - BS
G - AFOSR 89-0223
AFOSR 84-0034

6. AUTHOR(S)
Jose L. Castillo and Daniel E. Rosner

7. PERFORMING ORGANIZATION NAME(S) AND ADDRESS(ES)
HIGH TEMPERATURE CHEMICAL REACTION ENGINEERING LABORATORY
YALE UNIVERSITY
BOX 2159, YALE STATION
NEW HAVEN, CONNECTICUT 06520 U.S.A.

8. PERFORMING ORGANIZATION REPORT NUMBER

9. SPONSORING/MONITORING AGENCY NAME(S) AND ADDRESS(ES)
AFOSR/NA
Building 410
Bolling AFB DC 20332-6448

10. SPONSORING/MONITORING AGENCY REPORT NUMBER

11. SUPPLEMENTARY NOTES

12a. DISTRIBUTION/AVAILABILITY STATEMENT
Approved for public release; distribution is unlimited

12b. DISTRIBUTION CODE

13. ABSTRACT (Maximum 200 words)

Abstract—Deposition rates on targets cooled far below the dew point of undersaturated mainstreams have often been found to be surprisingly low and surface temperature dependent. A rational yet tractable theory to account for these observations is formulated and exploited in particular cases of current practical interest—e.g. the deposition of trace alkali sulfate vapors present in combustion products. The present physico-chemical model is based on the formation of a condensate aerosol near the deposition surface, with the resulting droplets (or particles) collected by the mechanism of thermophoresis [shown to be dominant, but previously neglected in related two-phase boundary layer (BL) analyses]. The vapor, assumed here to be in local equilibrium with the aerosol phase, is collected by the familiar mechanism of Fick (concentration) diffusion across the prevailing laminar BL (LBL), but the overly restrictive assumption $D_v \cong \alpha_a$ (unity Lewis number) is not made. As by-products of the calculation of the total (aerosol + vapor) deposition rate the position of nucleation onset, as well as the structure of the LBL on either side of this "fog-locus", are obtained. Encouraging agreement with limited available data on Na_2SO_4 deposition is obtained by assuming that the thermophoretic diffusivity of the resulting aerosol phase is about one decade smaller than the momentum diffusivity of the host combustion products.

14. SUBJECT TERMS
deposition, mass transfer, boundary layer theory, condensation, alkali sulfates, dew points

15. NUMBER OF PAGES
13

16. PRICE CODE

17. SECURITY CLASSIFICATION OF REPORT	18. SECURITY CLASSIFICATION OF THIS PAGE	19. SECURITY CLASSIFICATION OF ABSTRACT	20. LIMITATION OF ABSTRACT
Unclassified	Unclassified	Unclassified	UL

Chemical Engineering Science, Vol. 44, No. 4, pp. 925–937, 1989.
Printed in Great Britain

0009-2509/89 $3.00 + 0.00

THEORY OF SURFACE DEPOSITION FROM A UNARY DILUTE VAPOR-CONTAINING STREAM ALLOWING FOR CONDENSATION WITHIN THE LAMINAR BOUNDARY LAYER†

JOSE L. CASTILLO‡ and DANIEL E. ROSNER§
Department of Chemical Engineering, Yale University, New Haven, CT 06520, U.S.A.

(*First received* 11 *April* 1985; *accepted in revised form* 12 *September* 1988)

Abstract—Deposition rates on targets cooled far below the dew point of undersaturated mainstreams have often been found to be surprisingly low and surface temperature dependent. A rational yet tractable theory to account for these observations is formulated and exploited in particular cases of current practical interest—e.g. the deposition of trace alkali sulfate vapors present in combustion products. The present physico-chemical model is based on the formation of a condensate aerosol near the deposition surface, with the resulting droplets (or particles) collected by the mechanism of thermophoresis [shown to be dominant, but previously neglected in related two-phase boundary layer (BL) analyses]. The vapor, assumed here to be in local equilibrium with the aerosol phase, is collected by the familiar mechanism of Fick (concentration) diffusion across the prevailing laminar BL (LBL), but the overly restrictive assumption $D_v \cong \alpha_h$ (unity Lewis number) is not made. As by-products of the calculation of the total (aerosol + vapor) deposition rate the position of nucleation onset, as well as the structure of the LBL on either side of this "fog-locus", are obtained. Encouraging agreement with limited available data on Na_2SO_4 deposition is obtained by assuming that the thermophoretic diffusivity of the resulting aerosol phase is about one decade smaller than the momentum diffusivity of the host combustion products.

1. INTRODUCTION

1.1. *Motivation and applications*

Despite recent advances in the theory of chemical *vapor* deposition (CVD) and aerosol *particle* deposition, motivated in part by the needs of the electronics industry and the combustion/propulsion/power generation industry, little is yet known about commonly occurring situations in which both mechanisms operate simultaneously. One such class of problems is encountered even when the mainstream is itself completely free of particles; i.e. when the aerosol particles are formed within the cooler regions of the boundary layer (BL) near the deposition surface itself. Because of the resulting complexity of this two-phase mass transfer situation, previous investigators have *qualitatively* discussed this possibility in an effort to account for otherwise surprising deposition rate trends for targets cooled far below the prevailing dew point. The goal here is to provide a rational yet *quantitative* theory to allow useful engineering predictions of deposition rates in this interesting and commonly encountered mass transfer regime.

1.2. *Previous work*

Because of its engineering importance the behavior and rate of deposition of various condensible vapors on cold surfaces have often been experimentally studied [Johnstone *et al.* (1950), using mixtures of nitrogen and vapors of sulfur, *n*-butyl alcohol and water, Sjögren (*ca* 1959) and Ross (1965) (sulfuric acid), Hedley *et al.* (1966) (vanadium pentoxide), Hart *et al.* (1964) and Heywood and Womack (1969) (potassium sulfate), and Brown, (1967) and Santoro *et al.* (1984) (sodium sulfate)]. These studies have shown that there exists an initial increase in the deposition rate when the surface temperature, T_w, drops below the dew point, until a maximum deposition rate is reached. Interestingly enough, further decreases in T_w significantly *reduce* the deposition rate. This reduction has been qualitatively attributed to the condensation of the vapor inside the thermal BL (Brown, 1967). In fact, two sets of investigations reported direct observations of a fog region close to the cold surface (Johnstone *et al.*, 1950; Mori and Hijikata, 1973) comprised of submicron size droplets (Heywood and Womack, 1969). However, until now the only rational theoretical model that has been proposed to quantitatively explain such deposition rate results is that of Gardner (1968), which is adapted and extended here (see Section 2.1).

Toor (1971a and b) studied the formation of fog, and Mori and Hijikata (1973) and Hijikata and Mori (1973) the influence of condensation on *heat* transfer. These analyses assumed that in the fog region the vapors and the condensate droplets were in thermodynamic equilibrium, but they were not concerned

†Supported, in part, by Air Force Office of Scientific Research (under Grant AFOSR-84-0034) and NASA-Lewis Research Center (under Grants NAG-3-201 and 3-884).

‡Visiting Research Scientist, High Temperature Chemical Reaction Engineering Laboratory. On leave of absence from Departamento de Fisica Fundamental, UNED, Apdo 60141, Madrid 28080, Spain.

§Professor, Department of Chemical Engineering, and Director, High Temperature Chemical Reaction Engineering Laboratory. To whom correspondence should be addressed.

with the rate of deposition and considered that, in the two-phase region, the average velocity of the gas phase and the velocity of the liquid droplets were equal. In so doing, they have neglected the *thermophoretic* migration of droplets, shown to be crucial for similar aerosols in other contexts (Rosner, 1980).

1.3. *Outline of present paper*

In this paper a tractable theory of the behavior of unary dilute condensible vapors flowing near cold surfaces is presented. Condensation of the vapor within the thermal BL and its influence on the total deposition rate is taken into account. Since the importance of *thermophoretic transport* (the drift of condensate particles, liquid droplets or solid particles down the local temperature gradient) has recently been well established [e.g. see the recent reviews of Rosner (1980, 1986)] this mechanism of condensate transport toward the cold surface is included, as in the remarkable but little known pioneering study of turbulent BL transport by Gardner (1968). The assumptions underlying the present theoretical model and the associated equations are presented in Section 2. Section 3 then develops self-similar solutions for the vapor and condensate mass fraction equations, first in the simple case where there is no condensation of vapor inside the BL (dispersed condensate is *not* present) and then for the more interesting and previously unsolved case in which local condensation, indeed, occurs. Representative results for the deposition of Na_2SO_4 vapors from flowing combustion gases are given in Section 4, together with a comparison with available experimental measurements. Last, in Section 5, the main conclusions and their implications are summarized.

2. THEORETICAL MODEL AND GOVERNING EQUATIONS

2.1. *Underlying assumptions*

To simplify the problem without losing its essential new features the following defensible assumptions will be made:

(A1) The mass fraction of condensible vapor is sufficiently small (with respect to the mass fraction of noncondensible gas) so that the prevailing velocity and temperature fields are not affected by the thermophysical processes experienced by the relatively small amount of vapor (e.g. condensation, freezing, deposition).†

(A2) The condensible vapor behaves like an ideal gas. Thus, the relation between the vapor mass fraction ω_v, and vapor partial pressure, p_v, can be written as

$$\omega_v = \frac{1}{\rho}\left(\frac{p_v M_v}{RT}\right) \qquad (2.1\text{-}1)$$

where $\omega_v \equiv \rho_v/\rho$, M_v is the vapor molecular weight, and R is the universal gas constant.

(A3) Whenever the vapor is in contact with its condensate (liquid droplets, solid particles and liquid or solid deposit), they are in mutual thermodynamic equilibrium (Fig. 1). This requires that the characteristic residence time is much larger than the characteristic time required for the system to reach such equilibria. Making this approximation frees one from speculation about the *kinetics* of condensation, nucleation or freezing, as well as the kinetics of growth of liquid droplets or solid particles. Furthermore, for simplicity, the equilibrium vapor pressure over a small liquid droplet (or a solid particle) will be taken to be the same as on a flat liquid (solid) layer at the same temperature (i.e. the so-called Kelvin effect will be neglected). Therefore, there is no need to be concerned with the size (or number density) of droplets in the two-phase region, and interest will only be shown in the local *amount* of condensible material in each phase (vapor and either liquid droplets or solid particles, depending on the local temperature), irrespective of the number or sizes of these droplets or particles. Consequently, in the two-phase region the partial vapor pressure is equal to the equilibrium vapor pressure over a flat liquid (or solid) surface: thus an equilibrium mass fraction can be calculated from eq. (2.1-1) as

$$\omega_v^{eq} = \frac{1}{\rho}\left[\frac{p_v^{eq}(T)M_v}{RT}\right] \qquad (2.1\text{-}2)$$

which is only a function of local temperature {for constant ρ, as assumed below [assump-

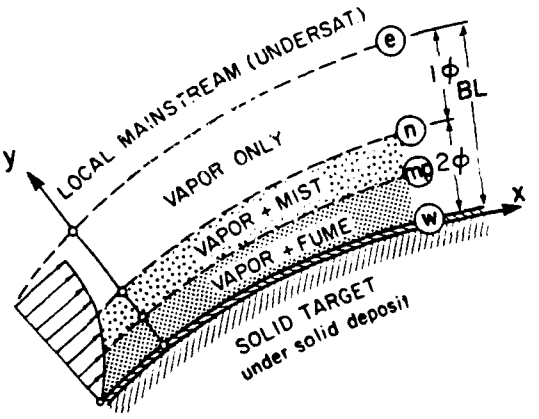

Fig. 1. Schematic of structure of laminar boundary layer near deposition surface showing inner zone(s) of two-phase (aerosol condensate) flow: primary *condensate* deposition mechanism is thermophoresis toward cooled surface.

†This assumption is self-consistent provided $\Delta\omega_v \ll (\alpha_h/D)^{1/3} c_p \Delta T/L$. In the present applications, while the right-hand side (RHS) is of order unity, the left-hand side (LHS) is only of order 10^{-5}. However, in 'highly loaded' systems (e.g. of interest in optical waveguide manufacture) latent heat release effects are appreciable even for dopants (Park and Rosner, 1989).

tion (A5)]}. Thus, $\omega_v = \omega_v^{eq}(T)$ in the two-phase (2ϕ) region and $\omega_v < \omega_v^{eq}$ in the single-phase (1ϕ) region. The validity of this assumption is discussed in Section 4.3. In a recent paper, Castillo and Rosner (1988a) have relaxed assumption (A3) to examine the influence of both a nonequilibrium between vapor and condensate and the Kelvin effect on the overall mass transfer rate.

(A4) The flow within the BL is steady and laminar. The usual BL approximations will be used and self-similarity will be assumed (see, for example, Schlichting (1968)].

(A5) All thermophysical properties of the gas mixture (momentum and thermal diffusivities, etc.) will be considered constant and equal to the values for the carrier gas at mainstream conditions.† Transport properties for the vapor (diffusion coefficient) and its dispersed condensate (thermophoretic coefficient) will also be taken to be constant. Lastly, the total 2ϕ system will be considered effectively incompressible, i.e. the total density will be assumed to be constant.

(A6) Thermal diffusion (Soret effect) will be neglected *for the vapor*. Thus, the difference between local carrier gas and vapor velocities is due only to the diffusion flux of the vapor down its own concentration gradient.

(A7) Condensate particles (liquid droplets or solid particles) do not appreciably migrate due to Brownian diffusion. Thus, the local difference between the condensate velocity and the carrier gas velocity is assumed to be only due to the thermophoretic drift of the condensate. This thermophoretic velocity will be taken at each position as that corresponding to an isolated particle in a uniform gas with the same temperature gradient. However, in contrast to Gardner (1968), the proportionality constant (dimensionless thermophoretic diffusivity) is allowed to be a parameter.

2.2. *Mass conservation equations*

Consider a system in which there are three "coexisting" constituents: an inert carrier gas (density ρ_{inert}), a condensible vapor (ρ_v) and the same substance in a condensed (dispersed) phase (ρ_c) (i.e. liquid droplets or solid particles depending on the local temperature).

Under assumption (A1), the total density and mass average velocity of the mixture are approximately equal to the values for the inert gas. Accordingly, the vapor mass fraction, $\omega_v \equiv \rho_v/\rho$, must satisfy the following partial differential equation (PDE) (Rosner, 1986):

$$\frac{\partial \omega_v}{\partial t} + \mathbf{v}\cdot\mathbf{grad}\,\omega_v = D_v\,\mathrm{div}\,\mathbf{grad}\,\omega_v - \frac{\dot{r}'''}{\rho} \quad (2.2\text{-}1)$$

where $\dot{r}'''$ denotes the local rate at which vapor mass is being transformed into condensate per unit volume and assumption (A6) has been used, i.e. the difference between $\mathbf{v}_v$ and $\mathbf{v}$ is the diffusion velocity of the vapor:

$$\rho_v(\mathbf{v}_v - \mathbf{v}) = \rho_v \mathbf{v}_{diff,v} = \mathbf{j}''_{diff,v} = -D_v\rho\,\mathbf{grad}\,\omega_v. \quad (2.2\text{-}2)$$

In the same way, the condensate mass fraction, $\omega_c \equiv \rho_c/\rho$, can be shown to satisfy the PDE

$$\frac{\partial \omega_c}{\partial t} + (\mathbf{v}+\mathbf{v}_T)\cdot\mathbf{grad}\,\omega_c = -\omega_c\,\mathrm{div}\,\mathbf{v}_T + \frac{\dot{r}'''}{\rho} \quad (2.2\text{-}3)$$

where assumption (A7) has been introduced, i.e. the condensate velocity is assumed to differ from the gas velocity by a thermophoretic velocity $\mathbf{v}_T$:

$$\mathbf{v}_c = \mathbf{v} + \mathbf{v}_T. \quad (2.2\text{-}4)$$

This thermophoretic velocity is normally written as

$$\mathbf{v}_T = \alpha_T D_c[-(\mathbf{grad}\,T)/T] \quad (2.2\text{-}5)$$

where α_T is a dimensionless "thermal diffusion factor". Actually, D_c is included here just to emphasize the similarity between eq. (2.2-5) and a diffusion velocity, but the value of the "thermophoretic diffusivity" $\alpha_T D_c$ does not really depend on D_c [which, in fact, is taken to be zero according to assumption (A7)]. Rather, it depends on the gas momentum diffusivity ν, the particle Knudsen number and the particle and carrier gas thermal conductivities; being $\alpha_T D_c \approx 0.54\,\nu$, irrespective of the particle radius, for a solid particle whose radius is much smaller than the mean free path of the gas molecules and whose thermal conductivity is much larger than that of the "host" gas (Talbot, 1981). This remarkably simple limiting case [the only case treated by Gardner (1968)] provides a useful first approximation for the magnitude of $\alpha_T D_c$ even for microdroplets, and motivates the introduction of the ratio $\alpha \equiv \alpha_T D_c/\nu$ in the analysis and parametric examples which follow.

2.3. *Host (carrier gas) flow field (external flow past a "wedge", $Re^{1/2} \gg 1$)*

The inviscid (potential) flow (external solution) which corresponds to the neighborhood of the forward stagnation point on a wedge (Fig. 2) with included angle β [$\beta = 2m/(m+1)$] has a "surface" velocity distribution of the form

$$u_e(x) = ax^m \quad (2.3\text{-}1)$$

where a is a constant. As is well known, two-dimensional stagnation region flow, as well as the BL on a flat plate at zero incidence, constitute particular cases

†Gökoğlu and Rosner (1984) compared numerical results for heat and mass transfer in laminar boundary layers (LBLs) with and without property variations for vapors in air and proposed a simple correlation scheme. They showed that, in general, for the range $0.25 \leqslant T_\infty/T_c \leqslant 4$ and for Lewis numbers (D/α_h) < 1 (as in the present case), the results for mass transfer considering constant properties differ no more that 18% from the results using actual property variations. In particular, for K_2SO_4 vapors in air, the difference was < 10% for the same range of temperature ratios. Thus, even for the lower values of T_∞/T_c considered the error made in the present analysis is acceptably small.

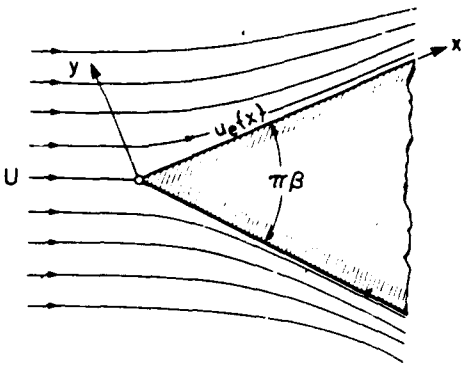

Fig. 2. Steady incompressible fluid flow past a wedge of opening angle $\pi\beta$: $Re_x^{1/2} \gg 1$.

of wedge flows, the former for $\beta = 1$ (i.e. $m = 1$), the latter for $\beta = 0$ (i.e. $m = 0$). On the other hand, the case $\beta = \frac{1}{2}$ ($m = \frac{1}{3}$) can easily be transformed into the flow near an axisymmetric stagnation point (Schlichting, 1968 p. 150) if, in the BL equations η(wedge) $= \eta$(rotational symmetry)$\sqrt{2}$.

The similarity variable $\eta(x, y)$ which leads to BL densities described by ordinary differential equations (ODEs) is

$$\eta \equiv y\{[u_e(x)]/(vx)\}^{1/2} = y(ax^{m-1}/v)^{1/2}. \quad (2.3\text{-}2)$$

The total mass conservation equation is automatically satisfied with the introduction of a dimensional stream function [and the corresponding nondimensional function $f(\eta)$]:

$$\psi(x, y) \equiv (va)^{1/2} x^{(m+1)/2} f(\eta). \quad (2.3\text{-}3)$$

Thus, the fluid velocity components become

$$u = \partial\psi/\partial y = ax^m f'(\eta) = u_e f'(\eta) \quad (2.3\text{-}4)$$

and

$$v = -\frac{\partial\psi}{\partial x} = -\frac{m+1}{2}(vax^{m-1})^{1/2}\left(f + \frac{m-1}{m+1}\eta f'\right) \quad (2.3\text{-}5)$$

where primes denote differentiation with respect to η. The x-momentum conservation equation then becomes the following well-known third-order nonlinear ODE for $f(\eta)$

$$f''' + \frac{m+1}{2} ff'' + m[1 - (f')^2] = 0 \quad (2.3\text{-}6)$$

with the boundary conditions

$$\text{at } \eta = 0: \quad f = f' = 0 \quad (2.3\text{-}7)$$

$$\text{at } \eta = \infty: \quad f' = 1. \quad (2.3\text{-}8)$$

2.4. *Temperature field*

In a steady state, using BL approximations (A4) and (A5), the energy equation which governs the host gas temperature distribution simplifies to

$$u\frac{\partial T}{\partial x} + v\frac{\partial T}{\partial y} = \alpha_h \frac{\partial^2 T}{\partial y^2} \quad (2.4\text{-}1)$$

α_h being the thermal diffusivity.

A self-similar solution is now sought for $T(x, y)$, i.e. $T(\eta)$, where $\eta(x, y)$ is defined by eq. (2.3-2). Thus, when the wall temperature is held constant and equal to T_w:

$$T = T_w + (T_\infty - T_w)\theta(\eta) \quad (2.4\text{-}2)$$

where T_∞ is the temperature at the mainstream, far from the wall, with boundary conditions

$$\theta(0) = 0 \text{ and } \theta(\infty) = 1. \quad (2.4\text{-}3)$$

Using eqs (2.3-2), (2.3-4) and (2.3-5) and eq. (2.4-2) in eq. (2.4-1):

$$\theta'' + \frac{m+1}{2} Pr f\theta' = 0 \quad (2.4\text{-}4)$$

where Pr is the Prandtl number ($Pr \equiv v/\alpha_h$).

The solution of eq. (2.4-4) with boundary condition (2.4-3) is given by [e.g. Spalding and Evans (1961)]:

$$\theta(\eta) = \frac{1}{\delta_T}\int_0^\eta \exp\left\{-\frac{m+1}{2} Pr \int_0^\phi f(\xi)\,d\xi\right\} d\phi \quad (2.4\text{-}5)$$

with

$$\delta_T \equiv \int_0^\infty \exp\left\{-\frac{m+1}{2} Pr \int_0^\phi f(\xi)\,d\xi\right\} d\phi. \quad (2.4\text{-}6)$$

(For a description of the numerical computation of δ_T see the end of Section 3.1.)

2.5. *Self-similar mass fraction equations and the prediction of deposition rates*

Assuming that the vapor mass fraction field depends on y and x only through η, i.e. $\omega_v = \omega_v(\eta)$, and using eqs (2.3-1), (2.3-3) and (2.3-4) in eq. (2.2-1), together with the BL approximations (A4), $\omega_v(\eta)$ must satisfy the second-order ODE

$$\frac{d^2\omega_v}{d\eta^2} + \frac{m+1}{2} Sc f\frac{d\omega_v}{d\eta} = Sc\,\dot{\omega}''' \quad (2.5\text{-}1)$$

where $Sc \equiv v/D_v$ is the Schmidt number, and

$$\dot{\omega}'''(\eta) \equiv \frac{\dot{r}'''(x, y)}{\rho u_e(x)} x = \frac{\dot{r}'''(x, y)}{\rho a x^{m-1}}. \quad (2.5\text{-}2)$$

Using the same relations in eq. (2.2-3), and taking into account eq. (2.2-5), the *condensate* mass fraction field, $\omega_c(\eta)$, is found to satisfy the first-order ODE

$$A\frac{d\omega_c}{d\eta} + B\omega_c = -\dot{\omega}''' \quad (2.5\text{-}3)$$

where the coefficients are, explicitly:

$$A(\eta) \equiv \frac{m+1}{2} f + \frac{\alpha}{T}\frac{dT}{d\eta} \quad (2.5\text{-}4)$$

$$B(\eta) \equiv \frac{\alpha}{T}\left[\frac{d^2T}{d\eta^2} - \frac{1}{T}\left(\frac{dT}{d\eta}\right)^2\right] \quad (2.5\text{-}5)$$

and α is the ratio of the particle "thermophoretic diffusivity" to the host gas momentum diffusivity, i.e.

$$\alpha \equiv \alpha_T D_v / \nu. \tag{2.5-6}$$

Equations (2.5-1) and (2.5-3) govern the amount of condensible material which exists in the vapor and condensate phase, respectively. In the following section these equations are solved in the two limiting cases: (1) when there is no condensate formation within the BL, i.e. $\omega_c = 0$ everywhere; and (2) when condensate forms, and the value of $\dot{\omega}'''(\eta)$ is such that thermodynamic equilibrium exists between the vapor and condensate phases, i.e. $\omega_v(\eta) = \omega_v^{eq}[T(\eta)]$. In any case, the local mass deposition rate of condensible material arriving as *vapor* will be

$$-j''_{v,w}(x) = -(\rho_v \mathbf{v}_v \cdot \mathbf{n}_w)_{y=0} = \rho D_v \left.\frac{\partial \omega_v}{\partial y}\right|_{y=0}$$

$$= \frac{\rho}{Sc}\left(\frac{u_e \nu}{x}\right)^{1/2} \left.\frac{d\omega_v}{d\eta}\right|_{\eta=0}.$$

The total deposition over a length L, measured along x from the forward stagnation point, $-j'_{v,w}(L)$, will therefore be

$$-j'_{v,w}(L) = \int_0^L [-j''_{v,w}(x)]\, dx$$

or, in terms of the behavior of $\omega_v(\eta)$ near the wall:

$$-j'_{v,w}(L) = \frac{\rho}{Sc}\frac{2}{m+1}(a\nu L^{m+1})^{1/2} \left.\frac{d\omega_v}{d\eta}\right|_{\eta=0}.$$

If the nondimensional vapor deposition rate $\mathcal{J}_v$ is defined as

$$\mathcal{J}_v \equiv \frac{m+1}{2\rho}(a\nu L^{m+1})^{-1/2}[-j'_{v,w}(L)] \tag{2.5-7a}$$

then

$$\mathcal{J}_v = \frac{1}{Sc}\left.\frac{d\omega_v}{d\eta}\right|_{\eta=0}. \tag{2.5-7b}$$

If condensate particles (liquid droplets or solid particles) are also present, this dispersed condensate will also deposit on the colder wall *via thermophoresis*. Defining a nondimensional condensate deposition rate $\mathcal{J}_c$ in a similar manner to $\mathcal{J}_v$:

$$\mathcal{J}_c \equiv \frac{m+1}{2\rho}(a\nu L^{m+1})^{-1/2}[-j'_{c,w}(L)] \tag{2.5-8a}$$

then

$$\mathcal{J}_c = \frac{T_\infty - T_w}{T_w \delta_T}\alpha\, \omega_c(\eta = 0). \tag{2.5-8b}$$

In more conventional notation, these nondimensional fluxes are simply related to the associated mass transfer Stanton numbers via

$$\mathcal{J}_v = (\omega_{v,\infty} - \omega_{v,w}) St_{m,v} Re_x^{1/2}$$

$$\mathcal{J}_c = (\omega_{v,\infty} - \omega_{v,w}) St_{m,c} Re_x^{1/2}$$

where, in the latter case, $St_{m,c}$ is *defined* using $\omega_{v,\infty}$ since $\omega_{c,\infty} = 0$

3. SELF-SIMILAR SOLUTIONS

3.1. *No-condensation case*

When the boundary conditions and parameters are such that condensate does not form within the BL then $\dot{\omega}''' = 0$ and $\omega_c = 0$, and the solution of eq. (2.5-1) is simply

$$\omega_v = \omega_{v,w} + (\omega_{v,\infty} - \omega_{v,w})\Gamma(\eta, 0) \tag{3.1-1}$$

where

$$\Gamma(\eta, \phi) = \frac{1}{\delta_v(\phi)}\int_\phi^\eta \exp\left[-\frac{m+1}{2} Sc \int_\phi^\zeta f(\xi)\, d\xi\right] d\zeta \tag{3.1-2}$$

and

$$\delta_v(\phi) = \int_\phi^\infty \exp\left[-\frac{m+1}{2} Sc \int_\phi^\zeta f(\xi)\, d\xi\right] d\zeta. \tag{3.1-3}$$

According to assumption (A3) the vapor is in thermodynamic equilibrium with the macroscopic deposit: therefore $\omega_{v,w} = \omega_v^{eq}(T_w)$. Thus, the nondimensional vapor deposition rate, given by eq. (2.5-7) becomes

$$\mathcal{J}_v = \frac{\omega_{v,\infty} - \omega_v^{eq}(T_w)}{Sc\, \delta_v(0)} \tag{3.1-4}$$

which is readily computed once $\omega_{v,\infty}$, $\omega_v^{eq}(T_w)$ and the diffusivity ratio Sc are known. The dew point wall temperature is defined as the minimum wall temperature at which $\mathcal{J}_v = 0$. It is clear from eq. (3.1-4) that

$$\omega_{v,\infty} = \omega_v^{eq}(T_{dp}) \tag{3.1-5}$$

so T_{dp} gives a measure of the value of $\omega_{v,\infty}$. In order to calculate the value of $\delta_v(0)$ [and δ_T, given by eq. (2.4-6), which is governed by a similar expression], it should be noted that from eq. (2.3-7), $f' = u/u_e$ and $f' \to 1$ when $\eta \to \infty$. In practice, f' reaches the value unity for a finite value of η. Thus, suppose the large η behavior of f is given by

$$f = \eta - b \text{ for } \eta \geq \eta_\infty \tag{3.1-6}$$

where b is a constant which depends on m. Then, from its definition [eq. (3.1-3)]:

$$\delta_v(0) = \int_0^{\eta_\infty} \exp\left[-\frac{m+1}{2} Sc \int_0^\phi f(\xi)\, d\xi\right] d\phi$$

$$+ \exp\left[\frac{m+1}{4} Sc(\eta_\infty - b)^2\right]$$

$$\times \exp\left(-\frac{m+1}{2} Sc \int_0^{\eta_\infty} f\, d\xi\right)$$

$$\times \left\{\left[\frac{\pi}{(m+1)\, Sc}\right]^{1/2}\right.$$

$$\left. - \int_0^{\eta_\infty - b} \exp\left(-\frac{m+1}{4} Sc\, \xi^2\right) d\xi\right\}. \tag{3.1-7}$$

This equation is also valid for δ_T by just changing Sc to Pr [see eq. (2.4-6)].

The values of $\delta_v(0)$ and δ_T have been computed using Simpson's rule and the values of $f(\eta)$ calculated using a Taylor expansion using the numerical values of f, f', f'' and f''' at given η values. The three former (f, f' and f'') quantities are tabulated by Schlichting (1968) [Table 7.1 (p. 129) for $m=0$ (in this case $\eta_\infty=7.8$, $b=1.72077$) and Table 5.1 (p. 90) for $m=1$ ($\eta_\infty=3.8$, $b=0.6482$) and $m=\frac{1}{3}$ ($\eta_\infty=5.6$, $b=0.9855$)]. In this last case the different nondimensionalizations have been taken into account [η (here)$=\sqrt{3}\zeta$ (Schlichting) and f (here)$=\sqrt{3}\phi$ (Schlichting)]. The value of f''' is obtained from eq. (2.3-6). Accurate values of expression (3.1-7) for certain combinations of m and Sc can also be found in Evans (1961, Table 3, p. 33); however, it should be noted that due to the different similarity variable used, $\delta_v(0)$ is equal to $[2/(m+1)]^{1/2}\times$(Evans tabulated value)$^{-1}$, and $\beta=2m/(m+1)$. Evans' table has been used the to check the program, and perfect agreement was obtained for the values of m (0, 1 and $\frac{1}{3}$) of greatest practical interest in the present mass transfer research program.

3.2. *Condensation within the BL*

In this more interesting (and previously unsolved) case a two-phase region exists near the wall in which there are condensate particles (liquid droplets or solid particles, depending on the local temperature) at local equilibrium with the vapor, and extending into the BL until a position given by $\eta=\eta_n$, i.e. the "interface" between the single- and the two-phase region is located at η_n. Then, the solution of eq. (2.5-1) for $\eta>\eta_n$ ($\dot\omega'''=0$ and $\omega_c=0$ in this region) is

$$\omega_v=\omega_{v,n}+(\omega_{v,\infty}-\omega_{v,n})\Gamma(\eta,\eta_n);\ \eta\geq\eta_n \tag{3.2-1}$$

with $\Gamma(\eta,\eta_n)$ given by eq. (3.1-2) and $\omega_{v,n}=\omega_v(\eta_n)$.

In the two-phase region, the condensate is in local equilibrium with the vapor, therefore

$$\omega_v=\omega_v^{eq}(T(\eta));\quad \eta\leq\eta_n \tag{3.2-2}$$

and continuity of vapor at η_n implies that $\omega_{v,n}=\omega_v^{eq}[T(\eta_n)]$. The mass fraction of condensate will be [solving eq. (2.5-3)]

$$\omega_c=\int_\eta^{\eta_n}\frac{\dot\omega'''(\phi)}{A(\phi)}\exp\left[-\int_\eta^\phi\frac{B(\xi)}{A(\xi)}\,d\xi\right]d\phi \tag{3.2-3}$$

with the function $\dot\omega'''(\eta)$ given by [from eqs (2.5-1) and (3.2-2)]

$$\dot\omega'''(\eta)=\frac{1}{Sc}\frac{d^2\omega_v^{eq}}{dT^2}\left(\frac{dT}{d\eta}\right)^2+\frac{m+1}{2}f\left(1-\frac{Pr}{Sc}\right)\frac{d\omega_v^{eq}}{dT}\frac{dT}{d\eta} \tag{3.2-4}$$

The nondimensional vapor deposition rate, $\mathcal{J}_v$, will be, using eqs (2.5-7) and (3.2-2):

$$\mathcal{J}_v=\frac{T_\infty-T_w}{Sc\,\delta_T}\left.\frac{d\omega_v^{eq}}{dT}\right|_{T_w} \tag{3.2-5}$$

In contrast, the nondimensional deposition rate of material in condensate form (transported by thermophoresis) is given by [eq. (2.5-8)]

$$\mathcal{J}_c=\frac{T_\infty-T_w}{T_w\delta_T}\alpha\omega_c(\eta=0). \tag{3.2-6}$$

The total nondimensional deposition rate will be

$$\mathcal{J}=\mathcal{J}_v+\mathcal{J}_c \tag{3.2-7}$$

where $\mathcal{J}_v$ is given by eq. (3.2-5) and $\mathcal{J}_c$ by eq. (3.2-6). It should be noted that the contribution $\mathcal{J}_v$ can be computed without solving the rest of the equations. In sharp contrast, to determine the deposition rate in condensate form, eq. (3.2-3) must be calculated at $\eta=0$.

To complete the solution of this system of equations the value of η_n must be established. This is done by using the fact that the flux of condensible material across $\eta=$constant surfaces must be continuous for any value of η; in particular, at $\eta=\eta_n$. Thus

$$(\rho_v\mathbf{v}_v\cdot\mathbf{n}_n)_{1\phi}=[\rho_v\mathbf{v}_v\cdot\mathbf{n}_n+\rho_c\mathbf{v}_c\cdot\mathbf{n}_n]_{2\phi}$$

where the subscripts 1ϕ and 2ϕ refer to the indicated quantity in the single-phase (two-phase) region, and $\mathbf{n}_n$ is a unit vector normal to the contour $\eta=\eta_n$ (pointing, say, into the two-phase region). But ρ_v must be continuous at η_n (otherwise the vapor diffusion flux would be infinite) and $\rho_c(\eta=\eta_n)=0$ [only when $\mathbf{v}_c\cdot\mathbf{n}_n$ is equal to zero could $\rho_c(\eta_n)$ be different from zero, but this is not the case of interest here: in fact, this condition was used to derive eq. (3.2-3)]. Therefore, continuity of vapor flux implies that, at $\eta=\eta_n$:

$$\left.\frac{d\omega_v}{d\eta}\right|_{1\phi}=\frac{d\omega_v^{eq}}{d\eta}\quad\text{at}\quad\eta=\eta_n. \tag{3.2-8}$$

Using eq. (3.2-1) to obtain the value at the single-phase side, there results

$$\frac{\omega_{v,\infty}-\omega_v^{eq}(T_n)}{\delta_v-\displaystyle\int_0^{\eta_n}\left[\exp\left(-\frac{m+1}{2}Sc\int_0^\phi f\,d\xi\right)\right]d\phi}=\frac{T_\infty-T_w}{\delta_T}\exp\left[\frac{m+1}{2}(Sc-Pr)\int_0^{\eta_n}f\,d\xi\right]\left.\frac{d\omega_v^{eq}}{dT}\right|_{T_n} \tag{3.2-9}$$

with $T_n=T_w+(T_\infty-T_w)\theta(\eta_n)$. Equation (3.2-9) allows one to compute the value of η_n. Once η_n is known, $\omega_c(\eta)$ is calculated from eq. (3.2-3) using eq. (3.2-4).

3.3. *Minimum wall temperature for the onset of BL condensation*

It is clear that the boundary between the non-condensation case and the case in which a two-phase (aerosol-containing) region appears adjacent to the solid body corresponds to the wall temperature $T_{w,n}$ at which the "interface" between the single- and the two-phase region just reaches the wall, that is, $\eta_n=0$. Imposing this condition in eq. (3.2-9) it is found that at $T_w=T_{w,n}$

$$\frac{\omega_{v,\infty}-\omega_v^{eq}(T_{w,n})}{\delta_v(0)}=\left.\frac{d\omega_v^{eq}}{dT}\right|_{T_{w,n}}\frac{T_\infty-T_{w,n}}{\delta_T} \tag{3.3-1}$$

Therefore at this temperature $\mathcal{J}_c = 0$ and $\mathcal{J}_v$ is given by either eq. (3.1-4) or eq. (3.2-6) (both yield the same value), and a plot of $\mathcal{J}$ $(= \mathcal{J}_v + \mathcal{J}_c)$ vs T_w will be continuous at $T_{w,n}$. Not only that, the *slope* of J will also be continuous at $T_{w,n}$ because it can be shown that

$$\left.\frac{d\mathcal{J}_c}{dT_w}\right|_{T_{w,n}} = \left.\frac{d\omega_i^{eq}}{dT}\right|_{T_{w,n}} \frac{1}{Sc}\left\{\frac{1}{\delta_T} - \frac{1}{\delta_i}\right\} - \frac{T_\infty - T_w}{Sc\,\delta_T} \times \left.\frac{d^2\omega_i^{eq}}{dT^2}\right|_{T_{w,n}} \tag{3.3-2}$$

$$\left.\frac{d\mathcal{J}_i^{2\phi}}{dT}\right|_{T_{w,n}} = -\frac{1}{Sc\,\delta_T}\left.\frac{d\omega_i^{eq}}{dT}\right|_{T_{w,n}} + \frac{T_\infty - T_w}{Sc\,\delta_T}\left.\frac{d^2\omega_i^{eq}}{dT^2}\right|_{T_{w,n}} \tag{3.3-3}$$

$$\left.\frac{d\mathcal{J}_i^{1\phi}}{dT_w}\right|_{T_{w,n}} = -\frac{1}{Sc\,\delta_i}\left.\frac{d\omega_i^{eq}}{dT}\right|_{T_{w,n}} \tag{3.3-4}$$

where superscripts 2ϕ and 1ϕ are used to distinguish between the values of $\mathcal{J}_i$ when there is condensation (two phases around the wall) [given by eq. (3.2-6)] and when there is no condensation (single phase near the wall) [given by eq. (3.1-4)], respectively. Thus, the slope of $\mathcal{J} = \mathcal{J}_i + \mathcal{J}_c$ is also continuous at $T_{w,n}$, except in the case of $\alpha = 0$ [eq. (3.3-2) is then not valid] which is a singular limit. Note that eqs (3.3-2)–(3.3-4) are general and the conclusion is not affected by the dependence of ω_i^{eq} on T.

4. COMPUTATIONAL PROCEDURES, RESULTS AND DISCUSSION

The particular values $m = 0$, $\frac{1}{3}$ and 1 have been considered, for which the Blasius function f describing the local velocity field of the host gas is well known [and tabulated, for example, in Schlichting (1968)]. As mentioned earlier, when the value of f was required at a nontabulated value of η, it was calculated by a Taylor expansion using the tabulated values of f, f' and f'' and the corresponding value of f''' from eq. (2.3-6) at the closest tabulated value of η. All integrals were here calculated using Simpson's rule, and the temperature at a given position within the thermal BL was computed from eq. (2.4-2) with $\theta(\eta)$ given by eq. (2.4-5).

In order to obtain the deposition rate, for given conditions T_∞, T_{dp} and T_w, the following steps should be followed:

(1) Using the diffusivity ratios Sc and Pr, compute δ_i and δ_T as indicated at the end of Section 3.1.
(2) The nondimensional deposition rate, if there is no BL condensation, is then calculated from eq. (3.1-4).
(3) The nondimensional vapor deposition rate, $\mathcal{J}_i$ (with condensation) is given by eq. (3.2-5). If this value is larger than the one obtained in step (2), condensation within the BL is not possible and the deposition rate is given by eq. (3.1-4).
(4) If $\mathcal{J}_i$ {with condensation [eq. (3.2-5)]} $< \mathcal{J}_i$ {without condensation [eq. (3.1-4)]}, the deposition in condensate form is given by eq. (3.2-6). In order to evaluate it numerically one must:

(4a) Compute the value of η_n at which eq. (3.2-9) is satisfied. It could be shown that when the different terms in eq. (3.2-9) are calculated at $\eta < \eta_n$ then the LHS > the RHS and the opposite is true for $\eta > \eta_n$. Thus η_n is found by starting at $\eta = 0$ and increasing the value of η until $|(\text{LHS/RHS}) - 1| < \varepsilon$, where ε is the required precision.
(4b) Once η_n is known, integral (3.2-3) is carried out, starting at η_n and ending at $\eta = 0$ with $\dot{\omega}'''(\eta)$ given by eq. (3.2-4), and $A(\eta)$ and $B(\eta)$ by eqs (2.5-4) and (2.5-5), respectively. It should be mentioned that the function $\dot{\omega}'''(\eta)$ is discontinuous at $\eta = \eta_n$: because $\dot{\omega}'''(\eta) \equiv 0$ for $\eta > \eta_n$ and is given by eq. (3.2-4) for $\eta < \eta_n$, the value given by eq. (3.2-4) at $\eta = \eta_n$ should be used in the first integration step in eq. (3.2-3).
(4c) The value obtained in step (4b) is used in eq. (3.2-6) and yields the nondimensional deposition rate in condensate form. Adding this value of $\mathcal{J}_c$ to $\mathcal{J}_v$ [step (3)] the total dimensionless deposition rate is obtained from which the absolute total deposition rate [e.g. the sum of vapor and condensed material fluxes expressed in (mg/h)/cm of depth transverse to the flow follows from the definitions in eqs (2.5-7a) and (2.5-8a)].

As illustrations of considerable current interest [see, for example, Santoro *et al.* (1984)], some results are presented here for dilute vapors of Na_2SO_4 in combustion products with thermophysical properties approximating those of air. Values of the alkali salt and air thermodynamic properties actually used are given in the Appendix.

4.1 *Deposition on the wall*

Figures 3–5 depict the deposition rates for $T_\infty = 1713$ K, $T_{dp} = 1400$ K and $m = 0$, $\frac{1}{3}$ and 1, respectively. Line e represents the deposition rate when condensation within the BL is either not possible or not considered. This deposition rate is equal to zero at $T_w = T_{dp}$ and increases as T_w decreases, tending to a plateau value given by $\omega_i^{eq}(T_{dp})/Sc\,\delta_v$ [i.e. $\omega_i^{eq}(T_w)$ is negligible in eq. (3.1-4)]. But by decreasing the wall temperature from $T_w = T_{dp}$, as soon as line e crosses the line given by eq. (3.2-5) (line a in Figs 3–5) small liquid droplets start to form near the surface and the total deposition is given by the deposition in vapor form (line a) and the contribution due to the condensate $\mathcal{J}_c$, and is represented by lines b, c and d for the thermophoretic coefficient α equal to 10^{-2}, 10^{-1} and 5×10^{-1}, respectively. For any value of α (except $\alpha = 0$) the total deposition is continuous (as well as the first derivative) at $T_w = T_{w,n}$, as shown in Section 3.3. The results are qualitatively similar for the three

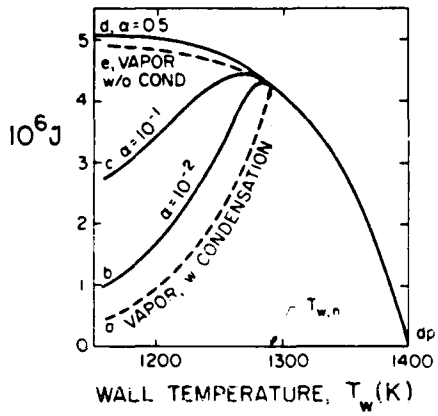

Fig. 3. Surface temperature dependence of total deposition rate of Na_2SO_4 as a function of condensate thermophoretic parameter α ($\equiv \alpha_T D_c/\nu$). Conditions: $T_\infty = 1713$ K, $T_{dp} = 1400$ K, flat-plate collector ($m = 0$).

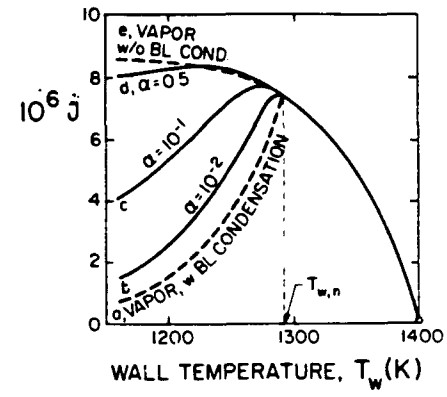

Fig. 5. Surface temperature dependence of total deposition rate of Na_2SO_4 as a function of condensate thermophoretic parameter α ($\equiv \alpha_T D_c/\nu$). Conditions: $T_\infty = 1713$ K, $T_{dp} = 1400$ K, two-dimensional (planar) stagnation line ($m = 1$).

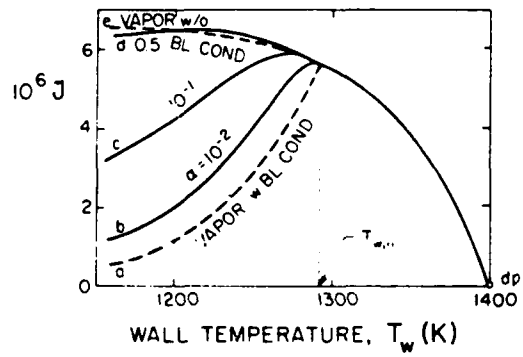

Fig. 4. Surface temperature dependence of total deposition rate of Na_2SO_4 as a function of condensate thermophoretic parameter α ($\equiv \alpha_T D_c/\nu$). Conditions: $T_\infty = 1713$ K, $T_{dp} = 1400$ K, axisymmetric stagnation point ($m = \frac{1}{2}$).

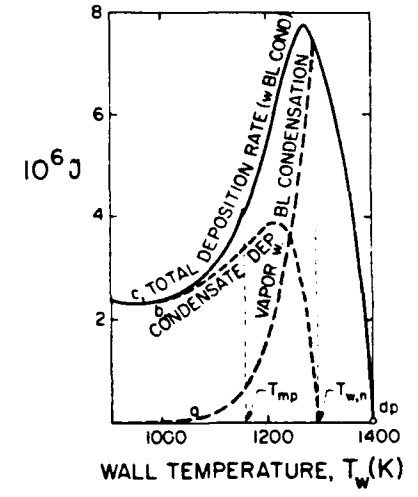

Fig. 6. Predicted effect of condensate freezing on the surface temperature dependence of the deposition rate of Na_2SO_4 condensate and vapor. Conditions: $T_\infty = 1713$ K, $T_{dp} = 1400$ K, two-dimensional (planar) stagnation line collector, α ($\equiv \alpha_T D_c/\nu$) = 0.1.

values of m, so what follows will be restricted to the most important special case: $m = 1$ (two-dimensional stagnation region).

Figure 6 is an extended version of Fig. 5 for $\alpha = 0.1$, in which wall temperatures below the melting point temperature for Na_2SO_4 have been included. It should be pointed out that $\mathcal{J}_v$ [with condensation (line a)] and therefore $\mathcal{J}$ [$= \mathcal{J}_v + \mathcal{J}_c$ (line c)] are discontinuous at $T_w = T_{mp}$ due to the discontinuity of $d\omega_v^{eq}/dT$ at this temperature. Line b represents the deposition rate in condensate form, which tends to zero when T_w approaches $T_{w,n}$ from below. Note that the maximum deposition rate corresponds to a wall temperature which is lower than $T_{w,n}$ and the distance from this maximum to $T_{w,n}$ increases as α increases, as can be observed in Fig. 5. The reduction in deposition rate due to condensation phenomena within the BL could be appreciable. For instance, for $T_w = 1000$ K, $\mathcal{J}_v$(no condensation)/$\mathcal{J}$(with condensation) = 3.66.

4.2. *Condensation and freezing points: BL structure*

As mentioned earlier, when T_w decreases below $T_{w,n}$ a two-phase region, in which the condensible substance exists in vapor form as well as forming liquid droplets or solid particles (depending on the local temperature), starts to develop near the cold surface. In Fig. 7 the position inside the BL at which condensate starts to form (locus of the "interface" between the two- and the single-phase region) is plotted vs the wall temperature as well as the locus of the melting point interface (position in the BL at which $T = T_{mp}$). The conditions are the same as for Fig. 6 but in this case neither η_n nor η_{mp} depend on the value of α. When $T_w < T_{mp}$, three different regions can be distinguished in the BL: an outermost region for $\eta > \eta_n$ in which the condensible substance exists only in dilute *vapor* form, an intermediate region in which liquid droplets are also present, and a third region, still closer to the wall, in which there exists vapor and *solid* particles. This third region does not exist for $T_{mp} < T_w < T_{w,n}$, and

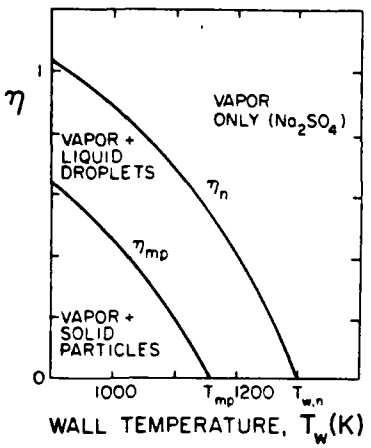

Fig. 7. Predicted locations in the laminar boundary layer at which Na_2SO_4 fog onset and fog freezing occur at various deposition surface temperatures. Conditions: $T_\infty = 1713$ K, $T_{dp} = 1400$ K, two-dimensional (planar) stagnation line.

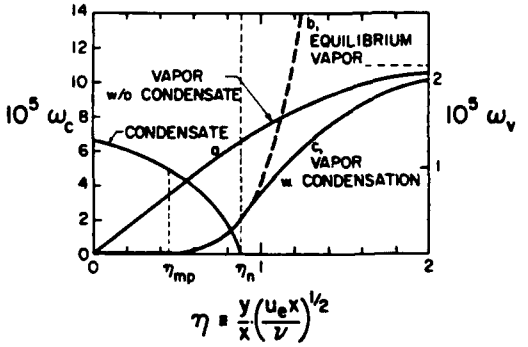

Fig. 8. Predicted distribution of Na_2SO_4 vapor and condensate across laminar boundary layer near deposition surface. Conditions: $T_\infty = 1713$ K, $T_{dp} = 1400$ K, $T_w = 1000$ K, two-dimensional (planar) stagnation line, $\alpha\ (\equiv \alpha_T D_c/\nu) = 0.1$.

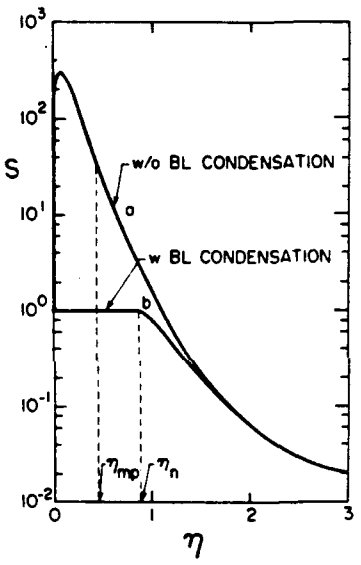

Fig. 9. Predicted distribution of Na_2SO_4 vapor saturation ratio across laminar boundary layer near deposition surface with (and without) condensation. Conditions: $T_\infty = 1713$ K, $T_{dp} = 1400$ K, $T_w = 1000$ K, two-dimensional (planar) stagnation line, $\alpha\ (\equiv \alpha_T D_c/\nu) = 0.1$.

only the first region is present for $T_w > T_{w,n}$. According to assumption (A3), the vapor is in thermodynamic equilibrium with the condensate at $\eta < \eta_n$ and the liquid droplets suddenly convert to solid particles when crossing the line $\eta = \eta_{mp}$. In some cases, as depicted in Fig. 11, the intermediate region does not exist (because $\eta_{mp} > \eta_n$) and solid particles are directly formed from the vapor upon entering the two-phase region.

In Fig. 8 the structure of the mass transfer BL is plotted for the same conditions as Fig. 6 and $T_w = 1000$ K. Line a represents the vapor mass fraction when condensation is not considered and line c when condensation is taken into account. Both have the same limit values, equal to $\omega_v^{eq}(T_w) \approx 1.55 \times 10^{-9}$ at the wall ($\eta = 0$) and equal to $\omega_{v,\infty} = \omega_v^{eq}(T_{dp}) \approx 2.18 \times 10^{-5}$ at the mainstream ($\eta \to \infty$). From Fig. 8 it can be seen that ω_v departs from the noncondensation value and meets the function $\omega_v^{eq}(T)$ (line b) at $\eta = \eta_n$. For $\eta < \eta_n$, lines b and c coincide as well as their slope at η_n [in fact, these were the conditions used to determine the value of η_n through eq. (3.2-9)]. On the other hand, ω_c, the condensate mass fraction, increases from the value zero at η_n and reaches its maximum value at the wall ($\approx 6.66 \times 10^{-5}$ in this particular case). The slopes of ω_c and ω_v^{eq} are discontinuous at η_{mp}.

In Fig. 9 the *saturation ratio*, $s \equiv \omega_v/\omega_v^{eq}$, is plotted inside the BL for the same conditions as Fig. 8. When condensation is considered, $s = 1$ inside the two-phase region ($\eta \leqslant \eta_n$). But if condensation were "not allowed", ω_v will be given by locus a of Fig. 8 and ω_v^{eq} by locus b, displaying a region in which $s > 1$ [reaching a maximum value of more than 300 very close to the wall (at $\eta \approx 0.084$)]. Of course, this maximum value of s (when condensation is "not allowed") increases when T_w decreases.

4.3. *Discussion of underlying assumptions*

Most of the assumptions underlying the present theory of deposition in the presence of BL condensation (see Section 2.1) are widely used and accepted in the literature on constant property BL theory. Therefore, assumptions (A1), (A2) and (A4) need not be discussed further here. However, a brief discussion of the range of validity of assumptions (A3) (saturation within the 2ϕ region) and (A5) and (A7) (size-insensitive, thermophoretically-dominated migration of dispersed condensate) is in order. Indeed, it is required that the dispersed condensate particles be large enough to neglect the Kelvin effect as well as Brownian diffusion, yet, unless the condensate particles are much smaller (or larger) than the prevailing mean free path, assumptions (A5) and (A7) also require that the change in condensate particle size across the 2ϕ region corresponds to a negligible change in thermophoretic diffusivity.

Fortunately, in the most commonly encountered engineering situations nucleation is not purely "homogeneous", but instead occurs on dispersed, pre-existing "nuclei", e.g. gaseous ions or "seed particles". In the case of liquid droplets it is easy to show that, in effect, it has been assumed that the Kelvin (effect) parameter

$$\mathscr{K} \equiv \frac{1}{\rho_l} \frac{M_v}{RT_\infty} \frac{2\sigma_l}{r_{p,\infty}} \tag{4.3-1}$$

is small, but the free-molecule growth law based Damköhler number:

$$(Dam)_{p,\text{seed growth}} = \frac{4\pi\alpha_m}{(du_e/dx)} \left(\frac{RT_\infty}{2\pi M_v}\right)^{1/2} N_{p,\infty} r_{p,\infty}^2 \tag{4.3-2}$$

which governs the "scavenging" kinetics of vapor by particles within the 2ϕ region near a stagnation point ($m=1$) is very *large*. In the applications of interest here, both conditions would be satisfied in mainstreams containing at least *ca* 10^4 nuclei/cm^3 above 10^{-1} μm diameter, corresponding to seed particle volume fractions which have to be above only 1/100 ppb. While generalizations of the present rational asymptotic theory [$\mathscr{K}\to 0$, $(Dam)_p \to \infty$] are currently in progress, its simplicity and generality should render it very useful for engineering estimates of the effects we set out to predict. Moreover, even if environmental conditions are such that the condensate particles are not much smaller (or larger) than the prevailing mean free path, their size is not expected to change by an order of magnitude during thermophoretic transit across the 2ϕ region. Accordingly, the assumption of constant $\alpha_T D_c/\nu$ should provide a useful first approximation in describing the more complex "polydispersed" condensate situation which will generally prevail within the inner, 2ϕ regions of such boundary layers.

4.4. *Comparison with available experiments*

Available experimental results for Na_2SO_4 vapors are based on deposition onto cooled cylindrical tubes immersed in a combustion gas stream. Although this is not the geometry considered here, due to the fact that the theoretical results are very similar for the different values of m (Section 4.1) at least a qualitative agreement is expected. To assess this level of agreement the experimental results have been multiplied by a constant factor, i.e. rescaled in each figure.

Figure 10 compares the experimental deposition rate of Na_2SO_4 vapors on a cylinder by Santoro *et al.* (1984) (their Fig. 11) with the theoretical results for deposition in a stagnation point configuration ($m=1$) with $\alpha=0.1$, and $T_{dp}=1000$°C. The theoretical curve is discontinuous at T_{mp} (when condensation is taken into account) but is continuous at the beginning of condensation ($T_{w,n}$), as was mentioned in Section 4.1. The experimental results are less scattered for $T<T_{mp}$ suggesting that the dispersion of data for $T_w \geq T_{mp}$ could be associated with "run-off" of the liquid. Evidently freezing does occur in these experiments. Clearly, the agreement between theory and experiment is much better when BL condensate formation is taken into account (present work; solid line for $T_w < T_{w,n}$) than when condensation is not considered (dashed line for $T_w < T_{w,n}$).

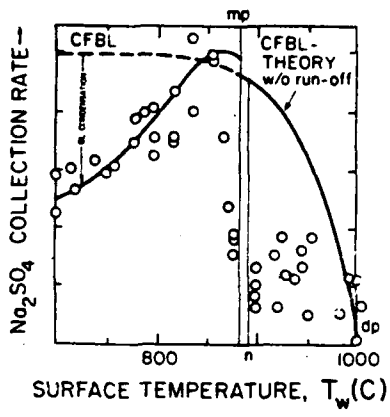

Fig. 10. Comparison of experimental and predicted surface temperature dependence of Na_2SO_4 deposition rate from an undersaturated stream of combustion products. Conditions: $T_\infty = 1713$ K, $T_{dp} = 1273$ K, two-dimensional (planar) stagnation line ($m=1$), α ($\equiv \alpha_T D_c/\nu$) = 0.1.

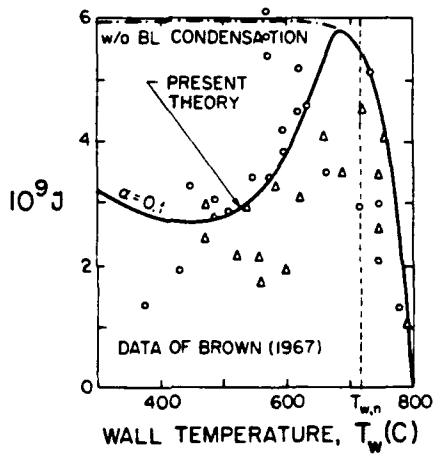

Fig. 11. Comparison of experimental and predicted surface temperature dependence of Na_2SO_4 deposition rate from an undersaturated stream of combustion products. Conditions: $T_\infty = 1523$ K, $T_{dp} = 1073$ K, two-dimensional (planar) stagnation line ($m=1$), α ($\equiv \alpha_T D_c/\nu$) = 0.1.

Figure 11 compares theoretical results for $m=1$, $\alpha=0.1$, $T_\infty = 1523$ K and $T_{dp} = 1073$ K with the experimental results of Brown (1967) (his Fig. 7). In this case, the wall temperature range is such that the *liquid* droplet region shown in Fig. 7 does not exist and solid particles are formed directly from the vapor entering into the two-phase region. While the scatter in these experimental results will clearly preclude a good fit with *any* theory, the agreement is certainly better when condensation is considered (present work, solid line) than when it is neglected (dashed line).

5. CONCLUSIONS AND IMPLICATIONS

To predict deposition rates under operating conditions in which the "dew point" is achieved *within* the thermal boundary layer, one must be able to predict the contribution associated with the collection of the newly formed condensate aerosol. Here the physical model of Gardner (1968) has been adapted and a rational yet tractable method developed for making such predictions for laminar boundary layers in the limiting case that vapor–liquid equilibrium is maintained in the two-phase (inner) region of the BL, and the dispersed condesnate is collected primarily by the mechanism of *thermophoresis*, with the parameter $\alpha_T D_p/\nu$ left arbitrary. Moreover, the restrictive assumption (Toor, 1971a) that the molecular diffusivities for vapor transport and heat transport are equal is avoided. Illustrative calculations are included for the deposition of sodium sulfate from initially undersaturated streams of combustion products (here $D/\alpha_h = 0.39$) exposed to actively cooled solid targets representing as turbine blades (above the Na_2SO_4 melting point) or heat exchanger surfaces cooled below the Na_2SO_4 freezing point. While agreement with experimental data in the available literature for the surprisingly low value $\alpha_T D_c/\nu \approx 0.1$ is encouraging, it seems clear that more precise data will be needed to draw definitive conclusions about the sufficiency of the present theory and the parameters appearing therein [e.g. particle thermophoretic diffusivity chosen by Gardner (1968) to be the theoretical upper limit 0.54]. Such experiments, underway in these laboratories, are reported elsewhere (Liang *et al.*, 1988; Rosner, 1988).

In the present work only "unary" vapor systems under LBL conditions when the mainstream is undersaturated have been explicitly considered. Two necessary and interesting extensions of this work (recently completed) deal with: (a) initially undersaturated *binary* systems (which nucleate far more readily in thermal BL) (Liang *et al.*, 1988; Castillo and Rosner, 1988b), and (b) unary systems under conditions when the mainstream is already a saturated two-phase (aerosol) mixture (Castillo and Rosner, 1989).

With the help of the abovementioned studies a comprehensive, quantitative picture of the important regimes of vapor and/or particle deposition is beginning to emerge, including their interesting mutual interactions and the role of local departures from vapor–liquid equilibrium (Castillo and Rosner, 1988a). Since these convective mass transfer phenomena appear in so many important technologies, this understanding should ultimately pay handsome dividends in the form of improved predictability and rational process optimization/control.

Acknowledgements—The authors gratefully acknowledge many helpful discussions and relevant computations/experiments involving their colleagues Drs J. Fernandez de la Mora (Mechanical Engineering Department, Yale University), B. Liang (Chemical Engineering Department, University of California at Berkeley), H. M. Park (Applied Mathematics, Brown University) and S. A. Gökoğlu (NASA–Lewis Research Laboratory), as well as G. Quinlivan (Yale Engineering Summer Research Program, 1984). Thanks are also due to HTCRE industrial affiliates (Babcock & Wilcox, General Electric, SCM Chemicals, Shell and Textron–Lycoming) for their support of the research activities in the generic area of vapor and particle deposition in high-temperature flow systems.

NOTATION

a	constant in eq. (2.3-1) describing $u_e(x)$
A	function defined by eq. (2.5-4)
b	constant in eq. (3.1-6)
B	function defined by eq. (2.5-5)
D	Fick diffusion coefficient
$(Dam)_p$	Damköhler number [eq. (4.3-1)]
f	Blasius' function [eq. (2.3-2)]
$\mathbf{j}''$	mass flux vector
$\mathcal{J}$	nondimensional mass flux at the wall
$\mathcal{K}$	Kelvin parameter [eq. (4.3-1)]
L	distance along x from the stagnation point
m	parameter defined in eq. (2.3-1) [$m = \beta/(2-\beta)$]
M_v	molecular weight of condensible vapor
$\mathbf{n}$	unit normal vector
$N_{p,\infty}$	number density of seed particles in mainstream (Section 4.3)
p_v	vapor pressure
Pr	Prandtl number [momentum/heat diffusivity ratio ($Pr = \nu/\alpha_h$)]
$r_{p,\infty}$	radius of seed particles in mainstream (Section 4.3)
$\dot{r}'''$	local vapor sink strength [eq. (2.2-2)]
R	universal gas constant
s	saturation ratio ($s \equiv \omega_v/\omega_v^{eq}$)
Sc	vapor Schmidt number ($Sc \equiv \nu/D_v$)
t	time
T	local fluid temperature
u_e	external (potential) flow velocity along x [eq. (2.3-1)]
$\mathbf{v}$	fluid velocity vector ($v_x \equiv u$, $v_y \equiv v$)
x	distance along the wall (measured from the stagnation point) (Fig. 2)
y	distance normal to the wall (Fig. 3)

Greek letters

α	normalized thermophoretic coefficient ($\alpha \equiv \alpha_T D_c/\nu$)
α_h	thermal (heat) diffusivity
α_m	accommodation coefficient
α_T	thermophoretic coefficient [eq. (2.2-5)]
β	included (wedge) angle (Fig. 2)
Γ	normalized vapor mass fraction [eq. (3.1-2)]
δ_T	parameter defined by eq. (2.4-6)
δ_v	function defined by eq. (3.1-3)
η	similarity variable $\{\eta = y[u_e(x)/\nu x]^{1/2}$
η_∞	value of η defined by eq. (3.1-6)
θ	dimensionless local temperature [eq. (2.4-2)]
ν	gas momentum diffusivity (kinematic viscosity)
ρ	density
ρ_l	density of the liquid inside a droplet
σ_l	droplet surface tension

ψ	stream function [eq. (2.3-5)]
ω_v	vapor mass fraction ($\omega_v = \rho_v/\rho_g$)
ω_c	condensate mass fraction ($\omega_c = \rho_c/\rho_g$)
$\dot{\omega}'''$	dimensionless vapor sink strength [eq. (2.5-2)]

Subscripts

c	condensate phase
diff	diffusion quantity
dp	dew point conditions
e	at the outer edge of the BL at station x (local "mainstream")
g	total gas (carrier gas + vapor)
p	pertaining to particle
inert	inert carrier gas
mp	at the melting point
n	at "interface" between the two- and single-phase regions
T	thermophoretic
v	vapor
w	at the wall
∞	at the mainstream

Superscripts

eq	equilibrium value over a flat condensate layer
1ϕ, 2ϕ	refer to quantity on the "interface" between the two- and single-phase regions at the two- or single-phase side, respectively
	derivative with respect to η

Miscellaneous

BL	boundary layer
CVD	chemical vapor deposition
LBL	laminar boundary layer
LHS	left-hand side
ODE	ordinary differential equation
PDE	partial differential equation
RHS	right-hand side

REFERENCES

Brown, T. D., 1967, Oil ash deposition. *Fuel Soc. J.* **18**, 28–43.

Castillo, J. L. and Rosner, D. E., 1988a, A nonequilibrium theory of surface deposition from particle-laden dilute condensible vapor-containing laminar boundary layer. *Int. J. Multiphase Flow* **14**, 99–120.

Castillo, J. L. and Rosner, D. E., 1988b, Theory of surface deposition from a binary dilute vapor-containing stream allowing for condensation within the laminar boundary layer. *Int. J. Multiphase Flow* (in press).

Castillo, J. L. and Rosner, D. E., 1989, Equilibrium theory of surface deposition from particle-laden dilute, saturated vapor containing laminar boundary layers. *Chem. Engng Sci.* **44**, 939–956.

Evans, H. L., 1961, Mass transfer through laminar boundary layers—3a. Similar solution of the b-equation when $B = 0$ and $\sigma > 0.5$. *Int. J. Heat Mass Transfer* **3**, 26–41.

Gardner, G. C., 1968, Mass transfer when diffusing vapor partially precipitates as fume, with special reference to potassium sulfate seed. Central Electricity Research Laboratories (Leatherhead, U.K.), Laboratory Note No. RD/L/N68/68.

Gökoğlu, S. A. and Rosner, D. E., 1984, Engineering correlations of variable property effects on laminar forced convection mass transfer for dilute vapor species and small particles in air. NASA Report CR-168322.

Hart, A. B., Gardner, G. C., Halstead, W. D., Laxton, J. W. and Tidy, D., 1964, Some factors in seed recovery. Paper 89, International Symposium Magnetohydrodynamic Electrical Power Generation, Paris.

Hedley, A. B., Brown, T. D. and Shuttleworth, A., 1966, Vanadium pentoxide deposition from combustion gases. *J. Engng Power* **88**, 173–178.

Heywood, J. B. and Womack, G. J. (Eds), 1969, *Open-cycle MHD Power Generation*, pp. 685–701. Pergamon Press, Oxford.

Hijikata, K. and Mori, Y., 1973, Forced convective heat transfer of a gas with condensing vapor around a flat plate. *Heat Transfer—Jap. Res.* **2**, 81–101.

Janz, G. J., Allen, C. B., Bansal, N. P., Murphy, R. M. and Tomkins, R. P. T., 1979, Physical property data compilations relevant to energy storage. II. Molten salts: data on single and multi-component salt systems. *NSRDS—NBS* **61**, Part II (U.S. Department Communication), 174.

Johnstone, H. F., Kelley, M. D. and McKinley, D. L., 1950, Fog formation in cooler-condensers. *Ind. Engng Chem.* **42**, 2298–2302.

Kohl, F. J., Stearns, C. A. and Fryburg, G. C., 1975, Sodium sulfate: vaporization thermodynamics and role in-corrosion flames, in *Metal–Slag–Gas Reactions and Processes* (Edited by Z. A. Foroulis and W. W. Smeltzer), pp. 649–664. Electrochemical Society Princeton, NJ.

Liang, B., 1987, Experimental studies of multicomponent deposition rate processes using flash evaporation technique. Ph.D. dissertation, Department of Chemical Engineering, Yale University.

Liang, B., Gomez, A., Castillo, J. L. and Rosner, D. E., 1988, Experimental studies of nucleation phenomena within thermal boundary layers—influence on chemical vapor deposition rate processes. Paper A5A, 1987 Annual Meeting of the American Association of Aerosol Research, *Chem. Engng Commun.* (in press).

Mori, Y. and Hijikata, K., 1973, Free convective condensation heat transfer with noncondensible gas on a vertical surface. *Int. J. Heat Mass Transfer* **16**, 2229–2240.

Park, H. M. and Rosner, D. E., 1989, Multiphase continuum theory of dopant redistribution across aerosol-laden laminar nonisothermal boundary layers. *Chem. Engng Sci.* **44**, 603–617.

Rosner, D. E., 1980, Thermal (Soret) diffusion effects on interfacial mass transport rates. *Physicochem. Hydrodynamics* **1**, 159–185.

Rosner, D. E., 1986, *Transport Processes in Chemically Reacting Flow Systems*. Butterworths, Stoneham, MA. Second printing 1988.

Rosner, D. E., 1988, Experimental and theoretical research on the deposition dynamics of inorganic compounds from combustion gases. Invited paper for the B. Levich Memorial Volume of *Physicochem. Hydrodynamics* **10**.

Ross, K., 1965, Condensation of sulfuric acid from flue gas on a cooled cylinder *Inst. Fuel J.* **38**, 273–277.

Santoro, G. J., Kohl, F. J., Stearns, C. A., Gökoğlu, S. A. and Rosner, D. E., 1984, Experimental and theoretical deposition rates from salt-seeded combustion gases of a Mach 0.3 burner rig. NASA TP 2225.

Schlichting, H., 1968, *Boundary Layer Theory*, 6th Edition. McGraw-Hill, New York.

Sjögren, A., *ca* 1959, Flue gas corrosion in boiler plants. Report from the Flue Gas Corrosion Research Committee, Danish Academy of Technical Sciences, Report No. 38, pp. 30–35.

Spalding, D. B. and Evans, H. L., 1961, Mass transfer through laminar boundary layers—3. Similar solutions of the b-equation. *Int. J. Heat Mass Transfer* **2**, 314–341.

Talbot, L., 1981, Thermophoresis—a review. In *Rarefied Gas Dynamics—Part I* (Edited by S. S. Fisher), *Prog. Astronaut. Aeronaut. (AIAA)* **74**, 467–488.

Toor, H. L., 1971a, Fog formation in boundary value problems. *A.I.Ch.E. J.* **17**, 5–14.

Toor, H. L., 1971b, Fog vaporization and condensation in boundary value problems. *Ind Engng Chem. Fundam.* **10**, 121–131.

APPENDIX: INPUT DATA (ILLUSTRATIVE CASES)

All figures presented in this paper correspond to dilute Na_2SO_4 vapors, with the inert "carrier" gas air at atmospheric pressure. According to assumption (A5) the gas thermodynamic properties are considered constant and equal to their values at the mainstream temperature, T_∞. Following assumption (A3), the vapor equilibrium mass fraction is given by

$$\omega_v^{eq} = \frac{1}{\rho}\frac{p_v^{eq}(T)M_v}{RT}. \qquad (A.1)$$

The following values were used in the numerical illustrations:

$M_v = 142.05$ g/mol

$\rho = 0.353/T_\infty$ g/cm^3

$R = 8.3143 \times 10^7$ erg mol K.

If

$$p_v^{eq}(T) = \exp\left(\gamma_l - \frac{\Lambda_l}{RT}\right) \text{ dyn/cm}^2,\ T \geq T_{mp}$$

for the equilibrium vapor pressure over a *liquid* condensate, and, over the solid:

$$p_v^{eq}(T) = \exp\left(\gamma_s - \frac{\Lambda_s}{RT}\right) \text{ dyn/cm}^2,\ T \leq T_{mp}$$

then $\gamma_l = 25.05$ and $\Lambda_l/R = 3.325 \times 10^4$ (Kohl *et al.*, 1975) and $\Lambda_s/R = 3.61 \times 10^4$ with γ_s such that both values for the vapor pressure coincide at the melting point temperature, $T_{mp} = 1157$ K. The value of Λ_s/R was calculated using the fact that $\Lambda_s = \Lambda_l + l_f$, were l_f is the latent heat of fusion, approximately equal to $l_f \approx 5.63$ kcal/mol (Janz *et al.*, 1979). Turning to the important diffusivity ratios governing this class of problems, the Prandtl number Pr was taken to be equal to 0.7 (air) and the vapor Schmidt number $Sc = 1.8$. For these values of Pr and Sc the following values of δ_T [eq. (2.4-6)] and $\delta_v(0)$ [eq. (3.1-3)] were obtained for the values of m of principal interest here:

m	δ_T ($Pr = 0.7$)	$\delta_v(0)$ ($Sc = 1.8$)
$m = 0$ (flat plate)	3.41669	2.45525
$m = \frac{1}{3}$ (axisymmetric stagnation point)	2.60279	1.82522
$m = 1$ (planar stagnation point)	2.01669	1.39912

The vapor mass fraction in the mainstream (specified in each figure) was obtained via the experimentally observed dew point temperature, using the relation

$$\omega_{v,\infty} = \omega_v^{eq}(T_{dp})$$

valid in the absence of appreciable thermal (Soret) diffusion of Na_2SO_4 vapor (Rosner, 1980).

REPORT DOCUMENTATION PAGE

Form Approved
OMB No. 0704-0188

1. AGENCY USE ONLY (Leave blank)	2. REPORT DATE	3. REPORT TYPE AND DATES COVERED
	1989	Journal Publication

4. TITLE AND SUBTITLE

EQUILIBRIUM THEORY OF SURFACE DEPOSITION FROM PARTICLE-LADEN DILUTE, SATURATED VAPOR CONTAINING LAMINAR BOUNDARY LAYERS† (U)

5. FUNDING NUMBERS

PE - 61102F
PR - 2308
SA - BS
G -AFOSR 89-0223
AFOSR 84-0034

6. AUTHOR(S)

Jose L. Castillo and Daniel E. Rosner

7. PERFORMING ORGANIZATION NAME(S) AND ADDRESS(ES)

HIGH TEMPERATURE CHEMICAL REACTION ENGINEERING LABORATORY
YALE UNIVERSITY
BOX 2159, YALE STATION
NEW HAVEN, CONNECTICUT 06520 U.S.A.

8. PERFORMING ORGANIZATION REPORT NUMBER

9. SPONSORING/MONITORING AGENCY NAME(S) AND ADDRESS(ES)

AFOSR/NA
Building 410
Bolling AFB DC 20332-6448

10. SPONSORING/MONITORING AGENCY REPORT NUMBER

11. SUPPLEMENTARY NOTES

12a. DISTRIBUTION/AVAILABILITY STATEMENT

Approved for public release; distribution is unlimited

12b. DISTRIBUTION CODE

13. ABSTRACT (Maximum 200 words)

Abstract—Mass deposition rates on cooled solid surfaces exposed to saturated mainstreams containing a dispersed condensate aerosol are influenced by both the thermophoretic capture of such particles and the inevitable scavenging of vapor that takes place during their transit through the thermal boundary layer (BL). A tractable asymptotic theory is presented which allows total mass deposition rates to be predicted from such coupled two-phase boundary layers on the realizable assumptions that the dispersed condensate: (i) is captured predominantly as a result of thermophoresis down the prevailing temperature gradient, and (ii) is able to maintain the condition of local vapor–condensate phase equilibrium (LVCE) throughout the thermal BL. It is shown that under such circumstances the total mass deposition rate can be conveniently split into three additive contributions, the simplest being the vapor contribution, which can be computed (based on LVCE) without a knowledge of the condensate contributions. The latter can themselves be split into two calculable portions—one associated with the deposition rate of the mainstream particles computed in the (hypothetical) absence of vapor scavenging, and one associated with the amount of condensate scavenged from the vapor during the process of particle thermophoresis across the thermal BL. The present formulation applies to carrier gas–vapor–condensate systems of any Prandtl number (Pr), vapor Schmidt number, dilute condensate mass fraction, dimensionless condensate particle thermophoretic diffusivity, and heat of vaporization. Illustrative numerical results are presented here for high Reynolds number, $Pr = 0.7$ (air-like) streams in forward stagnation-point flow (two-dimensional and axisymmetric) or flat-plate flow, for absolute surface temperatures in the range $0.5 \leq T_w/T_\infty \leq 1.0$, over the interesting ranges of dimensionless thermophoretic diffusivities ($\alpha_T D_c/\nu$) and latent heats [$\Lambda/(RT_\infty)$].

14. SUBJECT TERMS

vapor deposition, condensation, dew point, boundary layers, heterogeneous nucleation

15. NUMBER OF PAGES
18

16. PRICE CODE

17. SECURITY CLASSIFICATION OF REPORT	18. SECURITY CLASSIFICATION OF THIS PAGE	19. SECURITY CLASSIFICATION OF ABSTRACT	20. LIMITATION OF ABSTRACT
Unclassified	Unclassified	Unclassified	UL

Chemical Engineering Science, Vol. 44, No. 4, pp. 939–956, 1989.
Printed in Great Britain.

0009-2509/89 $3.00+0.00

EQUILIBRIUM THEORY OF SURFACE DEPOSITION FROM PARTICLE-LADEN DILUTE, SATURATED VAPOR CONTAINING LAMINAR BOUNDARY LAYERS†

JOSE L. CASTILLO‡ and DANIEL E. ROSNER§
Department of Chemical Engineering, Yale University, New Haven, CT 06520, U.S.A.

(*First received* 10 *July* 1985; *accepted in revised form* 12 *September* 1988)

Abstract—Mass deposition rates on cooled solid surfaces exposed to saturated mainstreams containing a dispersed condensate aerosol are influenced by both the thermophoretic capture of such particles and the inevitable scavenging of vapor that takes place during their transit through the thermal boundary layer (BL). A tractable asymptotic theory is presented which allows total mass deposition rates to be predicted from such coupled two-phase boundary layers on the realizable assumptions that the dispersed condensate: (i) is captured predominantly as a result of thermophoresis down the prevailing temperature gradient, and (ii) is able to maintain the condition of local vapor–condensate phase equilibrium (LVCE) throughout the thermal BL. It is shown that under such circumstances the total mass deposition rate can be conveniently split into three additive contributions, the simplest being the vapor contribution, which can be computed (based on LVCE) without a knowledge of the condensate contributions. The latter can themselves be split into two calculable portions—one associated with the deposition rate of the mainstream particles computed in the (hypothetical) absence of vapor scavenging, and one associated with the amount of condensate scavenged from the vapor during the process of particle thermophoresis across the thermal BL. The present formulation applies to carrier gas–vapor–condensate systems of any Prandtl number (Pr), vapor Schmidt number, dilute condensate mass fraction, dimensionless condensate particle thermophoretic diffusivity, and heat of vaporization. Illustrative numerical results are presented here for high Reynolds number, $Pr=0.7$ (air-like) streams in forward stagnation-point flow (two-dimensional and axisymmetric) or flat-plate flow, for absolute surface temperatures in the range $0.5 \leqslant T_w/T_\infty \leqslant 1.0$, over the interesting ranges of dimensionless thermophoretic diffusivities ($\alpha_T D_c/\nu$) and latent heats [$\Lambda/(RT_\infty)$].

1. INTRODUCTION

1.1. *Motivation and applications*

The R and D needs of high-technology materials processors (e.g. micro-electronic circuit components) and energy conversion device manufacturers (to reduce fouling and/or corrosion for components exposed to combustion products containing both condensible vapors and particulate matter [see, for example, Stearns *et al.* (1983)] have stimulated recent advances in our understanding of the laws governing *vapor* deposition (VD) and *particle* deposition (PD) [summarized, for example, in Rosner (1985) and Rosner and Atkins (1983)]. However, until recently, little attention has been directed to more complex, but commonly encountered, situations in which particle deposition and vapor deposition *occur together and interact* owing to interphase exchange processes within the gas-side boundary layers adjacent to the deposition surface. An instructive class of examples, recently treated in Castillo and Rosner (1989) occurs even when the mainstream is *undersaturated* and apparently free of particles (other than condensation nucleii). When the deposition surface is cooled sufficiently far below the vapor dew point, condensation occurs within the thermal boundary layer (BL), forming an aerosol which modifies the local vapor composition distribution and which is itself "attracted" to the collector by the hitherto neglected mechanism of thermophoresis [see, for example, Kosner and Kim (1985) and Rosner and Fernandez de la Mora (1982)]. In the present case a closely related (limiting) case, also commonly encountered in practice, is treated, viz. that in which the mainstream is already saturated with respect to a dispersed condensate present in the noncondensible carrier gas at low mass fraction, $\omega_{c,\infty}$. The focus is on the thermophoretically augmented deposition rate of this condensate and the amount of *vapor it scavenges in the course of its migration through the thermal BL*. These processes will be shown to dramatically modify the surface temperature dependence of the total deposition rate for targets cooled below the prevailing vapor dew point. For the present, particles large enough to inertially "drift" relative to the decelerating gas/vapor mixture [see, for example, Rosner and Fernandez de la Mora (1982, 1984) and Rosner (1986)] were precluded from consideration. Thus, the influence of submicron condensate particles whose surface area per unit volume (of mixture) is large enough to alter the simultaneous process of vapor deposition is considered explicitly.

†Supported, in part, by DOE-METC (under Contract DE-AC21-85MC22075) and Air Force Office of Scientific Research (under Grant 84-0034).

‡Postdoctoral Research Scientist, High Temperature Chemical Reaction Engineering Laboratory. On leave of absence from Departamento de Fisica Fundamental, UNED, Apdo 60141, Madrid 28080, Spain.

§Professor, Department of Chemical Engineering and Director, High Temperature Chemical Reaction Engineering Laboratory. To whom correspondence should be addressed.

1.2. *Outline of present paper*

It might appear that for interacting VD–PD situations as complex as those outlined above, recourse must be made to full-scale experiments and/or ancillary numerical computations of very limited generality. However, by introducing a series of simplifying, but realizable asymptotic assumptions, the problem of calculating each contribution to the total deposition rate is reduced to a tractable and general form, quite suitable for future engineering design/optimization studies. The assumptions which allow this treatment are outlined in Section 2.1, along with brief comments about their domain of validity. The treatment of the host gas forced convection momentum and energy density fields for steady laminar BL flow (Sections 2.2 and 2.3) is similar to that recently given in Castillo and Rosner (1989), but is reproduced here in abbreviated form for completeness. At the heart of the analysis are the mass balance equations governing the interacting vapor and dispersed condensate density fields (Section 2.4), and their consequences with respect to the individual deposition rate contributions. While generally useful, formal *quadrature results* are derived, and numerical illustrations are provided in Section 3 based on the methods outlined in Section 3.1. In particular, tabular and graphical results are obtained and displayed covering the most important range of parameters governing surface temperature, type of flow field (stagnation point or flat plate), particle thermophoretic diffusivity, and dimensionless heat of vaporization $[\Lambda/(RT_\infty)]$. The principal theoretical conclusions and their engineering implications are given in Section 4, which completes the present paper. Experiments are currently underway in the author's laboratory to verify some of these conclusions in well-characterized, seeded combustion gas situations [see, for example, Rosner and Atkins (1983), Rosner and Kim (1985) and Rosner and Liang (1986)], but at lower Reynolds numbers.

2. THERMOPHYSICAL MODEL AND GOVERNING EQUATIONS

2.1. *Underlying assumptions*

To simplify the problem and, at the same time, retain its most important characteristics, the following assumptions will be made:

(A1) The total amount of condensible material is very small compared to the amount of noncondensible (host or "carrier") gas. Thus, the host gas velocity and temperature fields are not appreciably affected by physical processes that the relatively small amount of condensible material undergoes (condensation, deposition).

(A2) The gas mixture flow is steady and laminar. The usual large Reynolds number BL approximations and self-similarity are exploited [see, for example, Schlichting (1968)].

(A3) Transport properties of the gas (momentum and heat diffusivities) are considered constant and equal to their values for the carrier gas under, say, local mainstream conditions. Also, the mass transport properties of the vapor (Fick diffusion coefficient) and condensate particles (thermophoretic coefficient) will be considered constant. Last, the total mixture will be considered incompressible, i.e. the total density is taken to be constant.

(A4) Thermal diffusion (Soret effect) will be neglected for the vapor. Thus, the difference between the velocities of the carrier gas and condensible vapor is due only to the Fick diffusion flux of the dilute vapor down its own concentration gradient.

(A5) Condensate particles exhibit no appreciable Brownian diffusion, i.e. the difference between the velocity of the condensate and the carrier gas is due only to a thermophoretic velocity of the condensate particles. At each position in the thermal BL this thermophoretic "drift" velocity will be taken as the one corresponding to an isolated particle in a uniform gas with the same temperature gradient [see, for example, Talbot (1981)], i.e.

$$\mathbf{v}_T = \alpha_T D_c [-(\mathbf{grad}\, T)/T] \qquad (2.1\text{-}1)$$

where α_T is a dimensionless "thermal diffusion factor". Actually, the dispersed condensate Brownian diffusivity D_c is included here just to emphasize the similarity between eq. (2.1-1) and a diffusion velocity, but the value of the "thermophoretic diffusivity" $\alpha_T D_c$ does not really depend on D_c (which, in effect, is taken to be zero in the analysis which follows). Rather, $\alpha_T D_c$ depends on the carrier gas *momentum* diffusivity, particle Knudsen number and particle/gas thermal conductivity ratio; being $\alpha_T D_c \simeq 0.54\nu$, irrespective of particle radius for particles whose radius is much smaller than the prevailing mean free path (of the carrier gas molecules) (Talbot, 1981). This remarkably simple limiting case provides a useful first approximation for $\alpha_T D_c$, and motivates the introduction of the parameter $\alpha (\equiv \alpha_T D_c/\nu)$ in the analysis which follows.

(A6) Whenever vapor and condensate particles coexist they are in mutual thermodynamic equilibrium.† This is equivalent to requiring that the characteristic condensate residence time is much larger than that required for such a (perturbed) two-phase dispersed system to (re)attain vapor–liquid (or vapor–solid) equilibrium. Making this asymptotic approximation frees one from the need to speculate about the condensation kinetics. Furthermore, for simplicity, the equilibrium vapor pressure over a small condensate particle (liquid droplet or solid particle) is taken to be the same as over a flat condensate layer at the same temperature (i.e. the so-called "Kelvin effect" will be neglected). Therefore, in what follows there is no need to be concerned with the size (or number density) of condensate particles, but only with the local *amount* of condensible material in each phase (vapor and condensate particles).

† See Castillo and Rosner (1988) for validity criteria of this assumption.

(A7) The condensible vapor behaves like an ideal gas, even when a dispersed condensate phase is also present. As a result of the abovementioned assumptions, the amount of condensible material in the vapor phase is fixed by the equilibrium value over a flat condensate surface at the local temperature, i.e.

$$\omega_v = \omega_v^{eq}(T) = \frac{1}{\rho}\frac{p_v^{eq}(T)M_v}{RT} \qquad (2.1\text{-}2)$$

which depends only on local temperature {for ρ = constant, as assumed [assumption (A3)]}. In what follows, the temperature dependence of p_v^{eq} will be written in the two-parameter Clausius–Clapeyron form:

$$p_v^{eq}(T) = \exp\left(\gamma - \frac{\Lambda}{RT}\right). \qquad (2.1\text{-}3)$$

2.2. *Host (carrier) gas flow field (wedge flow)*

The inviscid (external solution) velocity distribution corresponding to the flow past a symmetrical wedge (Fig. 1) of included angle $\pi\beta$ is given by

$$u_e(x) = ax^m \qquad (2.2\text{-}1)$$

where $\beta = 2m/(m+1)$, and a is a constant. Two-dimensional flow in the vicinity of a stagnation line, as well as the flow external to a thin BL on a flat plate at zero incidence, are particular cases of "wedge-flows", the former for $\beta = 1$ (i.e. $m = 1$), the latter for $\beta = 0$ (i.e. $m = 0$). Moreover, the special case of $\beta = \frac{1}{2}$ ($m = \frac{1}{3}$) can easily be transformed into the rotationally (axi-)symmetrical flow near a forward stagnation point [see, for example, Schlichting (1968, p. 150)].

As in any two-dimensional motion of a Newtonian fluid, the Prandtl BL equations can be written

$$u\frac{\partial u}{\partial x} + v\frac{\partial u}{\partial y} = u_e\frac{du_e}{dx} + \nu\frac{\partial^2 u}{\partial y^2} \qquad (2.2\text{-}2)$$

$$\frac{\partial u}{\partial x} + \frac{\partial v}{\partial y} = 0 \qquad (2.2\text{-}3)$$

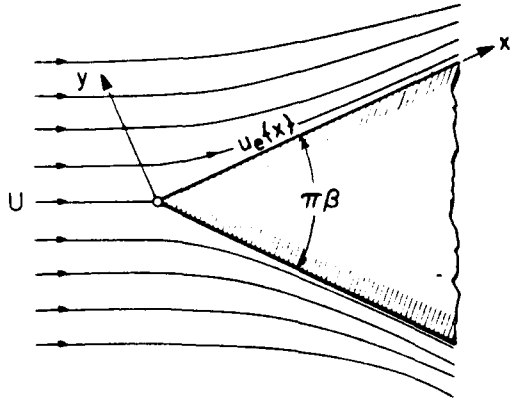

Fig. 1. Steady, nearly incompressible flow of a saturated, condensate-carrying gas past a cooled, solid wedge of opening angle $\pi\beta$; $Re_x^{1/2} \gg 1$.

with boundary conditions $u = 0$ (no slip) and $v = 0$ (no blowing) along the surface $y = 0$, and $u = u_e(x)$ at $y = \infty$.

A similarity variable $\eta(x, y)$ which allows the transformation of these equations to an *ordinary* differential equation (ODE) is

$$\eta = \frac{y}{x}\left(\frac{u_e x}{\nu}\right)^{1/2} = y(ax^{m-1}/\nu)^{1/2}. \qquad (2.2\text{-}4)$$

The local mass balance equation [eq. (2.2-3)] is automatically satisfied by the introduction of a stream function of the form

$$\psi(x, y) = (\nu a x^{m+1})^{1/2} f(\eta). \qquad (2.2\text{-}5)$$

Thus, the carrier fluid velocity components become

$$u = \partial\psi/\partial y = ax^m f'(\eta) = u_e f'(\eta). \qquad (2.2\text{-}6)$$

$$v = -\partial\psi/\partial x = -\frac{m+1}{2}(\nu a x^{m-1})^{1/2}\left(f + \frac{m-1}{m+1}\eta f'\right) \qquad (2.2\text{-}7)$$

where primes denote differentiation with respect to η. Introducing these expressions into the x-momentum balance equation [eq. (2.2-2)] the following well-known third-order nonlinear ODE for $f(\eta)$ is obtained:

$$f''' + \frac{m+1}{2}ff'' + m(1 - f'^2) = 0 \qquad (2.2\text{-}8)$$

with the "split" boundary conditions

$$f = 0, \quad f' = 0 \quad \text{at } \eta = 0 \qquad (2.2\text{-}9)$$

$$f' = 1 \quad \text{at } \eta = \infty. \qquad (2.2\text{-}10)$$

An important consequence of the assumptions (constant thermophysical properties and low vapor/condensed material mass fraction) is that the carrier gas momentum density (velocity) field can be found without considering the corresponding temperature and composition fields. Indeed, use will be made of tabular values of the dimensionless stream function $f(\eta)$ [see, for example, Schlichting (1968)] in computing all integrals which appear in the solutions for the corresponding temperature and composition fields.

2.3. *Temperature field*

In the steady state, using BL approximations (A2) and (A3), the partial differential equation which governs the temperature distribution $T(x, y)$ when $T_w < T_\infty$ is

$$u\frac{\partial T}{\partial x} + v\frac{\partial T}{\partial y} = \alpha_h\frac{\partial^2 T}{\partial y^2} \qquad (2.3\text{-}1)$$

α_h being the thermal (heat) diffusivity. Defining

$$\theta \equiv \frac{T}{T_\infty} \qquad (2.3\text{-}2)$$

when the wall temperature is held constant, θ admits a self-similar solution with the ODE for $\theta(\eta)$ becoming

$$\theta'' + \frac{m+1}{2} Pr\, f\theta' = 0 \qquad (2.3\text{-}3)$$

where Pr is the Prandtl number ($Pr = \nu/\alpha_h$) and the abovementioned dimensionless stream function appears as a coefficient in the convective term. The boundary conditions on $\theta(\eta)$ are clearly

$$\theta(0) \equiv \theta_w = T_w/T_\infty;\ \theta(\infty) = 1. \qquad (2.3\text{-}4)$$

The solution to eq. (2.3-3) can be written in the following *quadrature form* [see, for example, Spalding and Evans (1961)]:

$$\theta(\eta) = \theta_w + (1-\theta_w)\frac{1}{\delta}\int_0^\eta \exp\left[-\frac{m+1}{2} Pr \times \int_0^\phi f(\xi)\,d\xi\right] d\phi \qquad (2.3\text{-}5)$$

with

$$\delta \equiv \int_0^\infty \exp\left[-\frac{m+1}{2} Pr \int_0^\phi f(\xi)\,d\xi\right] d\phi. \qquad (2.3\text{-}6)$$

For a description of the computation of δ (needed, for example, to determine the local wall heat flux) see Castillo and Rosner (1989, Section 3.1).

2.4. *Mass fraction equations and deposition rates*

Under assumptions (A1)–(A5), the coupled BL equations for the mass fractions of condensible material in the vapor phase ($\omega_v = \rho_v/\rho$) and in the condensate phase ($\omega_c = \rho_c/\rho$) can be written (Castillo and Rosner, 1989) as

$$u\frac{\partial \omega_v}{\partial x} + v\frac{\partial \omega_v}{\partial y} = D_v\frac{\partial^2 \omega_v}{\partial y^2} - \frac{\dot r'''}{\rho} \qquad (2.4\text{-}1)$$

and

$$u\frac{\partial \omega_c}{\partial x} + (v+v_T)\frac{\partial \omega_c}{\partial y} = -\omega_c\frac{\partial v_T}{\partial y} + \frac{\dot r'''}{\rho} \qquad (2.4\text{-}2)$$

where v_T is the y-component of the condensate particle's thermophoretic velocity [given by eq. (2.1-1)] and $\dot r'''$ denotes the mass of vapor that is locally transforming into condensate phase per unit time and volume.

Under assumption (A2), ω_v and ω_c depend on x and y only through the similarity variable η. Therefore, using eqs (2.2-4), (2.2-6) and (2.2-7) in eqs (2.4-1) and (2.4-2), it is found that $\omega_v(\eta)$ satisfies the second-order ODE

$$\frac{d^2\omega_v}{d\eta^2} + \frac{m+1}{2} Sc f\frac{d\omega_v}{d\eta} = \dot\omega'''\, Sc \qquad (2.4\text{-}3)$$

whereas $\omega_c(\eta)$ satisfies the coupled but linear *first-order* ODE

$$A\frac{d\omega_c}{d\eta} + B\omega_c = -\dot\omega'''. \qquad (2.4\text{-}4)$$

In these equations the Schmidt number ($Sc = \nu/D_v$) and the functions

$$\dot\omega'''(\eta) \equiv \frac{\dot r'''(x,y)}{\rho u_e(x)}x \qquad (2.4\text{-}5)$$

$$A(\eta) \equiv \frac{m+1}{2} f + \frac{\alpha}{\theta}\frac{d\theta}{d\eta} \qquad (2.4\text{-}6)$$

$$B(\eta) \equiv -\frac{\alpha}{\theta}\frac{d\theta}{d\eta}\left(\frac{m+1}{2} Pr\, f + \frac{1}{\theta}\frac{d\theta}{d\eta}\right) \qquad (2.4\text{-}7)$$

where α is the nondimensional thermophoretic coefficient for the dispersed condensate:

$$\alpha \equiv \alpha_T D_c/\nu \qquad (2.4\text{-}8)$$

have been introduced.

As mentioned above, the interest here is in the case when far from the wall the gas is already saturated with respect to the condensible vapor [i.e. $\omega_{v,\infty} = \omega_v^{eq}(T_\infty)$] and condensate particles already exist in the mainstream [$\omega_c(\eta\to\infty) = \omega_{c,\infty}$]. Now consider that such a mixture flows past a surface maintained at a temperature, T_w, lower than T_∞ (i.e. $\theta_w \equiv T_w/T_\infty < 1$). Since the ODE for $\omega_c(\eta)$ [eq. (2.4-4)] is linear the solution ω_c can be split into two different contributions. The first is ω_c^0, which describes the evolution inside the boundary layer of the preexisting condensate particles as if they were not interacting with the vapor phase [therefore, ω_c^0 must satisfy eq. (2.4-4) with $\dot\omega'''$ set equal to zero (i.e. ω_c^0 is the solution of the "homogeneous" ODE and its boundary condition is $\omega_{c,\infty}^0 = \omega_{c,\infty}$)]. The second contribution (ω_c^v) takes into account the vapor scavenging that occurs by the particles as they drift across the thermal BL. Its boundary condition is $\omega_{c,\infty}^v = 0$ [i.e. ω_c^v is a particular solution of the inhomogeneous eq. (2.4-4)].

To reduce the number of parameters in this problem and thereby facilitate the presentation of general results (Section 3), define

$$\Omega_v \equiv \frac{\omega_v}{\omega_{v,\infty}} = \frac{\rho_v}{\rho_{v,\infty}} = \frac{\omega_v}{\omega_v^{eq}(T_\infty)} \qquad (2.4\text{-}9)$$

$$\Omega_c^v \equiv \frac{\omega_c^v}{\omega_{v,\infty}} \qquad (2.4\text{-}10)$$

$$\Omega_c^0 \equiv \frac{\omega_c^0}{\omega_{c,\infty}}. \qquad (2.4\text{-}11)$$

Note that both Ω_v and Ω_c^v are normalized with respect to $\omega_{v,\infty}$, whereas $\omega_{c,\infty}$ is used in Ω_c^0, emphasizing in this way their respective origins.

The ODEs governing these new dependent variables are [from eqs (2.4-3) and (2.4-4)], respectively:

$$\frac{d^2\Omega_v}{d\eta^2} + \frac{m+1}{2} Sc f\frac{d\Omega_v}{d\eta} = Sc\,\dot\Omega''' \qquad (2.4\text{-}12)$$

$$A\frac{d\Omega_c^v}{d\eta} + B\Omega_c^v = -\dot\Omega''' \qquad (2.4\text{-}13)$$

$$A\frac{d\Omega_c^0}{d\eta} + B\Omega_c^0 = 0. \qquad (2.4\text{-}14)$$

According to the vapor–condensate thermodynamic equilibrium assumption [assumption (A6)] $\omega_v(\eta) = \omega_v^{eq}(T(\eta))$; therefore, using eqs (2.1-2) (2.1-3) and (2.3-2):

$$\Omega_v = \Omega_v^{eq}(\theta(\eta)) = \frac{1}{\theta}\exp\left[\mathscr{L}\left(1-\frac{1}{\theta}\right)\right] \quad (2.4\text{-}15)$$

where

$$\mathscr{L} \equiv \Lambda/(RT_\infty). \quad (2.4\text{-}16)$$

Using eq. (2.4-15) in eq. (2.4-12):

$$\dot{\Omega}'''(\eta) = \dot{\Omega}_1'''(\eta) + \frac{1}{Sc}\dot{\Omega}_2'''(\eta) \quad (2.4\text{-}17)$$

where

$$\dot{\Omega}_1''' \equiv \frac{m+1}{2} f \frac{d\Omega_v^{eq}}{d\theta}\frac{d\theta}{d\eta} \quad (2.4\text{-}18)$$

and

$$\dot{\Omega}_2''' \equiv \frac{d^2\Omega_v^{eq}}{d\theta^2}\left(\frac{d\theta}{d\eta}\right)^2 - Pr\,\dot{\Omega}_1'''. \quad (2.4\text{-}19)$$

Then, the solution of eq. (2.4-13) with boundary condition $\Omega_c^v(\eta\to\infty) = 0$ can be written as

$$\Omega_c^v = \int_\eta^\infty \frac{\dot{\Omega}'''(\phi)}{A(\phi)}\exp\left[-\int_\eta^\phi \frac{B(\xi)}{A(\xi)}d\xi\right]d\phi \quad (2.4\text{-}20)$$

and the solution of eq. (2.4-14) with boundary condition $\Omega_{c,\infty}^0 = 1$ can be written as

$$\Omega_c^0 = \exp\left[\int_\eta^\infty \frac{B(\phi)}{A(\phi)}d\phi\right] \quad (2.4\text{-}21)$$

where the functions A and B have been given in eq. (2.4-6) and eq. (2.4-7), respectively, and $\dot{\Omega}'''$ is given by eq. (2.4-17).

The main interest here is in the mass *deposition rate* of vapor and condensate particles on the "cold" wall. The local mass deposition rate of condensible material *in vapor form* is

$$-j_{v,w}''(x) = \rho D_v\left(\frac{\partial\omega_v}{\partial y}\right)\Big|_{y=0} = \frac{\rho\omega_{v,\infty}}{Sc}\left(\frac{u_e v}{x}\right)^{1/2}\frac{d\Omega_v}{d\eta}\Big|_{\eta=0} \quad (2.4\text{-}22)$$

In contrast, the mass deposition rate of the condensate particles is

$$-j_{c,w}''(x) = -\rho_c v_T|_{y=0} = \rho\left(\frac{u_e v}{x}\right)^{1/2}\frac{1-\theta_w}{\delta\theta_w}\alpha(\omega_{v,\infty}\Omega_c^v + \omega_{c,\infty}\Omega_c^0)_{\eta=0}. \quad (2.4\text{-}23)$$

A kind of (modified) *mass transfer Stanton number* for the vapor is now defined, i.e.

$$St_{m,v} \equiv \frac{-j_{v,w}''}{\rho u_e \omega_{v,\infty}}. \quad (2.4\text{-}24)$$

Using eqs (2.4-15), (2.3-5) and (2.4-22):

$$St_{m,v} = Re_x^{-1/2}\frac{1-\theta_w}{Sc\,\delta\theta_w^2}\left(\frac{\mathscr{L}}{\theta_w}-1\right)\exp\left[\mathscr{L}\left(1-\frac{1}{\theta_w}\right)\right]. \quad (2.4\text{-}25)$$

Note that the present $St_{m,v}$ can easily be calculated once the parameters Sc, θ_w, $\mathscr{L}$ and $\delta(m, Pr)$ are specified. Since the deposition rate contribution due to the condensate particles is split into two parts, the dimensionless transfer coefficients are now defined:

$$St_{m,c}^v \equiv \frac{-j_{c,w}''^v}{\rho u_e \omega_{v,\infty}} \quad (2.4\text{-}26)$$

and

$$St_{m,c}^0 \equiv \frac{-j_{c,w}''^0}{\rho u_e \omega_{c,\infty}} \quad (2.4\text{-}27)$$

where $j_{c,w}''^0$ and $j_{c,w}''^v$ are contained in eq. (2.4-23). Accordingly

$$St_{m,c}^v = Re_x^{-1/2}\frac{1-\theta_w}{\delta\theta_w}\alpha\,\Omega_c^v\Big|_{\eta=0} \quad (2.4\text{-}28)$$

and

$$St_{m,c}^0 = Re_x^{-1/2}\frac{1-\theta_w}{\delta\theta_w}\alpha\exp\left[\int_0^\infty \frac{B(\phi)}{A(\phi)}d\phi\right]. \quad (2.4\text{-}29)$$

Note that these are not conventional mass transfer Stanton numbers {which are normally referred to the mass fraction *difference* "driving force" $(\omega_\infty - \omega_w)$ [cf., for example, Rosner (1986)]} but in the present case the above definitions are, in fact, more useful. Note also that $St_{m,v}$ and $St_{m,c}^v$ are referred to $\omega_{v,\infty}$, whereas $St_{m,c}^0$ is referred to $\omega_{c,\infty}$. Finally, the dependence of $St_{m,c}^v$ on the Schmidt number Sc can be explicitly extracted by defining

$$St_{m,c}^v = Re_x^{-1/2}\left(\mathscr{J}_1 + \frac{1}{Sc}\mathscr{J}_2\right) \quad (2.4\text{-}30)$$

Here

$$\mathscr{J}_i = \frac{1-\theta_w}{\delta\theta_w}\alpha\int_0^\infty \frac{\dot{\Omega}_i'''(\phi)}{A(\phi)}\times\exp\left[-\int_0^\phi \frac{B(\xi)}{A(\xi)}d\xi\right]d\phi \quad (2.4\text{-}31)$$

with $\dot{\Omega}_1'''$ given by eq. (2.4-18) and $\dot{\Omega}_2'''(\phi)$ by eq. (2.4-19).

Summarizing, in the present case:

$St_{m,v}\,Re_x^{1/2}$ = function $(m, Pr, Sc, \mathscr{L}, \theta_w)$ given by eq. (2.4-25) with the dependence on m and Pr through the value of δ,

$St_{m,c}^v\,Re_x^{1/2} = \mathscr{J}_1(m, Pr, \alpha, \mathscr{L}, \theta_w) + (1/Sc)\,\mathscr{J}_2(m, Pr, \alpha, \mathscr{L}, \theta_w)$ with $\mathscr{J}_i$ given by eq. (2.4-31), and

$St_{m,c}^0\,Re_x^{1/2}$ = function $(m, Pr, \alpha, \theta_w)$ given by eq. (2.4-29).

The computation of these functions is the subject of Section 3.

3. RESULTS AND DISCUSSION

3.1. *Numerical method*

Because of their practical importance the focus here is on the particular cases $m=0, \frac{1}{3}$ and 1, for which the dimensionless stream function f is well known and tabulated [e.g. in Schlichting (1968)]. When the value of f was required at a "nontabulated value" of η, it was calculated from a Taylor-series expansion using the tabulated values of f, f' and f'', and the corresponding value of f''' from the ODE (2.2-8), at the closest tabulated value of η.

In this paper all indicated integrals were numerically calculated using Simpson's algorithm. Although the integrals in eqs (2.4-29) and (2.4-31) extend from $\eta=0$ to $\eta=\infty$, in both cases the integrand is vanishingly small outside the thermal BL. Accordingly, these integrals were carried out by starting at $\eta=0$ and ending at the outer edge of the thermal BL, estimated via $\eta_{x,\mathrm{th}} \cong \eta_{x,\mathrm{mom}}/Pr^{1/2}$. Here $\eta_{x,\mathrm{mom}}$ is the outer edge of the momentum diffusion BL [the position at which $f'=1-\varepsilon$, where $\varepsilon(\ll 1)$ is the required precision]; on the other hand, at $\eta_{x,\mathrm{th}}$, $\theta=1-\varepsilon$, which was used as a test in the program.

The most important cases are those for which the carrier gas is essentially air (perhaps containing combustion products) and therefore the Prandtl number was fixed at the value $Pr=0.7$. For this Pr the δ values given by eq. (2.3-6) are (Castillo and Rosner, 1989):

$$\delta(m=0)=3.41669$$
$$\delta(m=\tfrac{1}{3})=2.60279$$
$$\delta(m=1)=2.01669. \qquad (3.1\text{-}1)$$

These values are required for $\mathrm{d}\theta/\mathrm{d}\eta|_{\eta=0}$ and to start the integrations. All numerical results presented below are for $Pr=0.7$.

Comments have already been made on the rationale for the ranges of θ_w ($\equiv T_w/T_\infty$) and α ($\equiv \alpha_T D_c/\nu$) covered in this paper. To this it should be added that since the main interest is in deposition of inorganic (alkali-containing) vapors from combustion products, with T_∞ values of about 1500 K, the value of $\mathscr{L} \equiv \Lambda/(RT_\infty)$] defined by eq. (2.4-16) is $\simeq 22$ (for Na_2SO_4) 19 for K_2SO_4, and 14 for NaCl. Accordingly, the range of $\mathscr{L}$ covered is from 10 to 30.

3.2. *Mass deposition rate of "noninteracting" particles*

As mentioned in Section 2.4, $St^0_{m,c}$ represents the deposition rate of the preexisting condensate particles as if they did not interact with the prevailing condensible vapor. Therefore, it also provides the deposition rate of any kind of particle for which assumption (A5) is valid, with the thermophoretic parameter constant through the laminar BL [cf. Goren (1977) and Gökoğlu and Rosner (1985)].

Numerical values of $St^0_{m,c}\,Re_x^{1/2}/\alpha$ are given in Table 1 (for $m=0$), Table 2 ($m=\frac{1}{3}$) and Table 3 ($m=1$), for three different values of α: $\alpha=0.5$ (close to the corresponding theoretical limit for particles in the free-molecule regime), $\alpha=0.1$ [which appears (Castillo and Rosner, 1989) to provide a good estimate for experimentally observed deposition rates of Na_2SO_4 condensate particles], and a lower value of $\alpha=0.01$ (which might describe the behavior of high-conductivity condensate particles in the near-continuum limit).

Table 1. Numerical values of the preexisting condensate particle mass transfer coefficient $St^0_{m,c}\,Re_x^{1/2}/\alpha$ as a function of the normalized wall temperature θ_w ($\equiv T_w/T_\infty$) for three different values of the condensate thermophoretic parameter α ($\equiv \alpha_T D_c/\nu$), for flat-plate collector ($m=0$)

θ_w	$\alpha=0.5$	$\alpha=0.1$	$\alpha=0.01$
0.98	5.925E−3	5.960E−3	5.971E−3
0.96	1.198E−2	1.213E−2	1.218E−2
0.94	1.818E−2	1.853E−2	1.865E−2
0.92	2.450E−2	2.515E−2	2.538E−2
0.90	3.095E−2	3.200E−2	3.240E−2
0.88	3.753E−2	3.909E−2	3.971E−2
0.86	4.424E−2	4.644E−2	4.734E−2
0.84	5.108E−2	5.404E−2	5.530E−2
0.82	5.805E−2	6.192E−2	6.362E−2
0.80	6.516E−2	7.007E−2	7.232E−2
0.75	8.349E−2	9.176E−2	9.587E−2
0.70	1.027E−1	1.155E−1	1.224E−1
0.65	1.227E−1	1.415E−1	1.524E−1
0.60	1.436E−1	1.699E−1	1.866E−1
0.55	1.654E−1	2.013E−1	2.259E−1
0.50	1.882E−1	2.358E−1	2.713E−1

Table 2. Numerical values of the preexisting condensate particle mass transfer coefficient $St^0_{m,c}\,Re_x^{1/2}/\alpha$ as a function of the normalized wall temperature θ_w ($\equiv T_w/T_\infty$) for three different values of the condensate thermophoretic parameter α ($\equiv \alpha_T D_c/\nu$), for an axisymmetric stagnation point ($m=\frac{1}{3}$)

θ_w	$\alpha=0.5$	$\alpha=0.1$	$\alpha=0.01$
0.98	7.778E−3	7.825E−3	7.838E−3
0.96	1.574E−2	1.593E−2	1.600E−2
0.94	2.387E−2	2.433E−2	2.449E−2
0.92	3.219E−2	3.304E−2	3.333E−2
0.90	4.067E−2	4.205E−2	4.255E−2
0.88	4.934E−2	5.138E−2	5.216E−2
0.86	5.818E−2	6.106E−2	6.220E−2
0.84	6.719E−2	7.108E−2	7.267E−2
0.82	7.639E−2	8.147E−2	8.362E−2
0.80	8.576E−2	9.223E−2	9.507E−2
0.75	1.100E−1	1.209E−1	1.261E−1
0.70	1.354E−1	1.524E−1	1.611E−1
0.65	1.620E−1	1.869E−1	2.008E−1
0.60	1.898E−1	2.250E−1	2.462E−1
0.55	2.189E−1	2.669E−1	2.983E−1
0.50	2.494E−1	3.133E−1	3.589E−1

Note that from eq. (2.4-29) it is clear that

$$\frac{\partial}{\partial\theta_w}\left(St^0_{m,c}\,Re_x^{1/2}/\alpha\right)\bigg|_{\theta_w=1} = -\frac{1}{\delta}. \qquad (3.2\text{-}1)$$

On the other hand, in the very special case when $\alpha\,Pr=1$, it can be shown that

$$St^0_{m,c} \simeq Re_x^{-1/2}\frac{1-\theta_w}{\delta}\,\alpha \quad (\alpha\,Pr=1). \qquad (3.2\text{-}2)$$

Table 3. Numerical values of the preexisting condensate particle mass transfer coefficient $St^0_{m,c}\,Re_x^{1/2}/\alpha$ as a function of the normalized wall temperature θ_w ($\equiv T_w/T_\infty$) for three different values of the condensate thermophoretic parameter α ($\equiv \alpha_T D_c/\nu$), for a two-dimensional (planar) stagnation line collector ($m=1$)

θ_w	$\alpha=0.5$	$\alpha=0.1$	$\alpha=0.01$
0.98	1.004E−2	1.010E−2	1.012E−2
0.96	2.031E−2	2.057E−2	2.064E−2
0.94	3.082E−2	3.141E−2	3.160E−2
0.92	4.155E−2	4.265E−2	4.302E−2
0.90	5.252E−2	5.429E−2	5.492E−2
0.88	6.371E−2	6.635E−2	6.733E−2
0.86	7.514E−2	7.885E−2	8.028E−2
0.84	8.679E−2	9.180E−2	9.380E−2
0.82	9.868E−2	1.052E−1	1.079E−1
0.80	1.108E−1	1.192E−1	1.227E−1
0.75	1.422E−1	1.563E−1	1.628E−1
0.70	1.751E−1	1.971E−1	2.081E−1
0.65	2.096E−1	2.419E−1	2.594E−1
0.60	2.457E−1	2.913E−1	3.181E−1
0.55	2.835E−1	3.459E−1	3.858E−1
0.50	3.231E−1	4.064E−1	4.644E−1

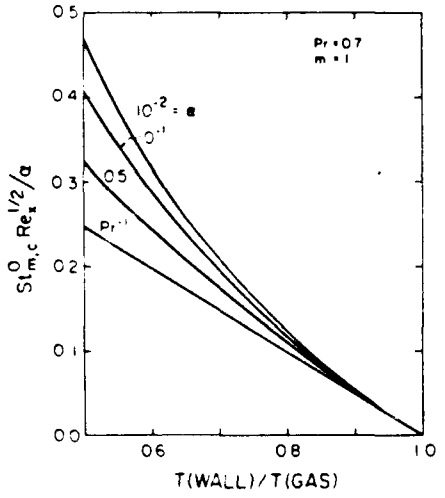

Fig. 2. Surface temperature dependence of the pre-existing condensate mass transfer coefficient $St^0_{m,c}\,Re_x^{1/2}/\alpha$ for different values of the condensate thermophoretic parameter α ($\equiv \alpha_T D_c/\nu$). Conditions: $Pr=0.7$, two-dimensional (planar) stagnation line ($m=1$).

In Fig. 2, the values of Table 3 together with the straight line corresponding to eq. (3.2-2) are plotted. It is observed that all cases tend to the slope given by eq. (3.2-1) when the wall temperature ratio θ_w tends to unity, in such a way that eq. (3.2-2) provides a good first approximation to $St^0_{m,c}$ for any value of α when θ_w is sufficiently close to the unity. When θ_w departs substantially from unity (i.e. for a highly cooled wall), $St^0_{m,c}$ is appreciably larger than the value given by eq. (3.2-2) (the opposite will be true for the hypothetical case $\alpha\,Pr>1$). It should be cautioned that while these are formally computed cases with θ_w as low as 0.5 (i.e. $T_w=\frac{1}{2}T_\infty$) the present results should be corrected for the inevitable effects of variable thermophysical properties which would not be negligible for temperature ratios so far from unity [see, for example, Gökoğlu and Rosner (1984b)].

3.3. *Deposition rate of the scavenged vapor*

The mass deposition rate (via condensate) of the vapor scavenged by the particles on their way through the thermal BL is described by $St^v_{m,c}$ [eq. (2.4-30)]. It is interesting to note that

$$\frac{\partial}{\partial\theta_w}(St^v_{m,c})\bigg|_{\theta_w=1}=0 \qquad (3.3\text{-}1)$$

i.e. $St^v_{m,c}$ starts at $\theta_w=1$ with zero slope.

Numerical values of $\mathcal{J}_1$ and $\mathcal{J}_2$ (describing the two parts of $St^v_{m,c}\,Re_x^{1/2}$ [cf. eq (2.4-31)] are given in Tables 4–6 [$m=0$ for $\alpha=0.5$ (Table 4), $\alpha=0.1$ (Table 5) and $\alpha=0.01$ (Table 6), respectively], Tables 7–9 ($m=\frac{1}{3}$ and the same values of α) and Tables 10–12 ($m=1$), for five different values of the heat-of-evaporation parameter $\mathcal{L}$ [$\equiv\Lambda/(RT_\infty)$]. Moreover, using the numerical values reported in Table 6, $St^v_{m,c}\,Re_x^{1/2}$ is plotted in Fig. 3 for $Sc=2$, using eq. (2.4-30). Note that for θ_w close to unity, $St^v_{m,c}$ increases with $\mathcal{L}$, whereas the opposite is true for lower values of θ_w. This is due to the different behavior of $\mathcal{J}_1$ and $\mathcal{J}_2$, as can be observed in Tables 4–12. Thus, for a given value of the thermophoretic diffusivity parameter α, $\mathcal{J}_1$ is always an increasing function of $\mathcal{L}$. In contrast, the contribution $\mathcal{J}_2$ increases with $\mathcal{L}$ for θ_w close to unity, but decreases as $\mathcal{L}$ increases for lower values of θ_w.

3.4. *Total deposition due to the presence of vapor in the mainstream*

Although $St^v_{m,c}$ measures a contribution to the deposition rate associated with the transport of con-

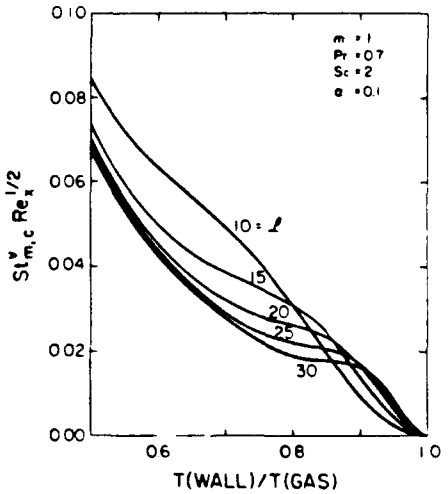

Fig. 3. Surface temperature dependence of the scavenged vapor deposition contribution $St^v_{m,c}\,Re_x^{1/2}$ for different values of the parameter $\mathcal{L}$. Conditions: $Pr=0.7$, $Sc=2$, $\alpha=0.1$, $m=1$.

Table 4. Numerical values of $\mathcal{J}_1$ (upper number) and $\mathcal{J}_2$ (lower number) defined by eq. (2.4-31) as functions of the normalized wall temperature θ_w ($\equiv T_w/T_\infty$) for a flat-plate collector ($m=0$), $\alpha=0.5$ and stated values of the parameter $\mathcal{L}$ [$\equiv \Lambda/(RT_\infty)$]

θ_w	$\mathcal{L}=10$	$\mathcal{L}=15$	$\mathcal{L}=20$	$\mathcal{L}=25$	$\mathcal{L}=30$
0.98	4.649E−4 2.274E−4	6.908E−4 8.688E−4	8.964E−4 1.747E−3	1.083E−3 2.785E−3	1.254E−3 3.918E−3
0.96	1.734E−3 1.636E−3	2.472E−3 4.619E−3	3.085E−3 8.031E−3	3.595E−3 1.140E−2	4.019E−3 1.446E−2
0.94	3.679E−3 4.607E−3	5.050E−3 1.106E−2	6.092E−3 1.720E−2	6.885E−3 2.212E−2	7.489E−3 2.555E−2
0.92	6.211E−3 9.151E−3	8.238E−3 1.929E−2	9.648E−3 2.708E−2	1.063E−2 3.175E−2	1.133E−2 3.365E−2
0.90	9.265E−3 1.510E−2	1.191E−2 2.830E−2	1.360E−2 5.609E−2	1.469E−2 3.880E−2	1.540E−2 3.798E−2
0.88	1.280E−2 2.220E−2	1.599E−2 3.725E−2	1.787E−2 4.334E−2	1.900E−2 4.299E−2	1.968E−2 3.924E−2
0.86	1.677E−2 3.013E−2	2.043E−2 4.549E−2	2.243E−2 4.854E−2	2.355E−2 4.478E−2	2.420E−2 3.855E−2
0.84	2.118E−2 3.857E−2	2.523E−2 5.262E−2	2.728E−2 5.180E−2	2.837E−2 4.487E−2	2.898E−2 3.695E−2
0.82	2.601E−2 4.720E−2	3.037E−2 5.844E−2	3.245E−2 5.347E−2	3.350E−2 4.399E−2	3.408E−2 3.517E−2
0.80	3.127E−2 5.575E−2	3.588E−2 6.292E−2	3.796E−2 5.397E−2	3.898E−2 4.272E−2	3.953E−2 3.364E−2
0.75	4.645E−2 7.528E−2	5.150E−2 6.921E−2	5.357E−2 5.288E−2	5.457E−2 4.017E−2	5.512E−2 3.191E−2
0.70	6.503E−2 9.067E−2	7.043E−2 7.139E−2	7.258E−2 5.207E−2	7.365E−2 4.017E−2	7.427E−2 3.308E−2
0.65	8.803E−2 1.019E−1	9.390E−2 7.309E−2	9.626E−2 5.365E−2	9.747E−2 4.287E−2	9.821E−2 3.645E−2
0.60	1.171E−1 1.107E−1	1.236E−1 7.677E−2	1.264E−1 5.812E−2	1.278E−1 4.794E−2	1.287E−1 4.170E−2
0.55	1.546E−1 1.199E−1	1.622E−1 8.380E−2	1.655E−1 6.561E−2	1.673E−1 5.545E−2	1.684E−1 4.901E−2
0.50	2.043E−1 1.321E−1	2.135E−1 9.509E−2	2.175E−1 7.660E−2	2.198E−1 6.593E−2	2.212E−1 5.897E−2

densate particles, in fact this material originates from the *vapor* in the mainstream (as can be seen from the definition of ω_c^v). Therefore, it could be said that the total mass deposition rate associated with the existing *vapor* in the mainstream is measured by the sum

$$St_{m,v} + St^v_{m,c}. \tag{3.4-1}$$

If it is assumed that there were no condensate particles in the mainstream at all, yet the conditions there were such that the gas was saturated [i.e. $\omega_{v,\infty} = \omega_v^{eq}(T_\infty)$ and $\omega_{c,\infty} = 0$] the above quantity would yield the total deposition rate on the cold surface. In fact, this is a limiting of the more general treatment of undersaturated mainstreams given by Castillo and Rosner (1989), one in which the "interface" between the single- and the two-phase region moves from within the thermal BL to its outer edge.

For purposes of illustration, this deposition rate is displayed in Fig. 4 for $m=1$, $Sc=2$, and $\mathcal{L}=20$, and three values of the dispersed condensate thermophoretic coefficient ($\alpha=0.5$, 0.1 and 0.01). The value of the contribution that arrives at the deposition surface as vapor ($St_{m,v}Re_x^{1/2}$) from eq. (2.4-25) is itself given by the dashed line d. Adding the $St^v_{m,c}$ contribution which arrives as condensate scavenged by the preexisting particles [eq (2.4-31)], based on the numerical values of $\mathcal{J}_1$ and $\mathcal{J}_2$ for $\mathcal{L}=20$ from Tables 10–12, the total deposition rate associated with vapor in the mainstream is obtained: see curves a ($\alpha=0.5$), b ($\alpha=0.1$) and c ($\alpha=0.01$), respectively. It is observed that for the higher values of the wall temperature parameter θ_w the

Table 5. Numerical values of $\mathscr{J}_1$ (upper number) and $\mathscr{J}_2$ (lower number) defined by eq. (2.4-31) as functions of the normalized wall temperature θ_w ($\equiv T_w/T_\infty$) for a flat-plate collector ($m=0$), $\alpha=0.1$ and stated values of the parameter $\mathscr{L}$ [$\equiv \Lambda/(RT_\infty)$]

θ_w	$\mathscr{L}=10$	$\mathscr{L}=15$	$\mathscr{L}=20$	$\mathscr{L}=25$	$\mathscr{L}=30$
0.98	9.689E−5	1.437E−4	1.861E−4	2.246E−4	2.594E−4
	1.858E−4	5.169E−4	9.492E−4	1.446E−3	1.978E−3
0.96	3.653E−4	5.183E−4	6.439E−4	7.470E−4	8.317E−4
	1.058E−3	2.530E−3	4.137E−3	5.666E−3	7.000E−3
0.94	7.790E−4	1.061E−3	1.270E−3	1.425E−3	1.540E−3
	2.767E−3	5.848E−3	8.590E−3	1.063E−2	1.189E−2
0.92	1.317E−3	1.726E−3	2.000E−3	2.184E−3	2.308E−3
	5.282E−3	9.938E−3	1.314E−2	1.471E−2	1.494E−2
0.90	1.963E−3	2.483E−3	2.798E−3	2.989E−3	3.106E−3
	8.486E−3	1.424E−2	1.697E−2	1.722E−2	1.593E−2
0.88	2.703E−3	3.312E−3	3.644E−3	3.826E−3	3.927E−3
	1.221E−2	1.829E−2	1.967E−2	1.813E−2	1.538E−2
0.86	3.527E−3	4.198E−3	4.528E−3	4.693E−3	4.776E−3
	1.625E−2	2.175E−2	2.113E−2	1.780E−2	1.396E−2
0.84	4.428E−3	5.136E−3	5.451E−3	5.594E−3	5.661E−3
	2.042E−2	2.441E−2	2.151E−2	1.667E−2	1.227E−2
0.82	5.399E−3	6.123E−3	6.414E−3	6.535E−3	6.588E−3
	2.452E−2	2.621E−2	2.103E−2	1.517E−2	1.066E−2
0.80	6.440E−3	7.160E−3	7.422E−3	7.525E−3	7.568E−3
	2.837E−2	2.717E−2	2.000E−2	1.362E−2	9.337F−3
0.75	9.347E−3	1.000E−2	1.020E−2	1.027E−2	1.030E−2
	3.611E−2	2.667E−2	1.659E−2	1.059E−2	7.433E−3
0.70	1.274E−2	1.330E−2	1.345E−2	1.351E−2	1.354E−2
	4.034E−2	2.399E−2	1.390E−2	9.225E−3	7.000E−3
0.65	1.676E−2	1.724E−2	1.737E−2	1.742E−2	1.745E−2
	4.126E−2	2.131E−2	1.265E−2	9.080E−3	7.331E−3
0.60	2.162E−2	2.205E−2	2.217E−2	2.223E−2	2.227E−2
	4.014E−2	1.977E−2	1.263E−2	9.671E−3	8.099E−3
0.55	2.766E−2	2.808E−2	2.821E−2	2.828E−2	2.832E−2
	3.861E−2	1.965E−2	1.352E−2	1.078E−2	9.233E−3
0.50	3.539E−2	3.583E−2	3.599E−2	3.607E−2	3.612E−2
	3.808E−2	2.085E−2	1.515E−2	1.241E−2	1.078E−2

direct vapor arrival term $St_{m,v}$ is the dominant one, whereas for lower values of θ_w, $St_{m,v}$ becomes negligible, with the scavenged vapor contribution arriving on condensate particles, measured by $St^v_{m,c}$, playing the major role. The total deposition rate due to the existence of *vapor* in the mainstream, given by eq. (3.4-1) is seen to exhibit a rather remarkable trend as the surface temperature is reduced below the dew point (here T_∞), never achieving the familiar "plateau" observed in simple vapor-only transport systems (Rosner *et al.*, 1979). Owing to condensate formation from the vapor BL, and its thermophoretically-driven transport to the surface, the mass deposition rate first rises to a maximum. If α is far below its theoretical maximum the thermophoretic transport of condensate cannot keep up with the reduced vapor flux and the total deposition rate drops to a value well below the first maximum before gradually recovering at much lower surface temperatures. These features also describe the *total* deposition rate when the mainstream contains a dispersed condensate with $\omega_{c,\infty} \ll \omega_{v,\infty}$ (see Section 3.5).

3.5. *Combined deposition rate*

The combined (condensate particle and vapor) deposition rate over a length L measured from the stagnation point will be given by

$$j'(L) = \int_0^L [j''_{v,w}(x) + j''_{c,w}(x)]\,dx \qquad (3.5\text{-}1)$$

where the fluxes j''_w and $j''_{c,w}$ are given by eq. (2.4-22)

Table 6. Numerical values of $\mathcal{J}_1$ (upper number) and $\mathcal{J}_2$ (lower number) defined by eq. (2.4-31) as functions of the normalized wall temperature θ_w ($\equiv T_w/T_\infty$) for a flat-plate collector ($m=0$), $\alpha=0.01$ and stated values of the parameter $\mathscr{L}$ [$\equiv \Lambda/(RT_\infty)$]

θ_w	$\mathscr{L}=10$	$\mathscr{L}=15$	$\mathscr{L}=20$	$\mathscr{L}=25$	$\mathscr{L}=30$
0.98	9.923E−6 7.263E−5	1.470E−5 1.828E−4	1.902E−5 3.231E−4	2.292E−5 4.819E−4	2.645E−5 6.499E−4
0.96	3.766E−5 3.929E−4	5.327E−5 8.773E−4	6.599E−5 1.390E−3	7.636E−5 1.865E−3	8.480E−5 2.267E−3
0.94	8.056E−5 1.002E−3	1.091E−4 1.993E−3	1.300E−4 2.832E−3	1.453E−4 3.415E−3	1.564E−4 3.735E−3
0.92	1.363E−4 1.880E−3	1.773E−4 3.328E−3	2.041E−4 4.232E−3	2.216E−4 4.576E−3	2.331E−4 4.495E−3
0.90	2.030E−4 2.975E−3	2.543E−4 4.677E−3	2.842E−4 5.308E−3	3.016E−4 5.138E−3	3.119E−4 4.530E−3
0.88	2.790E−4 4.218E−3	3.376E−4 5.872E−3	3.680E−4 5.934E−3	3.838E−4 5.136E−3	3.920E−4 4.068E−3
0.86	3.630E−4 5.532E−3	4.258E−4 6.799E−3	4.547E−4 6.106E−3	4.679E−4 4.726E−3	4.740E−4 3.374E−3
0.84	4.539E−4 6.837E−3	5.180E−4 7.396E−3	5.439E−4 5.897E−3	5.544E−4 4.091E−3	5.587E−4 2.655E−3
0.82	5.508E−4 8.059E−3	6.136E−4 7.653E−3	6.359E−4 5.418E−3	6.439E−4 3.388E−3	6.468E−4 2.029E−3
0.80	6.534E−4 9.135E−3	7.129E−4 7.597E−3	7.313E−4 4.785E−3	7.371E−4 2.726E−3	7.390E−4 1.544E−3
0.75	9.330E−4 1.088E−2	9.788E−4 6.464E−3	9.889E−4 3.136E−3	9.913E−4 1.554E−3	9.919E−4 8.923E−4
0.70	1.248E−3 1.105E−2	1.278E−3 4.773E−3	1.283E−3 1.992E−3	1.284E−3 1.048E−3	1.285E−3 7.144E−4
0.65	1.607E−3 9.899E−3	1.625E−3 3.335E−3	1.628E−3 1.443E−3	1.628E−3 9.113E−4	1.629E−3 7.089E−4
0.60	2.026E−3 8.072E−3	2.036E−3 2.458E−3	2.038E−3 1.273E−3	2.039E−3 9.244E−4	2.039E−3 7.629E−4
0.55	2.528E−3 6.278E−3	2.535E−3 2.080E−3	2.536E−3 1.286E−3	2.537E−3 1.001E−3	2.537E−3 8.495E−4
0.50	3.148E−3 4.992E−3	3.153E−3 2.018E−3	3.154E−3 1.390E−3	3.155E−3 1.121E−3	3.155E−3 9.669E−4

and eq. (2.4-23), respectively. Thus, if a dimensionless combined deposition rate is defined as

$$\mathcal{J} = \frac{m+1}{2\rho}(avL^{m+1})^{-1/2}[-j'(L)] \quad (3.5\text{-}2)$$

it is found that

$$\mathcal{J} = Re_x^{1/2}[\omega_{v,\infty}(St_{m,v} + St^{v}_{m,c}) + \omega_{c,\infty} St^{0}_{m,c}]. \quad (3.5\text{-}3)$$

The values of $\omega_{v,\infty}$ and $\omega_{c,\infty}$ appear in this expression due to the different definitions of $St_{m,v}$ and $St^{v}_{m,c}$ (both based on a reference flux defined with respect to $\omega_{v,\infty}$) and $St^{0}_{m,c}$ (defined with respect to $\omega_{c,\infty}$).

The behavior of the preexisting condensate $St^{0}_{m,c}$ [given by eq. (2.4-29)] was discussed in Section 3.2; the direct vapor contribution $St_{m,v}$ can easily be calculated from eq. (2.4-25) once $\delta(m, Pr)$ [eq. (2.3-6)] is known [values used here are given in eq. (3.1-1)]; and numerical values of $\mathcal{J}_1$ and $\mathcal{J}_2$ from which $St^{v}_{m,c}$ can be evaluated [eq. (2.4-30)] were given in Section 3.3.

To illustrate the resulting trends, values of $\mathcal{J}\, Re_x^{-1/2}/\omega_{v,\infty}$ are plotted in Fig. 5 for the particular case $m=1$, $Sc=2$, $\mathscr{L}=20$, $\alpha=0.1$, and different values of the mainstream condensate/vapor ratio $\omega_{c,\infty}/\omega_{v,\infty}$. Note that for $\omega_{c,\infty}/\omega_{v,\infty} \ll 1$ the deposition rate vs the surface temperature "fingerprint" is close to that described in Section 3.5. However, when $\omega_{c,\infty}/\omega_{v,\infty}$ greatly *exceeds* unity the behavior becomes dominated by the laws of thermophoretically dominated particle capture (Rosner and Kim, 1985).

4. CONCLUSIONS, IMPLICATIONS AND RECOMMENDATIONS

By invoking the realizable assumptions of a local vapor–condensate equilibrium within the thermal

Table 7. Numerical values of $\mathcal{J}_1$ (upper number) and $\mathcal{J}$ (lower number) defined by eq. (2.4-31) as functions of the normalized wall temperature $\theta_w (\equiv T_w/T_\infty)$ for an axisymmetric stagnation point ($m = \frac{1}{2}$), $\alpha = 0.5$ and stated values of the parameter $\mathscr{L}$ [$\equiv \Lambda/(RT_\infty)$]

θ_w	$\mathscr{L}=10$	$\mathscr{L}=15$	$\mathscr{L}=20$	$\mathscr{L}=25$	$\mathscr{L}=30$
0.98	6.159E−4	9.148E−4	1.187E−3	1.434E−3	1.658E−3
	2.125E−4	9.335E−4	1.932E−3	3.117E−3	4.415E−3
0.96	2.301E−3	3.278E−3	4.088E−3	4.759E−3	5.315E−3
	1.744E−3	5.177E−3	9.120E−3	1.302E−2	1.656E−2
0.94	4.888E−3	6.699E−3	8.070E−3	9.108E−3	9.896E−3
	5.091E−3	1.259E−2	1.972E−2	2.542E−2	2.939E−2
0.92	8.254E−3	1.092E−2	1.277E−2	1.405E−2	1.494E−2
	1.029E−2	2.212E−2	3.119E−2	3.658E−2	3.871E−2
0.90	1.231E−2	1.578E−2	1.798E−2	1.939E−2	2.029E−2
	1.717E−2	3.260E−2	4.164E−2	4.468E−2	4.361E−2
0.88	1.700E−2	2.117E−2	2.360E−2	2.504E−2	2.591E−2
	2.541E−2	4.301E−2	5.000E−2	4.941E−2	4.489E−2
0.86	2.227E−2	2.703E−2	2.959E−2	3.100E−2	3.181E−2
	3.466E−2	5.258E−2	5.592E−2	5.130E−2	4.392E−2
0.84	2.810E−2	3.333E−2	3.595E−2	3.731E−2	3.805E−2
	4.451E−2	6.081E−2	5.954E−2	5.122E−2	4.190E−2
0.82	3.449E−2	4.008E−2	4.270E−2	4.401E−2	4.471E−2
	5.459E−2	6.746E−2	6.126E−2	5.000E−2	3.971E−2
0.80	4.142E−2	4.730E−2	4.990E−2	5.116E−2	5.183E−2
	6.455E−2	7.250E−2	6.162E−2	4.836E−2	3.786E−2
0.75	6.138E−2	6.772E−2	7.027E−2	7.147E−2	7.214E−2
	8.714E−2	7.920E−2	5.981E−2	4.513E−2	3.582E−2
0.70	8.570E−2	9.241E−2	9.502E−2	9.630E−2	9.705E−2
	1.045E−1	8.099E−2	5.848E−2	4.506E−2	3.724E−2
0.65	1.157E−1	1.229E−1	1.258E−1	1.273E−1	1.282E−1
	1.167E−1	8.225E−2	6.008E−2	4.817E−2	4.121E−2
0.60	1.535E−1	1.616E−1	1.649E−1	1.666E−1	1.677E−1
	1.258E−1	8.592E−2	6.510E−2	5.405E−2	4.735E−2
0.55	2.023E−1	2.116E−1	2.156E−1	2.177E−1	2.191E−1
	1.350E−1	9.353E−2	7.362E−2	6.272E−2	5.586E−2
0.50	2.669E−1	2.780E−1	2.830E−1	2.857E−1	2.874E−1
	1.477E−1	1.061E−1	8.613E−2	7.479E−2	6.743E−2

boundary layer, and a thermophoretic diffusivity of condensate particles which is insensitive to particle size, the coupled two-phase laminar BL problem of predicting vapor and condensate deposition rates from initially saturated particle-laden streams is reduced to one of simple quadratures—i.e. the numerical computation of several explicit integrals. Interestingly enough, under these conditions it is found that the total mass deposition rate can be split into three additive contributions, each governed by a calculable mass transfer coefficient: a vapor transfer coefficient and two condensate mass transfer coefficients, one governing particle transport in the (hypothetical) absence of vapor scavenging, and one based on the scavenged vapor. This formalism allows rational, if approximate, predictions of vapor and condensate mass deposition rates over a rather wide range of system parameters of current interest, including those characterizing flow geometry, vapor Fick diffusivity and particle thermophoretic diffusivity, mainstream condensate mass fraction, carrier gas Prandtl number, dimensionless heat of condensate evaporation and wall/mainstream temperature ratio, subject to the remaining assumptions outlined in Section 2. Illustrative results are presented in Section 3 for important special cases (planar and axisymmetric stagnation point flow, flat-plate flow) of air-like gases (combustion products) in the parameter ranges $0.5 \leqslant T_w/T_\infty \leqslant 1.0$, $10^{-2} \leqslant \alpha_T D_c/\nu \leqslant 0.5$, and $10 \leqslant \Lambda/(RT_\infty) \leqslant 30$. These results reveal that the total deposition rate at surface temperatures below the mainstream dew point (Figs 2 and 3) "inherits" some

Table 8. Numerical values of $\mathcal{J}_1$ (upper number) and $\mathcal{J}_2$ (lower number) defined by eq. (2.4-31) as functions of the normalized wall temperature θ_w ($\equiv T_w/T_\infty$) for an axisymmetric stagnation point ($m=\frac{1}{3}$), $\alpha=0.1$ and stated values of the parameter $\mathscr{L}$ [$\equiv \Lambda/(RT_\infty)$]

θ_w	$\mathscr{L}=10$	$\mathscr{L}=15$	$\mathscr{L}=20$	$\mathscr{L}=25$	$\mathscr{L}=30$
0.98	1.279E−4 1.916E−4	1.896E−4 5.519E−4	2.455E−4 1.025E−3	2.962E−4 1.570E−3	3.421E−4 2.155E−3
0.96	4.825E−4 1.160E−3	6.841E−4 2.818E−3	8.494E−4 4.631E−3	9.849E−4 6.358E−3	1.096E−3 7.862E−3
0.94	1.029E−3 3.096E−3	1.400E−3 6.607E−3	1.674E−3 9.732E−3	1.877E−3 1.205E−2	2.028E−3 1.348E−2
0.92	1.740E−3 5.972E−3	2.277E−3 1.131E−2	2.635E−3 1.497E−2	2.875E−3 1.674E−2	3.036E−3 1.698E−2
0.90	2.593E−3 9.655E−3	3.274E−3 1.626E−2	3.684E−3 1.937E−2	3.931E−3 1.960E−2	4.081E−3 1.809E−2
0.88	3.569E−3 1.395E−2	4.364E−3 2.092E−2	4.793E−3 2.244E−2	5.028E−3 2.062E−2	5.156E−3 1.742E−2
0.86	4.655E−3 1.862E−2	5.527E−3 2.489E−2	5.952E−3 2.409E−2	6.161E−3 2.019E−2	6.266E−3 1.576E−2
0.84	5.840E−3 2.343E−2	6.757E−3 2.794E−2	7.158E−3 2.447E−2	7.338E−3 1.884E−2	7.421E−3 1.378E−2
0.82	7.117E−3 2.817E−2	8.048E−3 2.996E−2	8.415E−3 2.386E−2	8.566E−3 1.708E−2	8.631E−3 1.193E−2
0.80	8.482E−3 3.261E−2	9.402E−3 3.100E−2	9.731E−3 2.261E−2	9.856E−3 1.527E−2	9.908E−3 1.041E−2
0.75	1.228E−2 4.145E−2	1.311E−2 3.021E−2	1.334E−2 1.857E−2	1.343E−2 1.178E−2	1.346E−2 8.271E−3
0.70	1.671E−2 4.609E−2	1.739E−2 2.692E−2	1.757E−2 1.543E−2	1.764E−2 1.026E−2	1.767E−2 7.837E−3
0.65	2.192E−2 4.679E−2	2.249E−2 2.370E−2	2.264E−2 1.402E−2	2.270E−2 1.015E−2	2.273E−2 8.269E−3
0.60	2.821E−2 4.509E−2	2.871E−2 2.186E−2	2.886E−2 1.405E−2	2.892E−2 1.087E−2	2.896E−2 9.190E−3
0.55	3.600E−2 4.294E−2	3.648E−2 2.171E−2	3.664E−2 1.510E−2	3.672E−2 1.218E−2	3.676E−2 1.052E−2
0.50	4.594E−2 4.200E−2	4.645E−2 2.307E−2	4.663E−2 1.698E−2	4.672E−2 1.406E−2	4.677E−2 1.233E−2

Table 9. Numerical values of $\mathscr{J}_1$ (upper number) and $\mathscr{J}_2$ (lower number) defined by eq. (2.4-31) as functions of the normalized wall temperature θ_w ($\equiv T_w/T_\infty$) for an axisymmetric stagnation point ($m=\frac{1}{2}$), $\alpha=0.01$ and stated values of the parameter $\mathscr{L}$ [$\equiv \Lambda/(RT_\infty)$]

θ_w	$\mathscr{L}=10$	$\mathscr{L}=15$	$\mathscr{L}=20$	$\mathscr{L}=25$	$\mathscr{L}=30$
0.98	1.306E−5 6.796E−5	1.935E−5 1.736E−4	2.503E−5 3.085E−4	3.016E−5 4.615E−4	3.480E−5 6.237E−4
0.96	4.960E−5 3.862E−4	7.013E−5 8.693E−4	8.685E−5 1.382E−3	1.005E−4 1.858E−3	1.115E−4 2.261E−3
0.94	1.061E−4 1.018E−3	1.436E−4 2.037E−3	1.710E−4 2.901E−3	1.910E−4 3.502E−3	2.056E−4 3.833E−3
0.92	1.795E−4 1.956E−3	2.332E−4 3.478E−3	2.683E−4 4.428E−3	2.913E−4 4.793E−3	3.062E−4 4.711E−3
0.90	2.673E−4 3.151E−3	3.344E−4 4.968E−3	3.734E−4 5.644E−3	3.961E−4 5.465E−3	4.094E−4 4.820E−3
0.88	3.672E−4 4.528E−3	4.438E−4 6.315E−3	4.834E−4 6.385E−3	5.038E−4 5.526E−3	5.143E−4 4.376E−3
0.86	4.775E−4 6.001E−3	5.595E−4 7.382E−3	5.968E−4 6.628E−3	6.139E−4 5.127E−3	6.217E−4 3.658E−3
0.84	5.968E−4 7.478E−3	6.802E−4 8.089E−3	7.136E−4 6.442E−3	7.270E−4 4.463E−3	7.324E−4 2.894E−3
0.82	7.239E−4 8.873E−3	8.054E−4 8.415E−3	8.339E−4 5.945E−3	8.440E−4 3.710E−3	8.476E−4 2.219E−3
0.80	8.583E−4 1.011E−2	9.351E−4 8.386E−3	9.586E−4 5.265E−3	9.659E−4 2.992E−3	9.681E−4 1.692E−3
0.75	1.224E−3 1.213E−2	1.283E−3 7.167E−3	1.295E−3 3.456E−3	1.298E−3 1.708E−3	1.298E−3 9.850E−4
0.70	1.635E−3 1.236E−2	1.673E−3 5.281E−3	1.679E−3 2.190E−3	1.680E−3 1.158E−3	1.680E−3 7.980E−4
0.65	2.102E−3 1.105E−2	2.125E−3 3.670E−3	2.127E−3 1.590E−3	2.128E−3 1.017E−3	2.128E−3 8.006E−4
0.60	2.647E−3 8.955E−3	2.659E−3 2.694E−3	2.660E−3 1.412E−3	2.661E−3 1.041E−3	2.660E−3 8.683E−4
0.55	3.298E−3 6.901E−3	3.305E−3 2.283E−3	3.306E−3 1.437E−3	3.306E−3 1.135E−3	3.306E−3 9.721E−4
0.50	4.099E−3 5.440E−3	4.104E−3 2.228E−3	4.105E−3 1.563E−3	4.105E−3 1.277E−3	4.104E−3 1.111E−3

Table 10. Numerical values of $\mathcal{J}_1$ (upper number) and $\mathcal{J}_2$ (lower number) defined by eq. (2.4-31) as functions of the normalized wall temperature $\theta_w (\equiv T_w/T_\infty)$ for a two-dimensional (planar) stagnation line collector ($m = 1$), $\alpha = 0.5$ and stated values of the parameter $\mathcal{L} [\equiv \Lambda/(RT_\infty)]$

θ_w	$\mathcal{L} = 10$	$\mathcal{L} = 15$	$\mathcal{L} = 20$	$\mathcal{L} = 25$	$\mathcal{L} = 30$
0.98	7.975E−4 2.366E−4	1.184E−3 1.114E−3	1.536E−3 2.335E−3	1.856E−3 3.787E−3	2.146E−3 5.377E−3
0.96	2.983E−3 2.058E−3	4.248E−3 6.253E−3	5.295E−3 1.108E−2	6.162E−3 1.587E−2	6.881E−3 2.020E−2
0.94	6.339E−3 6.095E−3	8.683E−3 1.528E−2	1.045E−2 2.403E−2	1.179E−2 3.102E−2	1.281E−2 3.586E−2
0.92	1.071E−2 1.241E−2	1.416E−2 2.693E−2	1.654E−2 3.805E−2	1.819E−2 4.463E−2	1.933E−2 4.721E−2
0.90	1.597E−2 2.080E−2	2.045E−2 3.976E−2	2.328E−2 5.081E−2	2.508E−2 5.449E−2	2.624E−2 5.311E−2
0.88	2.205E−2 3.088E−2	2.743E−2 5.249E−2	3.054E−2 6.100E−2	3.238E−2 6.019E−2	3.348E−2 5.458E−2
0.86	2.888E−2 4.220E−2	3.500E−2 6.418E−2	3.828E−2 6.818E−2	4.008E−2 6.240E−2	4.110E−2 5.328E−2
0.84	3.643E−2 5.427E−2	4.315E−2 7.421E−2	4.648E−2 7.250E−2	4.821E−2 6.218E−2	4.915E−2 5.073E−2
0.82	4.469E−2 6.662E−2	5.186E−2 8.229E−2	5.519E−2 7.449E−2	5.685E−2 6.060E−2	5.773E−2 4.799E−2
0.80	5.367E−2 7.881E−2	6.118E−2 8.836E−2	6.448E−2 7.481E−2	6.606E−2 5.851E−2	6.691E−2 4.570E−2
0.75	7.945E−2 1.064E−1	8.750E−2 9.623E−2	9.072E−2 7.232E−2	9.224E−2 5.444E−2	9.308E−2 4.321E−2
0.70	1.108E−1 1.274E−1	1.193E−1 9.803E−2	1.226E−1 7.052E−2	1.242E−1 5.433E−2	1.252E−1 4.500E−2
0.65	1.495E−1 1.418E−1	1.586E−1 9.922E−2	1.622E−1 7.239E−2	1.641E−1 5.816E−2	1.652E−1 4.991E−2
0.60	1.982E−1 1.523E−1	2.083E−1 1.034E−1	2.125E−1 7.847E−2	2.147E−1 6.537E−2	2.162E−1 5.746E−2
0.55	2.609E−1 1.628E−1	2.726E−1 1.125E−1	2.777E−1 8.882E−2	2.805E−1 7.597E−2	2.823E−1 6.788E−2
0.50	3.439E−1 1.776E−1	3.580E−1 1.276E−1	3.643E−1 1.040E−1	3.678E−1 9.069E−2	3.701E−1 8.202E−2

Table 11. Numerical values of $\mathcal{J}_1$ (upper number) and $\mathcal{J}_2$ (lower number) defined by eq. (2.4-31) as functions of the normalized wall temperature θ_w ($\equiv T_w/T_\infty$) for a two-dimensional (planar) stagnation line collector ($m = 1$), $\alpha = 0.1$ and stated values of the parameter $\mathscr{L}$ [$\equiv \Lambda/(RT_\infty)$]

θ_w	$\mathscr{L} = 10$	$\mathscr{L} = 15$	$\mathscr{L} = 20$	$\mathscr{L} = 25$	$\mathscr{L} = 30$
0.98	1.652E−4	2.449E−4	3.171E−4	3.825E−4	4.418E−4
	2.400E−4	6.942E−4	1.291E−3	1.978E−3	2.715E−3
0.96	6.237E−4	8.843E−4	1.098E−3	1.273E−3	1.416E−3
	1.426E−3	3.478E−3	5.723E−3	7.859E−3	9.718E−3
0.94	1.331E−3	1.810E−3	2.164E−3	2.426E−3	2.621E−3
	3.789E−3	8.111E−3	1.195E−2	1.479E−2	1.654E−2
0.92	2.251E−3	2.944E−3	3.407E−3	3.715E−3	3.922E−3
	7.300E−3	1.385E−2	1.833E−2	2.048E−2	2.075E−2
0.90	3.354E−3	4.233E−3	4.761E−3	5.079E−3	5.271E−3
	1.180E−2	1.989E−2	2.367E−2	2.392E−2	2.204E−2
0.88	4.617E−3	5.641E−3	6.194E−3	6.494E−3	6.658E−3
	1.704E−2	2.557E−2	2.738E−2	2.511E−2	2.116E−2
0.86	6.021E−3	7.144E−3	7.689E−3	7.956E−3	8.090E−3
	2.275E−2	3.039E−2	2.935E−2	2.452E−2	1.909E−2
0.84	7.552E−3	8.730E−3	9.244E−3	9.473E−3	9.578E−3
	2.863E−2	3.407E−2	2.975E−2	2.284E−2	1.665E−2
0.82	9.202E−3	1.040E−2	1.086E−2	1.106E−2	1.114E−2
	3.440E−2	3.650E−2	2.896E−2	2.065E−2	1.437E−2
0.80	1.096E−2	1.214E−2	1.256E−2	1.272E−2	1.278E−2
	3.981E−2	3.772E−2	2.738E−2	1.841E−2	1.252E−2
0.75	1.587E−2	1.691E−2	1.721E−2	1.732E−2	1.736E−2
	5.053E−2	3.661E−2	2.238E−2	1.415E−2	9.944E−3
0.70	2.156E−2	2.243E−2	2.265E−2	2.273E−2	2.278E−2
	5.604E−2	3.247E−2	1.853E−2	1.233E−2	9.454E−3
0.65	2.826E−2	2.898E−2	2.917E−2	2.925E−2	2.930E−2
	5.669E−2	2.846E−2	1.683E−2	1.223E−2	1.001E−2
0.60	3.633E−2	3.697E−2	3.715E−2	3.724E−2	3.730E−2
	5.438E−2	2.620E−2	1.690E−2	1.314E−2	1.115E−2
0.55	4.633E−2	4.694E−2	4.714E−2	4.725E−2	4.731E−2
	5.155E−2	2.601E−2	1.820E−2	1.475E−2	1.279E−2
0.50	5.907E−2	5.971E−2	5.995E−2	6.007E−2	6.015E−2
	5.026E−2	2.768E−2	2.051E−2	1.706E−2	1.501E−2

Table 12. Numerical values of $\mathcal{J}_1$ (upper number) and $\mathcal{J}_2$ (lower number) defined by eq. (2.4-31) as functions of the normalized wall temperature θ_w ($\equiv T_w/T_\infty$) for a two-dimensional (planar) stagnation line collector ($m=1$), $\alpha=0.01$ and stated values of the parameter $\mathcal{L}$ [$\equiv \Lambda/(RT_\infty)$]

θ_w	$\mathcal{L}=10$	$\mathcal{L}=15$	$\mathcal{L}=20$	$\mathcal{L}=25$	$\mathcal{L}=30$
0.98	1.685E−5 9.461E−5	2.496E−5 2.407E−4	3.229E−5 4.270E−4	3.891E−5 6.381E−4	4.490E−5 8.616E−4
0.96	6.401E−5 5.139E−4	9.050E−5 1.155E−3	1.121E−4 1.835E−3	1.296E−4 2.464E−3	1.440E−4 2.995E−3
0.94	1.369E−4 1.335E−3	1.853E−4 2.667E−3	2.207E−4 3.793E−3	2.465E−4 4.574E−3	2.654E−4 5.000E−3
0.92	2.317E−4 2.539E−3	3.010E−4 4.505E−3	3.464E−4 5.727E−3	3.760E−4 6.188E−3	3.954E−4 6.071E−3
0.90	3.450E−4 4.054E−3	4.317E−4 6.379E−3	4.821E−4 7.230E−3	5.114E−4 6.985E−3	5.285E−4 6.145E−3
0.88	4.741E−4 5.783E−3	5.730E−4 8.045E−3	6.240E−4 8.110E−3	6.504E−4 6.996E−3	6.641E−4 5.521E−3
0.86	6.165E−4 7.614E−3	7.223E−4 9.337E−3	7.706E−4 8.353E−3	7.926E−4 6.435E−3	8.027E−4 4.571E−3
0.84	7.705E−4 9.434E−3	8.782E−4 1.017E−2	9.213E−4 8.060E−3	9.386E−4 5.556E−3	9.457E−4 3.582E−3
0.82	9.347E−4 1.114E−2	1.040E−3 1.051E−2	1.077E−3 7.388E−3	1.090E−3 4.583E−3	1.094E−3 2.723E−3
0.80	1.108E−3 1.263E−2	1.207E−3 1.042E−2	1.238E−3 6.501E−3	1.247E−3 3.668E−3	1.250E−3 2.061E−3
0.75	1.580E−3 1.501E−2	1.655E−3 8.798E−3	1.672E−3 4.207E−3	1.675E−3 2.064E−3	1.676E−3 1.186E−3
0.70	2.110E−3 1.517E−2	2.159E−3 6.413E−3	2.167E−3 2.637E−3	2.168E−3 1.392E−3	2.169E−3 9.626E−4
0.65	2.712E−3 1.346E−2	2.741E−3 4.415E−3	2.745E−3 1.907E−3	2.746E−3 1.225E−3	2.746E−3 9.702E−4
0.60	3.413E−3 1.082E−2	3.429E−3 3.224E−3	3.431E−3 1.697E−3	3.432E−3 1.259E−3	3.433E−3 1.056E−3
0.55	4.250E−3 8.277E−3	4.260E−3 2.732E−3	4.262E−3 1.734E−3	4.263E−3 1.378E−3	4.264E−3 1.185E−3
0.50	5.280E−3 6.487E−3	5.287E−3 2.673E−3	5.289E−3 1.892E−3	5.290E−3 1.553E−3	5.291E−3 1.356E−3

characteristics previously associated with pure vapor deposition (Rosner *et al.*, 1979; Castillo and Rosner, 1989; Rosner and Liang, 1986; Liang and Rosner, 1987) and some characteristics associated with pure thermophoretically dominated particle transport (Rosner and Kim, 1985; Gökoğlu and Rosner, 1984a), with the relative contributions scaling with the respective mass fractions, $\omega_{v,eq}(T_\infty)$ and $\omega_{c,\infty}$ in the saturated mainstream. Experiments are underway in the authors laboratory to test some of these predictions under well-defined seeded hydrocarbon/air flat flame conditions, but at Reynolds numbers lower than those assumed in the present BL theory ($Re^{1/2} \gg 1$).

The theory was also extended into the domain of nonnegligible particle loading, of importance in many material processing applications (Park and Rosner, 1989; Rosner and Park, 1988). This analysis, and its predecessor for undersaturated mainstreams (Castillo and Rosner, 1989), provide the theoretical background necessary to examine the consequences of relaxing the simplifying assumption that the condensate surface area per unit volume is large enough to maintain a vapor–condensate equilibrium everywhere within the thermal BL (Castillo and Rosner, 1988; Rosner and Liang, 1988). While nonequilibrium situations will undoubtedly be encountered in specific applications, the simplicity and generality of the present asymptotic cases, and the insights obtained from their investigation, amply justify their quantitative examination here. Since these two-phase convective mass transfer phenomena are important in a wide variety of materials processing—and energy con-

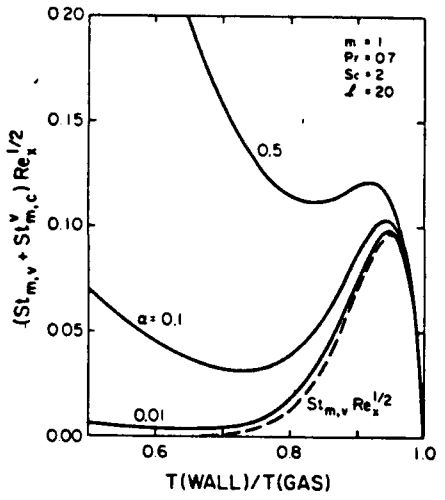

Fig. 4. Surface temperature dependence of the direct vapor contribution $St_{m,v}\,Re_x^{1/2}$ (dashed line d) and the sum $(St_{m,v}+St^{v}_{m,c})\,Re_x^{1/2}$ associated with the presence of vapor in the mainstream for different values of condensate thermophoretic parameter α. Conditions: $Pr=0.7$, $Sc=2$, $\mathscr{L}=20$, $m=1$.

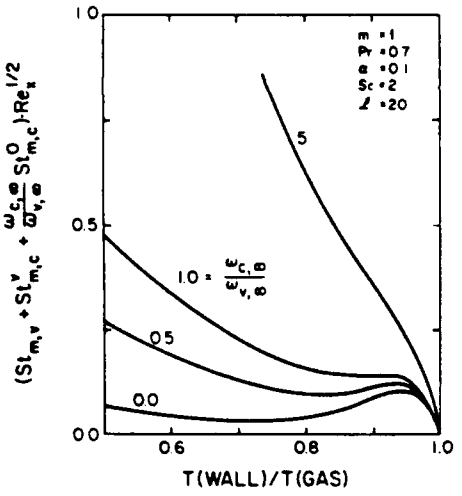

Fig. 5. Surface temperature dependence of the *combined* dimensionless mass transfer coefficient $\{[St_{m,v}+St^{v}_{m,c}+(\omega_{c,\infty}/\omega_{v,\infty})St^{0}_{m,c}]\,Re_x^{1/2}\}$ for two-dimensional (planar) stagnation line collector ($m=1$) and $Pr=0.7$, $\alpha=0.1$, $Sc=2$, $\mathscr{L}=20$, and stated values of the mainstream condensate/vapor ratio parameter $\omega_{c,\infty}/\omega_{v,\infty}$.

version—technologies, this new body of quantitative results should prove useful for making rapid engineering design predictions, and for interpreting experimental data obtained in the laboratory or field under conditions of combined (interactive) particle and vapor deposition.

Acknowledgements—The authors greatefully acknowledge many helpful discussions with present and former High Temperature Chemical Reaction Engineering Laboratory colleagues: J. Fernandez de la Mora (Mechanical Engineering Department, Yale University), R. Nagarajan (IBM, San Jose), B. Liang (University of California at Berkeley), H. M. Park (Brown University), A. D. Eisner (Northrup), S. A. Gökoğlu (NASA–Lewis Laboratory), R. Israel (GE, Nela Park), A. Gomez (ME/ChE, Yale) and P. Garcia-Ybarra (UNED). They are also indebted to the U.S. government agencies (Air Force Office of Scientific Research and DOE–METC) whose financial support made possible these fundamental studies and their publication

NOTATION

a	constant in eq. (2.2-1)
A	function defined by eq. (2.4-6)
B	function defined by eq. (2.4-7)
D	diffusion coefficient
f	Blasius function [eq. (2.2-5)]
j''	local deposition rate
$\mathscr{J}$	combined dimensionless deposition rate [eq. (3.5-2)]
$\mathscr{J}_i$	functions defined by eq. (2.4-31)
L	distance along the wall from the stagnation point
$\mathscr{L}$	parameter defined by eq. (2.4-16)
m	parameter defined in eq. (2.2-1) $[m=\beta/(2-\beta)]$
M_v	molecular weight of vapor
p_v	vapor pressure
Pr	Prandtl number $(Pr=\nu/\alpha_h)$
r'''	local rate of vapor consumption [eq. (2.4-1)]
R	universal gas constant
Re_x	Reynolds number $(Re_x=u_e x/\nu)$
Sc	vapor Schmidt number $(Sc=\nu/D_v)$
St_m	mass transfer Stanton number [eqs (2.4-24), (2.2-26) and (2.2-27)]
t	time
T	temperature field
u_e	external (potential) flow velocity along x [eq. (2.2-1)]
$\mathbf{v}$	velocity field (u, v)
x	distance along the wall from the stagnation point (Fig. 1)
y	distance normal to the wall (Fig. 1)

Greek letters

α	normalized thermophoretic coefficient $(\alpha=\alpha_T D_c/\nu)$
α_h	thermal diffusivity
α_T	thermophoretic factor [eq. (2.1-1)]
β	included (wedge) angle (Fig. 1)
γ	constant in eq. (2.1-3)
δ	function defined by eq. (2.3-6) $[\delta\{Pr, m\}]$
η	similarity variable $[\eta=(y/x)(u_e x/\nu)^{1/2}]$
θ	dimensionless temperature field $(\theta=T/T_\infty)$
Λ	constant in eq. (2.1-3)
ν	momentum diffusivity (gas kinematic viscosity)
ρ	density
ψ	stream function [eq. (2.2-5)]
ω_v	vapor mass fraction $(\omega_v=\rho_v/\rho)$

ω_c condensate mass fraction ($\omega_c \equiv \rho_c/\rho$)
$\dot{\omega}'''$ dimensionless vapor consumption [eq. (2.4-5)]
Ω normalized mass fractions [eqs (2.4-9)–(2.4-11)]
$\dot{\Omega}'''$ normalized vapor consumption ($\dot{\Omega}''' = \dot{\omega}'''/\omega_{v,\infty}$)
$\dot{\Omega}_i'''$ functions defined by eqs (2.4-18) and (2.4-19)

Subscripts

c condensate particles
T thermophoretic
v vapor
w at the wall
∞ at mainstream

Superscripts

eq equilibrium value over a flat layer of condensate
0 corresponding to the preexisting condensate particles
v corresponding to the vapor scavenged by the particles
derivative with respect to η

REFERENCES

Castillo, J. L. and Rosner, D. E., 1988, A nonequilibrium theory of surface deposition from particle-laden, dilute, condensible vapor-containing laminar boundary layer. *Int. J. Multiphase Flow* **14**, 99–120.

Castillo, J. L. and Rosner, D. E., 1989, Theory of surface deposition from a unary dilute vapor-containing stream allowing for condensation within the laminar boundary layer. *Chem. Engng Sci.* **44**, 925–937.

Gökoğlu, S. A. and Rosner, D. E., 1984a, Correlation of thermophoretically-modified small particle diffusional deposition rates in forced convection systems with variable properties, transpiration cooling and/or viscous dissipation. *Int. J. Heat Mass Transfer* **28**, 639–645; see also, 1986, *Chem. Engng Commun.* **44**, 107–119.

Gökoğlu, S. A. and Rosner, D. E., 1984b, Engineering correlations of variable-property effects on laminar forced convection mass transfer for dilute vapor species and small particles in air. NASA CR-168322.

Gökoğlu, S. A. and Rosner, D. E., 1986, Thermophoretically-augmented forced convection mass transfer rates to solid walls across non-isothermal laminar boundary layers. *AIAA J.* **24**, 172–179.

Goren, S. L., 1977, Thermophoresis of aerosol particles in the laminar boundary layer on a flate plate. *J. Colloid Interface Sci.* **61**, 77–85.

Liang, B., Gomez, A., Castillo, J. L. and Rosner, D. E., 1988, Experimental studies of nucleation phenomena within thermal boundary layers—influence on chemical vapor deposition rate processes. Paper A5A, 1987 Annual Meeting of the American Association of Aerosol Research, *Chem. Engng Commun.* (in press).

Liang, B. and Rosner, D. E., 1987, Laboratory studies of binary salt CVD in combustion gas environments. *A.I.Ch.E. J.* **33**, 1937–1948.

Park, H. M. and Rosner, D. E., 1989, Multiphase continuum theory of dopant redistribution across aerosol-laden laminar nonisothermal boundary layers. *Chem. Engng Sci.* **44**, 603–617.

Rosner, D. E., 1985, Mass transfer across combustion gas thermal boundary layers—power production and materials processing implications, in *Heat Transfer in Fire and Combustion Systems* (Edited by C. K. Law, Y. Jaluria, W. W. Yuen and K. Miyasaka), pp. 3–8. HTD **45**, American Society of Mechanical Engineers, New York.

Rosner, D. E., 1986, *Transport Processes in Chemically Reacting Flow Systems*. Butterworth, Stoneham, MA. Second printing 1988.

Rosner, D. E. and Atkins, R. M., 1983, Experimental studies of salt/ash deposition rates from combustion products using optical techniques, in *Fouling and Slagging Resulting from Impurities in Combustion Gases* (Edited by R. Bryers), pp. 469–492. Engineering Foundation, New York.

Rosner, D. E., Chen, B. K., Fryburg, G. C. and Kohl, F. J., 1979, Chemically frozen multicomponent boundary layer theory of salt and/or ash deposition rates from combustion gases. *Combust. Sci. Technol.* **20**, 87–106.

Rosner, D. E. and Fernandez de la Mora, J., 1982, Correlation and prediction of thermophoretic and inertial effects on particle deposition from non-isothermal turbulent boundary layers, in *Particulate Laden Flows in Turbomachinery* (Edited by W. Tabakoff, C. T. Crowe and D. B. Cale), pp. 85–94. American Society of Mechanical Engineers, New York.

Rosner, D. E. and Fernandez de la Mora, J., 1984, Boundary layer effects on particle impaction and capture. *A.S.M.E. Trans.—J. Fluid Engng* **106**, 113–114.

Rosner, D. E. and Kim, S. S., 1984, Optical experiments on thermophoretically augmented submicron particle deposition from 'dusty' high temperature gas flows. *Chem. Engng J.* **29**, 147–157.

Rosner, D. E. and Liang, B., 1986, Laboratory studies of the deposition of alkali sulfate vapors from combustion gases using a flash-evaporation technique. *Chem. Engng Commun.* **42**, 171–196; see also *Chem. Engng Commun.* **64**, 27–46.

Rosner, D. E. and Park, H. M., 1988, Thermophoretically augmented mass-, momentum- and energy-transfer rates in high particle mass loaded laminar forced convection systems. *Chem. Engng Sci.* **43**, 2689–2704.

Schlichting, H., 1968, *Boundary Layer Theory*, 6th Edition. McGraw-Hill, New York.

Spalding, D. B. and Evans, H. L., 1961, Mass transfer through laminar boundary layers—3. Similar solutions of the b-equation. *Int. J. Heat Mass Transfer* **2**, 314–341.

Stearns, C. A., Kohl, F. J. and Rosner, D. E., 1983, Combustion system processes leading to corrosive deposits, in *Proceedings of the NACE International Conference on High Temperature Corrosion* (Edited by R. Rapp), pp. 441–450. NACE-6, National Association of Corrosion Engineers, Houston, TX. Also NASA TM-81752.

Talbot, L., 1981, Thermophoresis—a review, in *Rarified Gas Dynamics: Part I* (Edited by S. S. Fisher), *Prog. Astron. Aeronaut. (AIAA)* **74**, 467–488.

REPORT DOCUMENTATION PAGE

Form Approved
OMB No. 0704-0188

1. AGENCY USE ONLY (Leave blank)	2. REPORT DATE	3. REPORT TYPE AND DATES COVERED
	1989	Journal Publication

4. TITLE AND SUBTITLE

BOUNDARY LAYER COAGULATION EFFECTS ON THE SIZE DISTRIBUTION OF THERMOPHORETICALLY DEPOSITED PARTICLES(v)

5. FUNDING NUMBERS

PE - 61102F
PR - 2308
SA - BS
G - AFOSR 89-0223

6. AUTHOR(S)

H.M.Park and Daniel E. Rosner

7. PERFORMING ORGANIZATION NAME(S) AND ADDRESS(ES)

HIGH TEMPERATURE CHEMICAL REACTION ENGINEERING LABORATORY
YALE UNIVERSITY
BOX 2159, YALE STATION
NEW HAVEN, CONNECTICUT 06520 U.S.A.

8. PERFORMING ORGANIZATION REPORT NUMBER

9. SPONSORING/MONITORING AGENCY NAME(S) AND ADDRESS(ES)

AFOSR/NA
Building 410
Bolling AFB DC 20332-6448

10. SPONSORING/MONITORING AGENCY REPORT NUMBER

11. SUPPLEMENTARY NOTES

12a. DISTRIBUTION/AVAILABILITY STATEMENT

Approved for public release; distribution is unlimited

12b. DISTRIBUTION CODE

13. ABSTRACT (Maximum 200 words)

Abstract—In highly loaded aerosol flow systems of industrial interest, to what extent is the particle size distribution (PSD) in a deposit altered by inevitable *coagulation* events within the thin two-phase "boundary layer" adjacent to the collecting surface? As a timely example, under typical optical waveguide preform deposition conditions (which include thermophoretically dominated submicron particle deposition at high particle mass loadings), we predict that, while Brownian diffusion plays a negligible role in determining the total particle mass deposition rate, Brownian coagulation (along with gas shear) plays an important role in determining the *size distribution of the depositing particles* of doped silica. Since the size spectrum of the depositing particles, here assumed to be spherical, will strongly influence all thermophysical and structural properties of the porous deposited glass, our mathematical model illustrative calculations can be used to circumvent the difficult problem of optically probing the thin laminar thermal boundary layer to infer this size spectrum information. Moreover, an understanding of "PSD shifts" induced by coagulation in the immediate vicinity of sampling probes surfaces (including "thermophoretic sampling" recently applied in organic soot research) can be used to correct electron-microscope-inferred particle size/shape distributions for the systematic effects of coagulation within such boundary layers in systems with higher particle mass loadings

14. SUBJECT TERMS

coagulation, thermophoresis, deposition, high mass loading, boundary layer theory, aerosols, optical waveguides

15. NUMBER OF PAGES

7

16. PRICE CODE

17. SECURITY CLASSIFICATION OF REPORT	18. SECURITY CLASSIFICATION OF THIS PAGE	19. SECURITY CLASSIFICATION OF ABSTRACT	20. LIMITATION OF ABSTRACT
Unclassified	Unclassified	Unclassified	UL

Chemical Engineering Science, Vol 44, No 10, pp 2225–2231, 1989
Printed in Great Britain

0009 2509/89 $3.00 + 0.00

BOUNDARY LAYER COAGULATION EFFECTS ON THE SIZE DISTRIBUTION OF THERMOPHORETICALLY DEPOSITED PARTICLES†

H. M. PARK‡ and DANIEL E. ROSNER§
Department of Chemical Engineering, Yale University, New Haven, CT 06520, U.S.A.

(*Accepted in revised form* 10 *March* 1989)

Abstract—In highly loaded aerosol flow systems of industrial interest, to what extent is the particle size distribution (PSD) in a deposit altered by inevitable *coagulation* events within the thin two-phase "boundary layer" adjacent to the collecting surface? As a timely example, under typical optical waveguide preform deposition conditions (which include thermophoretically dominated submicron particle deposition at high particle mass loadings), we predict that, while Brownian diffusion plays a negligible role in determining the total particle mass deposition rate, Brownian coagulation (along with gas shear) plays an important role in determining the *size distribution of the depositing particles* of doped silica. Since the size spectrum of the depositing particles, here assumed to be spherical, will strongly influence all thermophysical and structural properties of the porous deposited glass, our mathematical model/illustrative calculations can be used to circumvent the difficult problem of optically probing the thin laminar thermal boundary layer to infer this size spectrum information. Moreover, an understanding of "PSD shifts" induced by coagulation in the immediate vicinity of sampling probes/surfaces (including "thermophoretic sampling" recently applied in organic soot research) can be used to correct electron-microscope-inferred particle size/shape distributions for the systematic effects of coagulation within such boundary layers in systems with higher particle mass loadings.

INTRODUCTION

In most previous particle deposition rate theories [see, for example, Friedlander (1977) and Rosner (1989) (who explicitly considered convection/Brownian diffusion); and Goren (1977), Rosner and Park (1988) and Park and Rosner (1986, 1987) (who considered thermophoretically driven submicron aerosol particle transport through nonisothermal combustion product gases)] it has been assumed that the suspended particles were spherical and remained constant in diameter up to the moment of deposition. However, as is well known, aerosols are unstable with respect to coagulation, and, especially in highly loaded aerosol systems, coagulation may exert an important influence on system or product performance. In previous investigations of thermophoretic deposition rates under conditions of high particle mass loading we could neglect particle coagulation phenomena by exploiting the fact that since the thermophoretic diffusivity, $\alpha_T D_p$ remains nearly constant with respect to the particle Knudsen number for submicron particles in atmospheric pressure combustion products (Rosner, 1980), particle coagulation does *not* affect the resulting aerosol deposition rate (Rosner and Park, 1988). However, in many industrial applications, including the manufacture of "preforms" for optical waveguides, the *size distribution of the depositing particles* will exert a strong influence on the porosity and other important microstructural properties of the deposit (Tassopoulos *et al.*, 1989), thereby affecting all subsequent processing (e.g. drying, spinning etc.) (Keiser, 1983). As a useful first step in the prediction of size distribution "shifts" for thermophoretically deposited particles we present here a simple mathematical model that describes particle coagulation behavior across nonisothermal highly-loaded "dusty-gas" laminar boundary layers (BLs).

THEORETICAL FORMULATION

Overall BL flow structure

If we neglect particle *inertial* drift [see Rosner and Park (1988, Appendix)], the Eulerian BL flow equations for highly particle mass loaded systems treated as a continuum are [see, for example, Fernandez de la Mora and Rosner (1982) and Rosner and Park (1988)] a mixture mass balance, x-momentum balance, mixture energy balance and total particle mass (irrespective of particle size) balance. In their self-similar forms these equations, combined with an appropriate mixture equation of state $\{\rho = [pM_g/(RT)](1-\omega_p)^{-1}\}$ and boundary conditions, were derived and solved numerically by Rosner and Park (1988) to obtain the overall boundary layer structure and wall transfer rates of x-momentum, mass and energy, under parametric conditions relevant to optical waveguide processing. It was pointed out [Rosner and Park (1988, Appendix 5)] that, while the explicitly considered

†Originally submitted May 1987 to *Chemical Engineering Science*. Based, in part, on H. M. Park's PhD dissertation, Department of Chemical Engineering, Yale University (1987).

‡Graduate Research Assistant, High Temperature Chemical Reaction Engineering Laboratory, Yale University. Present address: Center for Fluid Mechanics, Brown University, Providence, RI 02912, U.S.A.

§Director, High Temperature Chemical Reaction Engineering Laboratory, and Professor, Department of Chemical Engineering, Yale University. Author to whom correspondence should be addressed.

the case of "monodispersed" submicron particles in the absence of coagulation, because of the particle size independence of the particle thermophoretic diffusivity, $\alpha_T D_p$, our earlier solutions for the distribution of the *total particle mass fraction*, ω_p, remain valid even in the case of nonnegligible coagulation (due to Brownian motion, gas shear, . . .).

Because of our present interest in the *size distribution of the thermophoretically deposited particles* (here considered spherical, assuming rapid coalescence), to the abovementioned set of equations we now add the following set of particle balance equations. These steady-state Eulerian balance equations [see, for example, Rosner (1986)] one for each selected size class k ($k = 1, 2, \ldots$) and corrected to apply to particles in a variable density mixture, equate the net outflow/volume of particles by convection and thermophoretic drift, to the net rate at which particles of this size class are "born" as a result of "binary" coagulation events [see, for example, Friedlander (1977)]. In our present notation (see Fig.1), after making the now-familiar $(Re)^{1/2} \gg 1$ laminar oundary layer (LBL) approximations, [see, for example, Schlicting (1979)] they can be written as:

Particle (size class) balance equations:

$$u\frac{\partial n_k}{\partial x} + v\frac{\partial n_k}{\partial y} = (1-\omega_p)\alpha_T D_p \frac{\partial \ln T_g}{\partial y}\frac{\partial n_k}{\partial y} - n_k \operatorname{div} \mathbf{v}_p + \frac{1}{2}\sum_{i+j=k} \beta(d_i, d_j)\, n_i n_j - n_k \sum_{i=1}^{\infty} \beta(d_i, d_k)\, n_i \qquad (2\text{-}1)$$

where n_k = particle number density of size class k ($k = 1, 2, \ldots$); $\mathbf{v}_p$ = particle velocity field given by

$$\mathbf{v}_p \equiv \begin{bmatrix} u_p \\ v_p \end{bmatrix} = \begin{bmatrix} u \\ v - (1-\omega_p)\alpha_T D_p \dfrac{\partial \ln g}{\partial y} \end{bmatrix}$$

and $\beta(d_i, d_j)$ = collision frequency function which depends on the sizes of the colliding particles and on local properties of the system such as temperature, pressure etc.

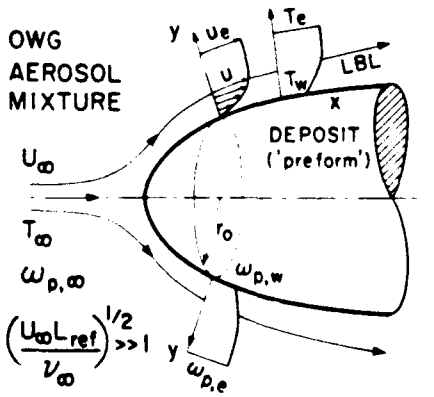

Fig. 1. High Reynolds number viscous flow configuration; body-oriented boundary layer coordinate system and nomenclature, axisymmetric case ($k = 1$) shown.

In the "source" term containing the factor: $(1/2)\beta(d_i, d_j)\, n_i n_j$ the notation $i+j=k$ indicates that the summation is taken only over those collisions for which $d_i^3 + d_j^3 = d_k^3$ (i.e. those binary encounters which "populate" size class d_k).

Thus, in addition to the LBL equations already stated/solved in Park (1987) and Rosner and Park (1988), we now (subsequently) solve the particle coagulation equations, which, in BL (ξ, η) coordinates, take the form

$$P(\xi,\eta)\frac{\partial n_k}{\partial \eta} + Q(\xi,\eta)\frac{\partial n_k}{\partial \xi} + S(\xi,\eta)\, n_k + \frac{1}{2}\sum_{i+j=k} \beta(d_i, d_j)\, n_i n_j - n_k \sum_{i=1}^{K} \beta(d_i, d_k)\, n_i = 0 \qquad (k = 1, 2, \ldots K) \quad (2\text{-}2)$$

where f is the dimensionless (Blasius) stream function, $g \equiv T/T_e$, and, in the notation of Rosner and Park (1988):

$$P(\xi,\eta) \equiv (1-\omega_p)\alpha_T D_p \frac{\rho^2 u_e^2}{2\xi}\left(\frac{r}{L_{ref}}\right)^{2\kappa}\frac{\partial \ln g}{\partial \eta} + \rho_e \mu_e u_e^2 \left(\frac{r_0}{L_{ref}}\right)^{2\kappa}\left(\frac{f}{2\xi} + \frac{\partial f}{\partial \xi}\right)$$

$$Q(\xi,\eta) \equiv -\rho_e \mu_e u_e^2 f' \left(\frac{r_0}{L_{ref}}\right)^{2\kappa} \qquad (2\text{-}3)$$

$$S(\xi,\eta) \equiv \frac{1}{\rho}\rho_e \mu_e u_e^2 f' \left(\frac{r_0}{L_{ref}}\right)^{2\kappa}\frac{\partial \rho}{\partial \xi} - \frac{1}{\rho}\rho_e \mu_e u_e^2 f' \left(\frac{r_0}{L_{ref}}\right)^{2\kappa}\frac{\partial \rho}{\partial \eta}\left(\frac{f}{2\xi} + \frac{\partial f}{\partial \xi}\right) + \frac{\rho_e u_e^2}{2\xi}\left(\frac{r_0}{L_{ref}}\right)^{2\kappa}\frac{\partial}{\partial \eta}\left[(1-\omega_p)\alpha_T D_p \rho \frac{\partial \ln g}{\partial \eta}\right]$$

where η and ξ are the "stretched" coordinates given by

$$\eta(x, y) \equiv (2\xi)^{1/2} u_e \int_0^y \rho\, dy$$

and

$$\xi(x, y) \equiv \int_0^x \rho_e \mu_e u_e \left[\frac{r_0(x)}{L_{ref}}\right]^{2\kappa} dx$$

$$\kappa = \begin{cases} 1 & \text{for axisymmetric LBL flow (cf. Fig. 1)} \\ 0 & \text{for planar LBL flow} \end{cases}.$$

The appropriate boundary conditions on the n_k values are simply that, at $\eta = \infty$, $n_k \to n_{k,e}$ (specified). Note that, since the PDEs for the n_k are first-order, no condition on the $n_{k,w}$ need be specified—indeed, it is the relative $n_{k,w}$ values which we seek.

As before, to solve this additional set of (hyperbolic) PDEs we used the finite-difference method of Keller (1974), applied extensively to the BL situations by Cebeci and Smith (1974) and Cebeci and Bradshaw (1976). This scheme is unconditionally stable and appropriate for the present highly implicit, nonlinear problem. The overall solution scheme is shown in Figure 2.

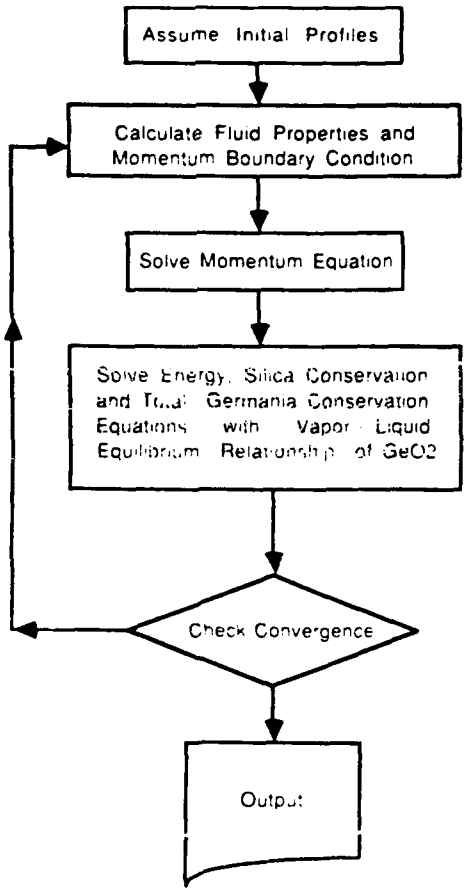

Fig. 2. Program logic diagram for numerically solving the coupled laminar boundary layer balance equations and suspended particle coagulation equations (general (nonself-similar) case).

Coagulation kernels

Particle collision and coalescence lead to a reduction in the total number density of particles and an accompanying increase in their average diameter. If the number of collisions occurring per unit time per unit volume between the two classes of particle of diameters d_i and d_j is written in the "mass-action" form: $\beta\langle d_i, d_j\rangle n_i n_j$, then $\beta\langle d_i, d_j\rangle$ is the so-called collision frequency function or collision "kernel" These "rate constants" depend on the sizes of the colliding particles and on the local properties of the system, such as temperature and pressure. Of course, to solve the coagulation rate equations we must specify the form of $\beta\langle d_i, d_j\rangle$, which, as discussed below, is determined by the mechanism of particle collision. In all coagulation estimates below we assume that each encounter is "successful"—i.e., there are no apreciable barriers to "sticking" and coalescence.

Brownian coagulation. Aerosol particles collide as a result of their Brownian motion in the high-temperature "background" gas. For particles much larger than the prevailing gas mean-free-path the particle–particle collision process is diffusion-limited (Smoluchowski) and $\beta\langle d_i, d_j\rangle$ is given by [see, for example, Friedlander (1977)]

$$\beta\langle d_i, d_j\rangle = \frac{2k_B T}{3\mu_g}\left(\frac{1}{d_i}+\frac{1}{d_j}\right)(d_i+d_j). \tag{2-4}$$

For particles much smaller that the prevailing carrier gas mean-free-path the relevant collision frequency can be obtained from the kinetic theory of "hard-sphere" gases, leading to

$$\beta\langle d_i, d_j\rangle = \left(\frac{1}{8}\right)^{1/6}\cdot\left(\frac{6k_B T}{\tilde{\rho}_p}\right)^{1/2}\cdot\left(\frac{1}{d_i^3}+\frac{1}{d_j^3}\right)^{1/2}(d_i+d_j)^2 \tag{2-5}$$

where $\tilde{\rho}_p$ is the intrinsic particle density. Fuchs (1964) has proposed a general interpolation formula for β_{ij}, which takes into account the transition from the above mentioned "free-molecule" regime to the "continuum" range. We adopted Fuchs' interpolation formula for the numerical calculations described below, i.e.

$$\beta\langle d_i, d_j\rangle = \frac{R_{ij}}{R_{ij}+(l_i^2+l_j^2)^{1/2}} + \frac{4D_{ij}(1+\tilde{A}Kn_i)(1+\tilde{A}Kn_j)}{(\bar{c}_i^2+\bar{c}_j^2)^{1/2}R_{ij}} \tag{2-6}$$

where $R_{ij}=R_i+R_j$; $R_i=$ radius of particle i; $l_i=$ mean-free-path for particle i; $\tilde{A}=1.257+0.4\times\exp(-1.1/Kn_i)$ (parameter in the Stokes–Cunningham correction to the mobility of particles at Knudsen number Kn_i); and $\bar{c}_i=\left(\frac{8k_B T}{\pi m_i}\right)^{1/2}$ (mean thermal speed of particle i). Before discussing other coagulation mechanisms it is relevant to observe that, even though in these environments thermophoresis dominates the Brownian diffusion as a mechanism for microparticle transport to the macroscopic surface, this does *not* imply that Brownian motion will necessarily make an insignificant contribution to the rate of particle–particle encounters *within* the LBL.

Laminar shear-induced coagulation. Particles of finite diameter in a laminar shear flow will encounter one another because of their relative motion. This mechanism is described by a collision kernel $\beta\langle d_i, d_j\rangle$ (Friedlander, 1977) of the form

$$\beta\langle d_i, d_j\rangle = \frac{4}{3}\left(\frac{d_i}{2}+\frac{d_i}{2}\right)^3\cdot\left|\frac{\partial u}{\partial y}\right| \tag{2-7}$$

where $|\partial u/\partial y|$ is the local deformation rate ("shear rate") of the gas mixture in the BL.

As is well known, there is also a lift force on particles which "slip" relative to a shear flow [see, for example, Saffman (1965)]. In general, this phenomenon causes a differential velocity which would also give rise to coagulation. However, in the present case the (inertial) particle stopping times are small enough to render the required "slip" negligible. Thus, when the so-called "diffusion model" for treating such a two-phase mixture is valid [see Rosner and Park (1988) and Park and

Rosner (1989)] this vorticity-induced "lift" mechanism of coagulation can be neglected.

While not pursued further here, it is interesting to note that, if the coagulating particles did not quickly coalesce to form spheres, then nonspherical particles of all orientations would be present within the thermal LL. Recent work of Garcia-Ybarra and Rosner (1989) reveals that even nonspherical particles of equal size but different orientations (cf. $-\mathbf{grad}\ T$) would overtake one another in such an environment. Moreover, Brownian rotation of nonspherical particles in a temperature gradient will also bring about encounters due to particle drift perpendicular to $-\mathbf{grad}\ T$. The rate constants and consequences of these "new" mechanism of coagulation will be treated/discussed elsewhere (Garcia-Ybarra *et al.*, 1988).

RESULTS AND DISCUSSION

For illustrative purposes Figure 3 shows a comparison of coagulation rate constants for particles of, say, 0.2 μm diameter (the particle diameter in the mainstream) interacting with particles of diameters between 0.02 and 2 μm. The shear-induced coagulation kernel β_{shear} is based on $|\hat{c}u/\hat{c}y| = 10^3\ s^{-1}$, a value typical of the BL flow region in some optical waveguide manufacturing processes. Note that, while Brownian coagulation is initially dominant under these conditions, shear-induced coagulation is by no means negligible, and at 1500 K becomes comparable to Brownian coagulation for "monomers" interacting with "hexamers" (particle volume equal to six primary particles).

Figure 4 shows our predicted results for the size distribution of depositing particles when we assume for simplicity that in the local mainstream (station ©) all particles are of the same size ($d_p = 0.2\ \mu$m). Here the total coagulation kernel β_{ij} has been assumed to be the sum of Brownian coagulation kernel, β_{Brown}, and local shear coagulation kernel, β_{shear}. Our results show that even if the particles are all of the same size (i.e. "monodisperse") at the outer edge of the BL, significant particle coagulation occurs *within* the LBL due to both the particle Brownian motion and the intense fluid shear. Indeed, nonnegligible concentrations of even the "hexamer" are indicated at the "dusty gas"/deposit interface. Of course, in practice, a significant amount of (Brownian) coagulation would also occur *outside* of the BL. However, considering the experimental difficulty of optically measuring the particle size distribution (PSD) within very thin nonisothermal BLs, and the more straightforward measurement of the particle size distribution in the local mainstream (outside the BL), the present mathematical model and numerical methods could be judiciously combined with the experimentally measured mainstream PSD to infer the size distribution of the depositing particles.

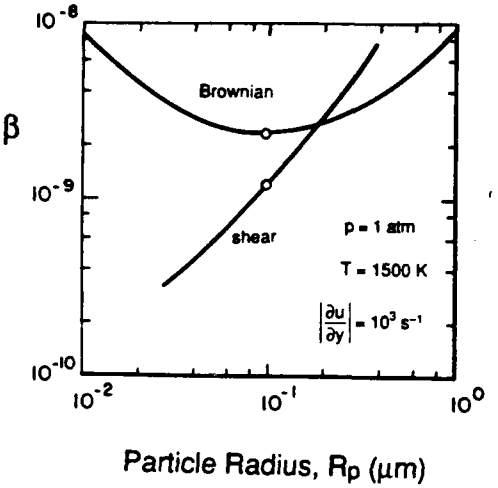

Fig. 3. Comparison of suspended particle coagulation rate constants β $\{[(\text{particles/cm}^3)\ (\text{s})]^{-1}\}$ for binary collisions with a "test" particle of diameter 0.2 μm.

Since the dimensionless particle mass transfer coefficient, St_m, or the closely related capture fraction, η_{cap}, are, generally, particle-size-dependent [see, for example, Friedlander (1977) and Rosner (1986, 1988b)], and the mainstream is usually "polydispersed" (multisized), there will, of course, be a calculable "shift" in the PSD across the BL, *even in the absence of BL coagulation processes* [see, for example, Rosner and Tassopoulos (1989)]. However, an additional shift and broadening can occur due to BL *coagulation* processes emphasized here. In the present cases, this can be anticipated whenever the characteristic time for coagulation is not negligible on the time-scale of particle drift across the BL. The ratio of these two characteristic times, which can be regarded as a coagulation "Damköhler number" (Rosner, 1986; Rosner and Park, 1988), can be written as†

$$(Dam)_{coag} = \frac{\dfrac{\delta_T^2}{(\alpha_T D_p)}\dfrac{T_w}{T_e - T_w}}{\left(\dfrac{2}{9}N_{p,e}\dfrac{k_B T_e}{\mu_{g,e}}\right)^{-1}} \approx \frac{4\pi C_{slip}\dfrac{m_g}{m_p}\omega_{p,e}}{9(Kn_L Nu_h)^2\left(\dfrac{\alpha_T D_p}{\nu_g}\right)_e\left(\dfrac{T_e - T_w}{T_w}\right)} \quad (3\text{-}1)$$

for Brownian coagulation of a single size class. Accordingly, PSD shifts associated with Brownian coagulation in a thermophoretically dominated BL should be expected whenever $(Dam)_{coag}$ given by eq. (3-1) is not negligible compared to unity. Note that the product $(Kn_L Nu_h)$ is the ratio of the gas mean-free-path to the (slope) thickness of the thermal BL, δ_T, and C_{slip} is the Stokes–Cunningham "slip" correction factor [see, for example, Friedlander, (1977)]. For completeness, the analogous parameter $(Dam)_{coag}$ governing the importance of BL coagulation in

†Equation (3-1) corrects a typographical error (of omission) in eqs (A5-1) and (A5-3) of Rosner and Park (1988) (absence of the exponent -1 in the expression for t_{coag}).

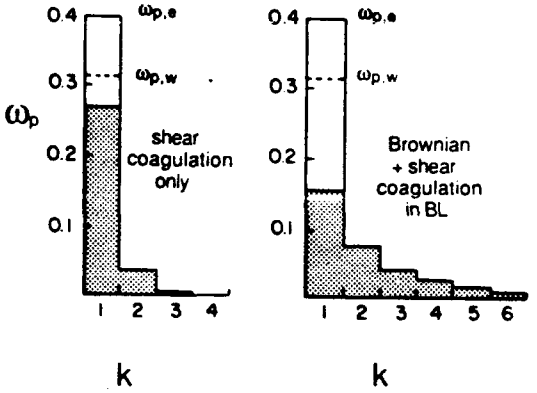

Fig. 4. Predicted mass fraction distribution of the depositing particle (at station (w)) (see Fig. 2).

nearly) isothermal convective-diffusion systems can be written:

$$(Dam)_{coag} = \frac{\left(\frac{\delta_m^2}{D_p}\right)}{\left(\frac{2}{9}N_{p,e}\frac{k_B T_e}{\mu_{g,e}}C_{slip}\right)^{-1}} \cong \frac{8\left(N_{p,e}d_p\frac{\pi L^2}{4}\right)}{3(Nu_m)^2}\frac{m_g}{m_p}\omega_{p,e}$$

again revealing the importance of the particle mass loading, $\omega_{p,e}$. Here, $N_{g,e}$ is the *gas* molecule number density and $Nu_m (= Re\,Sc\,St_m)$ is the nondimensional mass transfer coefficient (Nusselt number or Sherwood number) based on the reference target dimension L [see, for example, Rosner (1986)].

We expect, and are currently studying, the decisive role of the PSD of thermophoretically depositing particles on the microstructure and thermophysical properties of the porous glass "preform" (Tassopoulos *et al.*, 1989). Indeed, this investigation, combined with its predecessors (Rosner and Park, 1988; Park and Rosner, 1988a–c) sets the stage for long overdue quantitative studies of the important relationship between deposition mechanism, state of aerosol agglomeration and deposit properties—information that would evidently be useful in many technologies involving "powdery" deposits.

CONCLUSIONS AND IMPLICATIONS

We have developed and illustrated a mathematical model that predicts, under typical high particle mass loading conditions, the size distribution of thermophoretically depositing particles if the PSD of the local mainstream (outside the BL) is specified. Here, we have assumed that the principal mechanisms of aerosol particle coagulation within the nonisothermal LBL are Brownian coagulation and laminar shear coagulation, both of which are found to make nonnegligible contributions under conditions typical of industrial processes used in optical waveguide manufacture [see, for example, Keiser (1983)].

In the present class of applications (thermophoretically dominated deposition of particles with $Sc \equiv \nu/D_p \gg 1$, $Kn_p \gg 1$) it is interesting that BL coagulation does not appreciably alter the total mass deposition rate. but, rather, broadens the size distribution of depositing particles—inevitably leading to more "open", porous deposits (Tassopoulos *et al.*, 1989). More generally, BL coagulation would be expected to alter (usually reduce) the total mass deposition rate by virtue of the attendant reduction in effective Brownian diffusivity.

Since the depositing particle size distribution helps to determine important structural and thermophysical properties of the resulting deposits (e.g. porosity, permeability, thermal conductivity, . . .), properties which strongly influence the subsequent materials processing (e.g. drying, melting, consolidation, . . .) in optical waveguide manufacture, the present mathematical model and illustrative results may have important practical implications. This formulation/brief discussion can also serve as a rational starting point for subsequent mathematical models which, depending upon the specific environment, will inevitably require further refinements.

Finally, this approach can lead to a quantitative understanding of transport/coagulation-induced "shifts" in PSD which inevitably occur in "intrusive" sampling schemes [see, for example, Eisner and Rosner (1985) and Dobbins and Megaridis (1987)], enabling inferences of mainstream PSDs from observed (e.g. electron microscope) PSDs on the target.

Acknowledgements—We are indebted to the U.S. Department of Energy–Pittsburgh Energy Technology Center, whose financial support (under Grant DE-FG22-86PC90756) helped make possible this study and its publication. Thanks are also due to Drs J. Abbott, D. Powers, J. L. Castillo and P. Garcia-Ybarra for their helpful comments on this work. The support of our High Temperature Chemical Reaction Engineering Laboratory Industrial Affiliates (Shell, SCM Chemicals and Textron–Lycoming) is also gratefully acknowledged.

NOTATION

$\tilde{A}$	parameter in Cunningham–Millikan "slip" correction factor [eq. (2-6)]
$\bar{c}_i$	mean thermal speed of particle i
C_{slip}	Cunningham–Millikan slip correction factor
Dam_{coag}	Damköhler number governing particle coagulation
d_i	diameter of (spherical) particle i
D_{ij}	Brownian diffusion coefficient for particle j with respect to particle i
D_p	particle Brownian diffusivity in mixture
f	dimensionless (Blasius) stream function [eq. (2-3)]
g	dimensionless temperature ratio (T/T_e)
k	mixture thermal conductivity

k_B	Boltzmann constant
k_g	gas phase thermal conductivity
Kn_i	Knudsen number (l/d_i)
Kn_L	Knudsen number based on target dimension L
l	gas mean-free-path
l_i	mean-free-path for particle i
L	characteristic dimension of target
L_{ref}	reference length
m_g	mass of gas molecule
m_p	mass of particle
M_g	molecular weight of gas
n_k	particle number density of size class k
N_p	particle total number density
Nu	Nusselt number (dimensionless transfer coefficient)
p	pressure of gas phase
P	function defined by eq. (2-3)
Q	function defined by eq. (2-3)
r	radial coordinate in axisymmetric geometry (Fig. 1)
$r_0(x)$	radial coordinate to local body surface (Fig. 1)
R	ideal gas constant
Re	Reynolds number
R_i	radius of spherical particle i
R_{ij}	$R_i + R_j$
S	function defined by eq. (2-3)
Sc	Schmidt number (momentum/mass diffusivity ratio) (ν/D_p)
T	mixture temperature
T_g	gas temperature
T_p	particle temperature
u	x-direction mass-averaged velocity (Fig. 1)
v	y-direction mass-averaged velocity
$\mathbf{v}_g$	gas phase velocity vector
$\mathbf{v}_p$	particle phase velocity vector [eq. (2-1)]
x	distance along the wall (Fig. 1)
y	distance locally normal to the wall (Fig. 1)

Greek letters

α_T	thermal diffusion factor for particle transport
β	coagulation rate constant
δ_m	Brownian boundary layer (slope) thickness
δ_T	thermal boundary layer (slope) thickness
η	similarity variable defined after eq. (2-3)
κ	index (0 for planar flow, 1 for axisymmetric flow)
μ	dynamic viscosity of mixture
ν_g	gas momentum diffusivity [$\equiv(\mu/\rho)_g$] (kinematic viscosity)
ξ	streamwise variable defined after eq. (2-3)
ρ	mass density of mixture
ρ_p	intrinsic mass density of each particle
ω_p	particle mass fraction in mixture

Subscripts

B	Boltzmann
coag	pertaining to microdroplet coagulation
e	at the outer edge of the boundary layer
g	gas phase
k	pertaining to size class k ($k = 1, 2, \ldots, K$)
L	pertaining to reference length L
m	pertaining to *mass* transfer
p	particle phase
T, h	pertaining to *heat* transfer (thermal BL)
w	at the wall (surface of the particulate deposit)

Abbreviations

LBL	laminar boundary layer
OWG	optical waveguide
PSD	particle size distribution

Operators

div	(spatial) divergence
| |	absolute value
grad	spatial gradient

REFERENCES

Cebeci, T. and Bradshaw, P., 1976, *Momentum Transfer across Boundary Layers*. McGraw-Hill, New York.

Cebeci, T. and Smith, A. M. O., 1974, *Analysis of Turbulent Boundary Layers*. Academic Press, New York.

Dobbins, R. A. and Megaridis, C., 1987, Morphology of flame-generated soot as determined by thermophoretic sampling. *Langmuir* (ACS) **3**, 254–259.

Fernandez de la Mora, J. and Rosner, D. E., 1982, Effects of inertia on the diffusional deposition of small particles to spheres and cylinders at low Reynolds numbers. *J. Fluid Mech.* **125**, 379–395.

Friedlander, S. K., 1977, *Smoke, Dust and Haze—Fundamentals of Aerosol Behavior*. J. Wiley, New York.

Fuchs, N. A., 1964, *Mechanics of Aerosols*. Pergamon Press, New York

Garcia-Ybarra, P. and Rosner D. E., 1989, Thermophoretic properties of nonspherical particles and large molecules. *A.I.Ch.E. J.* **35**, 139–147.

Garcia-Ybarra, P., Rosner, D. E. and Park, H. M., 1988, Investigation of two new coagulation mechanisms for nonspherical particles in a thermal boundary layer. High Temperature Chemical Reaction Engineering Laboratory, Yale University (in preparation).

Goren, S. L., 1977, Thermophoresis of aerosol particles in the laminar boundary layer on a flat plate. *J. Colloid Interface Sci.* **61**, 77–85.

Keiser, G., 1983, *Optical Fiber Communications*. McGraw-Hill, New York.

Keller, H. B., 1974, Accurate difference methods for nonlinear two-point boundary value problems. *SIAM J. numerical analysis* **11**, 305–320.

Park, H. M., 1987, Thermophoretically augmented mass, momentum and energy transfer rates in high particle mass loaded laminar forced convection systems. PhD dissertation, Department of Chemical Engineering, Yale University.

Park, H. M. and Rosner, D. E., 1989a, Multiphase continuum theory of dopant redistribution across aerosol-laden laminar nonisothermal boundary layers. *Chem. Engng Sci.* **44**, 603–617.

Park, H. M. and Rosner, D. E., 1989b, Combined inertial and thermophoretic effects on particle deposition rates in highly loaded dusty-gas systems. *Chem. Engng Sci.* **44**, 2233–2244.

Park, H. M. and Rosner, D. E., 1989c, Thermophoretically induced phase-separation in highly mass-loaded dusty gas mixtures. High Temperature Chemical Reaction Engineer-

ing. Laboratory Publication No. 162, Yale University (prepared for submission to *A.I.Ch.E. J.*).

Rosner, D. E., 1980, Thermal (Soret) diffusion effects on interfacial mass transport rates. *Physicochem. Hydrodynamics* **1**, 159–185.

Rosner, D. E., 1986, *Transport processes in Chemically Reacting Flow Systems*. Butterworths, Stoneham, MA. Second printing 1988.

Rosner, D. E., 1989, Total mass deposition rates from 'polydispersed' aerosols. *A.I.Ch.E. J.* **35**, 164–167.

Rosner, D. E. and Park, H. M., 1988, Thermophoretically augmented mass-, momentum- and energy-transfer rates in high particle mass loaded laminar forced convection systems. *Chem. Engng Sci.* **43**, 2689–2704 [NB add exponent -1 to expression for t_{coag} in eqs (A5-1) and (5-3)].

Rosner, D. E. and Tassopoulos, M., 1989, Mass deposition rates from streams containing 'polydispersed' particle populations of arbitrary spread. *A.I.Ch.E. J.* (in press).

Saffman, P. G., 1965, The lift on a small sphere in a slow shear flow. *J. Fluid Mech.* **22**, 385–400.

Schlicting, H., 1979, *Boundary Layer Theory*, 7th Edition. McGraw-Hill, New York.

Tassopoulos, M., O'Brien, J. and Rosner, D. E., 1989, Theoretical approach to establish particle deposition mechanism/deposit microstructure relationships. *A.I.Ch.E. J.* (in press).

REPORT DOCUMENTATION PAGE

Form Approved
OMB No. 0704-0188

1. AGENCY USE ONLY (Leave blank)	2. REPORT DATE	3. REPORT TYPE AND DATES COVERED
	1991	Journal Publication

4. TITLE AND SUBTITLE
"High Temperature Kinetics of Solid Boron Gasification by $B_2O_3(g)$: Chemical Propulsion Implications" (U)

5. FUNDING NUMBERS
PE - 61102F
PR - 2308
SA - BS
G - AFOSR 89-0223

6. AUTHOR(S)
R. Zvuloni, A. Gomez and D.E.Rosner

7. PERFORMING ORGANIZATION NAME(S) AND ADDRESS(ES)
HIGH TEMPERATURE CHEMICAL REACTION ENGINEERING LABORATORY
YALE UNIVERSITY
BOX 2159, YALE STATION
NEW HAVEN, CONNECTICUT 06520 U.S.A.

8. PERFORMING ORGANIZATION REPORT NUMBER

9. SPONSORING/MONITORING AGENCY NAME(S) AND ADDRESS(ES)
AFOSR/NA
Building 410
Bolling AFB DC 20332-6448

10. SPONSORING/MONITORING AGENCY REPORT NUMBER

11. SUPPLEMENTARY NOTES

12a. DISTRIBUTION/AVAILABILITY STATEMENT
Approved for public release; distribution is unlimited

12b. DISTRIBUTION CODE

13. ABSTRACT (Maximum 200 words)

New flow reactor measurements are reported of the intrinsic kinetics of the gasification of solid boron by each of these important vapors: $B_2O_3(g)$, $O_2(g)$, $CO_2(g)$, and $H_2O(g)$ at surface temperatures between 1330 and 2050 K. For illustrative purposes, our data for the remarkably efficient $B_2O_3(g)/B(s)$ reaction and the $O_2(g)/B(s)$ reaction are used to discuss the expected sequence of rate-controlling processes for the combustion of individual B(s) particles in air under typical ramjet conditions. A diagram of (log-) particle diameter vs (log-) chamber pressure is shown to be particularly useful for this purpose, as well as to display the onset of noncontinuum behavior and the locus of expected particle extinction due to passivation associated with the kinetically controlled onset of condensed B_2O_3 on the gas/solid interface. In this way we show that, whereas most previous boron particle combustion and extinction laboratory experiments have been performed in the regime of gas-phase diffusion control, under conditions of actual ramjet interest the gas/solid kinetics for the efficient $B_2O_3(g)/B(s)$ reaction and the slower $O_2(g)/B(s)$ reaction, as well as noncontinuum transport effects, become rate limiting.

14. SUBJECT TERMS
boron, boric oxide vapor, heterogeneous kinetics, chemical propulsion, gas/solid reactions, flow reactors

15. NUMBER OF PAGES
5

16. PRICE CODE

17. SECURITY CLASSIFICATION OF REPORT	18. SECURITY CLASSIFICATION OF THIS PAGE	19. SECURITY CLASSIFICATION OF ABSTRACT	20. LIMITATION OF ABSTRACT
Unclassified	Unclassified	Unclassified	UL

High Temperature Kinetics of Solid Boron Gasification by $B_2O_3(g)$: Chemical Propulsion Implications

R. Zvuloni,* A. Gomez,† and D. E. Rosner‡
Yale University, New Haven, Connecticut 06520 USA

New flow reactor measurements are reported of the intrinsic kinetics of the gasification of solid boron by each of these important vapors: $B_2O_3(g)$, $O_2(g)$, $CO_2(g)$, and $H_2O(g)$ at surface temperatures between 1330 and 2050 K. For illustrative purposes, our data for the remarkably efficient $B_2O_3(g)/B(s)$ reaction and the $O_2(g)/B(s)$ reaction are used to discuss the expected sequence of rate-controlling processes for the combustion of individual B(s) particles in air under typical ramjet conditions. A diagram of (log-) particle diameter vs (log-) chamber pressure is shown to be particularly useful for this purpose, as well as to display the onset of noncontinuum behavior and the locus of expected particle extinction due to passivation associated with the kinetically controlled onset of condensed B_2O_3 on the gas/solid interface. In this way we show that, whereas most previous boron particle combustion and extinction laboratory experiments have been performed in the regime of gas-phase diffusion control, under conditions of actual ramjet interest the gas/solid kinetics for the efficient $B_2O_3(g)/B(s)$ reaction and the slower $O_2(g)/B(s)$ reaction, as well as noncontinuum transport effects, become rate limiting.

I. Introduction

BECAUSE the combustion of boron in an oxygen-containing gas has an appreciable potential, considering all possible chemical elements in terms of gravimetric and especially volumetric energy density, it has been recognized as a potentially attractive fuel (see, e.g., Ref. 1). At typical anticipated operating conditions (temperature, pressure, gaseous environment) and based on its thermochemical properties, boron burns as a solid particle.[2,3] Because of the necessarily short combustor residence times, the required particle diameters are sufficiently small that the burning is expected to be kinetically limited during most, if not all, of the burning time.[3,4] Nevertheless, experimental and theoretical research in the late 1960s and early 1970s[5-7] concentrated on diffusion-controlled combustion, revealing only some of the features of boron particle combustion of the underlying semimetal. Indirect determination of some kinetic parameters during ignition appears in recent work.[8] Diffusion-controlled quasi-steady surface oxidation of boron (like carbon) is found to be a two-step process since ambient O_2 molecules can react in the gas phase with boron suboxides to form B_2O_3, i.e., O_2 does not necessarily reach the particle surface. In such cases the higher boron oxide vapor, $B_2O_3(g)$, is the main surface gasifier, playing the same role as CO_2 in carbon gasification. However, as the particle gets smaller, this picture is expected to break down since the following new phenomena become involved: 1) kinetics (homogeneous and heterogeneous) begins to dominate over vapor phase diffusion, and 2) when the particle diameter becomes comparable to the gas mean free path, the individual particle flowfield is no longer continuum and, hence, the transfer of heat and mass to/from the particle exhibits new characteristics. B_2O_3 condensate may play an important role under these conditions also. Under kinetically controlled surface oxidation conditions, $B_2O_3(c)$ may be present on the boron particle surface as a continuous submicroscopic layer or as patches, even at temperatures higher than the (equilibrium) condensation temperature. Only by experimentally studying the surface reaction kinetics (below) can we reliably determine the conditions leading to bare or covered surface behavior in such nonequilibrium cases.

Except for a qualitative understanding, until now a lack of experimental data, especially for the less predictable surface kinetics, has precluded accurate predictions of boron particle combustion behavior (via surface and gas phase kinetics/transport theoretical/numerical models) in the kinetically limited, and possibly noncontinuum, regime.

To appreciate the relative importance of the previously mentioned chemical reactions (homogeneous and heterogeneous) and transport processes we have summarized the preliminary calculations in Fig. 1. The diagonal straight lines on our

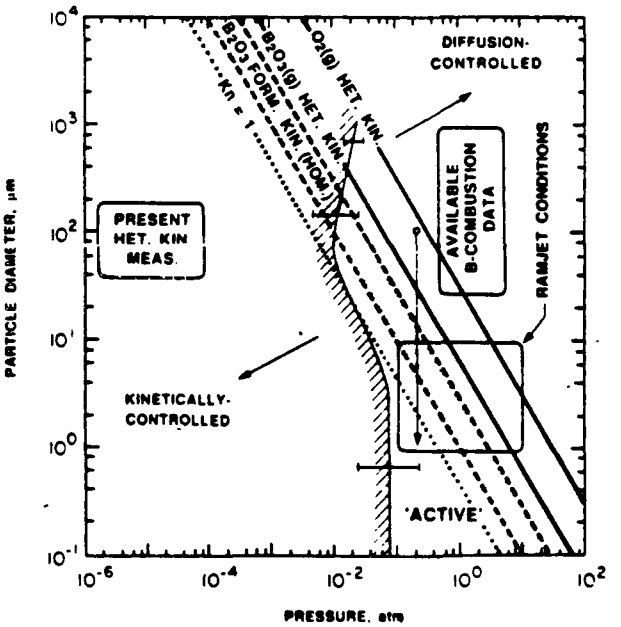

Fig. 1 Boron particle combustion map displaying expected: 1) diffusion-controlled or kinetically controlled regimes for $B_2O_3(g)$ and $O_2(g)$ reactions with the surface, 2) transition to noncontinuum behavior, and 3) extinction due to surface passivation.

Received Jan. 14, 1989; revision received Jan. 4, 1990.

*Graduate Research Assistant, Department of Chemical Engineering, High Temperature Chemical Reaction Engineering Laboratory.
†Assistant Professor, Mechanical Engineering.
‡Professor, Department of Chemical Engineering; Director, High Temperature Chemical Reaction Engineering Laboratory. #170

proposed (log) particle diameter vs (log) total pressure plane define loci of transition from the diffusion-controlled regime to the kinetically controlled regime for surface reactions of $B_2O_3(g)$ and $O_2(g)$ with solid boron and for the $B_2O_3(g)$ homogeneous formation reaction. Also shown is the Knudsen number locus $Kn = 1$, i.e., approximately when the continuum approach fails. A knowledge of the relative position of these three locii gives a clearer picture of what are likely to be the important gaseous species and rate-controlling mechanisms in the history of a burning particle. In constructing this figure (see Sec. IV for details), we estimated the homogeneous kinetics and the $O_2(g)/B(s)$ kinetics based on previous fragmentary results. We deliberately assumed the upper limit surface reaction probability, $\epsilon = 1$, for the $B_2O_3(g)/B(s)$ kinetics (which, remarkably, was found to be close to the measured reaction probabilities; see Sec. III) and concluded that this heterogeneous reaction would be important over more than one order of magnitude in particle diameter and, hence, three orders of magnitude in particle mass [the vertical segment from the O_2 kinetics locus, based on $\epsilon \approx 0.2$, where $B_2O_3(g)$ becomes the dominant species, until the homogeneous kinetics locus below which $B_2O_3(g)$ does not have adequate time to be formed]. Since ϵ for the $B_2O_3(g)/B(s)$ reaction turned out to be somewhat smaller, this interval would be even broader. Motivated, in part, by these initial estimates our objective was to study experimentally, under well-defined conditions, the intrinsic kinetics of the high-temperature surface reaction between solid boron and $B_2O_3(g)$ (structurally OBOBO, with a central B-O-B angle in the range 95-125 deg). For comparison purposes we also briefly examined the reagents $O_2(g)$, $CO_2(g)$, and $H_2O(g)$.

II. Experimental Techniques

Principles and experimental techniques for measuring the intrinsic kinetics of efficient gas/solid reactions at realistic reagent pressures without encountering external transport limitations have been developed at this laboratory and are discussed in detail elsewhere.[9,10] It was found that under conditions of small specimen size, high gas velocity, and subatmospheric pressure, a laboratory test environment appropriate for such kinetic measurements can be achieved. For monitoring the boron gasification rate we utilize a technique called microwave induced plasma emission spectroscopy (MIPES),[11-14] a sensitive yet simple chemical element detection technique capable of instantaneous measurements, together with high-temperature flow-reactor techniques developed earlier in our laboratory.[9,15-18]

Our experiments have been performed in a transonic, low-pressure (ca. 0.5 Torr), steady-flow chemical reactor (Fig. 2). We developed an electrically heated platinum boat source and obtained measurable amounts of $B_2O_3(g)$ effusing through a slit (0.5-mm width) at known conditions (ca. $T = 1450$ K, at which the equilibrium vapor pressure is reported[19] to be about 0.2 Pa). Under equilibrium conditions it is known that $B_2O_3(l)$ vaporizes predominantly to $B_2O_3(g)$ with less than 0.1% boron suboxides simultaneously present.[19] The downstream boron filament specimen (obtained via AVCO Specialty Materials), of 0.142-mm diam, was electrically heated to the desired temperature (calculated from optical pyrometer measurements using a spectral emittance of 0.69, see Ref. 14 for details) and attacked by the selected gaseous reactant ($B_2O_3, O_2, \ldots$) in crossflow using Ar as the carrier gas. The reaction product stream, collected through a skimmer immediately downstream of the central (uniform temperature) region of the filament, meets an opposed jet of argon metastable atoms Ar^* generated by the microwave plasma discharge.[11] This leads to reaction product excitation and subsequent characteristic radiation emission. (In an earlier configuration,[12] we found that B_2O_3 condensed on the reactor walls was then removed by Ar^* and diffused back into the central probe volume, thereby interfering with such measurements. Our modified counterflow geometry successfully eliminates this problem.) Emission of the strongest boron line, at 249.7 nm, coming from neutral boron atoms,[20] was focused by a 35-mm f1 fused silica lens onto the slit of a 0.5-m monochromator (Jarrel-Ash, Model 84-110), with the signal collected into a photomultiplier tube (Hamamatsu, R212) and the output converted to a voltage signal by a picoammeter (Gencom, Model 1012). Since the reactant $B_2O_3(g)$ itself contains the element B, a signal is, of course, obtained even without surface reaction. Therefore, the change in signal over the reactant contribution, and over the boron filament sublimation signal, is the signal assigned to the surface reaction to form B-containing vapor products. A linear output vs boron element mass flow rate was obtained over ca. 4 decades of B-flow rate. Further details of the experimental procedure are given elsewhere.[14]

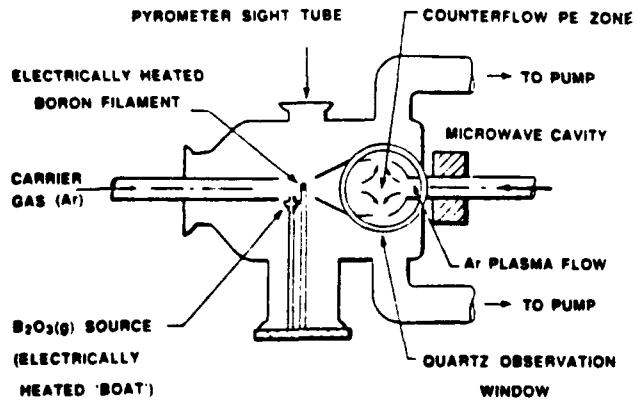

Fig. 2 Flow reactor configuration for kinetic studies of gas/solid reactions using product detection via microwave induced plasma emission spectroscopy (MIPES).

III. Experimental Results

In Fig. 3, we present our results for the surface reaction rate between solid boron and individual, important anticipated gaseous species as a function of the inverse of the solid surface temperature. Reaction rate results are shown in terms of a reaction probability ϵ, a nondimensional overall rate constant for the (nonelementary) surface reaction, defined as the ratio of the net flux of boron atoms, irrespective of speciation, emerging from the surface as a result of chemical reaction, to the arrival flux of the gaseous reactant B_2O_3, or $O_2, \ldots$ on the

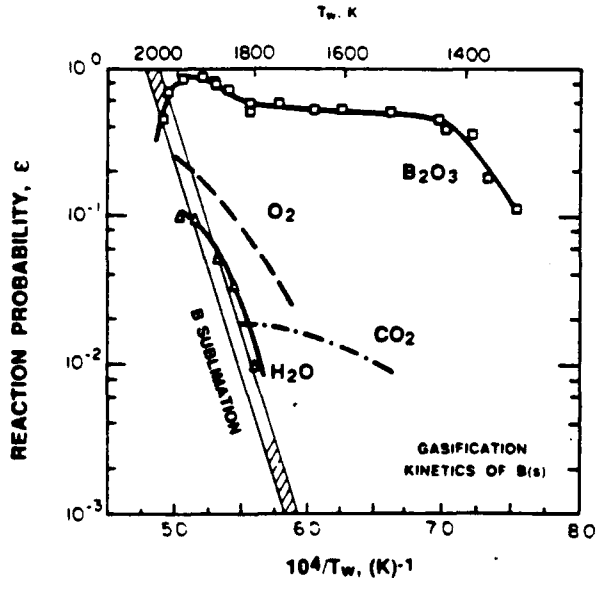

Fig. 3 Reaction probabilities for gasification of solid boron by $B_2O_3(g)$, $O_2(g)$, $H_2O(g)$, and $CO_2(g)$ at reactant pressure of the order of 10^{-2} Pa.

surface. Accordingly, this presentation is independent of the identity of the reaction products. The boron sublimation branch (ca. 132 Kcal/mole) shows what would be the contribution to the apparent reaction probability from the boron atom flux subliming into a vacuum (the left line pertains to the heavy reactant molecule B_2O_3 and the right line pertains to the lighter molecules O_2, H_2O). The $O_2(g)$ and O(g) reactions on high temperature boron surfaces have been studied before using different experimental conditions and techniques.[15] We repeated a portion of the $O_2(g)/B(s)$ reaction study using the present MIPES technique and found similar behavior.[21] In both cases, the reaction probability in the active regime (relatively insensitive to surface temperature) is ca. $\epsilon = 0.2$. Our new results for the $B_2O_3(g)/B(s)$ reaction are presented here in greater detail, along with a discussion (Sec. IV) of their propulsion implications. This reaction probability was measured over a surface temperature range from 1330 to 2060 K at an estimated partial pressure of 10^{-2} Pa. Remarkably high reaction probabilities ($\epsilon = 0.5$) were inferred, exhibiting very low sensitivity to surface temperature over the range 1450–1800 K. Boron gasification by $B_2O_3(g)$ is evidently more efficient than boron gasification by $O_2(g)$, $H_2O(g)$, or $CO_2(g)$ and is comparable to that attained (over a narrower temperature interval) by atomic oxygen, O(g).[15] At still higher surface temperatures, the $B_2O_3(g)/B(s)$ reaction probability rises to a maximum of $\epsilon = 0.9$ near 1950 K and then falls steeply. Below about 1450 K, we also observed a sharp reduction in reaction probability. The conditions at which this fall-off occurs (the so-called active-to-passive transition[18]) are of primary importance for predicting particle extinction, as discussed below. The slope of the Arrhenius curve (on the log ϵ vs $1/T$ plane) at each point gives the local overall activation energy of the surface reaction and provides valuable clues about the detailed surface processes.[14] In the aforementioned fall-off regime, this slope is found to correspond to about 60 Kcal/mole. Also shown are our MIPES estimates for B(s) gasification by measured gaseous fluxes of $H_2O(g)$ or $CO_2(g)$. It can be seen that H_2O contributes B atoms to the gaseous environment at about the same rate as boron sublimation at the measured temperatures, 1800–2000 K. The observed reaction probability for B(s) attacked by $CO_2(g)$ is 0.01–0.02 in the temperature range 1500–1900 K, with much lower and T-dependent apparent activation energies.

In Fig. 4, we summarize our results for the active-to-passive transition locus of the $B_2O_3(g)/B(s)$ reaction as inferred from experiments similar to the ones summarized in Fig. 3 but at different B_2O_3 pressures. The resulting transition condition establishes a locus that effectively divides the $p_{B_2O_3}$-T field into two qualitatively different regimes. The active regime is characterized by high reaction probabilities with low apparent activation energies. The passive regime is characterized by lower reaction probabilities and higher activation energy (the transition was found to be more abrupt as $p_{B_2O_3}$ is reduced). We have also estimated theoretically the active-to-passive transition locus based on a quasi-equilibrium approach[9,14,22] and obtained the same general trend: the expected transition temperature increases with B_2O_3 partial pressure. (However, the QE-predicted slope was slightly different from that observed; see Ref. 14 for further details.)

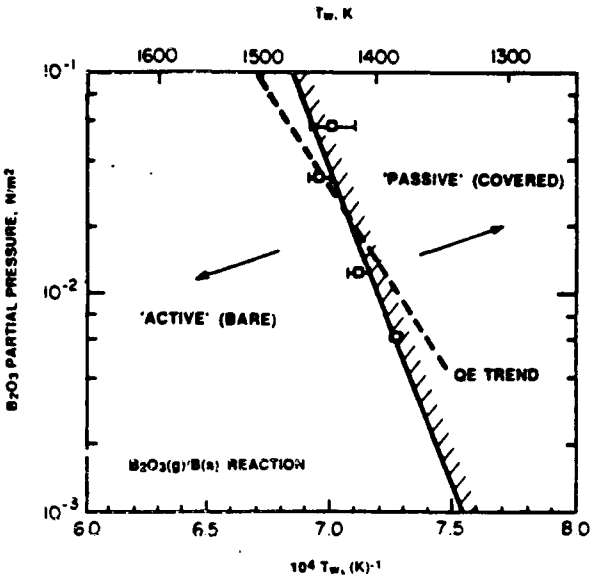

Fig. 4 Active-to-passive transition locus. Solid line: experimentally determined[14]; dashed line: inferred from quasi-equilibrium theory.

IV. Chemical Propulsion Implications

As pointed out previously, measurements of the true rates of these surface reactions (without diffusional falsification) enable us for the first time to estimate the relative importance of the reaction/diffusion processes during the burning history of boron particle in an oxygen-containing environment. In Fig. 1, we include four different kinds of information on the suggested logarithmic graph of particle diameter vs total pressure. A typical gas temperature of 2000 K was chosen for these calculations. The locus of unit Knudsen number (transition to noncontinuum behavior) at this temperature is also shown. Separated by the diffusion-to-kinetics transition loci, large particles at high pressures experience diffusion-controlled particle combustion and small particles at low pressures lead to kinetically controlled combustion, possibly in a free-molecular flowfield (on the scale of the individual particle diameter). The loci for the $O_2(g)/B(s)$ and $B_2O_3(g)/B(s)$ reactions, consistent with our gas/solid kinetic measurements (cf., Fig. 3) together with the $B_2O_3(g)$ homogeneous formation [oxidation of the suboxides BO(g) and $(BO)_2(g)$] kinetics shown on this map, display an estimate of when the kinetics of each of these reactions is expected to become important compared to the relevant diffusional transfer of these species. While O_2 diffuses from the ambient toward the boron surface, if B_2O_3 forms in the gas phase near the surface its diffusion rate is enhanced by a calculable factor (F_{rxn}[23] here estimated to be about twofold), compared to simple diffusion in the absence of homogeneous reaction. The homogeneous kinetics band shown here covers the range of results from the highest possible bimolecular collision rate (left boundary) to an estimated overall formation rate of B_2O_3 from boron suboxides (right boundary). We based our nonelementary reaction rate estimate on fragmentary experimental measurements[24-26] and theoretical estimates summarized in Ref. 27 for selected gaseous elementary reactions between boron-containing species and oxygen-containing species; i.e., the rate of homogeneous $B_2O_3(g)$ formation was estimated by deducing what would be the rate determining step from the possible rate constants appearing in Ref. 27. Homogeneous formation of atomic oxygen in the B,O system was predicted to be negligible compared to $B_2O_3(g)$ formation in Ref. 27 and consequently is not considered further here. Since our measurements of the kinetics of the $B_2O_3(g)/B(s)$ reaction indicated higher reaction probabilities than for the competing $O_2(g)/B(s)$ surface reaction we conclude (i.e., based on the relative position of the locii) that $B_2O_3(g)$ would be the main B(s) gasifier in the kinetic regime if it can be formed at an adequate rate in the gas phase diffusion boundary layer. Consequently, a boron particle of diminishing size at constant pressure (see the vertical path in Fig. 1) will exhibit a slower combustion rate under a critical size when homogeneous kinetics begins to limit the formation of $B_2O_3(g)$ (thereby causing the direct $O_2(g)/B(s)$ reaction to be the main surface reaction) even though conditions favor active kinetics for both surface reactions. Another important feature of these kinetically controlled combustion processes is possible extinction due to the transition from active to passive behavior for

the surface oxidation reaction. Since the overall oxidation reaction is exoergic, when the reaction rate falls, less chemical energy is released and the particle surface temperature necessarily drops. This unidirectional process leads to a further reduction in the reaction rate and the particle surface temperature, ultimately causing extinction. We estimated the active-to-passive locus (the curved boundary on the graph) based on our rather preliminary active-to-passive transition data for the $O_2(g)/B(s)$ reaction [data similar to Fig. 4 for the $B_2O_3(g)/B(s)$ reaction]. Then using a quasisteady energy balance for an individual particle, assuming maximum radiation losses, we estimated particle temperatures as a function of particle diameter and total pressure (at $T_g = 2000$ K and $p_{O_2}/p \approx 0.20$) and the conditions under which passivation should occur due to the (temperature dependent) formation of a protective $B_2O_3(c)$ layer (i.e., Fig. 4). Although this locus is independent of particle diameter in the free-molecular regime, in the continuum kinetically controlled surface reaction regime the slope of the curve is determined by the solution of the energy balance and, therefore, is not known a priori. We find that, in the continuum regime, lower pressures are needed for extinction by passivation compared to the free-molecular regime. On the same graph we also present three rectangular domains of practical interest: 1) the domain of most previous experimental boron particle combustion research, which is essentially in the diffusion-controlled domain; 2) the domain of oxygen pressure and specimen size in which we have been measuring true gas/solid reaction kinetic data (not falsified by gaseous diffusion); and 3) the domain of principal ramjet interest, which falls between the domains of diffusion-controlled and kinetically controlled reaction and also between continuum to free-molecular flow domains. Thus, in such applications one cannot defend simplifying assumptions frequently made as to the rate-controlling steps and local flow fields.

V. Conclusions

Our experiments lead us to conclude that $B_2O_3(g)$ is a very efficient reactant for gasifying solid boron at high temperature—much more so than other possible stable reactants [$O_2(g)$, $H_2O(g)$, $CO_2(g)$] of chemical propulsion interest. Not only is $B_2O_3(g)$ found to be locally comparable to O(g) (cf. Refs. 15 and 17) but it is efficient over a much broader surface temperature range. It follows that, provided there is adequate residence time (in the gaseous boundary layer near a burning particle) to form $B_2O_3(g)$ by the vapor phase oxidation of boron suboxides [BO, $(BO)_2$,...], the $B_2O_3(g)/B(s)$ heterogeneous reaction will be the most important channel through which B(s) is gasified. We estimate that at atmospheric pressure boron particles under about 30-μm diam would undergo kinetically limited combustion and the surface attack would be governed by the $B_2O_3(g)/B(s)$ reaction until the particle diameter reached ca. 3 μm. This means that a particle of, say, 30-μm initial diameter would deliver as much as 99.9% of its mass and energy under conditions of $B_2O_3(g)/B(s)$ rate control, whereas, if we considered a particle of 10-μm initial diameter, 97.8% of its mass and energy would be delivered under the same conditions. Under ca. 3 μm particle diameter, we estimate that the particle surface would be attacked mainly by $O_2(g)$, thereby reducing the gasification rate by some 2-3 times. From the above arguments, we conclude that this transition to the $O_2(g)/B(s)$ surface reaction would not be important for initially large particles (say, 10-30 μm) since the relative amount of mass and energy released at this latter stage would be negligible. However, fine fuel particles (about 3-μm initial diameter or less) would undergo kinetically controlled surface reaction by the slower $O_2(g)/B(s)$ reaction with a correspondingly slower energy release rate. Furthermore, at about 1-μm diameter, the burning particle boundary layer can evidently no longer be considered a continuum. Thus, continuum-to-free molecular transition flow theories should be included in simulation calculations if an appreciable fraction of energy is expected to be released under such conditions. Our calculations also indicate that near atmospheric pressure a small solid boron particle undergoes heterogeneous reaction in the kinetically active regime and would be likely to remain in this regime through its entire burning time. This implies that a successfully ignited particle in the environments considered here should not extinguish due to a possible reduction of the surface gasification rate resulting from "surface passivation" by $B_2O_3(c)$.

With the help of experimental measurements for several important gas/solid reactions, we have shown that it is possible to identify the chemical kinetic and physical phenomena likely to play a dominant role at each stage in the combustion history of a solid boron fuel particle. These considerations should be included in future mathematical models. As is well known, in practice, hydrogen- and/or carbon-containing species may also be present and thus complicate the simple picture illustrated here for the B/O system. However, using the same general strategy, i.e., experimentally obtaining the missing necessary information (which in most cases today falls in the area of chemical kinetics of homogeneous and, especially, heterogeneous reactions: see, e.g., Ref. 28) under well-defined conditions, combined with environmentally specific transport calculations, one can identify the appropriate phenomena to include in a sufficiently comprehensive model of boron particle combustion in airbreathing propulsion systems.

Acknowledgments

The authors are indebted to the U.S. Air Force Office of Scientific Research, whose financial support (under Grants AFOSR 84-0034 and 89-0223) made possible this study and its publication. Thanks also are due to A. Gany, A. Fontijn, B. Halpern, P. C. Nordine, and R. Weber for their helpful comments. This manuscript and Refs. 14 and 28 are based on R. Zvuloni's 1990 Yale University Ph.D. Dissertation.

References

[1]Gany, A., and Netzer, D. W., "Fuel Performance Evaluation for Solid-Fueled Ramjet," *International Journal of Turbo and Jet Engines*, Vol. 2, 1985, pp. 157-168.

[2]Paule, R. C., and Margrave, J. L., "A Langmuir Determination of the Sublimation Pressure of Boron," *Journal of Physical Chemistry*, Vol. 67, 1963, pp. 1368-1370.

[3]Glassman, I., Williams, F. A., and Antaki, P., "A Physical and Chemical Interpretation of Boron Particle Combustion," *Proceedings of the 20th Symposium on Combustion*, Combustion Inst., Pittsburgh, PA, 1984, p. 2057-2064.

[4]Mulcahy, M. F. R., and Smith, I. W., "Kinetics of Combustion of Pulverized Fuel: A Review of Theory and Experiment," *Review of Pure and Applied Chemistry*, Vol. 19, 1969, pp. 81-108.

[5]King, M. K., "Ignition and Combustion of Boron Particles and Clouds," *Journal of Spacecraft and Rockets*, Vol. 19, No. 4, 1982, pp. 294-306.

[6]Faeth, G. M., "Status of Boron Combustion Research," Report of the Boron Combustion Specialists Workshop, U.S. Air Force Office of Scientific Research, Oct. 1984.

[7]Mohan, G., and Williams, F. A., "Ignition and Combustion of Boron on O_2/Inert Atmospheres," *AIAA Journal*, Vol. 10, No. 6, 1972, pp. 776-783.

[8]Li, S. C., Williams, F. A., and Takahashi, F., "An Investigation of Combustion of Boron Suspensions," *Proceedings of the 22nd Symposium on Combustion*, Combustion Inst., Pittsburgh, PA, 1989, pp. 1951-1960.

[9]Rosner, D. E., "High Temperature Gas-Solid Reactions," *Annual Review of Materials Science*, Vol. 2, 1972, pp. 573-606.

[10]Rosner, D. E., and Nordine, P. C., "Mass Transport Requirements and a New Technique for Studying the Intrinsic Kinetics of High Temperature Gas/Liquid Reactions," *Physical Chemistry in Metallurgy, Proc. Darken Conf.*, edited by R. M. Fisher, U.S. Steel Corp., Monroeville, PA, 1976, pp. 496-499.

[11]Stedman, H., and Setser, W., "Chemical Applications of Metastable Rare Gas Atoms," *Progress in Reaction Kinetics*, Vol. 6, 1971, pp. 193-238.

[12]Oner, A., "Application of MIPES to the Study of Gas/Solid

Reactions," Ph.D. Dissertation, Dept. of Chemical Engineering, Yale University, New Haven, CT, 1985.

[13]Gomez, A., Zvuloni, R., and Rosner, D. E., "Flow Reactor Studies of the Kinetically-Controlled Oxidation of B(s) by $B_2O_3(g)$ Using Microwave-Induced Plasma Emission Spectroscopy: Preliminary Results," 1987 Technical Meeting—The Combustion Inst.-Eastern States Sections, Nov. 2, 1987, NBS (now NIST), Gaithersburg, MD.

[14]Zvuloni, R., Rosner, D. E., and Gomez, A., "High Temperature Kinetics of Solid Boron Gasification by Its Higher Oxide $B_2O_3(g)$: Flow Reactor Techniques, Rate Measurements and Their Implications," *Journal of Physical Chemistry* (to be published).

[15]Rosner, D. E., and Allendorf, H. D., "Kinetic Studies of the Attack of Refractory Materials by Oxygen Atoms and Chlorine Atoms," *Proceedings of the 3rd International Symposium on High Temperature Technology*, Butterworths, London, 1969, pp. 707-719.

[16]Rosner, D. E., and Allendorf, H. D., "Kinetics of Elemental Boron Chlorination by Chlorine Atoms and Chlorine Molecules," *Journal of Physical Chemistry*, Vol. 72, No. 12, 1968, pp. 4159-4162.

[17]Rosner, D. E., and Allendorf, H. D., "Kinetics of the Attack of Refractory Materials by Dissociated Gases," *Heterogeneous Kinetics at Elevated Temperatures*, edited by W. Worrell, Plenum, NY, 1970, pp. 231-251.

[18]Rosner, D. E., and Allendorf, H. D., "High Temperature Kinetics of the Oxidation and Nitridation of Pyrolytic Silicon Carbide in Dissociated Gases," *Journal of Physical Chemistry*, Vol. 74, 1970, pp. 1829-1839.

[19]Hildenbrand, D. L., Hall, W. F., and Potter, N. D., "Thermodynamics of Vaporization of Lithium Oxide, Boric Oxide, and Lithium Metaborate," *Journal of Chemical Physics*, Vol. 39, No. 2, 1963, pp. 296-301.

[20]Phelps, F. M. (ed.), *M.I.T. Wavelength Tables*, Vol. 2, MIT Press, Cambridge, MA, 1969.

[21]Gomez, A., Zvuloni, R., and Rosner, D. E., "Flow Reactor Studies of Boron Vaporization and Kinetically-Controlled Oxidation Using Microwave-Induced Plasma Emission Spectroscopy: Preliminary Results," 1986 Technical Meeting—The Combustion Inst.-Eastern States Sections, Dec. 12, 1986, San Juan, PR, and Joint Meeting of the French and Italian Sections of the Combustion Inst., June 16, 1987, Amalfi, Italy.

[22]Batty, J. C., and Stickney, R. E., "Quasi-equilibrium Treatment of Gas-Solid Reactions," *Journal of Chemical Physics*, Vol. 51, No. 10, 1969, pp. 4475-4492.

[23]Rosner, D. E., *Transport Processes in Chemically Reacting Flow Systems*, Butterworths, MA, 1986 (second printing 1988).

[24]Oldenborg, R. C., "Gas-Phase Oxidation of Boron Compounds," Abstracts of the 1987 AFOSR/ONR Contractors Meeting on Combustion, Pennsylvania State Univ., June 1987.

[25]DiGiuseppe, T. G., and Davidovits, P., "Boron Atom Reactions. II. Rate Constants with O_2, SO_2, CO_2, and N_2O," *Journal of Chemical Physics*, Vol. 74, No. 6, 1981, pp. 3287-3291.

[26]Llewellyn, I. P., Fontijn, A., and Clyne, M. A. A., "Kinetics of the Reaction $BO + O_2 \rightarrow BO_2 + O$," *Chemical Physics Letters*, Vol. 84, No. 3, 1981, pp. 504-508.

[27]Yetter, R. A., Cho, S. Y., Rabitz, H., Dryer, F. L., Brown, R. C., and Kolb, C. E., "Chemical Kinetic Modeling and Sensitivity Analyses for Boron-Assisted Hydrocarbon Combustion," *Proceedings of the 22nd Symposium on Combustion*, Combustion Inst., Pittsburgh, PA, 1989, pp. 919-927.

[28]Zvuloni, R., and Rosner, D. E., "Gasification Rate of Solid Boron in Mixtures of $B_2O_3(g)$ and Water Vapor," *Journal of Propulsion and Power* (to be published).

HIGH TEMPERATURE CHEMICAL REACTION ENGINEERING LABORATORY
YALE UNIVERSITY
BOX 2159, YALE STATION
NEW HAVEN, CONNECTICUT 06520 U.S.A.

FLOW REACTOR STUDIES OF THE HIGH TEMPERATURE GASIFICATION KINETICS OF SOLID BORON AND CARBON AND THEIR CHEMICAL PROPULSION IMPLICATIONS

A Dissertation

Presented to the Faculty of the Graduate School

of

Yale University

in Candidancy for the Degree of

Doctor of Philosophy

By

Roni Zvuloni

May, 1990

FLOW REACTOR STUDIES OF THE HIGH TEMPERATURE GASIFICATION KINETICS OF SOLID BORON AND CARBON AND THEIR CHEMICAL PROPULSION IMPLICATIONS

Roni Zvuloni
Yale University
1989

Abstract

Intrinsic heterogeneous kinetics of the high temperature gasification of solid boron, carbon, and boron-carbide by several important vapors are investigated utilizing newly designed low-pressure Transverse Filament Flow Reactor techniques, together with a sensitive, 'real-time', Microwave Induced-Plasma Emission Spectroscopy element detection technique. Reactions of solid boron with each of the vapors: $B_2O_3(g)$, $O_2(g)$, $CO_2(g)$, and $H_2O(g)$, as well as mixtures of $B_2O_3(g)$ and $H_2O(g)$, are investigated. The carbon reaction with $B_2O_3(g)$ and the boron-carbide reaction with $B_2O_3(g)$ and $O_2(g)$ were also measured in an effort to identify key surface reactions in ramjet combusors utilizing boron-containing hydrocarbons fuels. Experimental conditions covered surface temperatures between 1300 K and 2100 K and reactant partial pressures between *ca.* 10^{-3} to 10^{-1} Pa. Quasi-Equilibrium (QE) theory was used to provide complementary information on the thermodynamically favored surface product distribution.

Results revealed remarkably high reaction probabilities for $B_2O_3(g)$ attacking boron and pyrolytic carbon, with a maximum close to unity near 2000 K, much higher than that for the $O_2(g)$/B(s) reaction and comparable to that previously observed for atomic reactants, *e.g.*, O-atom attack of boron. The $CO_2(g)$ and $H_2O(g)$ contribution to B(s) gasification is modest. $B_4C(s)$ was found to be an excellent protective material in an oxidizing environment of $O_2(g)$ or $B_2O_3(g)$. Transition conditions for 'passivation' of the $B_2O_3(g)$/B(s) reaction were identified experimentally and found to be in qualitative agreement with Quasi-Equilibrium model predictions

QE results provided ancillary information on the partial pressure distributions of the gaseous products. For the $B_2O_3(g)/B(s)$ system the reaction products are primarily the *monomer* BO in the high temperature regime, 1500-2200 K and the *dimer* $(BO)_2$ in the intermediate temperature regime, *ca.* 1050-1500 K. Under the conditions investigated, the addition of hydrogen-containing species (*e.g.* $H_2O(g)$) to the oxygen/boron system resulted mainly in hydrogen products in the form of H and H_2 rather than complex products (*i.e.*, containing B,O, and H atoms). QE results for the $B_2O_3(g)/C(s)$ reaction revealed that at temperatures higher than *ca.* 1600 K the main gaseous products were CO molecules and B atoms while in the lower temperature range, *ca.* 1100-1600 K the main QE-predicted surface reaction products were the dimer $(BO)_2$ and CO at comparable partial pressures. QE results together with the experimental measurements of the observed (overall) kinetics of the gasification of boron, graphite, and boron-carbide, provided the basis for our analysis, of the mechanistic implications (*i.e.* elementary steps) of each of these reactions.

Our data for the remarkably efficient $B_2O_3(g)/B(s)$ reaction and the $O_2(g)/B(s)$ reaction have also been used to discuss the expected sequence of rate-controlling processes for the *combustion* of individual B(s) particles in air under typical ramjet conditions. A diagram of (log-) particle diameter *vs.* (log-) chamber pressure is shown to be particularly useful for this purpose, as well as to display the onset of non-continuum behavior and the locus of expected particle *extinction* due to "passivation" associated with the kinetically-controlled onset of condensed B_2O_3 on the gas/solid interface. In this way, we have shown that, while most previous boron particle combustion and extinction laboratory experiments were performed in the regime of *gas-phase diffusion control*, under conditions of actual ramjet interest the *gas/solid kinetics* for the efficient $B_2O_3(g)/B(s)$ reaction and the slower $O_2(g)/B(s)$ reaction, as well as non-continuum transport effects, become rate-limiting.

As an important 'by product' of this research, we also present details of flow reactor improvements and current capabilities of the MIPES detection technique.